Modelling refraction of waves over tidal channels

A numerical study focusing on the performance of spectral wave models with respect to bottom refraction

I.M.H. van der Reijden

TU Delft

Modelling refraction of waves over tidal channels

A numerical study focusing on the performance of spectral wave models with respect to bottom refraction

by:
I.M.H. (Ineke) van der Reijden

to obtain the degree of Master of Science
at the Delft University of Technology,
section: Hydraulic Engineering - Coastal Engineering,

to be defended publicly on Tuesday February 18, 2020 at 13:30h.

The image on the front page shows a part of the Ems-Dollard estuary (Waddenvereniging, Henk Postma (wad-mooi.nl))

Student number: 4381254
Project duration: May 15, 2019 – February 18, 2020
Thesis committee:
Dr. ir. M. Zijlema, Delft University of Technology
Dr. ir. V. Vuik, Delft University of Technology, HKV Consultants
Ir. P. Oosterlo, Delft University of Technology
Dr. ir. H. Steetzel, Arcadis Consultancy

TU Delft

ARCADIS Design & Consultancy for natural and built assets

Acknowledgements

This report is written for the completion of the master 'Coastal Engineering' of the section Hydraulic Engineering at Delft University of Technology. The project took up nine months and is the largest project I have worked on so far. For this thesis I have collaborated with Arcadis Zwolle, who provided me with the needed computational power, a working place and useful conversations. Thereby, I would like to thank all colleagues of Arcadis of the group RKZ and office Zwolle in general.

For a successful completion of this report, there are several people who deserve personal acknowledgement. First of all, I would like to thank my current thesis committee for their time and feedback. Here a special thanks goes to my chairman Marcel Zijlema for his suggestions and supportive comments. Also, I would like to thank Henk Steetzel for his practical view and help, Vincent Vuik for his sharp comments and Patrick Oosterlo for his feedback even though he only joined at the last months of the project. Despite the fact that I am thankful that Patrick wanted to join the committee, the reason why was less joyful. In the last months of the project an unexpected replacement for my former committee member Gerbrant van Vledder was needed. During the project Gerbrant gave me helpful advice, provided me the REFRAC executable and many Matlab files. For this I am still very grateful.

Last but not least, I would like to thank Nathanaël Geleynse of Arcadis for his great help, enthusiasm and honest interest in the project. He was always ready to help or to discuss the content. In addition, he provided me with the needed data and information, for which I am thankful. To conclude, I thank all friends and family who supported me during the past months.

I.M.H. van der Reijden
Zwolle, February 2020

Abstract

For the design of coastal structures, the hydraulic loads that act on the coast should be known. These are often based on extrapolation of measurements. However, if the physical relation is unknown, large errors could be made. Therefore, a numerical model can be set up to take the most important processes into account.

Yet, uncertainties are present in these numerical models as well. Taking for example the spectral wave model SWAN, it is hypothesised that the wave bottom refraction is not always properly modelled. The refraction process occurs due to a difference in depth and hence wave celerity along a crest, which causes wave turning to shallower regions. In case a channel is present along a wave path, the wave may turn away from the channel and stick to the channel edge. Previous studies concluded that SWAN overestimates this refraction process, leading to an underestimation of waves entering the channel. In case a coastal protection structure is present across the channel, the hydraulic loads here could thus be seriously underestimated. This problem leads to the following research question to be answered:
How can the representation of wave refraction over tidal channels be improved in spectral wave models?

This study uses the model SWAN in which different sensitivities are tested to assess the effect on refraction. The focus will be on the spatial and directional resolution as well as the wave propagation scheme that SWAN uses to discretise the propagation terms, which are the default SORDUP scheme and the optional BSBT scheme. From previous studies it is known that also physical processes could impact the bottom refraction, however these are only addressed shortly in this study. The aim of this study is to analyse the current performance of SWAN with respect to refraction and to assess how this performance can be improved.

First, an analysis of a simple schematic channel case is made in SWAN and a ray-tracing model called REFRAC, where waves propagate from shallow to deeper water. Physical source terms and wind wave-growth were not taken into account in this part. It is found that a coarser spatial resolution can lead to a weaker wave refraction, causing the wave height along the upwave channel edge, i.e. the side where waves come from, to decrease with 0-11cm (0-11%). Also a coarser directional resolution and the BSBT scheme can lead to weaker refraction. It is concluded that this is caused by the way SWAN determines the turning rate, which is underestimated by SWAN compared to the theory of Snellius. On the other hand, an overestimation of wave refraction was observed for cases were waves should enter the channel. This is partly caused by the increased diffusion. The directional spreading increases, causing a larger fraction of energy to refract away from the channel.

Secondly, these findings were taken into practice in a study of the Eastern Wadden Sea, specifically along the Ems channel, where waves propagated from deeper to shallower water. It was found that if again the source terms are deactivated, SWAN and REFRAC give a similar result. Yet, a coarser spatial resolution and the BSBT scheme showed less wave penetration from offshore into the Ems channel. The directional resolution has minor impact on the solution in this case. Finally, the storm of January 2017 was simulated in SWAN after which a comparison was made to measurements. It was found that SWAN underestimated the wave energy for frequencies<0.15Hz, which is in accordance with previous studies. However, this did not improve by refining the resolution in both spatial and directional domain or by applying a different propagation scheme. Yet, the prediction of the significant wave height improved along the channel edge with a refined spatial resolution.

Based on these case studies, it can be concluded that SWAN indeed overestimates the wave refraction due to bottom gradients if waves propagate to shallower water. In case waves travel to deeper water, refraction can be underestimated. If all physical source terms are deactivated, the effects of resolution on refraction are clearly visible. Including the source terms diminishes this effect. Along the channel edges, effects of increased spatial resolution are notable giving a significant wave height of 12-14cm (6-9%) closer to the measured condition. On the other hand, the effects at the coast near Uithuizerwad are negligible. The tidal flat in between the channel and the coast causes a larger impact of other physical settings and the bottom schematisation. Therefore it is recommended to perform further research to the implementation of these physics, such as the non-linear triad interactions and depth-induced wave breaking. It is expected that the relative importance of these processes is larger than the refraction process near the coast.

Contents

List of Figures

List of Tables

List of Symbols

Latin characters

a	Wave amplitude	[m]
b	Width between two wave rays	[m]
c	Wave celerity	[m/s]
c_g	Wave group velocity	[m/s]
c_θ	Wave direction velocity	[°/s]
c_σ	Rate of change in frequency space	[Hz/s]
Cr	Courant number	[-]
d	Water depth	[m]
$E(f,\theta)$	Wave energy density	[J/m^2/Hz/°]
$E_{variance}(f,\theta)$	Variance density = m_0	[m^2 / Hz /°]
E	Total wave energy	[J/m^2]
f	Wave frequency	[Hz]
f_{max}	Maximum wave frequency	[Hz]
f_{min}	Minimum wave frequency	[Hz]
$\overline{f}$	Mean wave frequency	[Hz]
g	Gravitational acceleration = 9.81	[m/s^2]
H_{m0}	Spectral significant wave height	[m]
H_{max}	Maximum wave height	[m]
H_{rms}	Root mean squared wave height	[m]
H_s	Significant wave height	[m]
k	Wave number = 2π/L	[m^{-1}]
L	Wave length	[m]
m	Direction along wave ray = s	[-]
m_0	Zeroth order spectral moment	[m^2]
m_n	nth order spectral moment	[m^2]
msc	Number of bins in frequency space	[-]
N	Wave action density	[m^2/Hz^2/degr^2]
R	Ray curvature	[m]
RB	Relative Bias	[%]
$RMSE$	Root Mean Squared Error	[m]
S_{bfr}	Bottom friction dissipation term	[m^2/Hz]
S_{in}	Wind input term	[m^2/Hz]
S_{nl3}	Non-linear triad wave-wave interaction term	[m^2/Hz]
S_{nl4}	Non-linear quadruplet wave-wave interaction term	[m^2/Hz]
S_{surf}	Depth-induced wave breaking term	[m^2/Hz]
S_{tot}	Total source terms	[m^2/Hz]
S_{wc}	White-capping term	[m^2/Hz]
t	Time	[s]
T	Wave period	[s]
T_{m01}	Mean wave period	[s]
T_{m02}	Mean wave period	[s]
$T_{m-1,0}$	Low-frequency mean wave period	[s]
T_p	Peak wave period	[s]
$\vec{U}$	Flow velocity vector	[m/s]
U_{10}	Wind velocity at 10 m height	[m/s]
x	Horizontal distance in directional space	[m]
y	Vertical distance in directional space	[m]

Greek characters

β	Bottom slope	[-]
η	Surface elevation	[m]
θ	Wave direction	[°]
θ_{ch}	Nautical channel angle	[°]
θ_{cr}	Critical refraction angle	[°]
θ_{in}	Incoming mean wave direction = θ_i	[°]
θ_{mean}	Mean wave direction	[°]
λ	Number of wave lengths	[-]
ρ_w	Water density = 1025	[kg/m^3]
σ	Relative frequency	[Hz]
ω	Wave frequency	[rad/s]

1 Introduction

1.1. Background

All over the world, cities have been build along rivers and in delta regions. They are protected against flooding by engineering solutions such as dikes, dunes and hydraulic structures. For a proper design, it is essential to have knowledge about the hydraulic loads acting on the coast. Often, extrapolation of measurements is performed to obtain these loads in extreme conditions. However, since the behaviour of hydrodynamic and wave processes is sometimes unknown, large extrapolation errors could occur. Especially during extreme storm conditions, which are considerably stronger than most measured conditions, this error could be significant. Instead of using these extrapolation techniques, there is a need to capture the physics properly in a numerical model.

For the Wadden Sea basin, this was first pointed out by Arcadis (2015) in the 'Rekenexperiment', performed in 2014 and 2015. Following up on this study, the 'POV Waddenzeedijken: Risiconanalyse HR' is performed by Steetzel (2019). This study uses a model train covering both the North Sea and the Wadden Sea area. Storms generated at the Northern North Sea create waves that travel towards the Wadden Sea and the Dutch coast. Delft3D-FLOW (Deltares, 2015) is used to calculate the currents and water levels throughout the domain. The spectral wave model SWAN (Booij et al., 1999) is used for the wave characteristics. Taking into account the interaction between water levels, currents and waves, this method should give a physically more realistic representation compared to the currently used method of WBI2017 (Helpdesk-Water, 2020). However, there are still some uncertainties in both models that remain unanswered.

1.2. Problem statement

One process that is under discussion is the modelling of channel bottom refraction in SWAN. For obliquely incoming waves, the channel causes a water depth gradient along the wave crest. In shallow water, the wave celerity is dependent on the water depth by c=$\sqrt{gd}$, where g is the gravitational acceleration and d the water depth. Therefore, the wave part in deeper water moves faster than the part in shallower water. This causes the wave to change its direction towards the shallower region, i.e. away from the channel. Figure 1.1 shows the wave pattern around the Macleay river mouth north of South West Rocks, Australia. The offshore waves are coming from the north east on the image. At both the north and south side of the river, sedimentation takes place. This causes shallower areas at the river sides where waves start to break. At the southern side, waves turn towards the shallower area from offshore. At the upper channel side, it can be seen that the waves refract away from the channel onto the shallower areas. It can be noted that refraction is essentially a 2D process. Therefore, the complexity of a problem increases quickly and the analytical solution cannot be determined that easily anymore. Hence, it becomes necessary to solve refraction with a numerical wave model. Multiple examples are available of these models, such as the mentioned SWAN model. Also so-called ray-tracing models exist, for example the model REFRAC. These models focus on wave propagation and refraction patterns.

Multiple studies (Dusseljee et al., 2014; Groeneweg et al., 2015; Alkyon, 2009b) found that SWAN overestimates the refraction process. Especially low-frequency waves, say smaller than 0.2 Hz, tend to turn out of the channel too much. In cases like the Wadden Sea basin, tidal flats are present outside of the channels. Offshore waves entering through the channels turn to the tidal flats where the energy is dissipated. Hence, the penetration of wave energy into the basin is underestimated by SWAN in these cases (Alkyon, 2009b; Groeneweg et al., 2015). Consequently, this leads to an underestimation of the wave height and period near the dike. For future reference, the definitions of low and higher frequency waves that are used in this study are shown in figure 2.1.

It is hypothesized that better results may be obtained when increasing the *resolution* in spatial and/or di-

Figure 1.1: Refraction due to a channel near South West Rocks, Austalia (Google, 2019). At the upper part of the channel, the waves turn away from the channel.

rectional space. Alkyon (2009a) found in a Wadden Sea study that at 'Pieterburenwad' a higher directional resolution resulted in an improved prediction of low-frequency wave height H_{10} and H_{20}. This better prediction may suggest a better modelling of the system in general, including the refractive behaviour.

Another explanation for the underestimation of low-frequency wave penetration in channels can be found in the wave physics as discussed by Groeneweg et al. (2015) and Groeneweg et al. (2014). They state that non-linear wave-wave interactions are not modelled correctly, leading to too little low-frequency waves entering the basin. The non-linear interactions under discussion are called *triads*, which are interactions between two waves. It is stated that the formulation in which these triads are taken into account is insufficient. A possibility to solve this problem is to introduce a new triad formulation. However, this is outside the scope of this thesis.

1.3. Research questions

The above stated problems lead to the following research question to be answered:

How can the representation of wave refraction over tidal channels be improved in spectral wave models?

The question is divided into the following sub-questions:

1. How does the refraction process in SWAN compare with the analytical solution of REFRAC?
2. How well is the refraction process over channels in tidal basins represented by both wave models?
3. What spatial resolution is required to accurately predict bottom refraction of waves?
4. How does the directional resolution influence the bottom refraction process?
5. What is the sensitivity of the model accuracy with respect to the wave propagation scheme in SWAN concerning the refractive behaviour?
6. How do other nearshore wave processes influence the refraction process in SWAN inside the Wadden Sea basin?

1.4. Objective

Simulations will be performed with the spectral wave model SWAN and the ray-tracing model REFRAC to assess the current performance of SWAN and REFRAC concerning refraction. The aim of this study is to get insight in the way SWAN handles refraction and to identify the dependency of the solution on different model

settings. Based on this study, one can retrieve better insight in the accuracy with which spectral wave models represent refraction and how this can be improved.

1.5. Thesis outline

Throughout the report, an increase in complexity will be present. First, the background of relevant wave theory is given and the wave models that will be used are introduced. This knowledge will be used to give an assessment of refraction in wave models for a simplistic academic case. Finally, a realistic case study will be introduced concerning the Eastern Wadden Sea area. Here the previously gained knowledge will be taken into practice. Both the schematic and realistic case will be used to acquire the final conclusions. The different components of this thesis are presented in the following chapters:

- Chapter 2 gives relevant wave theory, such as the principles of wave energy and the refraction process;
- Chapter 3 contains background and underlying equations of the wave models SWAN and REFRAC;
- Chapter 4 introduces a schematic channel case, where the fundamental behaviour of refraction in wave models is assessed. Simplicity is the key in this chapter, neglecting realistic physical wave behaviour;
- Chapter 5 contains a case study of the Wadden Sea area. An analysis is given on how the wave refraction is represented by wave models in a more realistic case;
- Chapter 6 discusses all findings of this research. Additionally, extra information of specific subjects is given that is not fully treated in the previous chapters.
- Finally, chapter 7 gives the final conclusions and recommendations.

2
Wave theory

2.1. Linear wave theory

Small amplitude waves can be described by *linear wave theory*. This theory considers a harmonic wave of which the surface elevation can be approximated by (Holthuijsen, 2007):

$$\eta(x,t) = a\sin(\omega t - kx) \tag{2.1}$$

Most often this theory is well suitable to describe deep water waves. The amplitude of these waves is small relative to water depth and wave length and the bottom friction can be neglected. Other underlying assumptions of linear wave theory are (Holthuijsen, 2007):

- The water is incompressible with constant density;
- Bottom and surface are impermeable to water particles;
- Wind and Coriolis force are excluded, so waves are gravity-driven only;
- Fluid particles are irrotational.

For free harmonic waves, which are subject to gravity only, the radian frequency, ω, is related to the wave number, k. This relation is called the dispersion relationship and is given in equation 2.2.

$$\omega^2 = gk\tanh kd \tag{2.2}$$

This relationship can be written in terms of propagation speed by using c= ω/k. It can also be expressed by the wave length, see equation 2.3.

$$c = \sqrt{\frac{g}{k}\tanh kd}, \quad L = \frac{gT^2}{2\pi}\tanh\left(\frac{2\pi d}{L}\right) \tag{2.3}$$

Hence, the wave speed is dependent on the wave number and water depth. In reality a sea-state does not consist of one single harmonic wave, but a combination of multiple waves with different frequencies. In this case the waves add up to form a wave group travelling with its own group velocity equal to the speed of the surface envelope. According to Holthuijsen (2007), the group velocity of a wave group can be described by equation 2.4. For deep water it follows that $c_g = \frac{1}{2}c$ and for shallow water $c_g = c$. Since the wave energy propagates with the group, the group velocity should be used in calculating wave energy propagation.

$$c_{group} = c_g = \frac{\partial\omega}{\partial k} = nc \tag{2.4}$$

With:

$$n = \frac{1}{2}\left(1 + \frac{2kd}{\sinh 2kd}\right) \tag{2.5}$$

As a wave approaches shallower water, shallow water processes deform the wave leading to an increase in non-linearity. If the non-linearity becomes too large, the linear wave theory is no longer valid. Especially in shallow coastal zones, like the Wadden Sea basin, the non-linearity is strong. In this case the balance equations cannot be approximated by a sinus function and the shallow water equations need to be solved consisting of the mass and momentum balance. A method which uses these equations is the theory of Boussinesq (Holthuijsen, 2007).

2.2. Spectral wave energy

Another option is to calculate the amount of *wave energy* instead of solving the free surface by the shallow water equations. In this case the energy balance is used, which is given in equation 2.6 in absence of the source/sink terms (SWAN-team, 2019a). Here θ denotes the wave energy direction. The wave height and period, which are often the most important parameters for coastal design, can be derived from the wave energy density spectrum. An example of such a spectrum is given in figure 2.1. This figure also contains the definitions of long and short waves, hence low and high frequency waves, that will be used in this study.

$$\frac{\partial E}{\partial t} + \nabla_{\vec{x}} \cdot (\vec{c}_g E) + \frac{\partial c_\theta E}{\partial \theta} = 0 \tag{2.6}$$

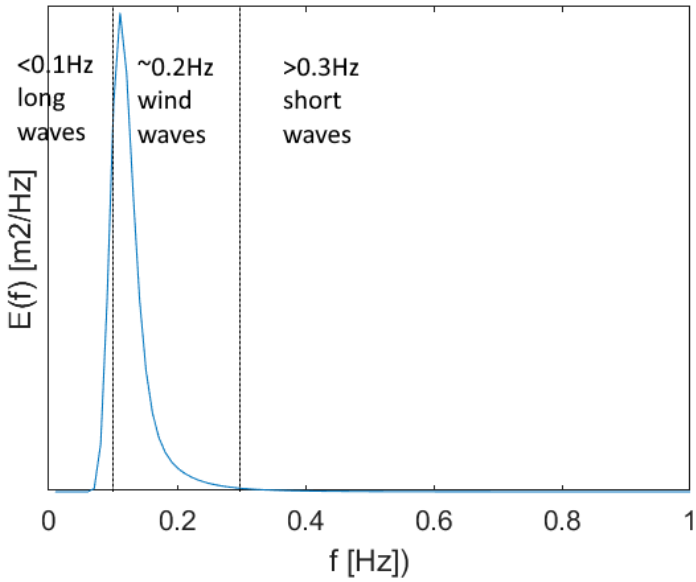

Figure 2.1: Example of a variance density spectrum, E(f), following the JONSWAP shape (Holthuijsen, 2007).

For determining H_{m0}, first the zeroth order spectral moment, m_0, should be calculated. This spectral moment is also called the *variance* and can be calculated from the variance density spectrum. The variance density is often used in literature and is coupled to the energy density by equation 2.7. For a 2D spectrum, the variance density is a function of the wave frequency and direction. In other words, the energy is distributed over multiple wave components with characteristic frequency and direction. Taking the integral of the variance density over both frequency and direction gives the variance m_0, see equation 2.8. This is a measure for the total amount of energy present in all wave components. The significant wave height H_{m0} can be calculated using equation 2.9.

$$E_{energy}(f,\theta) = \rho g E_{variance}(f,\theta) \tag{2.7}$$

$$m_n = \int\int f^n E(f,\theta) d\theta df \quad \rightarrow \quad m_0 = \int\int E(f,\theta) d\theta df = E_{variance} \tag{2.8}$$

$$H_{m0} = 4\sqrt{m_0} \tag{2.9}$$

The spectral mean wave period $T_{m-1,0}$ can be calculated by equation 2.10. This period gives more weight to the low-frequency wave components due to the multiplication with f^{-1}. Commonly, this parameter is used for coastal safety design in the Netherlands. Also the peak period T_p can be used, which is approximately equal to $1.1 T_{m-1,0}$ for a JONSWAP shape (Lorenzo et al., 2000). This ratio is dependent on the spectral shape.

$$T_{m-1,0} = \frac{m_{-1}}{m_0} \tag{2.10}$$

With the spectral approach, the total amount of wave energy and variance can thus be determined. As mentioned previously, the energy propagation, i.e. flux, is dependent on the group velocity and thus equals Ec_g. The system should be flux conservative, hence a conservation balance can be derived. With this balance, all processes that impact the energy propagation are captured.

2.3. Wave refraction

When waves approach shallower water, their propagation is affected in two different ways. Firstly, due to a reducing depth the wave celerity reduces. However, the energy flux Ec_g along a wave path should be conserved. Therefore, a reduced celerity results in an increase of wave energy and hence wave height. This process is called shoaling and takes place in the transition from deeper to shallower water. At some point the waves become too steep, which causes them to break.

Another process caused by bottom variations is wave refraction. As already explained in some detail in the introduction, bottom refraction is caused by depth variations along a wave crest. The different water depths cause a variation in wave celerity, since in shallow water $c = \sqrt{gd}$, where the highest celerity is found in deeper water. This causes a change in wave orientation towards the shallower side. Refraction thus affects the wave direction instead of the wave height.

Refraction can occur in different situations. First, consider the case of alongshore parallel depth contours and a uniform coast. If a normal incident wave approaches the coast, the water depth along the wave crest is constant and hence there is no depth gradient along the crest. The wave celerity is equal and thus no refraction occurs. However, if the angle of incidence is oblique to the coast there will be a depth gradient present along the crest. Therefore this wave will refract, causing normal incident waves at the coast, see figure 2.2. Obviously, in case a more complex bathymetry is present with no parallel depth contours, refraction will occur for both normal incident and oblique incident waves.

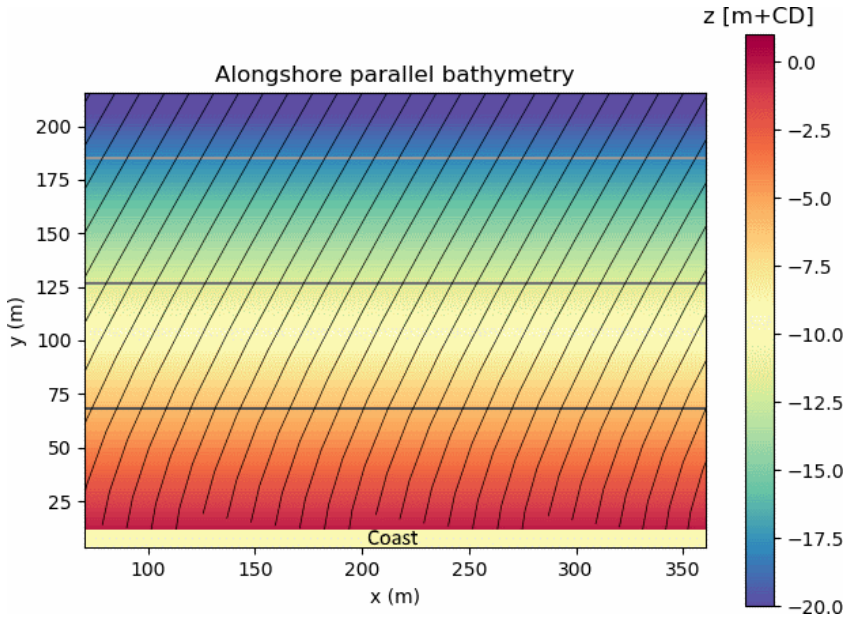

Figure 2.2: Refraction for alongshore parallel depth contours with the coast at the south, created with REFRAC (Refrac-team, 2019) using T=5s and θ_{in}=30°N.

The directional turn per unit forward distance is given in equation 2.11, with m in wave crest direction. This equation is valid for stationary computations with a spatially varying depth and no currents (Holthuijsen, 2007). The minus sign is the result of the definition of $\Delta\theta$, which is negative for clockwise direction. A positive $\Delta c/\Delta m$ leads to clockwise $\Delta\theta$, and thus a negative value.

$$\frac{d\theta}{dn} = -\frac{1}{c}\frac{\partial c}{\partial m} \tag{2.11}$$

Solving the above equation gives the change in wave direction along a wave ray. With parallel depth contours, the above equation reduces to Snel's law given in equation 2.12.

$$\frac{\sin\theta}{c} = \text{constant} \tag{2.12}$$

Looking at two points with respectively celerities c_1 and c_2 and directions θ_1 and θ_2, Snel's law becomes:

$$\frac{\sin\theta_1}{c_1} = \frac{\sin\theta_2}{c_2}$$
$$\sin\theta_2 = \frac{c_2}{c_1}\sin\theta_1 \tag{2.13}$$

In Snel's law the angle is given between the wave ray and the normal to the depth contours. From Snel's law it can be readily seen that for waves approaching the coast, e.g. $c_2 \rightarrow 0$, the wave direction reduces to zero as well. Hence, theoretically they always attack the coast perpendicular for parallel depth contours.

The approach described above is called *Lagrangian*, meaning that the coordinates follow the wave propagation. Since this method does not take non-linear interactions into account and wave rays are able to cross each other, an *Eulerian approach* may be more suitable in coastal zones (Holthuijsen, 2007). In the Eulerian approach the domain is discretised in geographical space, after which the wave conditions are determined per spatial cell. Inherently, the Eulerian method induces additional numerical diffusion compared to the Lagrangian approach. Instead of calculating the turning rate in the direction of the wave ray, the Eulerian method uses the change in wave direction over time moving with wave energy (Holthuijsen, 2007). The change over time is determined from the expression of $d\theta/dn$ and using the velocity of the wave energy, c_g. This eventually leads to $\Delta\theta = d\theta/dn c_g \Delta t$, and hence the equation as given by 2.14. Here c_θ gives the directional turn per unit time, also known as turning rate.

$$c_\theta = -\frac{c_g}{c}\frac{\partial c}{\partial m} \tag{2.14}$$

Channel refraction

In case a channel is present across the wave path, the fast change in bathymetry obviously changes the orientation of an oblique incident wave. According to research done by Riezebos (2014) and Dusseljee et al. (2014), obliquely incoming waves, θ_i, with an angle smaller than a *critical angle*, θ_{cr}, with respect to the channel axis get refracted and will not cross the channel. Figure 2.3 gives a schematic overview of the definitions of these angles. Instead of crossing the channel, the energy will accumulate on the channel edge in this case. The critical angle, θ_{cr}, for waves to refract such that they do not cross the channel, can be derived with Snel's law, of which follows that $\theta_{cr} = \arccos(c_1/c_2)$. This critical angle can be used to predict if waves are able to enter and cross a channel.

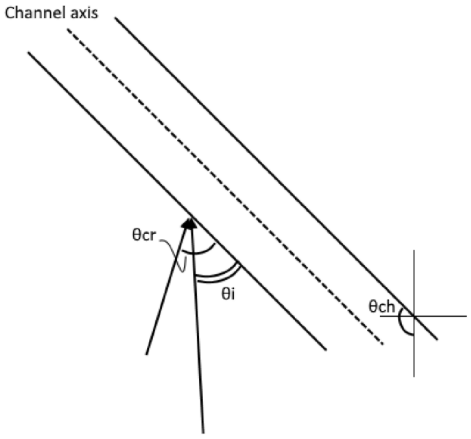

Figure 2.3: Explanation of the critical and incoming angle. The incoming angle equals $\theta_{ch} + \theta_i$ in case the nautical convention is used.

Following from the definition of θ_{cr}, the critical angle is dependent on the difference in water depth and wave frequency. A larger difference in water depth will cause the critical angle to increase, hence a larger fraction of wave directions will accumulate at the channel edge. The fact that a larger depth gradient will cause more refraction is comprehensible. For wave frequency the opposite is true. Higher wave frequencies lower the critical angle, leading to more wave directions that can cross the channel. Concluding, short waves feel the bottom less and hence get less refracted than long waves.

3
Wave models

The refraction process and other wave processes can be modelled using numerical wave models. Specifically for refraction, the model REFRAC is introduced. This model solves the trajectories of the wave rays for a specific wave condition. The equations are rather fundamental, from which the analytical solution can be approximated. Due to the simplicity, the application of this model is limited. When considering more complex cases with broad wave spectra, a spectral wave model such as SWAN is preferable. These models are based on conservation of wave energy in the considered domain.

3.1. Ray-tracing model REFRAC

As mentioned, REFRAC can be used to get an impression of the theoretical wave refraction that is present for a given bathymetry. This is done by computing the trajectories of the wave rays in a Lagrangian way for one single wave component. The model requests a wave height and period as well as a starting angle of the wave ray. Since the rays are computed for only one frequency component, the model is not suitable for broad incoming wave spectra. In those cases, it can only be used as a first impression of the influence of the bathymetry on different wave components. If the spectrum is very narrow in both frequency and directional space, REFRAC is able to predict the analytic refractive behaviour accurately.

3.1.1. Assumptions

To calculate the trajectories of the wave rays, the following assumptions are made:

- Wave rays do not interact with each other. Therefore, crossing of rays can occur which reduces the distance between the wave rays to zero. Theoretically, this results in an infinite growth of the wave amplitude. This phenomenon of infinite growth of wave amplitude at crossing rays is also called a caustic and leads to unrealistic amplitudes. Hence, the theory is not valid near these wave ray crossings (Holthuijsen, 2007).
- Bottom friction, wave breaking and wind input are neglected by REFRAC. This also holds for non-linear wave interactions.

3.1.2. Underlying equations

The rays start at the imposed starting point with a certain starting angle. With this angle and depth, the location of the x, y and θ of the following ray point can be calculated. The change in x,y and θ along a wave ray is given by equation 3.1. Here s is the coordinate along the wave ray and R the ray curvature (Refrac-team, 2019). According to Dingemans (1997), it can be assumed that the amplitude of the wave does not change significantly over one wave length. Therefore, for correct modelling of refraction it is sufficient to have a mesh size equally large as the wave length. In this sense, REFRAC uses the rate of change in the parameters over the number of wave lengths, λ.

From Refrac-team (2019) it is given that $dp/ds = 1/\lambda$, leading to the final equations of 3.2.

$$\frac{dx}{ds} = \cos\theta, \quad \frac{dy}{ds} = \sin\theta, \quad \frac{d\theta}{ds} = \frac{1}{R} \tag{3.1}$$

$$\frac{dx}{dp} = \lambda\cos\theta, \quad \frac{dy}{dp} = \lambda\sin\theta, \quad \frac{d\theta}{dp} = \frac{\lambda}{R} = \sin\theta\frac{\partial\lambda}{\partial x} - \cos\theta\frac{\partial\lambda}{\partial y} \tag{3.2}$$

Since the depth is given and the wave period is fixed, the local wave length can be calculated at each grid point. The wave lengths on the grid points are used to determine the local wave length at a ray point. Since then the wave length and the wave angle at the ray point are known, the derivatives of equation 3.2 can be determined and hence the x,y and θ at the following ray point. This process is repeated until the wave ray is

completed. The used solving method for the derivatives is the 4th order Runge-Kutta scheme (Refrac-team, 2019).

3.2. Spectral model SWAN

Considering more general wave models, there are many spectral wave models available, such as SWAN, MIKE21 and WAVEWATCH 3 (Cavaleri et al., 2018). These models are based on the balance of spectral energy density. The models are phase-averaged, meaning that the statistical parameters will be retrieved from the energy balance. Another type of wave models are based on time-dependent mass and momentum balances. These phase-resolving models, e.g. the mild-slope, Boussinesq-type equations and non-hydrostatic shallow water equations, are able to resolve the sea surface and hence calculate processes like diffraction and refraction accurately (Adytia and van Groessen, 2012). However, due to a larger computational demand, these model types are only suitable in case of small domains. Therefore, this study will focus on the performance of the phase-averaged models, specifically the SWAN model. SWAN is a third generation phase averaging spectral wave model designed for coastal waters, meaning that it solves the spectral wave energy balance including physical wave processes as source terms. The wave energy is distributed over the relative frequencies σ and wave directions θ in an energy density spectrum (SWAN-team, 2019a). For intermediate to shallow waters, this spectrum is often chosen as a JONSWAP shape if no spectra are known, named after the North Sea experiment performed by Hasselmann et al. (1973).

3.2.1. Spectral energy balance

Instead of the energy density, SWAN uses the action density defined as $N(x,y,t,\sigma,\theta) = E(x,y,t,\sigma,\theta)/\sigma$. The action density is, in contrast to the energy density, conserved along its wave characteristic in case a current is present (SWAN-team, 2019a). 2D SWAN entails the presence of these ambient currents and thus it is necessary to use the action density. Since the quantity is conserved, an action balance equation can be derived, denoted in equation 3.3 for Cartesian coordinates (SWAN-team, 2019a).

$$\frac{\partial N}{\partial t} + \nabla_{\vec{x}}[(\vec{c}_{\text{g,relative}} + \vec{U})N] + \frac{\partial c_\sigma N}{\partial \sigma} + \frac{\partial c_\theta N}{\partial \theta} = \frac{S_{\text{tot}}}{\sigma} \tag{3.3}$$

With:

N	=	action density [kg/m/s]
σ	=	relative frequency [Hz]
θ	=	spectral direction [°]

The first term describes the local change of action over time. In a stationary computation, this term reduces to zero. The second term accounts for wave propagation in spatial domain. Since $\vec{c}_g$ is depth dependent, this term also contains shoaling effects (Holthuijsen, 2007). The third term takes the derivative to σ, describing the change of action density over frequencies. The last term of the left hand side contains the change in directions of the wave, in other words, refraction (Holthuijsen, 2007).

The right hand side of the action balance equation exists of the term S_{tot}, which contains all physical processes that lead to dissipation, generation or redistribution of wave energy (SWAN-team, 2019a). S_{tot} can be divided into (SWAN-team, 2019a):

$$S_{tot} = S_{in} + S_{nl4} + S_{nl3} + S_{wc} + S_{bfr} + S_{surf} \tag{3.4}$$

With:

S_{in}	=	Wind input [m^2/Hz]
S_{nl4}	=	Non-linear quadruplet wave-wave interactions [m^2/Hz]
S_{nl3}	=	Non-linear triad wave-wave interactions [m^2/Hz]
S_{wc}	=	White-capping [m^2/Hz]
S_{bfr}	=	Bottom friction [m^2/Hz]
S_{surf}	=	Depth-induced wave breaking [m^2/Hz]

3.2.2. Numerical schemes

All of the content in this subsection is based on the Technical documentation of SWAN (SWAN-team, 2019a).

Discretisation

Time discretisation is chosen independently of the space discretisation in SWAN. Discretisation in time is performed by using implicit Euler, which is unconditionally stable. Spatial discretisation could be done in multiple ways. The first option is first order upwind, which together with the time discretisation is called *BSBT* (Backward in Space, Backward in Time), see equation 3.5. However, a disadvantage of this scheme is the diffusive behaviour. Therefore, the higher order *SORDUP* (Second ORDer UPwind) and *Stelling/Leendertse* schemes are suggested. These schemes are applied if structured grids are used. However, in case an *unstructured* grid is used, only the first order multidimensional upwind scheme is employed (Ilia and ODonnell, 2018).

$$\begin{aligned} \frac{\partial c_{g,x}}{\partial x} &\approx \frac{(c_{g,x}N)_i - (c_{g,x}N)_{i-1}}{\Delta x} \\ \frac{\partial c_{g,y}}{\partial y} &\approx \frac{(c_{g,y}N)_j - (c_{g,y}N)_{j-1}}{\Delta x} \end{aligned} \tag{3.5}$$

For stationary computations the SORDUP scheme is used as default option, see equation 3.6 for the approximation. This scheme is second order accurate in space and first order in time, however this time accuracy is not relevant since the computation is stationary. Compared to the upwind scheme, SORDUP creates less numerical diffusion without significant increase of computational effort.

$$\begin{aligned} \frac{\partial c_{g,x}}{\partial x} &\approx \frac{3(c_{g,x}N)_i - 4(c_{g,x}N)_{i-1} + (c_{g,x}N)_{i-2}}{2\Delta x} \\ \frac{\partial c_{g,y}}{\partial y} &\approx \frac{3(c_{g,y}N)_j - 4(c_{g,y}N)_{j-1} + (c_{g,y}N)_{j-2}}{2\Delta y} \end{aligned} \tag{3.6}$$

If the computation is performed nonstationary, the default scheme is that of Stelling and Leendertse. The accuracy is second order for both time and space. This scheme creates less diffusion than both the SORDUP and upwind scheme. Furthermore, it is unconditionally stable and the action flux is conserved along a wave characteristic.

Discretisation is also performed in the spectral domain (σ, θ). Here a combination of an upwind and central scheme is applied. In case only the first order upwind scheme is used, the solution shows diffusive behaviour. The disadvantage of the second order central scheme is the production of oscillations which are physically unrealistic. Since the error in the solution takes place near the blocking frequency for both schemes, the diffusion partly compensates the spurious oscillations if a combination of both schemes is applied. Section 3.2.3 gives more detailed information on the schemes that are used in the spectral domain.

In case the directional resolution $\Delta\theta$ is chosen too coarse, the *garden-sprinkler effect* may occur (Booij and Holthuijsen, 1987). The spatial distribution of the initial spectrum is discretised into a number of distributions, dependent on the amount of directional bins. If this is chosen too coarse and the spectrum is narrow with a large propagation distance (swell), then the spectrum will not spread smoothly in space as would be the case in the ideal situation (Booij and Holthuijsen, 1987). Instead, the energy stays in the spectral bands which is visible in the solution as bands of energy, just as with a garden sprinkler, and is purely numerical. To prevent this effect, one can either reduce the directional resolution or choose a numerical scheme that provides more diffusion.

Solving method

To solve the numerical equations, SWAN utilises the so called *sweep* method. Here the spatial domain (x,y) is divided into four directional quadrants. During a sweep the propagation energy is calculated for one quadrant, which will be repeated for all four quadrants independently. The interaction and transfer of energy between the quadrants is determined by iteration. The incoming energy of one cell should equal the outgoing energy of the cell next to it. This balance is solved in an iterative manner by SWAN, which requires a minimum amount of wet points where balance is achieved and a maximum number of iterations.

3.2.3. Implementation of refraction

Concerning the spectral action balance of equation 3.3, the refraction is included by the derivative to θ, where $c_\theta = \frac{d\theta}{dt}$ denotes the *turning rate*. The wave group velocity is given by $\vec{c}_g = \frac{d\vec{x}}{dt}$. From these equations, the Courant number as stated in equation 3.7 can be derived. For a stable solution, it should hold that Cr ≤ 1.

$$Cr = \frac{|c_\theta|}{c_g}\frac{\delta x}{\delta \theta} \tag{3.7}$$

In previous SWAN versions, the turning rate was given by equation 3.8 (SWAN-team, 2019a), with the right hand side in Cartesian coordinates. Here k denotes the wave number, d the water depth and σ the wave frequency, m is in the direction of the wave crest. When the depth gradient is too large, the c_θ increases too much causing Cr to become larger than 1. A depth gradient can be large due to large bottom gradients, but also a coarse computational grid may cause large depth gradients over one computational step.

$$c_\theta = -\frac{1}{k}\frac{\partial \sigma}{\partial d}\frac{\partial d}{\partial m} = \frac{\sigma}{\sinh 2kd}\left(\frac{\partial d}{\partial x}\sin\theta - \frac{\partial d}{\partial y}\cos\theta\right) \tag{3.8}$$

To decrease the dependency of the turning rate on the water depth, an alternative formulation was proposed as given in equation 3.9. Physically these equations are equal, however, in numerical sense equation 3.9 is less sensitive to depth variations (SWAN-team, 2019a). Both equations can be turned on in SWAN by stating 'NUM DIR DEP' and 'NUM DIR WNUM' respectively for equation 3.8 and 3.9.

$$c_\theta = -\frac{c_g}{c}\frac{\partial c}{\partial m} \tag{3.9}$$

Equation 3.9 holds for stationary computations without presence of currents (Holthuijsen, 2007). In general, SWAN does not compute the rate of change over a wave ray. Instead, the domain is partitioned in a meshed grid. Therefore, equation 3.9 is rewritten in Cartesian coordinates to retrieve the turning rate per grid cell, see equation 3.10. Instead of Cartesian coordinates, the equation can also be rewritten to spherical coordinates following the same principle.

$$c_\theta = \frac{c_g}{c}\left(\frac{\partial c}{\partial x}\sin\theta - \frac{\partial c}{\partial y}\cos\theta\right) \tag{3.10}$$

By assuming parallel depth contours this equation reduces to Snel's law:

$$\frac{\sin\theta}{c} = \text{constant} \tag{3.11}$$

According to Groeneweg et al. (2015), the non-linear triad interactions are not accounted for properly in SWAN. This is due to the fact that SWAN uses the 1D LTA Triad formulation (Groeneweg et al., 2015). The non-linear sub- and superharmonic interactions are 2D processes, therefore these are not modelled in the applied 1D formulation. Inside the surf zone, the superharmonics transfer energy back to lower frequencies. The energy is transferred to the difference-frequency ($f_1 = f_3 - f_2$), for which the angle is outside the directional range $[\theta_2, \theta_3]$. This thus leads to a broadening of the directional domain (Herbers et al., 1999). The process of transferring energy to lower frequencies is not taken into account by the LTA method and thus by SWAN. Therefore, the increased directional spreading is also absent. This leads to less energy in directions greater than the critical angle and hence stronger refraction along the channel edge. The confinement of energy at the edge hampers wave energy to cross the channel, thus leading to underestimation of wave energy inside and downwave of the channel. The assessment of triads is not the main focus of this thesis and will only be addressed shortly.

Discretisation of the refraction term

The refraction term of equation 3.3 can be approximated in SWAN with first order upwind, central differences or a combination of both schemes. Therefore, a hybrid scheme is introduced in equation 3.12 (SWAN-team, 2019a). A distinction is made between clockwise and counter-clockwise directions, i.e. $c_\theta < 0$ and $c_\theta > 0$ respectively.

$$c_\theta N|_{i,j,l,m+1/2} = \begin{cases} (1-0.5\nu)c_\theta N|_{i,j,l,m} + 0.5\nu c_\theta N|_{i,j,l,m+1}, & \text{if counter-clockwise} \\ (1-0.5\nu)c_\theta N|_{i,j,l,m+1} + 0.5\nu c_\theta N|_{i,j,l,m}, & \text{if clockwise} \end{cases} \tag{3.12}$$

In equation 3.12 the parameter $\nu \in [0,1]$, where first order upwind is given by $\nu = 0$ and central difference by $\nu = 1$. From this it follows that in case central difference is applied, the refraction action term in bin m can be approximated by:

$$\left(\frac{(c_\theta N)_{m+1} - (c_\theta N)_{m-1}}{2\Delta\theta}\right)^n_{i,j,l} \tag{3.13}$$

In case of upwind, e.g. $\nu = 0$, the approximation of the refraction term for a counter-clockwise case with $c_\theta > 0$ yields:

$$\left(\frac{(c_\theta N)_m - (c_\theta N)_{m-1}}{\Delta\theta}\right)^n_{i,j,l} \tag{3.14}$$

and for a clockwise case with $c_\theta < 0$:

$$\left(\frac{(c_\theta N)_{m+1} - (c_\theta N)_m}{\Delta\theta}\right)^n_{i,j,l} \tag{3.15}$$

By default $\nu = 0.5$ is chosen in SWAN (SWAN-team, 2019a). It follows that this scheme induces less numerical diffusion than the first order upwind, also less oscillations will be created than with central differences. For the counter-clockwise case, the approximation for refraction with $\nu = 0.5$ becomes:

$$\left(\frac{(c_\theta N)_{m+1} - 2(c_\theta N)_m - 3(c_\theta N)_{m-1}}{4\Delta\theta}\right)^n_{i,j,l} \tag{3.16}$$

whereas for a clockwise case the following approximation is retrieved:

$$\left(\frac{3(c_\theta N)_{m+1} - 2(c_\theta N)_m - (c_\theta N)_{m-1}}{4\Delta\theta}\right)^n_{i,j,l} \tag{3.17}$$

4

Schematic case: Harbour channel

In this chapter a harbour channel inspired on Riezebos (2014) and Dusseljee et al. (2014) is considered. Dusseljee et al. (2014) compared the performance of SWAN to experimental measurements and the phase resolving wave-flow model SWASH. The study consisted of a navigation channel of a harbour with flat bottoms at the side of the channel. It was found that SWAN underestimated the amount of waves that was able to enter and cross the navigation channel compared to measurements and the model SWASH.

In this thesis, a comparison will be made between the refractive behaviour in SWAN and REFRAC for different sensitivities, considering a very simplistic case. In contrast to Dusseljee et al. (2014), the intention is to isolate the refraction process rather than create a replica of reality. Therefore, all additional wave processes will be neglected. This approach is not realistic, however it is thought to give more fundamental knowledge on the refraction process itself. From literature it is known that the tendency of waves to physically refract is largely dependent on water depth and wave frequency. Therefore, an important part is to observe the numeric behaviour for varying frequency. Since the bathymetry is set, variations in depth will not be considered.

4.1. Monochromatic boundary conditions

The bathymetry as used in this study is given in figure 4.1 and is created in Delft3D-Quickin (Deltares, 2015).

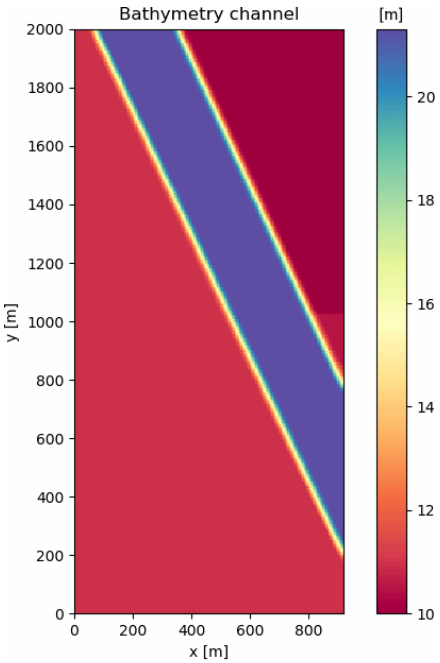

Figure 4.1: Bathymetry of the channel that is considered, bottom depth in m.

The resolution of the bathymetry is 5x5m, resulting in 184 meshes in x-direction and 400 meshes in y-direction. In order to prevent interpolation errors, the resolutions of the computational grid will be chosen as multiples of 5m. The channel slopes have a gradient of approximately 1:5. The angle of the channel axis with the x-axis is 65°. For full control of the system, the sill that was present in Dusseljee et al. (2014) is removed from the bathymetry. Also the widening of the channel is not taken into account in this case.

The 2D SWAN simulation will be performed without currents and wind input. For a clean comparison with REFRAC, the *source terms in SWAN are turned off.* In this way the waves do not interact with each other and no wave breaking occurs. Boundary conditions (BC) will be set to the southern and western boundary, where the BC are imposed parametric with a constant wave height of 1m. Since REFRAC gives the ray propagation for one single wave component, the wave climate imposed in SWAN should approach this as much as possible. This can be done by reducing the frequency range and the directional spreading of the wave spectra. To accommodate this, the spectrum option 'BIN' will be used. According to SWAN-team (2019b), this option creates a spectrum in which all energy is stored in the frequency bin closest to the imposed wave period.

The width of the directional distribution can be expressed with the function $\cos^m(\theta - \theta_{peak})$ (SWAN-team, 2019b). Either the power m or the standard deviation in degrees is requested in SWAN. To come to a narrow distribution it is thus required to choose a large m, say m=1000, or a narrow deviation in the order of 0.5°. For this study, it is chosen to set the power to m=1000 such that SWAN ensures that the directional distribution is narrow. An important note for these small distributions is that the directional resolution should be sufficient to accommodate the spectral width. Therefore, also the directional resolution should be chosen small. For m=1000, SWAN advises to choose a directional bin size smaller than 2.562°. Hence, to follow this advise the directional resolution will first be set to 2°, i.e. 180 bins. Figure 4.2 gives an example of a resulting 2D spectrum that is imposed to SWAN. As can be seen the peak frequency is at 0.1 Hz, which corresponds to the imposed peak frequency of 10s.

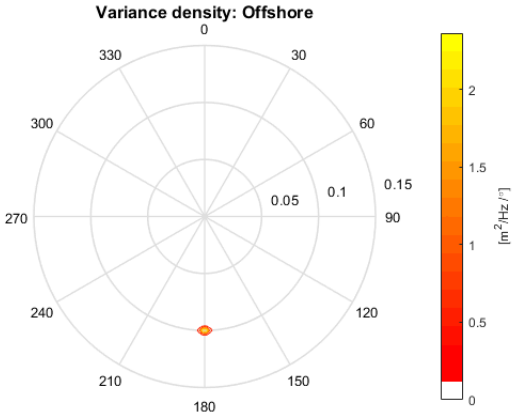

Figure 4.2: 2D spectrum imposed at the southern boundary for Tp=10s and θ=180°. The spectrum is plotted as waves 'coming from' 180°N.

As mentioned earlier, the frequency distribution is limited to approach a monochromatic wave. Therefore, the frequency range can be chosen narrow. Since it is not possible to have only one frequency bin present in SWAN, the frequency range is divided in two bins, of which the middle frequency equals the imposed peak frequency. The frequencies have a logarithmic distribution equal to $f_{i+1} = \gamma f_i$, of which follows that $\gamma = 1 + \Delta f/f$. Often $\Delta f/f = 0.1$ is chosen as constant. However, since a smaller bin size is preferable in this case, $\Delta f/f$ will be chosen equal to 0.05, resulting in $\gamma = 1.05$. The number of frequency bins is then determined by equation 4.1. Here f_{min} and f_{max} are respectively the minimum and maximum of the frequency range.

$$msc = \log\left(\frac{f_{max}}{f_{min}}\right) / \log(\gamma) \tag{4.1}$$

In this case the number of frequency bins is known, however f_{min} and f_{max} should be determined. The middle frequency should equal the peak frequency, and is thus known. Then f_{min} and f_{max} are determined by respectively dividing and multiplying the peak frequency with γ. Then equation 4.1 is fulfilled.

For example, taking again the case of T_p=10s leads to f_p=0.1s. Subsequently it follows that:

$$\begin{aligned} f_{min} &= \frac{f_p}{\gamma} = \frac{0.1}{1.05} = 0.095\,\text{Hz} \\ f_{max} &= f_p\gamma = 0.1 \cdot 1.05 = 0.105\,\text{Hz} \end{aligned} \tag{4.2}$$

Filling this into equation 4.1 gives:

$$\begin{aligned} msc &= \log\left(\frac{f_{max}}{f_{min}}\right) / \log(\gamma) \\ &= \log\left(\frac{0.105}{0.095}\right) / \log(1.05) \\ &= 2. \end{aligned} \tag{4.3}$$

4.2. Model variants

Different aspects are chosen which are thought to be of influence on the performance of SWAN. These are in order of expected importance:

- Initial wave frequency;
- Initial wave direction;
- Spatial and directional resolution;
- Numerical scheme for refraction term;
- Propagation scheme of SWAN.

Also, a situation without taking refraction into account will be tested. It is thought that this will not necessarily improve the prediction of refraction, but is useful for understanding the patterns if refraction would be absent. The parameters or settings to be used for each variant are given in table 4.1.

Table 4.1: Variants that will be treated for the harbour channel case.

Type	**Variant**	**Characteristics**
Incoming wave period	Tp1	T_p= 5s
	Tp2	T_p= 10s
	Tp3	T_p= 15s
Incoming wave direction	DIR1	180°N
	DIR2	200°N
	DIR3	220°N
Spatial resolution	5x5m	$\Delta x, \Delta y$ = 5x5m
	10x10m	$\Delta x, \Delta y$ = 10x10m
	20x20m	$\Delta x, \Delta y$ = 20x20m
Directional resolution	DR1	6° (60 bins)
	DR2	2° (180 bins)
	DR3	1° (360 bins)
Refraction scheme	CDD0	Central differences (CDS)
	CDD0.5	Combination CDS and UPW
	CDD1	First order upwind (UPW)
Propagation scheme	BTBS	BTBS scheme
	SORDUP	SORDUP scheme
Refraction	REF0	off

With these variants the effects of all parameters and settings are assessed systematically. Also combinations of variants will be simulated, creating a matrix of variants. This results many simulations to be performed. Obviously these cannot all be presented here, therefore the most important results will be shown.

In general, a certain number of grid points is needed per wave length. The wave length is dependent on the water depth and wave period, therefore the smallest wave length will occur for T_p=5s at the smallest depth of 10m. By using the dispersion relation[1], it is found that for these conditions the wave length becomes equal to approximately 37m. With a grid size of 5m, there will be a maximum of 7 grid points per wave length. On the other hand, if the wave period is 15s and the water depth 21.3m, then the wave length becomes 144m. With a grid size of 5m there will thus be a maximum of 28 grid points per wave length.

[1] For this indication it is assumed that the dispersion relation is valid. This is justified since all non-linear terms are turned off and a single wave component is considered. It is known that SWAN uses a slightly different method for determining the wave length, however this matches the results of the dispersion relation in this case.

4.3. Computational results of refraction

4.3.1. Theoretical approach

Before going into SWAN and REFRAC, figure 4.3 gives the critical wave direction of the harbour channel which is computed with equation 4.4. The wave celerities are calculated with the dispersion relationship using d_1=11m and d_2=21.3m. Comparing the calculated wave lengths with results from SWAN and REFRAC gives an error of less than 0.5%, which is considered negligible, therefore the dispersion relation is again valid here. The critical wave direction equals the critical wave angle, θ_{cr}, plus the angle of the channel axis, θ_{ch}. This conversion is needed since θ_{cr} is given relative to the channel axis, see figure 2.3 for the convention. Since θ_{ch}=155°N for this case, this is the minimal critical wave direction as can be seen for high frequencies in figure 4.3. For these short waves, i.e. f>0.35Hz, the waves are not affected by the bottom and hence the critical angle is low. Waves coming from directions above the critical angle will cross the channel.

$$\theta_{cr} = \arccos\left(\frac{c_1}{c_2}\right) \tag{4.4}$$

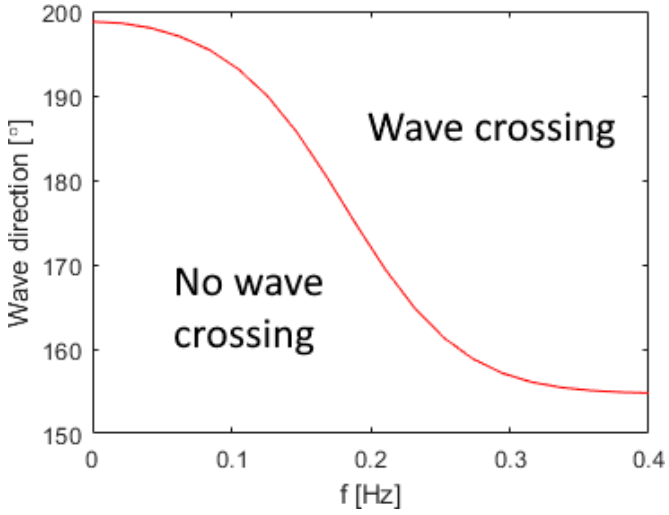

Figure 4.3: Critical wave direction as function of frequency for the harbour channel, directions larger than the critical wave direction will cross the channel.

From figure 4.3 it can be derived that for T_p=10s, i.e. f=0.1Hz, the critical wave direction equals approximately 194°N. The critical angles and directions for all frequency variants are given in table 4.2 in one decimal accuracy.

Table 4.2: Critical wave directions for the different peak frequency variants.

Tp	f	Crit. wave angle	Crit. wave dir.
5s	0.20Hz	17.3°	172.1°N
10s	0.10Hz	39.1°	193.8°N
15s	0.067Hz	42.1°	196.8°N

According to theory, only the waves of T_p=5s should be able to cross the channel for an incoming wave direction of 180°N, i.e. from the south. All frequency variants should be able to cross the channel for incoming wave directions 200°N and 220°N. However, since the critical angles of T_p=10s and 15s are close to the incoming wave direction of 200°N, it is expected that these waves will enter the channel. However, they will not leave it at the other side in the considered domain for higher periods.

4.3.2. REFRAC application

Following from the REFRAC results, all considered wave periods are able to enter the channel for wave direction>200°N. This is consistent with theory, since all critical wave directions are below 200°N. The REFRAC results for a wave period of 10s is given in figure 4.4, for T=5s and 15s one is referred to appendix B.1. The

aforementioned critical angles can be quickly observed. For a low wave period of 5s all wave rays are able to enter the channel as corresponds to theory. For higher wave periods, e.g. 10s and 15s, the waves refract at the channel edge for an incoming direction of 180°N, since this is below the critical angle. This as well conforms with the expectations. Noticeable is that the wave rays do not remain parallel to each other and hence they cross. This is most likely caused by the schematisation of the bathymetry. Since the refraction angle is largely depth-dependent, a small deviation in bottom depth causes differences in ray orientation along the channel axis. This is in itself an important finding, meaning that also in REFRAC errors are present due to interpolation of the bathymetry. It should be noted that most attention will be on the upwave, e.g. western, channel edge, since the incoming wave direction is unaltered here.

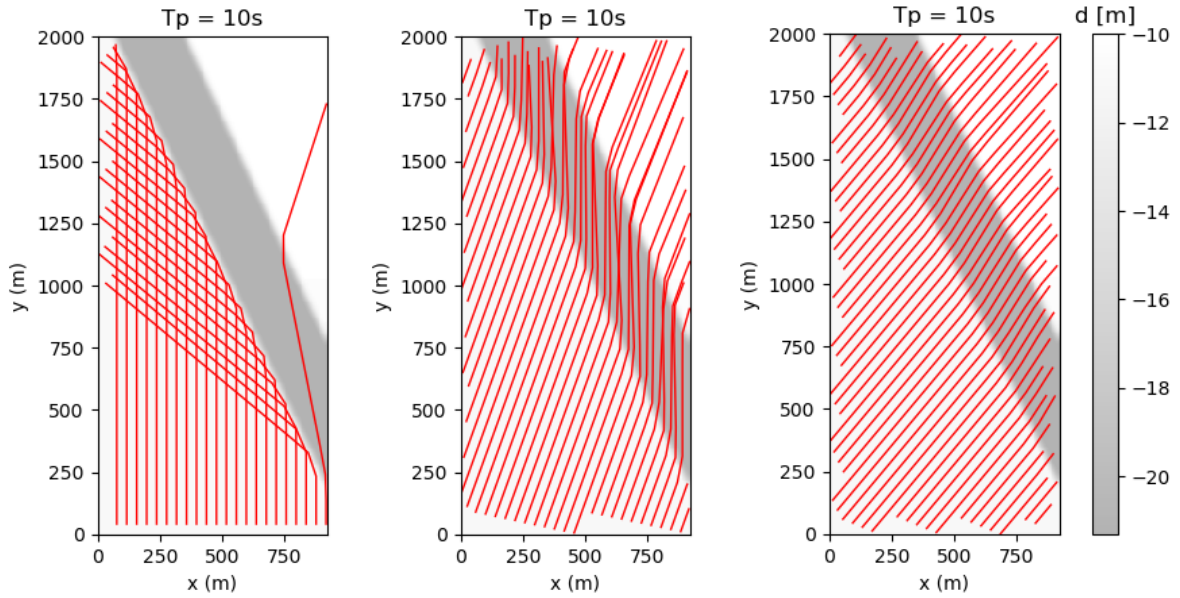

(a) Incoming wave 180°N (b) Incoming wave 200°N (c) Incoming wave 220°N

Figure 4.4: Wave rays according to REFRAC for different incoming wave directions for T=10s, H_{in}=1m.

Instead of looking at equal wave directions for all wave period variants, one can also zoom in on the critical angle of the specific wave period. This is done in figure 4.5 for T=10s, equal figures for the other period variants are given in appendix B.1. It can be observed that a part of the wave energy gets refracted off the channel edge at the critical angle. Still some waves do enter or even cross the channel. For a wave direction of only 1° lower than the critical direction, most waves get refracted and there is only a very limited amount of waves that enters the channel. Hence, for the cases and domain considered, there are practically no wave rays that cross the channel for a wave direction below the critical direction. Additionally, one may observe that for incoming angles above the critical angle all wave rays enter the channel. In some cases the considered domain is too short. Here waves that entered the channel are not able to leave the channel in the domain. For the case of T_p=5s there are also wave rays entering the domain at the east boundary. These will not be modelled in SWAN and will therefore be neglected here.

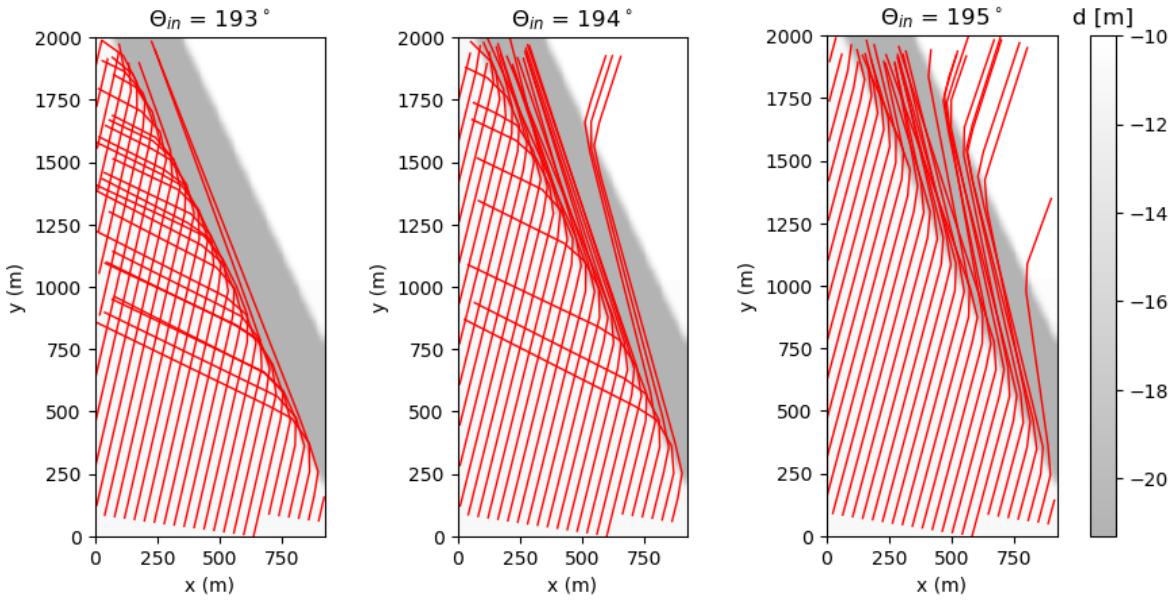

(a) Incoming wave 193°N (b) Incoming wave 194°N (c) Incoming wave 195°N

Figure 4.5: Wave rays according to REFRAC for wave directions around the critical angle of 194°N for T=10s, H_{in}=1m.

4.3.3. SWAN application

From here the results of the SWAN model will be considered. First, an assessment is done on the performance of SWAN when refraction is turned off. In this case only shoaling plays a role, see appendix B.2 for details. Here it can be seen that irrespective of the applied grid properties, the result is equal. This is an important conclusion, because it entails that all differences seen between the grid variants are likely caused by the modelling of the refraction term. For the directional resolution it is a different story. As long as the resolution is below the recommended 2.5°, thus >140 bins, the directional resolution does not affect the solution in case refraction is excluded. However for variant DR1 with 6° resolution, the resolution is too coarse to catch the directional spreading of the incoming wave, leading to a higher wave height in the entire domain. Since the imposed wave field is not represented properly by 60 bins, this variant will from now on be left out.

Effects of spatial resolution

Figures 4.6 and 4.7 give the distribution of the wave height for different grid resolutions. The smallest size of 5x5m is shown in absolute sense, the coarser grid variants are given relative to this fine grid. First of all, the significant wave height inside the channel is higher than at the flats due to wave refraction. This is caused by convergence of wave rays in the channel. In theory the wave height alteration is given by $H_2 \propto \sqrt{b_1/b_2}H_1$, where b is the width between the wave rays. The stronger the refraction is, the more the wave rays converge causing the wave height at the second point, with larger d, to increase.

Secondly, it can be observed that at the downwave channel side bands of energy ('stripes') become present for the finest grid. This could mean that a directional resolution of 2° is not sufficient for a grid size of 5x5m. Another reason could be that schematisation errors of the bathymetry propagate through the domain. The effect impacts the comparison with coarser grid points, since here the energy is more spread over the domain due to diffusivity. More attention for the cause of these 'stripes' is given in the coming paragraph 'Influence of directional resolution'. This is the main cause for the observed differences at T_p=5s. In vision of refraction all variants perform equally well, since the amount of energy crossing the channel in total is approximately the same and shows similar behaviour to REFRAC.

For a higher period of T_p=10s, differences between the grid variants with respect to the refractive behaviour are more pronounced. For coarser grids, the wave height inside and across the channel reduces while the wave height in front and along the channel edge increases. Notable is that for a period of 10s, the wave energy

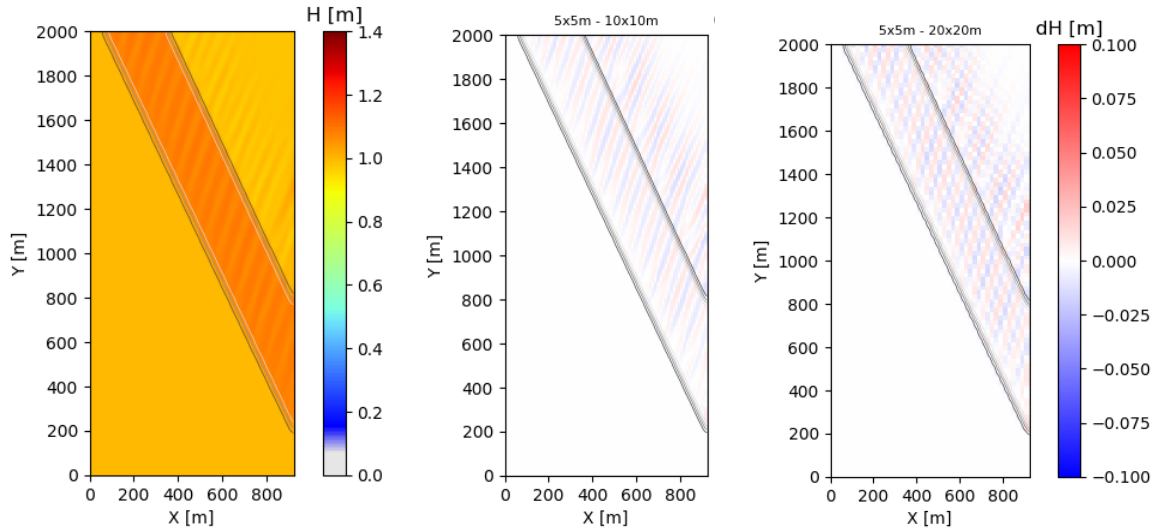

(a) grid size: 5x5m (b) grid size: 5x5-10x10m (c) grid size: 5x5-20x20m

Figure 4.6: Wave height according to SWAN for T_p=5s, $H_{s,in}$=1m and θ=200°N. Directional resolution=2°.

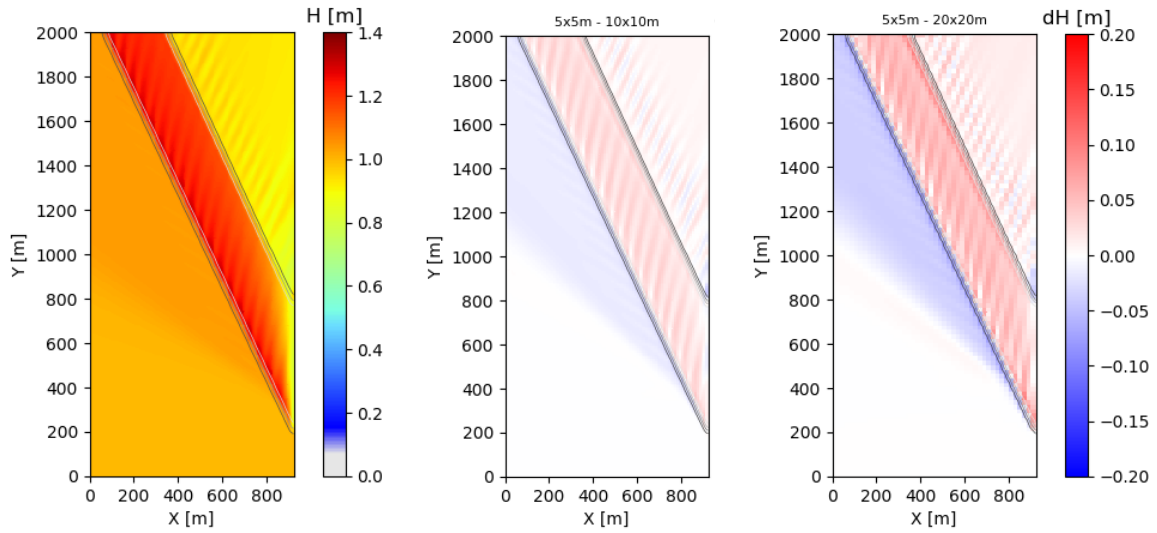

(a) grid size: 5x5m (b) grid size: 5x5m - 10x10m (c) grid size: 5x5m - 20x20m

Figure 4.7: Wave height according to SWAN for T_p=10s, $H_{s,in}$=1m and θ=200°N. Directional resolution=2°.

at the downwave side of the channel is significantly lower for a coarser grid. The wave height distribution for a period of 15s is similar. However, in case of T_p=15s there is no distinct difference downwave of the channel. The amount of wave energy that refracts away from the channel is order 10 cm higher for coarse grids, leading to a smaller amount of wave energy entering the channel. From REFRAC it followed that there is only a small amount of wave rays that is able to cross the channel, which is in line with the SWAN results. Since the amount of crossing waves is limited, the wave height at the downwave side is not much different for coarser grids as most wave energy stays in the channel for all grid variants.

Direction dependency

All figures shown above belong to a wave direction of 200°N, i.e. waves coming from south-southwest. However, in case other directions are considered, the results become slightly different. It can be readily observed that the accuracy of modelling with either coarse and fine grids is strongly dependent on the incoming wave

direction and frequency and hence the tendency to refract. For cases where refraction plays a negligible role, i.e. low periods or a small incoming angle with the channel normal, the solution approximates the case where refraction is turned off and the differences between the grid variants are negligible. However if the refraction is dominant, one can see that the grid resolution does affect the solution.

Figure 4.8 gives the absolute wave heights for a 5x5m grid size and the relative wave height for a 20x20m grid size compared to a 5x5m mesh size. The plots are made for a period of 10s, meaning the critical direction for refraction is 194°N. Only the 20m grid variant is shown, since the 10m grid variant gives equal patterns with slightly less absolute difference. Appendix B.3 gives the absolute values of the wave height for both the 5x5m and 20x20m grid sizes and difference plots for additional wave directions and periods in figures B.6 to B.13.

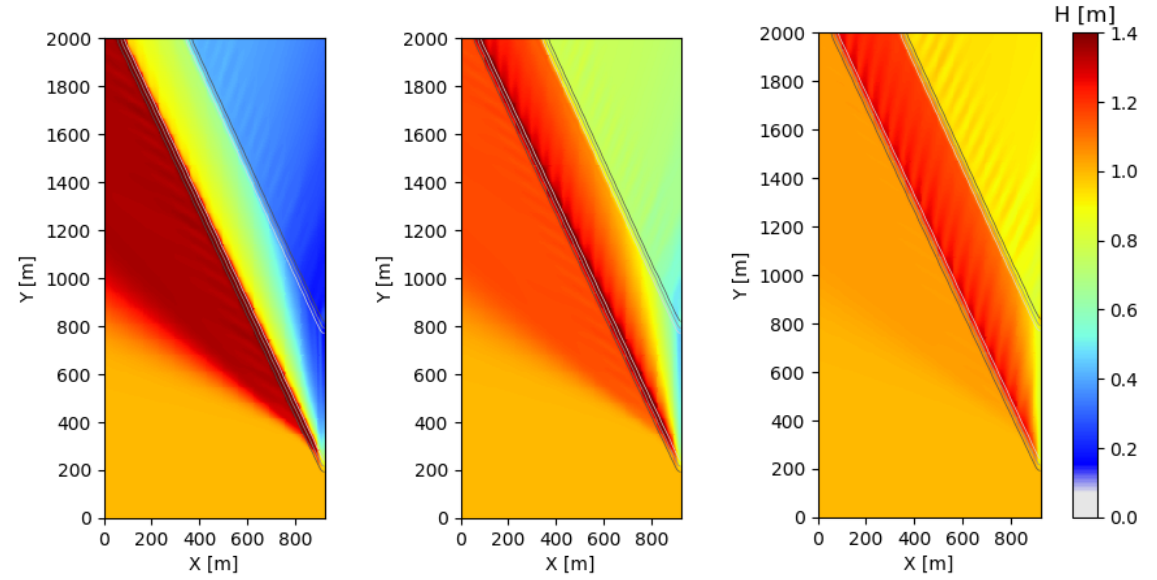

(a) Incoming wave 190° (b) Incoming wave 195° (c) Incoming wave 200°

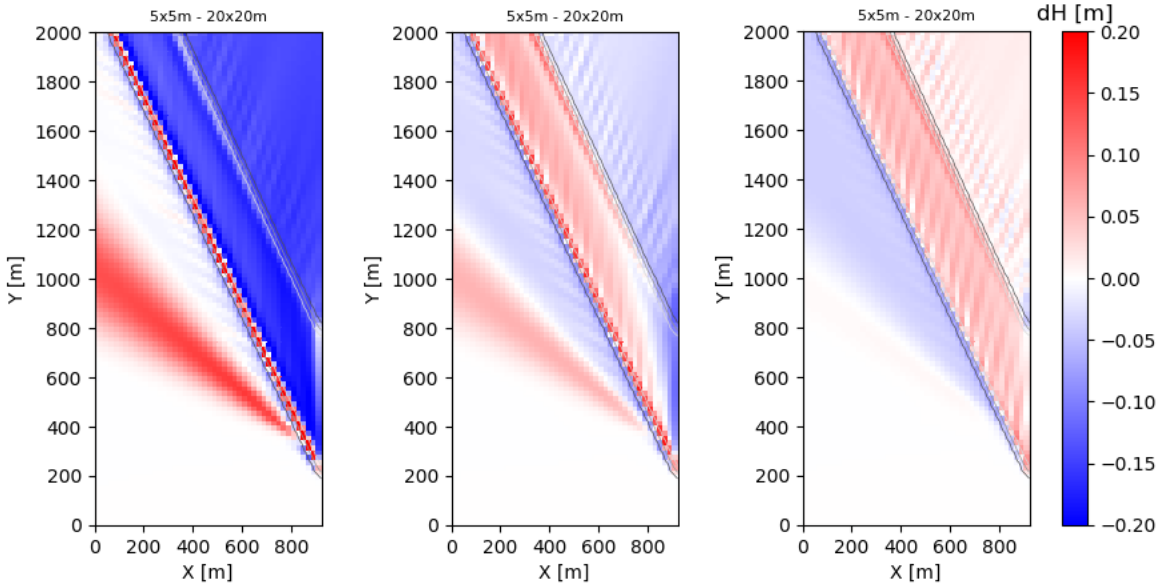

(d) Incoming wave 190° (e) Incoming wave 195° (f) Incoming wave 200°

Figure 4.8: Upper: absolute significant wave height of a 5x5m grid; Lower: relative height of a 20x20m grid to 5x5m grid, for different incoming wave directions. For all plots T_p=10s.

Incoming wave directions that are significantly larger than the critical direction, e.g. ≥15° larger, show neg-

ligible effect of the grid resolution to the accuracy of the solution, see also appendix B.3. This is true for all considered wave periods. However, when the wave angle becomes closer to the critical angle, the differences between the grid variants pronounce. Above the critical angle, where waves should enter the channel, the coarse grid underestimates the wave height inside the channel with respect to the finer grid. On the other hand, wave directions lower than the critical angle, where waves should refract off the channel edge, show a higher wave height for coarser grids inside and across the channel. This may be partly due to the fact that at the right boundary wave energy may enter the channel at the last grid cell. This boundary effect propagates through the entire channel, leading to serious errors for coarse grids. Yet, also diffusion and schematisation of the bathymetry play a role. For wave direction far below the critical angle, the differences reduce again, since in both cases all waves refract away from the channel. Interesting to notice is the evolution from 4.8(d) to (e) and (f). Here (e) is really the transition between (d) and (f), having more wave energy in the channel but lower across the channel for a fine grid. Of course this can be explained by the fact that 4.8(e) occurs at the critical angle. From the results, the importance of the critical angle arises.

From the above results a consistent pattern can be deduced for the influence and hence necessity of a proper grid resolution. For all cases the results varied most near the critical wave direction, which varies with wave frequency. Additionally, the differences become more pronounced with increasing wave period as these are more affected by refraction.

There were two variations visible in figure 4.8. First, the situation where the wave height inside the channel and in some cases across the channel is larger for fine grids. This matches with the hypothesis made beforehand based on literature. A second behaviour that can be observed is strongly visible for wave directions tending parallel to the channel axis. REFRAC shows all wave rays to refract away from the channel in these cases. For example, at a wave direction of 180°N, the wave rays refract for a period >6s. Observing the SWAN results for T_p=10s and θ=180°N shows a similar behaviour for the fine grid of 5x5m. However, a coarser grid gives a larger amount of energy inside and across the channel than is expected.

In cases where the incoming wave direction is more than 15° larger than the critical wave direction, the grid resolution has no influence on the accuracy of the solution. In these cases the use of a coarse grid might even be preferred since this gives a more smoothed solution, see figure 4.9. The finer grid of 5m shows a strong influence of the schematisation of the bathymetry propagating through the domain. In principle, this solution should be equal to the situation without refraction as given in figure B.5(a). Hence, a more diffuse solution is preferable if the role of wave refraction is small.

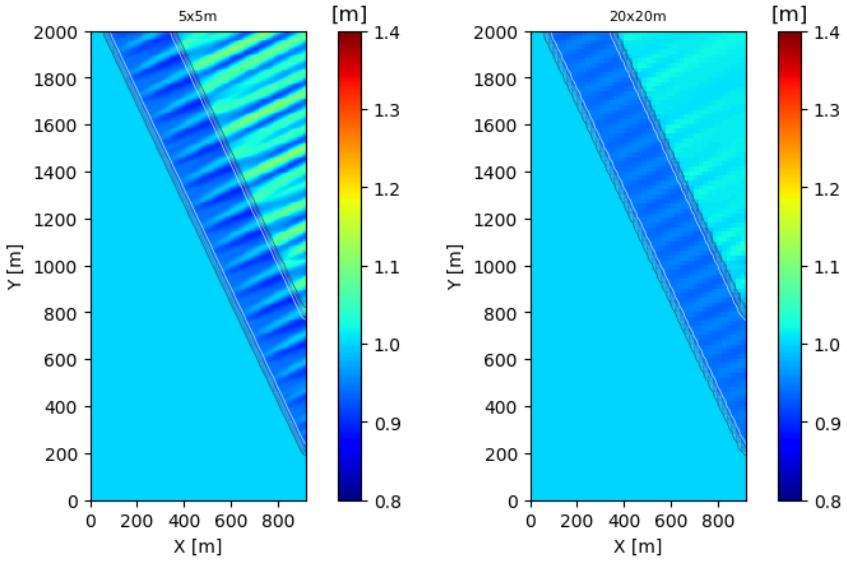

(a) grid size = 5x5m (b) grid size = 20x20m

Figure 4.9: Significant wave height for a wave direction of 245°N for two grid size variants. The wave direction equals the orientation of the channel normal.

Influence of directional resolution

In vision of the non-diffusive behaviour for fine grids, tests are performed to check the effect of the resolution in spectral space. It could be that the non-diffusivity is caused by a too coarse directional resolution compared to the spatial resolution. To check this hypothesis, a comparison will be made with a 1° resolution instead of the previously used 2° bin width. Also the effect on the refractive behaviour is part of investigation, as this leads back to the main question of this study.

First, from figure B.10 it followed that T_p=10s and an incoming wave from 190°N and 210°N are of most interest for directional resolution variants. Therefore the wave height plots of these directions are shown in figure 4.10. Also a difference plot is given between the wave heights of the 360 and 180 directional bin variants, i.e. 1° and 2° resolution.

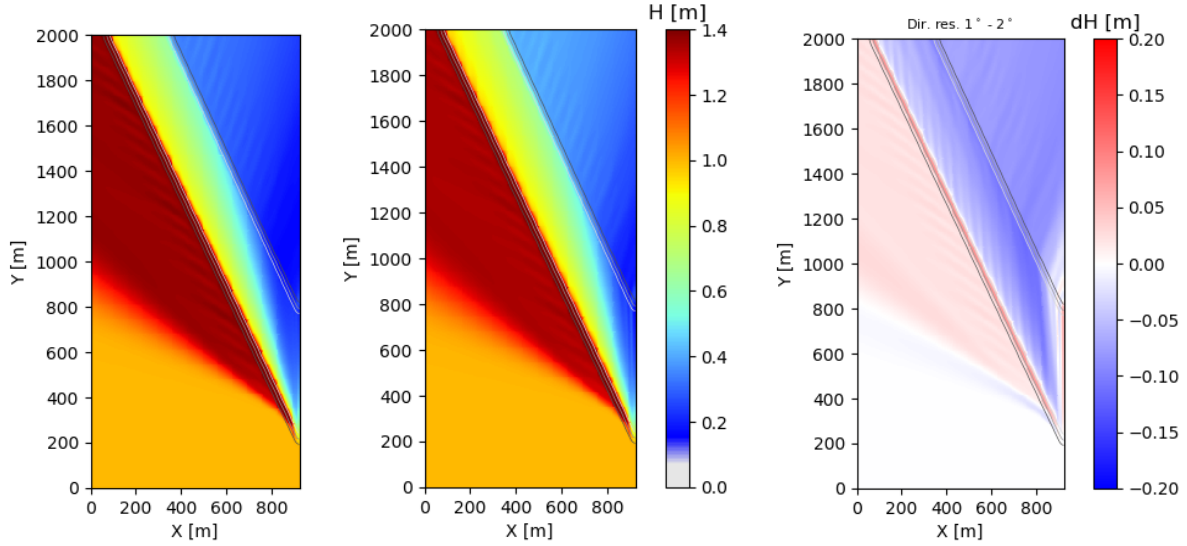

(a) DR3, incoming wave: 190°N (b) DR2, incoming wave: 190°N (c) DR3 - DR2, incoming wave: 190°N

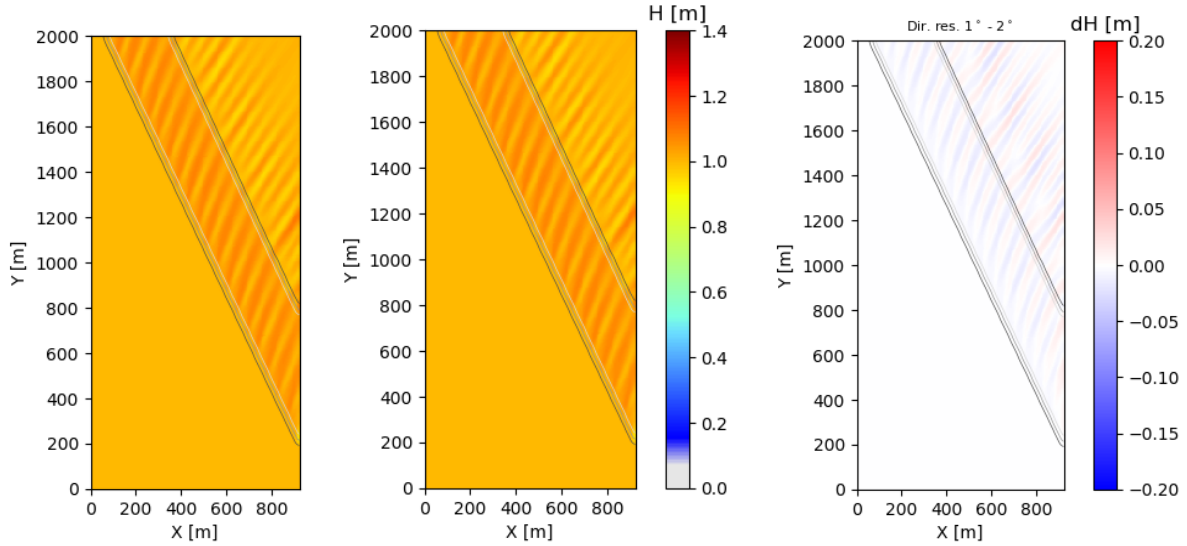

(d) DR3, incoming wave: 210°N (e) DR2, incoming wave: 210°N (f) DR3-DR2, incoming wave: 210°N

Figure 4.10: Significant wave height of a 5x5m grid for different incoming wave directions and directional resolutions, for all plots T_p=10s. DR3=1°(360 bins), DR2=2°(180 bins).

In the upper plot it can be clearly seen that for these wave conditions the finer resolution leads to more wave refraction. Since the wave direction is lower than the critical angle, this is also the expected behaviour. Hence, it can be clearly seen that the finer resolution models the refraction better. The order to which the wave height differs is approximately equal to that of the spatial grid variants.

From the lower plots it can be seen that the solutions are both equally non-diffusive. To go one step further, a simulation is performed with 3600 directional bins, hence a resolution of 0.1°. Still, the bands are present in the solution, they are even exaggerated as can be seen in figure B.14. Hence the before stated hypothesis can be rejected, as the directional resolution does not improve this behaviour. This leads to the conclusion that it is primarily caused by the way the bottom slopes are schematised. Small inaccuracies are captured by the fine resolutions and propagate through the solution due to a lack of numerical diffusion. This behaviour is also known as the garden-sprinkler effect (Booij and Holthuijsen, 1987).

Influence of numerical schemes

Refraction scheme

From theory it is known that the upwind scheme, CDD=1, tends to be more diffusive than the central differences, CDD=0. It is thus expected that the wave height will be more smoothed out over the domain for the upwind scheme. Figures 4.11 and 4.12 give the wave height distributions of the variants as well as the absolute difference between them. In theory, all waves should refract off the channel for θ_{in}=180°N. The wave energy inside the channel for central differences is however significant. On the other hand, also the amount of wave energy that refracts off the channel is larger if central differences is applied.

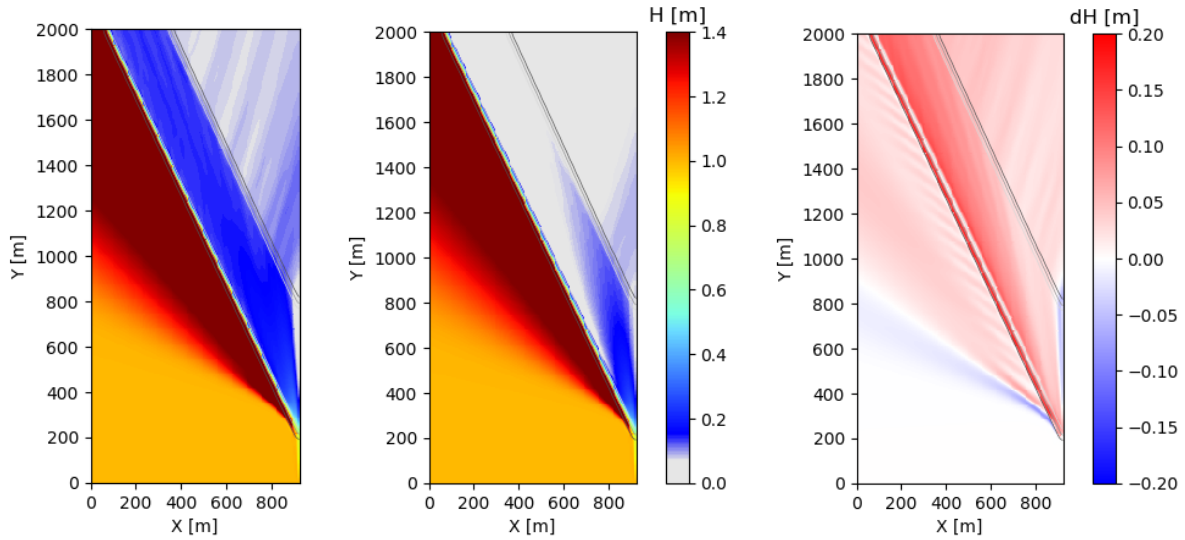

(a) CDD0: Central differences (b) CDD1: Upwind (c) CDD1 - CDD0

Figure 4.11: Significant wave height for different refraction schemes. θ_{in}=180°N and T_p=10s.

Comparing figure 4.11(b) to the REFRAC result of figure 4.4(a) shows a very similar result. Here it can be nicely seen that schematisation of the bathymetry causes some wave energy to enter and cross the channel. Both in SWAN and REFRAC this occurs at the same location. Hence the upwind scheme models the refraction process more accurate and is preferred for this case. Considering the case of θ_{in}=200°N, no waves should refract away from the channel. However, it can be clearly seen that in case upwind is used waves do refract off the channel. Furthermore, figure 4.12(b) clearly shows a more diffusive behaviour. Based on this situation, one may say that CD gives a better result, even though upwind is more diffusive.

It can be concluded that both schemes have their advantages and disadvantages. The diffusivity of the upwind scheme together with a better modelling for angles smaller than the critical angle makes this a preferable scheme. However, for angles larger than the critical angle and steep slopes, the refractive behaviour is too large for the upwind scheme. In the sense of modelling refraction, the central differences is thus preferred

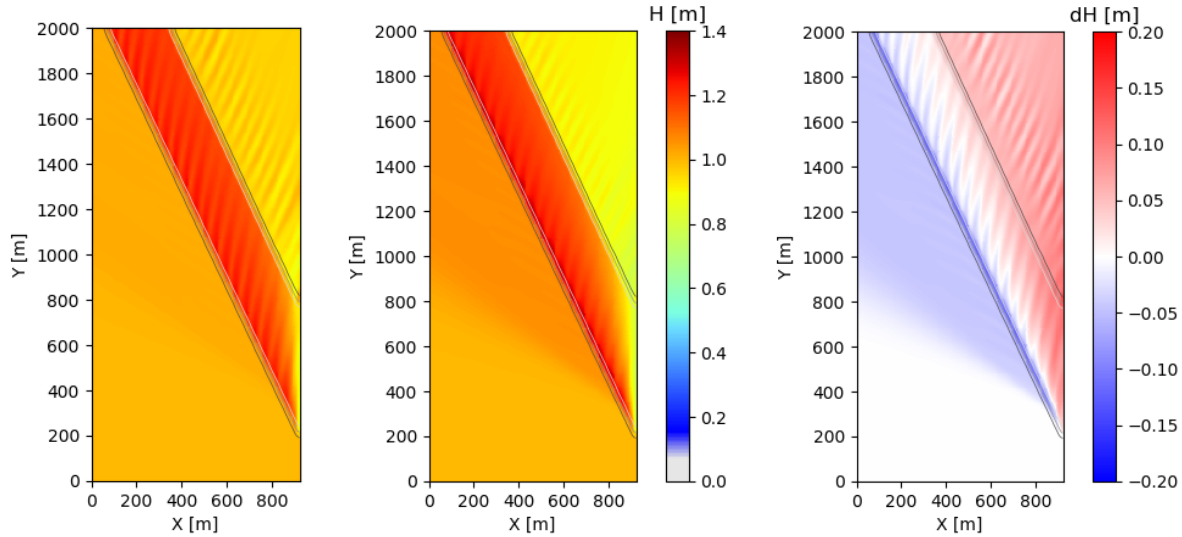

(a) CDD0: Central differences (b) CDD1: Upwind (c) CDD1 - CDD0

Figure 4.12: Significant wave height for different refraction schemes. θ_{in}=200°N and T_p=10s.

here. The combination of the two, which is the default setting with CDD=0.5, cooperates the advantages of both schemes. Figures 4.13 and 4.14 show the central differences, CDD=0, and upwind, CDD=1, schemes compared to the default scheme with CDD=0.5. From figure 4.13 it can be concluded that the default solution is mostly determined by the upwind scheme. On the other hand, figure 4.14 shows that the default solution is a true combination of the CD and upwind schemes. Therefore it is thought that switching to one of the two does not lead to any improvements in modelling refraction and hence the default is still the most accurate solution.

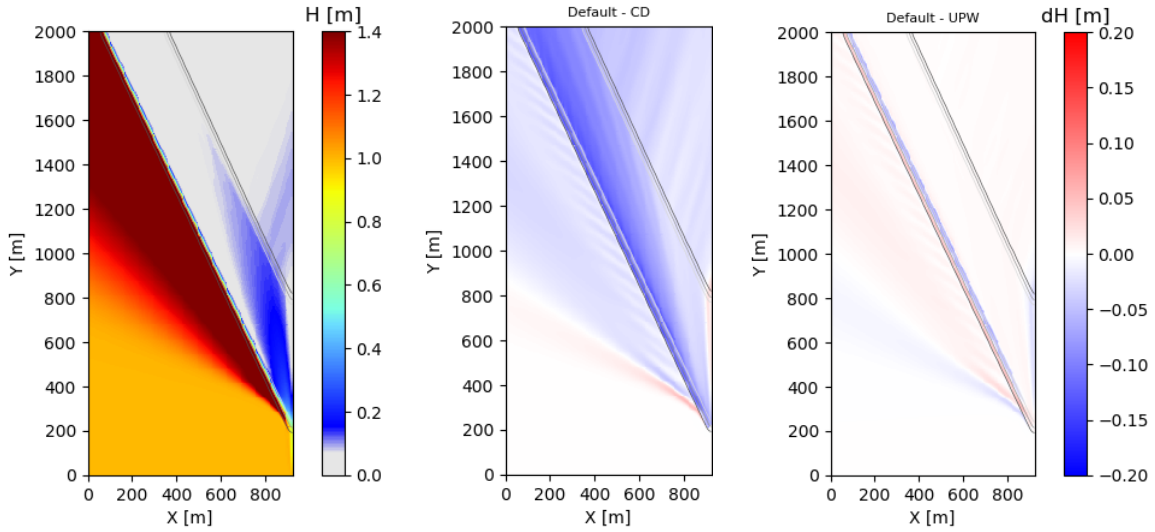

(a) Default CDD0.5 (b) CDD0.5 - CDD0 (c) CDD0.5 - CDD1

Figure 4.13: Significant wave height of a 5x5m grid for different numerical schemes for a period of 10s and a wave direction of 180°N.

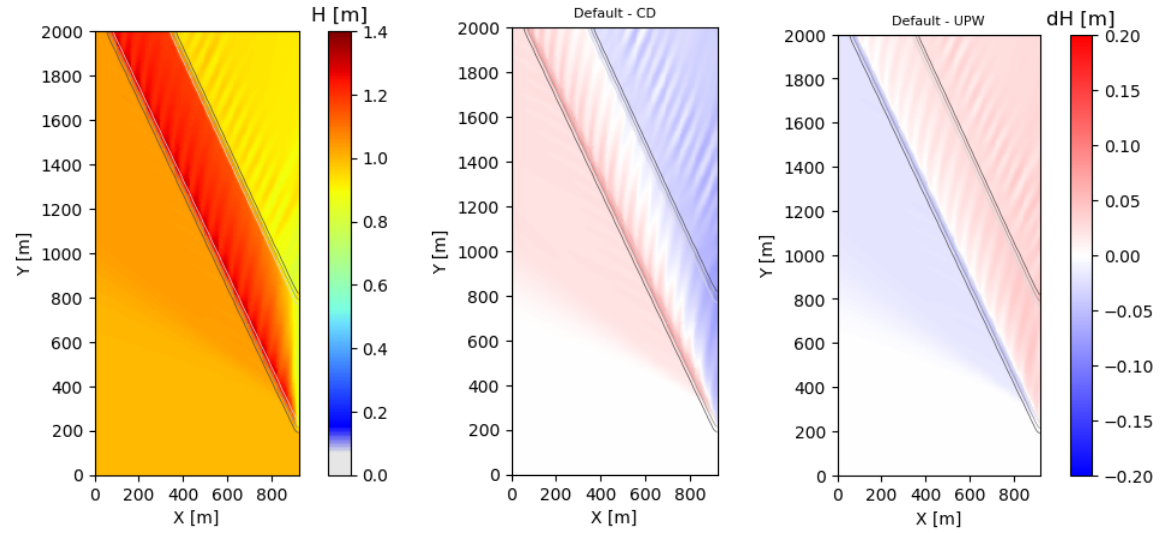

(a) Default CDD0.5 (b) CDD0.5 - CDD0 (c) CDD0.5 - CDD1

Figure 4.14: Significant wave height of a 5x5m grid for different numerical schemes for a period of 10s and a wave direction of 200°N.

Propagation scheme

The default scheme as used by SWAN to approximate the action balance is the second order SORDUP scheme. The alternative BSBT scheme is a first order upwind scheme, hence again introducing numerical diffusion. This can be clearly seen in figure 4.16(b), where the solution is much smoother at the downwave channel side. Furthermore, the BSBT scheme shows a stronger refractive behaviour for an incoming wave of 200°N. On the other hand, figure 4.15 shows a stronger refraction when applying the SORDUP scheme. This enhanced refraction is also what is expected according to theory and REFRAC. Concluding, the default SORDUP scheme shows the most accurate solution for both wave directions. The presented figures only show the case for a wave period of 10s, however the conclusions also hold for the other wave periods.

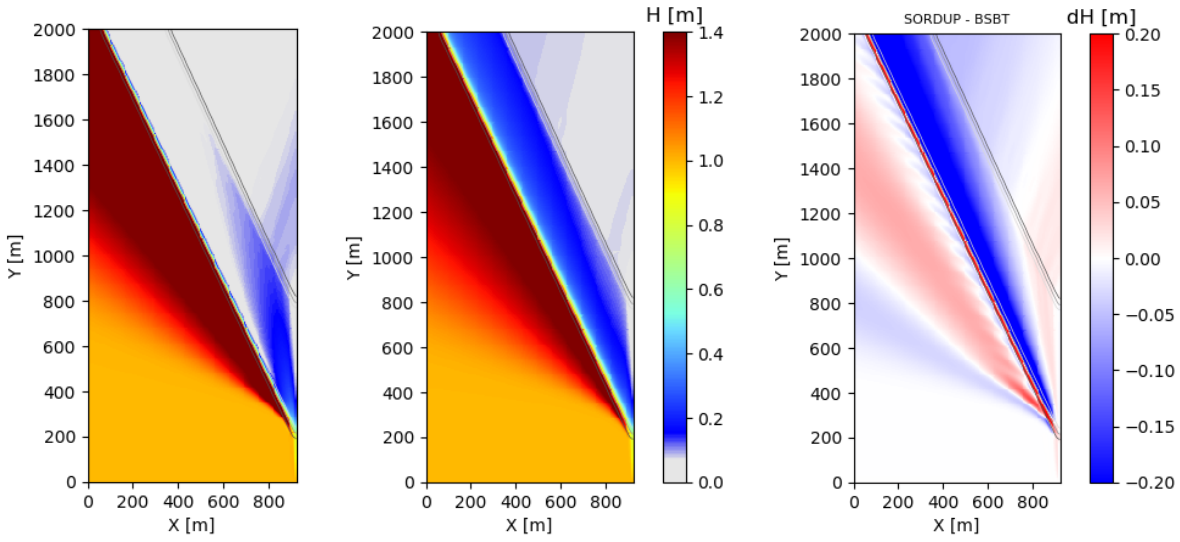

(a) Default SORDUP (b) BSBT (c) SORDUP - BSBT

Figure 4.15: Significant wave height for different action balance solving schemes. θ_{in}=180°N and T_p=10s.

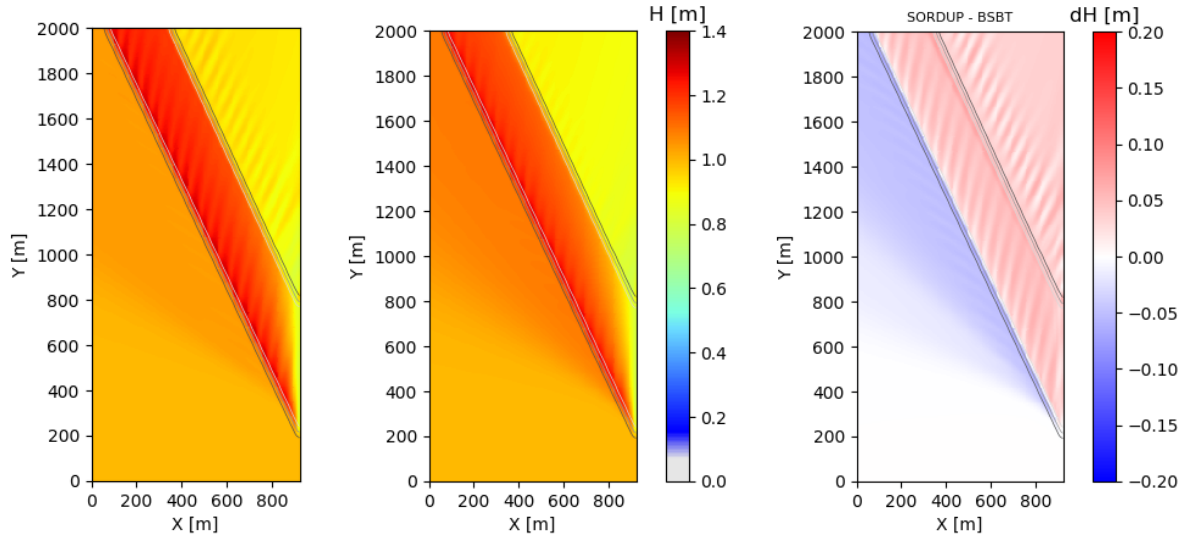

(a) Default SORDUP (b) BSBT (c) SORDUP - BSBT

Figure 4.16: Significant wave height for different action balance solving schemes. θ_{in}=200°N and T_p=10s.

4.4. Quantitative effects of spatial resolution

This section focuses on the required mesh width for the considered bathymetry. The most important conclusions are presented here, more details and additional figures are given in appendix C. To assess the accuracy of the model, the focus will mainly be on the significant wave height distribution. The smallest mesh width that is applied has a length of 1m in both x- and y-direction, this is chosen as reference case. Consequently, the root mean squared error, RMSE, and relative bias, RB, in wave height will be determined for larger mesh widths with respect to the reference width of 1m.

The RMSE indicates the discretisation error of the grid. As can be seen in figure 4.17, this error is logarithmic dependent on mesh width and could thus be interpreted as a convergence error. Hence, the relation between RMSE and mesh width Δx follows equation 4.5. Here p is is the slope of the graph, where a larger slope indicates a higher order of accuracy. Figure 4.17 shows a larger rms-error for large wave periods or coarse meshes. The lines for p=1 and p=2 are also given in the graphs, from which can be concluded that the order of accuracy for T_p=5s ~ p=1-1.6 and for T_p=10,15s ~ p=1.2-2.

$$\begin{aligned} RMSE &\propto \Delta x^p \\ \log(RMSE) &\propto p\log(\Delta x) \end{aligned} \tag{4.5}$$

Comparing the RMSE of the period variants for the corresponding critical wave directions shows that these errors are in the same order. As mentioned, the critical angles of the different period variants are: T_p=5s: 172°N, T_p=10s: 194°N and T_p=15s: 197°N. When considering a mesh width of 10m, the RMSE of the periods at the corresponding wave directions become:

- T_p=5s : 5-7 cm
- T_p=10s : 6 cm
- T_p=15s : 5-10 cm

When considering the total direction range of 170-200°N, the characteristic errors for the different period variants are as given in table 4.3. Here the mean RMSE as well as the minimum and maximum RMSE are given for each wave period and mesh width. From this table it follows that the error made by a 2m compared to 1m mesh width leads to negligible differences. However, the error starts to become significant from a grid size of around 10m. Due to the limited directional range, the RMSE is lower for the period of 5s. The minimum, maximum and mean error for the 10s and 15s variants are in the same order for each grid variant. Therefore, it can be concluded that the wave period on itself does not impact the accuracy of the grid variant

significantly. It influences the critical wave direction, on which the accuracy of the simulation depends. So it is an indirect influence on the accuracy of modelling refraction.

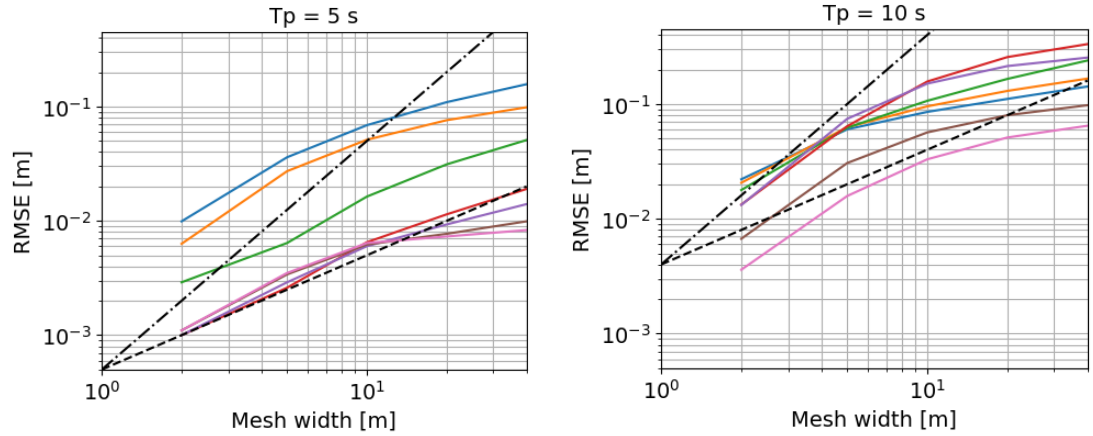

(a) Wave period of 5s

(b) Wave period of 10s

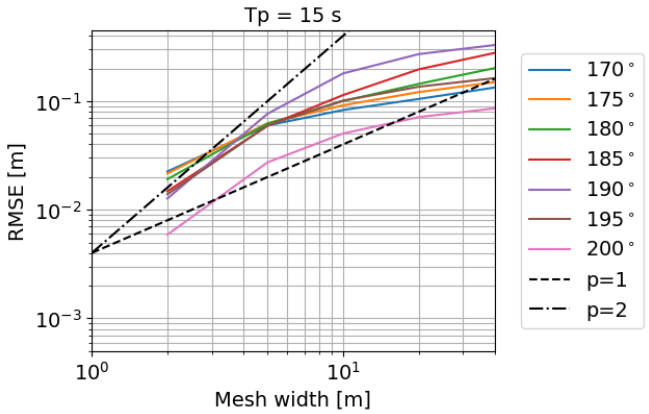

(c) Wave period of 15s

Figure 4.17: RMSE as function of mesh width for different wave directions and periods on a log-log scale, where the line p corresponds to the relation RMSE $\propto \Delta x^p$. The RMSE is determined based on the whole domain by using SORDUP and H_s=1m

Table 4.3 also shows the minimum, maximum and mean relative bias of the significant wave height. This is on average lower than the RMSE, due to the cancelling of wave height differences. This is not taken into account by the RMSE and may lead to negative minimum values for the RB. It follows that the maximum values are always positive, meaning that on average the wave heights for the coarser grids are larger than for the finer grids. This suggests that refraction is most times underestimated by SWAN for coarser grids. To get a more sounding representation of the refraction process, it may be better to split the area in two sections. The first covers the area upwave of the channel and the second covers the area inside and across the channel, see appendix C. The downwave channel side shows to have some boundary influences. To get a proper assessment of only the refraction process, the conclusions will be mostly based on the upwave side of the channel, i.e. side 1. The results of the RMSE and RB for side 1 are given in table 4.4. For positive RB it holds that the wave heights of the coarser grids are on average larger than of the finer grids. In this case more waves get refracted for the coarse grid. Following from table 4.4, the influence of refraction is rather small. The RMSE does not exceed 11cm (11%) and the RB is close to 0% most of the times. Despite this, it can be seen that the maximum and (negative) minimum RB do increase for coarser grids. Furthermore, the wave direction where the largest positive RB occurs is 175°and 200°N for respectively T_p=5s and T_p=10, 15s. Since a large area of side 1 is not influenced by the channel, this decreases the RB. Appendix C tables C.2 to C.5 give the RMSE and RB per side for all considered combinations of wave period, direction and mesh width.

Table 4.3: Bandwidths of the RMSE and RB for T_p=5s, 10s and 15s resulting from different mesh widths. The RMSE is determined based on the whole domain by using SORDUP and H_s=1m

		RMSE [m]			**RB [%]**		
	mesh width	*min*	*mean*	*max*	*min*	*mean*	*max*
T_p=5s	2m	0.00	0.00	0.01	0.0	0.0	0.1
	5m	0.00	0.01	0.04	0.0	0.2	1.0
	10m	0.01	0.02	0.07	0.0	0.5	2.7
	20m	0.01	0.04	0.11	-0.1	0.9	5.0
	40m	0.01	0.05	0.16	-0.2	1.4	7.6
T_p=10s	2m	0.00	0.01	0.02	0.0	0.2	0.4
	5m	0.02	0.05	0.07	-0.2	1.4	3.5
	10m	0.03	0.10	0.16	-0.5	3.3	8.5
	20m	0.05	0.14	0.26	-0.7	5.8	15.6
	40m	0.06	0.19	0.33	-0.7	8.4	20.9
T_p=15s	2m	0.01	0.02	0.02	-0.1	0.2	0.5
	5m	0.03	0.06	0.08	-0.2	1.5	3.8
	10m	0.05	0.10	0.18	-0.5	3.5	10.5
	20m	0.07	0.15	0.27	-0.7	6.1	16.6
	40m	0.09	0.19	0.33	-0.6	8.7	20.2

Table 4.4: Bandwidths of the RMSE and RB for T_p=5s, 10s and 15s resulting from different mesh widths when *only taking side 1 into account.* The minimum value for RB can become negative and may act as the maximum negative value. This is for example the case in the last row, where the absolute value of the minimum is larger than the max value.

		RMSE [m]			**RB [%]**		
	mesh width	*min*	*mean*	*max*	*min*	*mean*	*max*
T_p=5s	2m	0.00	0.00	0.01	0.0	0.1	0.2
	5m	0.00	0.01	0.03	0.0	0.2	1.1
	10m	0.00	0.01	0.05	0.0	0.3	1.7
	20m	0.00	0.02	0.06	-1.0	0.2	1.7
	40m	0.00	0.02	0.08	-1.9	0.0	1.4
T_p=10s	2m	0.00	0.01	0.03	-0.1	0.1	0.2
	5m	0.01	0.03	0.05	-1.0	0.1	0.6
	10m	0.02	0.05	0.06	-2.3	0.0	1.3
	20m	0.03	0.06	0.08	-3.4	-0.2	2.0
	40m	0.04	0.07	0.11	-4.3	-0.6	2.5
T_p=15s	2m	0.00	0.01	0.03	-0.3	0.1	0.2
	5m	0.01	0.04	0.05	-1.3	0.0	0.7
	10m	0.02	0.05	0.07	-2.3	-0.1	1.4
	20m	0.04	0.06	0.08	-3.0	-0.3	2.0
	40m	0.05	0.08	0.11	-3.6	-0.7	2.3

Concluding all, it is found that a resolution of order 5-10m is sufficient to predict refraction for this case. For a resolution of 10m, the maximum error of the western channel side becomes order 7cm (7%). For wave periods where waves should not enter the channel, the (positive) RB increases for coarser grids and SWAN thus shows to underestimate refraction for coarser resolutions, leading to more wave energy entering the channel. In case waves should enter the channel, the opposite takes place and SWAN overestimates refraction stronger for coarser resolutions leading to less energy in the channel. Related to this, one can compare the predicted crest turning according to Snel's law and the equation as used by SWAN. From this comparison it is found that a resolution of 10m leads to a crest turning of 4.5° and 5.2° according to SWAN and Snellius respectively in case T_p=10s and θ_{in}=195°N. The fact that SWAN underestimates refraction for shallow to deep water also

emerges here and is thus caused by the determination of the crest turning. A resolution of 5m leads to an almost identical crest turning of respectively 2.4° and 2.6°. Hence it is concluded that the resolution of 10m was already sufficiently small to model refraction properly. The overestimation of refraction that takes place at for example T_p=10s and 200°N is not a result of the turning rate but is thought to be caused by (numerical) diffusion.

4.5. Critical refraction angle in SWAN vs theory

In case the bathymetry is fixed, the critical angle is only dependent on the wave frequency. In theory, no waves should refract off the channel edge if the wave direction is larger than the critical angle. However, in the previous sections it was found that in cases where waves are able to enter the channel in theory, SWAN still shows refractive behaviour. This behaviour becomes stronger with coarser grids and by applying the BSBT scheme.

To assess this, a quantitative analysis of the critical angle according to SWAN is performed. A comparison will be made between this angle and the theoretical critical angle based on Snel's law[2]. Since it is already known that the critical angle is strongly dependent on the wave frequency, the influence of the wave period on the difference in critical angle will be analysed first. This will be done by taking a sequence of wave periods ranging from 4-15s. A *resolution of 5m* and a *SORDUP* scheme are taken as numerical settings. A wave height of 1m is imposed to the boundary and is not modified on its way to the channel, since the source terms are turned off. Therefore, the wave height just in front of the channel should in theory also be 1m. To assess this, eight points just in front of the channel are chosen, see appendix D for the locations of these points. The mean of these points should be equal to the wave height that is imposed to the boundary if refraction is absent. The relative difference between the incoming wave height and the wave height in front of the channel is then determined using equation 4.6. It is assumed that for a difference smaller than 0.5% the refractive behaviour is negligible. Hence if equation 4.6 is true, the critical angle is found. This 0.5% is chosen arbitrarily, therefore appendix D contains the critical angles found in SWAN when allowing a 5% difference. With this a bandwidth can be created for the results.

$$\frac{\overline{H}_{s,chan.edge} - H_{s,in}}{H_{s,in}} * 100\% < 0.5\% \tag{4.6}$$

Table 4.5 shows the critical angle for refraction according to theory and SWAN for the different wave periods. The angles are the *nautical wave directions*, hence 180°N means waves coming from the *south*. The angles are rounded to one decimal numbers to prevent large rounding errors to be present. Results are not reliable for wave periods smaller than or equal to 4s, since the critical wave direction becomes too small. In these cases the waves do not counter the channel in the domain considered. The domain is simply too small in y-direction for these wave directions.

Table 4.5: Critical wave directions according to theory and SWAN for different wave periods. The critical angle is expressed as the nautical wave direction in this table. Conditions: mesh width=5m, numerical scheme=SORDUP.

Tp [s]	**4**	**5**	**6**	**7**	**8**	**9**	**10**	**11**	**12**	**13**	**14**	**15**
theoretical angle	161.7	172.1	180.8	186.6	190.1	192.3	193.8	194.8	195.5	196	196.4	196.8
SWAN angle	169.2	179.7	188.6	195.3	199.2	201.5	203.1	204.1	205	205.6	206	206.5
error [*degr*]	*7.5*	*7.6*	*7.8*	*8.7*	*9.1*	*9.2*	*9.3*	*9.3*	*9.5*	*9.6*	*9.6*	*9.7*
error [%]	4.6%	4.4%	4.3%	4.7%	4.8%	4.8%	4.8%	4.8%	4.9%	4.9%	4.9%	4.9%

The *error* is the difference compared with the theoretical angle, e.g. $|\theta_{in,swan} - \theta_{in,theory}|$. From table 4.5 it follows that there is a maximum and minimum error that is present for the applied settings. An overestimation of the critical angle by SWAN implies that the refractive behaviour is too strong in SWAN, since wave directions above this angle are able to enter the channel. It can be seen that the overestimation of the critical angle will not be larger than 10° for the 5x5m grid in combination with the SORDUP scheme. For long waves, i.e. high periods, the critical angle should be constant according to theory. This is also visible in the SWAN

[2]It should be noted that the theoretical computed wave angles correspond with the REFRAC results. This verifies the reliability of the theoretical results.

results, only the absolute value of the angle in SWAN is between 9.5-10° higher than what is predicted by theory, see figure 4.18. Overall, the error in wave angle shows a similar shape to the function of the theoretical critical angle. For low periods and hence low critical angles, the absolute error is lower than for high periods and thus high critical angles. Concerning the relative error, the error varies from 4.3-4.9% for respectively low and high periods, see the last row of table 4.5. Here the relative error is determined by dividing the error by the theoretical angle. SWAN thus overestimates the critical angle with on average 4.7% relative to the theoretical value for this case. The deviation in relative error for the different wave periods is rather limited, with a slightly larger error for high periods. Concerning the directional spreading of the imposed spectrum, it can be noted that a small amount of energy is present up to 7° from the mean direction. This thus explains a part of the error found for the 5x5m grid and hence the prediction shows to be quite well for lower periods. Considering the case where 5% wave height difference is allowed, the error ranges from 4.2-4.6° which is relatively 2.3-2.5%, see appendix D. Hence, SWAN predicts the critical angle well for a 5x5m grid, where the prediction is slightly better for lower wave periods.

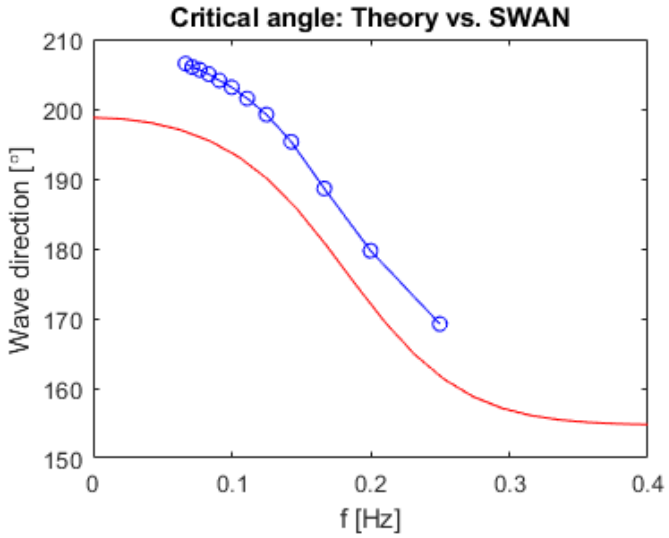

Figure 4.18: Critical angle as function of wave frequency according to SWAN and the theory of Snellius. The blue line represents the SWAN results and the red line corresponds with the theoretical function $\theta_{crit} = 155 + \arccos(c_1/c_2)$, where 155 equals the angle of the channel axis with the nautical north. Conditions: mesh width=5m, numerical scheme=SORDUP.

Subsequently, the influence of the grid resolution and numerical schemes on the refraction angle is assessed. Three wave period cases will be chosen, which are T_p=5s, 10s and 15s. For each combination of wave period and grid resolution, the critical angle is determined. The same is done for all combinations of wave period and numerical scheme. For the grid resolution variants a SORDUP numerical scheme is chosen in all cases. For the numerical scheme variants the 5x5m grid is taken for all cases.

Table 4.6 summarises the outcomes for the different variants. Here the angle represents the critical wave direction, where waves larger than this angle can enter the channel. It can be seen that SWAN overestimates the critical angle with 8-16°, thus a larger wave direction is needed to enter the channel. The absolute error increases with larger wave periods in all cases, which confirms the earlier findings.

Focusing on the resolution variants, it can be observed that the error increases for coarser grids. Additionally, the range of the error over the wave period and hence the influence of the period increases for these coarser grids. Where the error ranges between 8-10° for a fine mesh width, it varies between 11-16° for coarser meshes. Thus, the error made in the critical angle is more dependent on the wave period in case of coarser meshes. Furthermore, it can be noted that the deviation of the error from the grids becomes larger for higher periods. Where the error of the different grids ranges between 8-11° for low periods, it varies between 10-16° for large wave periods. From this it can be concluded that a finer resolution is of greater interest for larger wave periods.

Table 4.6: Critical angle according to SWAN results for grid resolutions of 5m,10m and 20m and the SORDUP and BSBT scheme at different wave periods.

			Tp [s]		
			5	**10**	**15**
Theory	-	*angle [degr]*	*172*	*194*	*197*
grid resolution	5x5m	angle [degr]	180	204	207
		error [deg]	8	10	10
		rel. error [%]	4.7%	5.2%	5.1%
	10x10m	angle [degr]	182	206	210
		error [deg]	10	12	13
		rel. error [%]	5.8%	6.2%	6.6%
	20x20m	angle [degr]	183	209	213
		error [deg]	11	15	16
		rel. error [%]	6.4%	7.7%	8.1%
Numerical scheme	SORDUP	angle [degr]	180	204	207
		error [degr]	8	10	10
		rel. error [%]	4.7%	5.2%	5.1%
	BSBT	angle [degr]	183	208	212
		error [degr]	11	14	15
		rel. error [%]	6.4%	7.2%	7.6%
Solving method for c_θ : DEP	5x5m	angle [degr]	181	204	207
		error [degr]	9	10	10
		rel. error [%]	5.2%	5.2%	5.1%
	10x10m	angle [degr]	183	206	210
		error [deg]	11	12	13
		rel. error [%]	6.4%	6.2%	6.6%
	20x20m	angle [degr]	184	210	213
		error [deg]	12	16	16
		rel. error [%]	7.0%	8.1%	8.1%

Concerning the differences between the SORDUP and BSBT schemes, one finds similar conclusions. Interesting is that the overestimation of a coarse grid of 20x20m is in the same order as the error of the BSBT scheme, meaning that they overestimate refraction similarly. The overestimation of the critical angle is slightly less for the BSBT scheme for larger wave periods. Wave height distributions of all angles from table 4.6 are given in appendix D.

As a side note, the influence of the solving formula for c_θ is given in the last row of table 4.6. As mentioned in section 3.2.3, there are different possibilities to solve c_θ, either by taking the derivative to bottom depth, DEP, or to the wave number, WNUM. It was thought that the equation with the derivative to the wave number is less sensitive to bottom variations. Therefore, this is the default option in SWAN from version 41.01 (SWAN-team, 2019a). To check this hypothesis, the critical angle is computed with SWAN in case the option DEP is used, hence the formulation with derivative to bottom depth. Interestingly, the errors are similar to those for the default case. The error is only slightly higher compared to the default WNUM, especially for lower periods. Noteworthy is that the error is less sensitive to the wave period when using option DEP.

Since both formulas for c_θ give approximately the same results for the total solution, this corroborates the statement that the overestimation of refraction by coarser grids is not caused by determining the turning rate. Again, the crest turning of both options of SWAN can be compared to Snel's law. Taking Δx=10m, T_p=10s and θ_{in}=195°N leads to a crest turning of 4.5°, 4.2° and 5.2°. Option DEP gives a larger underestimation in crest turning compared to Snel's law, however the differences are small. For more details about the crest turning, one is referred to appendix E.

4.6. Concluding notes

As already known from literature, the wave frequency largely impacts the rate of refraction. Low-frequency waves tend to refract stronger in SWAN, this trend is also visible in REFRAC. The critical angle theory derived from Snel's law supports this. Following this theory, waves should be able to enter the channel if the incoming wave angle is *larger* than the critical angle for refraction. The following points summarise the most important conclusions made with respect to refraction based on the different variant studies:

- For a case from shallow to deeper water, SWAN overestimates the refraction process if the incoming wave direction is larger than the critical direction for refraction. This leads to less wave energy inside the channel and more energy on the tidal flats. On the contrary, a larger amount of wave energy is found in and across the channel if the wave direction is smaller than the critical direction. SWAN thus underestimates the refraction process for these cases. Comparing the crest turning based on Snel's law and the method of SWAN shows that SWAN underestimates the crest turning with respect to Snel's law. Thus the underestimation of refraction by SWAN from shallow to deeper water can be explained by the determination of the turning rate.
- Both the spatial and directional resolution influence the predicted refraction in SWAN. The effect is dependent on the strength of the refraction process, hence the wave orientation with respect to the critical angle for refraction. For incoming wave directions 5-15° below the critical angle, where waves cannot enter the channel, the largest differences between the grid variants occur. For cases where the wave direction is much larger than the critical direction (>15° smaller), where waves should enter the channel, no significant differences are found between the resolution variants. When taking a mesh width of 1m as reference, grid sizes smaller than 10m are considered sufficient for a proper simulation of refraction, allowing a maximum error of order 7cm (7%) in wave height at the upwave channel edge. Taking only the upwave channel side into account, a coarse resolution of 40m underestimates the wave height with a maximum of 11cm (11%). Highest errors were found for wave directions just below the critical angle, were coarser grids show to underestimate refraction, leading to more wave energy entering the channel.
- For all considered frequencies, the RMSE was approximately equal at the corresponding critical angle. This leads to the conclusion that the accuracy of modelling refraction is not directly dependent on wave frequency. The critical angle changes with frequency and this, in combination with the incoming wave direction, influences the accuracy of modelling refraction.
- The critical angle for refraction is overestimated by SWAN, which implies that more wave energy is trapped at the upwave channel side for relatively large angles with the channel axis. Considering mesh widths of 5 to 20m, the error varies between 8-15°(4.5-8%), where largest errors are found for the coarse grid of 20m. Additionally, the error increased for larger wave periods, both in absolute and relative sense. The overestimation of the critical angle is independent of the formulation for c_θ, hence this is not causing the overestimation. It can thus be explained by the discretisation of the action balance terms and the larger diffusion for coarse grids, which increases the directional spreading. Yet, it should be noted that a part of the error is also caused by the initial directional spreading that is present in the imposed spectrum of SWAN.
- The default hybrid scheme is thought to be the best solving scheme for the refraction term in the action balance. Other options showed to give a less accurate representation and hence they do not lead to an improvement compared to the default.
- According to (SWAN-team, 2019a), BSBT is known to induce numerical diffusion. This behaviour can also be observed in this study. Additionally, the default SORDUP scheme gave a more accurate prediction due to second order accuracy instead of the first order BSBT scheme. Based on the presented results, it is thought that the SORDUP scheme is preferred when considering the modelling of refraction.

Relating the outcome to the geometric characteristics that are present may give a more standardised conclusion. For this case Δx=10m is sufficient for a proper modelling of refraction. Considering that the channel slope has a gradient of 1:5, with a length of approximately 50 m, there will be around 5 grid points on the channel slope with Δd=2m. For large domains, often only order one to ten grid points are present crossing the entire channel. Still, the fact that the differences between a coarse and fine grid may become order 10cm on 1m wave height underlines the importance of a sufficient grid resolution.

5

Case study: Eastern Wadden Sea

The previous chapter gave insights in the modelling of refraction for a simple academic case. Here the importance of the critical angle and the order of the observed error were denoted. Since the domain consisted of a straight channel with a flat bottom outside the channel, the waves were not altered in front of the channel. Of course, this schematisation will not be present in a true coastal system. Therefore, a more realistic scenario will be considered in this chapter to take the gained knowledge into practice.

5.1. Study area

The characteristics of the area that will be chosen should be roughly similar to the channel of chapter 4. There should be a channel present with relatively steep slopes, since the schematic channel had slopes of 1:5. Preferably, measurement data is available so that boundary conditions can be retrieved and a comparison with the results is possible. Following from these requirements, it is chosen to focus on the Eastern Wadden Sea area. This area consists of many small and large channels with tidal flats between them. Therefore, refraction plays an important role in this area.

Specifically at the Ems channel, there is an ongoing measurement campaign, 'Meerjarige Veldmetingen,' for the present and near future (Waterschap-Noorderzijlvest, 2020). Additionally, wave data from previous years is measured by wave buoys that are already present along the Ems channel, see figure 5.1. The current attention for this area shows that still a lot of research is needed and hence gives the relevance of this case study.

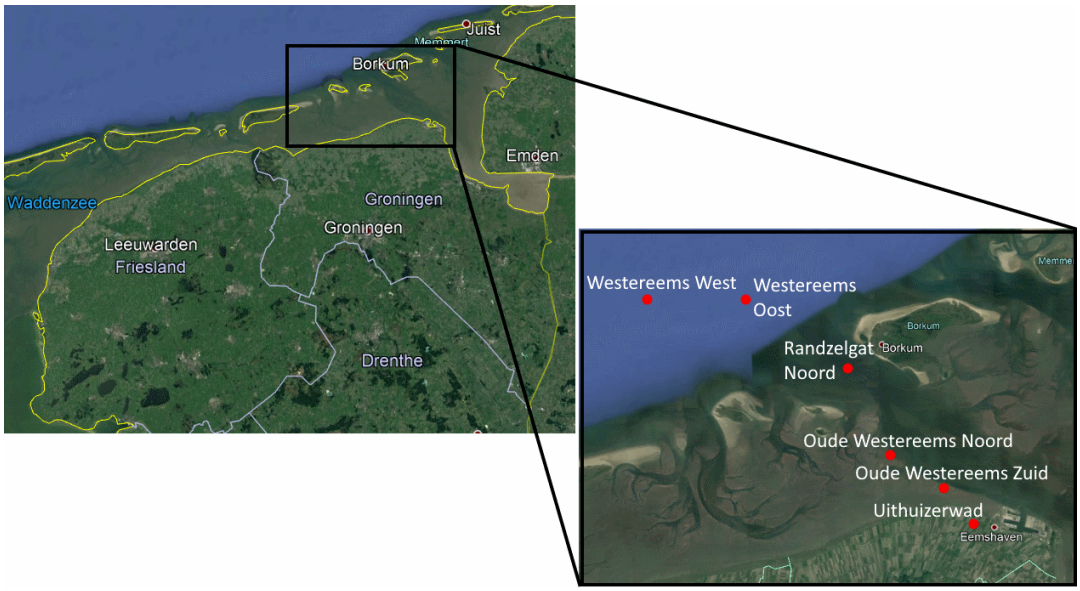

Figure 5.1: Location of the domain of interest and measurement buoys in the Eastern Wadden Sea (Rijkswaterstaat, 2019; Google, 2019).

Obviously, the results will be less pronounced as for the schematic channel of chapter 4. Since the orientation of the channel changes continuously, the critical angle for refraction will alter as well. Therefore, even with a constant wave field the wave direction will at some point be equal or near the critical angle for refraction. Largest model errors were found close to this angle. Additionally, the wave direction itself will vary over the

considered domain due to contribution of refraction. Furthermore, the channel slope varies from 1:15 to approximately 1:60 instead of a constant slope of 1:5. The fact that the slope is milder, leading to a different change in water depth over grid length, and varies along the channel will influence the modelling of refraction. Lastly, the source terms were neglected in the academic channel case and a monochromatic wave was assumed. When considering a realistic case, it is inevitable that source terms, such as wave breaking, should be taken into account and a realistic wave spectrum should be imposed. Previously, the main focus was on the wave height distribution for observing refractive behaviour. If the source terms and a complex wave spectrum are taken into account, these will also influence the wave height distribution and may compensate or amplify the refraction patterns. Since refraction mostly impacts the wave direction, there will be attention for the 2D wave spectra in the last sections as well. Yet, first a monochromatic wave case is considered in section 5.3.

5.2. Bathymetry and grid properties

The used bathymetry is retrieved from Vaklodingen data of Rijkswaterstaat, which has a resolution of 20m. The bottom depths of the dataset are measured once every 3-6 years. The bathymetry of the Eastern Wadden Sea is given in figure 5.2(a).

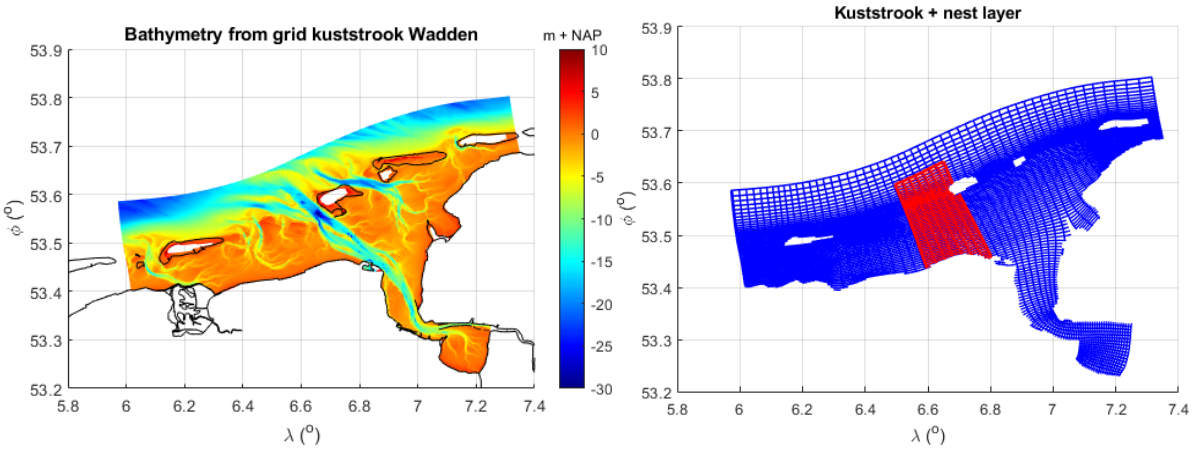

(a) Bathymetry (b) Grid and nest layer

Figure 5.2: Bathymetry corresponding to the Eastern part of the kuststrook grid, based on interpolated Vaklodingen data of 2010-2016; Kustrook grid as used in SWAN; red: outline of the nested grids.

This bathymetry is interpolated to a part of the 'kuststrook Wadden model' grid, which is a curvilinear grid that covers the entire Wadden Sea area. Figure 5.2(b) gives the grid that is used in the SWAN simulation. The red area covers the grid of the nested runs, which will be used later up in this study. The advantage of a curvilinear grid with respect to the rectangular grid is that the coastline can be captured more effectively. However, REFRAC requires a rectangular grid and hence a rectangular grid will be used in the comparison of SWAN with REFRAC, see figure 5.3. Note that Spherical coordinates where used in figure 5.2 while the Cartesian convention is used in figure 5.3.

The x-axis of the grid is imposed under an angle of 10° with respect to the Cartesian x-axis. Furthermore, the starting point of the grid, i.e. the lower left corner, is set to (X,Y) = (227123,605736). A mesh width of 100m is initially chosen in both grid directions, leading to (280,220) meshes in respectively x and y direction of the grid. This resolution is also used for the bathymetry.

5.3. Synthetic wave conditions

A monochromatic wave condition will be imposed to the Ems estuary to enable the comparison of SWAN with REFRAC. Again, the directional spreading will be chosen very narrow and the source terms are turned off at first. It is known that for example wave breaking will play a significant role in this area, however this should be neglected for the comparison to REFRAC. Both in REFRAC and SWAN, the monochromatic case will be performed in Cartesian coordinates. For further information about the SWAN settings, one is referred

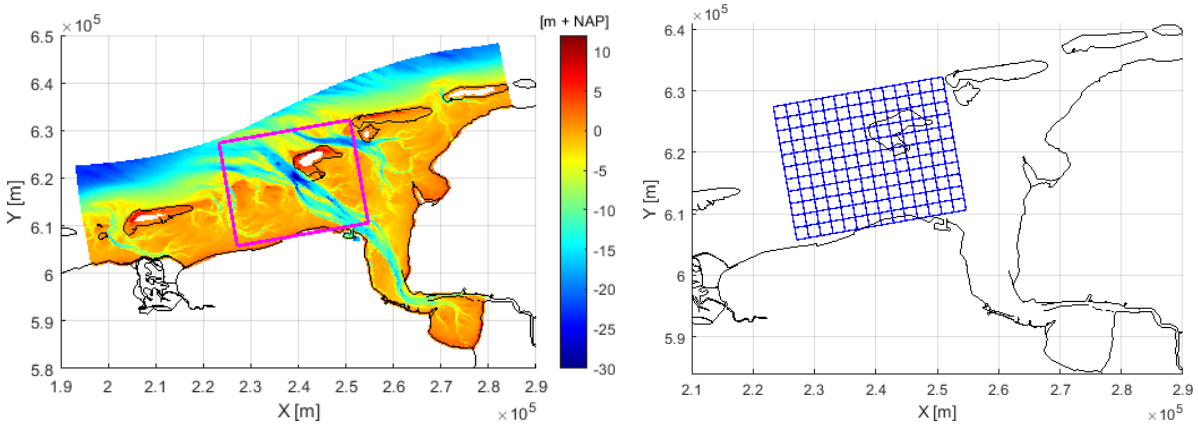

(a) Grid selection and bathymetry (b) Rectangular grid

Figure 5.3: Grid and batymetry that will be used in REFRAC and SWAN for the monochromatic wave conditions. In reality, the grid is 20 times finer than given in figure b.

to section 4.1.

The same wave conditions as for the schematic channel will be used here as well, which are a significant wave height of H_s=1m and a period varying between:

- T_p = 5s
- T_p = 10s
- T_p = 15s

The water level will vary between 0m and 2m relative to the reference level (NAP). The wave direction will be varied to observe the behaviour of wave rays for different incoming wave directions. All direction from west to east-northeast with intervals of 10° will be simulated. Not all cases will be presented in this report, however the most important features will be shown. Other wave direction outside the given range are in general of minor importance for this area. Concluding, in nautical convention the wave direction will range from -90 to 70°N. Boundary conditions will be imposed to the northern boundary in all cases. Additionally, west and east boundary conditions will be imposed respectively for western and eastern incoming waves.

5.3.1. REFRAC approach

First, analytical wave ray patterns will be calculated with REFRAC. Figure 5.4 gives the wave rays as calculated by REFRAC for T=10s and a water level of 2m. Similar figures for the wave periods of 5s and 15s are given in appendix F.2. These figures only cover part of the wave directions that were simulated and are thought to be representative. Only the cases for a water level of 2m are shown here, the same figures for a water level of 0m are given in appendix F.1. It can be concluded that shorter wave periods penetrate better into the Wadden Sea basin. This is visible for incoming wave directions between 300-350°N, where the waves come in close to parallel to the Ems channel axis. Large period waves refract stronger out of the channel onto the flats besides the Ems channel. This mode of refraction is different to the schematic channel case, since the waves came in from the side of the channel there. Interestingly, one may observe that for wave directions of around 0°N, refraction of long period waves causes wave rays to propagate into the channel instead of crossing it, which occurs for short periods. Therefore, more wave energy is present inside the basin for long period waves coming from the northern side.

Considering a water level of 0m, the waves coming from east and west are not able to propagate through the Wadden Sea basin. This is due to many flats that are just above the water level blocking the waves from reaching the Ems channel. During high tide and/or storm conditions, the water level will be higher than the here presumed zero level. It can be concluded that the refractive behaviour is lower for a higher water level. This enhances the wave penetration of both long and short period waves. Additionally, the tidal flats are largely submerged for a 2m water level, hence the wave blocking at the sides of the domain is less. This results in a larger amount of wave energy inside the basin for westerly or easterly waves for higher water levels. When

these side waves approach the channel, the resulting refraction mode corresponds more to the schematic case. Thus, two refraction modes are present in these Wadden Sea cases. Waves can start inside the channel with an equal orientation to the channel, after which they tend to refract out of the channel axis. Secondly, waves can approach a channel obliquely and may stick to the channel edge instead of crossing it. Of course, the refractive behaviour is dependent on the critical angle, which on itself depends on the depth difference and wave frequency. The figures presented here and in appendix F show that the result of T=10s is comparable to that of T=15s. This is due to the fact that the critical angle approaches a constant for lower frequencies.

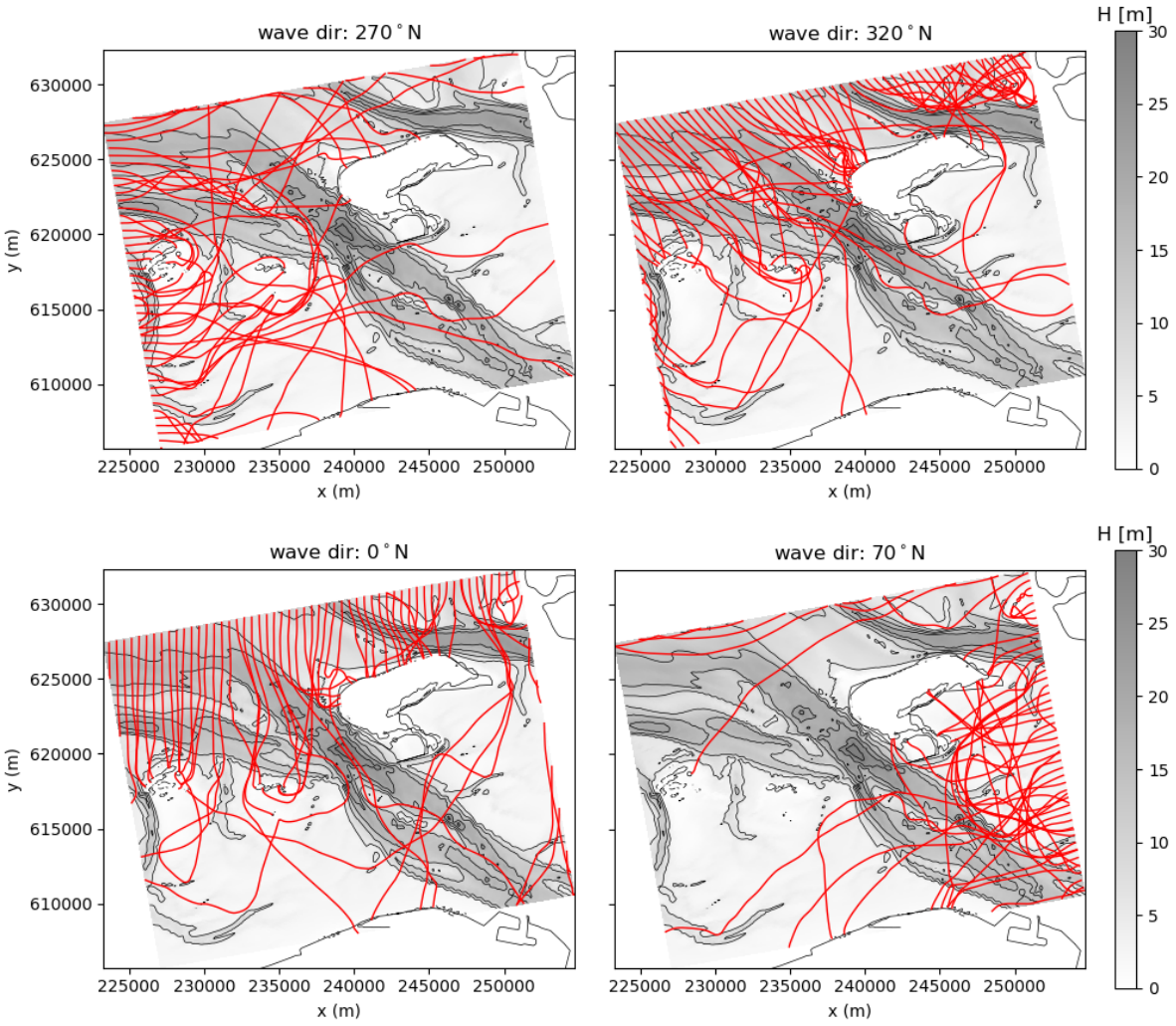

Figure 5.4: Wave rays according to REFRAC for a *period of T=10s* and water level = 2m.

Conclusion of REFRAC approach

From this section some conclusions can be given with respect to refraction at the Ems channel.

- Waves that are oriented parallel to the channel axis tend to refract out of the channel. This refractive behaviour is stronger for larger periods. When a water level of 0m with respect to the reference level is considered, the wave penetration of long period waves appears to be very limited.
- For a water level of 2m it is found that the wave penetration through the Ems channel is significantly larger than for a 0m water level. Also the wave propagation inside the Wadden Sea basin itself is larger, since there are less emerged flats that block the waves. The largest wave penetration from offshore is thus present for wave directions between 300-350°N for shorter wave periods and higher water levels.
- For the schematic channel case, the results for a period of 10s and 15s were similar due to the fact that the critical angle becomes constant for low frequencies. Where this constancy over frequency begins is

dependent on the relative depth difference. For the depth changes present in the Wadden Sea, the critical angle should theoretically be in the same order for both the 10s and 15s period. It is thus expected that the differences in wave refraction and hence penetration are small between these periods. This is also what follows from the REFRAC results.

5.3.2. SWAN approach

The same cases will now be considered using a SWAN simulation to get insight on the general behaviour of the waves according to SWAN in this area. The results of this are presented in figure 5.5 for a period of 10s. The water level is set to 2m, for simulations concerning other wave periods and a water level of 0m one is referred to appendix G. In this appendix, also wave rays from SWAN are shown for both the 0m and 2m water level. Initially, a mesh width of 100m is applied together with a directional resolution of 1°. The numerical scheme that is used is the SORDUP scheme. Later on in this section, variants will be presented on these settings.

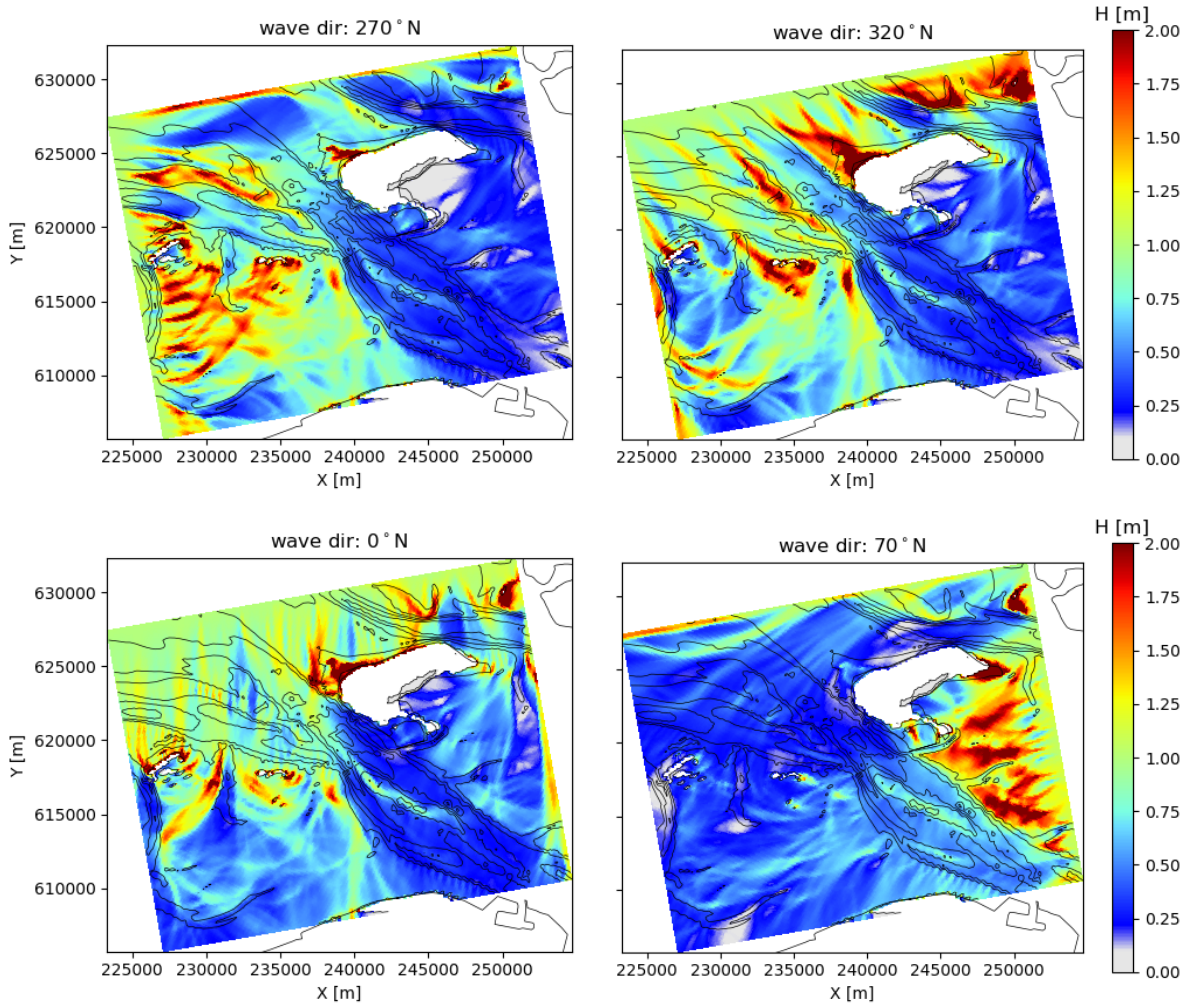

Figure 5.5: Wave height according to SWAN (propagation terms only) for T_p=10s and water level = 2m.

From the figures it can be observed that most wave penetration will be present in case the wave direction is close to parallel to the Ems channel axis. This is true for both SWAN and REFRAC. Furthermore, it is again found that the wave penetration is larger for small wave periods compared to the long wave periods. Different patterns of refraction can be seen in the figures, which are present in both REFRAC and SWAN. First of all, offshore of the islands the wave rays converge, leading to a significant increase in wave height at the island coasts. Secondly, it can be nicely observed that the elevated bottom inside the Ems channel ensures waves to get trapped here. The wave ray, and hence wave energy, meanders on top of the small flat since it is not able to enter the channel anymore. This can for example be seen on the bottom left plot of both figure 5.4 and

figure 5.5 for REFRAC and SWAN respectively.

Appendix F.1 and F.2 show the wave height along the wave rays according to REFRAC. Here a ray distance of 10m is assumed, therefore the rays are very close to each other. This causes caustics to become present where rays converge or cross, for more informations about caustics one is referred to section 3.1.1. Comparing the wave height of REFRAC with the SWAN results, leads to the conclusion that the largest differences inside the basin are observed for incoming waves from 310-360°N for all period variants. Here, REFRAC shows a larger amount of wave energy that is present inside the channel near the coast, whereas this is not present in SWAN. This is an example of caustics to become visible in the REFRAC results, leading to unrealistic high wave heights. Interestingly, the differences become less clear for larger wave periods since here the waves refract out of the channel before entering the basin for both models. Hence, the SWAN results are comparable to REFRAC in absolute sense. Overall, the patterns of REFRAC and SWAN are comparable, giving confidence in both models.

According to previous studies, the penetration of low-frequency waves into the Wadden Sea basin is underestimated by SWAN compared to measurements (Alkyon, 2009a; Groeneweg et al., 2014). It was suggested that this was due to an enhanced wave refraction, causing waves to turn out of the channel and dissipate on the tidal flats. This hypothesis can not yet be substantiated with the figures presented here, since also REFRAC shows a large amount of long period waves to be refracted out of the Ems channel. Yet, focusing on a wave direction of 320°N, it can be observed that SWAN gives a relatively large amount of wave energy at the upwave channel edge for a water level of 0m, see figure 5.6. Focusing on the channel above Borkum, one might see large differences between SWAN and REFRAC, where SWAN shows a lower wave height inside the channel. These are some details that suggest a stronger refractive behaviour in SWAN. When applying a water level of 2m, the situation becomes as given in figure 5.7. For this case, the wave height at the coast is similar for both models. Also at the other locations, the results are more similar. From this it is suggested that the SWAN results approach REFRAC better for a water level of 2m. In general, an increase in water level causes the depth gradient to reduce, and hence the wave turning rate decreases. Therefore, wave refraction is smaller and the waves are able to penetrate further into the basin. The hypothesis that SWAN performs better for higher water levels will be treated in the last part of the following section. The wave ray patterns for both a water level of 0m and 2m are shown in respectively the upper and lower plots of figure 5.8. In general, the characteristics match well between both models.

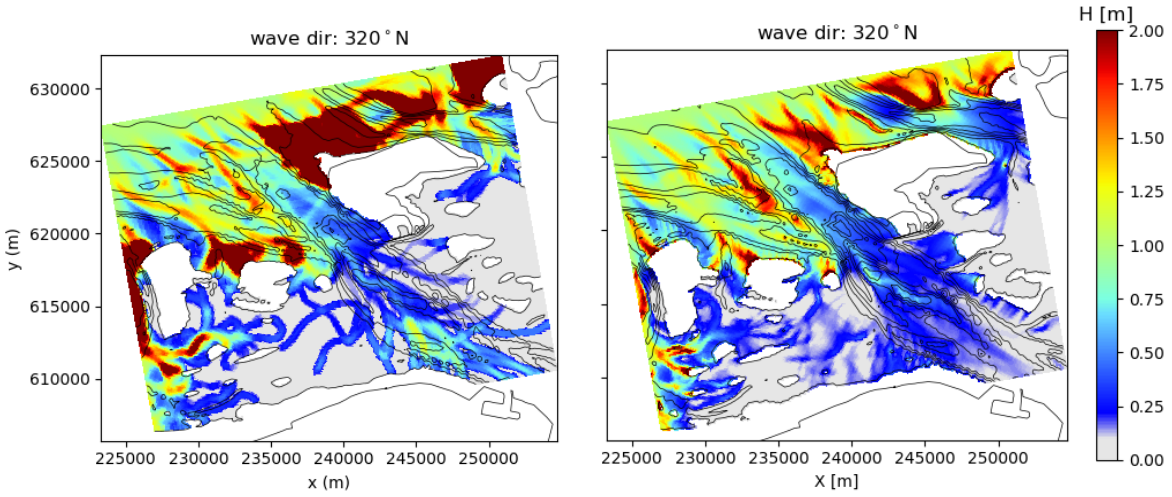

Figure 5.6: Wave height according to left: REFRAC and right: SWAN for T_p=10s and water level =0m.

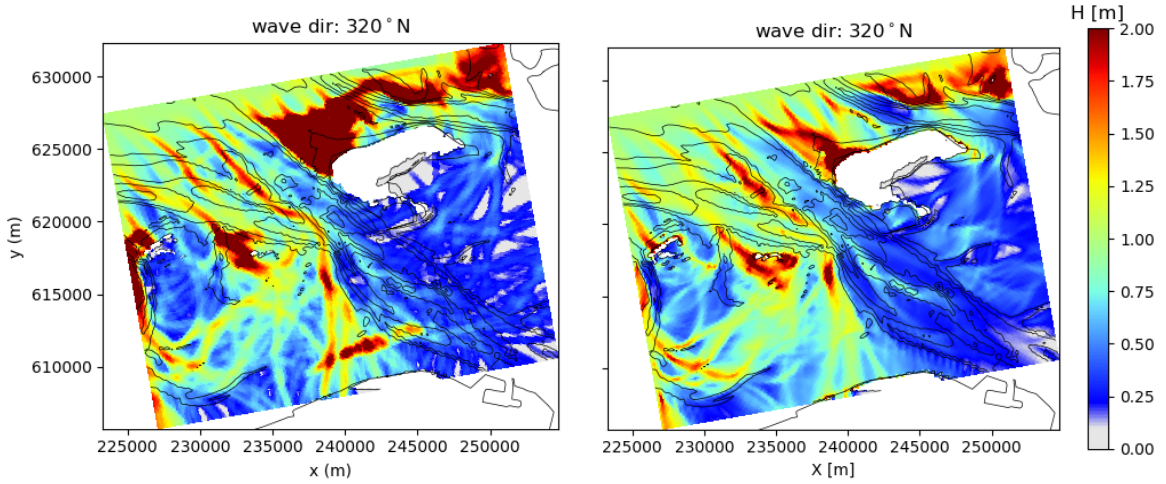

Figure 5.7: Wave height according to left: REFRAC and right: SWAN for T_p=10s and water level = 2m.

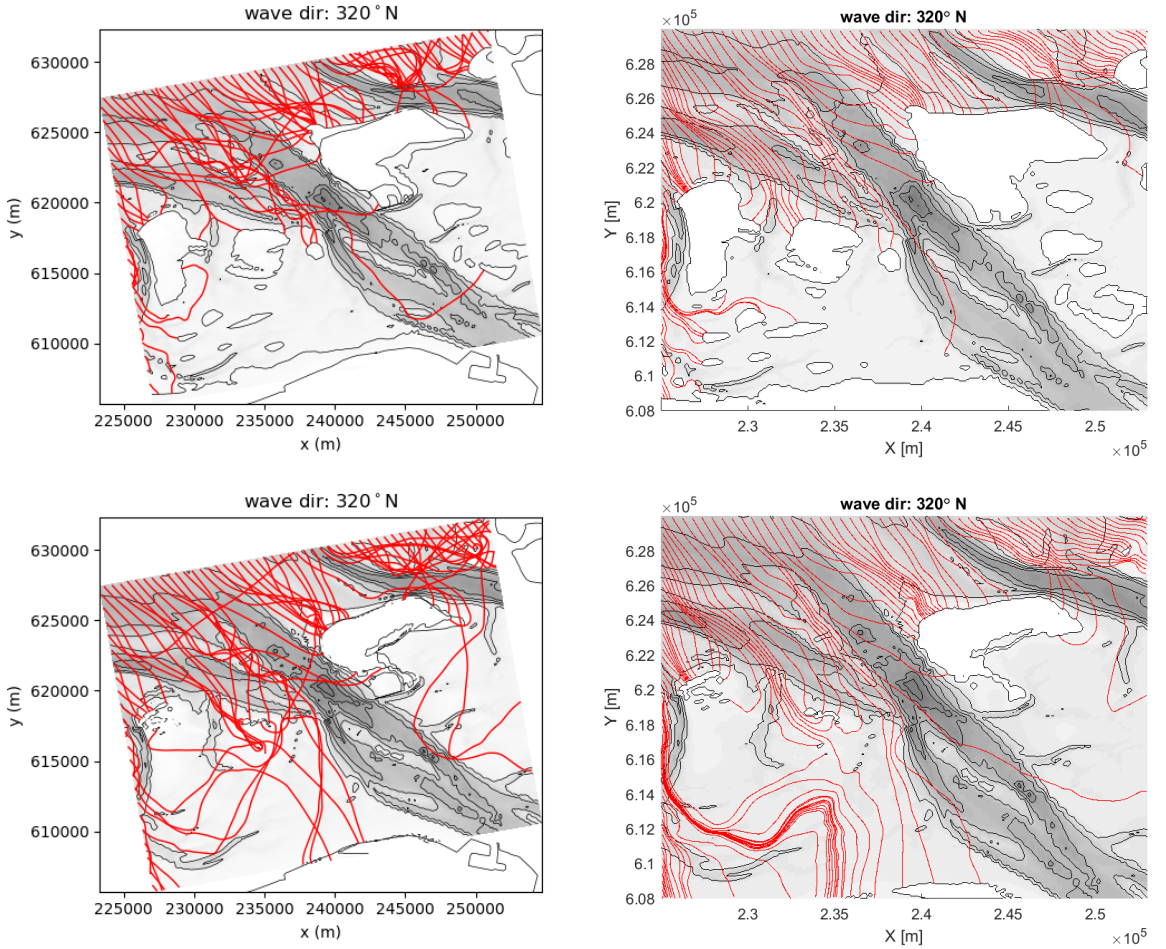

Figure 5.8: Wave rays according to left: REFRAC and right: SWAN for T_p=10s and a water level of upper: 0m and lower: 2m.

Influence of spatial resolution

In the above results, a fixed mesh width of 100m was applied. In this paragraph this will be varied to check the influence of the spatial grid resolution. Two variations for the reference mesh width of 100m will be con-

sidered, which are respectively *50m* and *200m*. For both cases, the implemented bathymetry will still have a mesh width of 100m. For all considered cases the SORDUP scheme will be applied.

Figures 5.9 and 5.10 give difference plots of the wave height for varying mesh widths and a water level of 2m. Figure 5.9 shows an incoming wave direction of 270°N, whereas figure 5.10 shows a wave coming from 320°N. Appendix G.3.1 gives the same figures, only then for a water level of 0m. All variants are considered relative to the grid size of 100m. From these figures, several conclusions can be drawn.

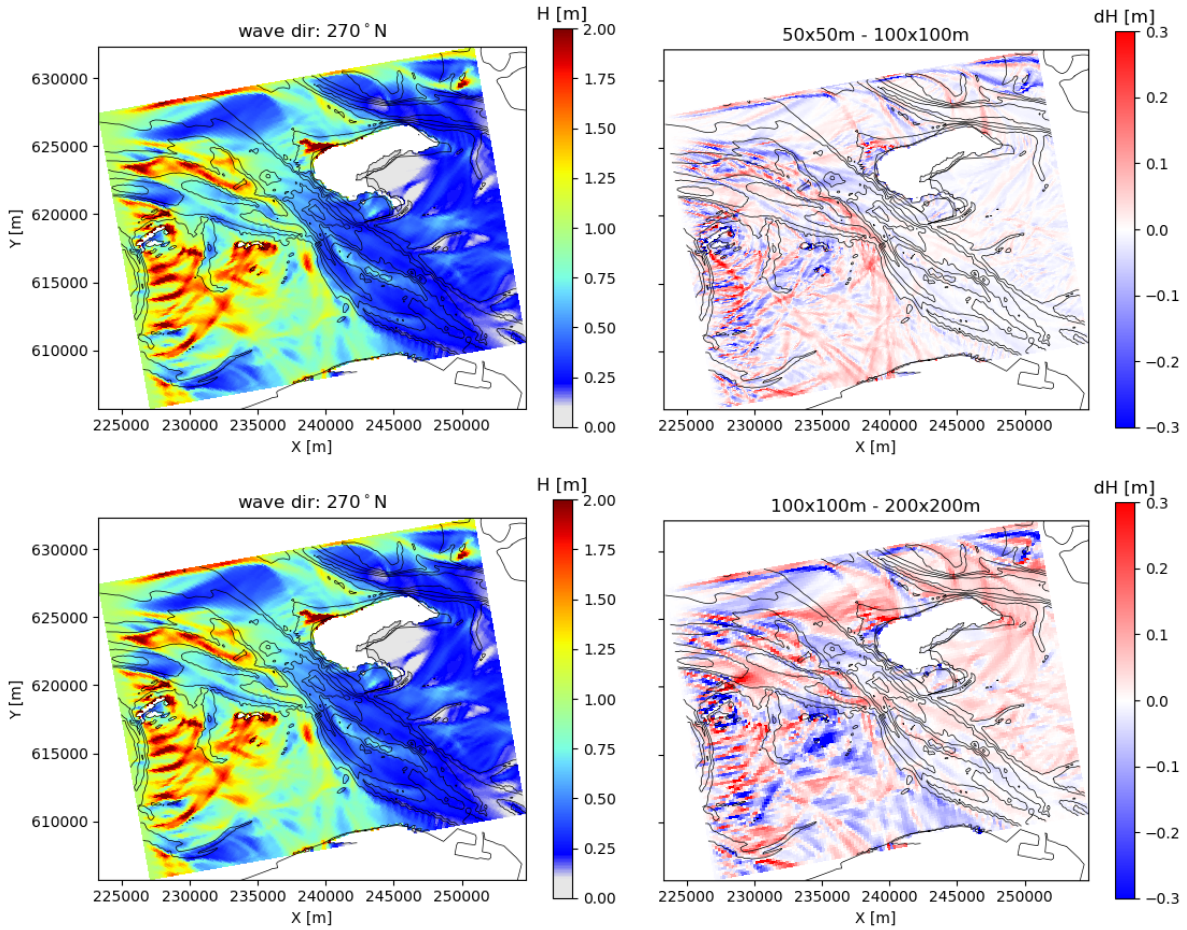

Figure 5.9: Left: wave height plot for a mesh width of 100m; Right: Wave height difference for the mesh width of 50m and 200m for respectively the upper and lower plot. conditions: wave direction of 270°N, T_p=10s and η=2m.

First of all, it can be seen that the differences between a 100m and 200m grid are larger than between the 50m and 100m grid. This could however be caused by a different schematisation of the bathymetry. To check this, some cross-sections have been made of the bathymetry for the different grid sizes. The bathymetry of the 50m and 100m grid are equal, since the 50m mesh width is interpolated from the 100m resolution bathymetry. For the 200m mesh width it follows that some small deviations are present. However, in most cases these are small. Still, it could be causing enhanced differences in wave energy. To go one step further, simulations have been performed with a mesh width of 25m. These results are given in appendix G.3.2. It follows that the wave height differences between the 50m and 25m mesh width are relatively small. Especially at the coast, which is in fact the area of most interest, there is negligible wave height difference.

Considering the cases with an incoming wave of 270°N, more waves are able to cross the channel for a finer grid at the ebb delta.The blue area inside the channel of the upper plot of figure 5.9 suggests that the waves are directed stronger into the channel for the coarser grid. From the lower plots of figure 5.9 it can be noted that also inside the basin a larger part of the wave energy is able to cross the channel for the finer grid.

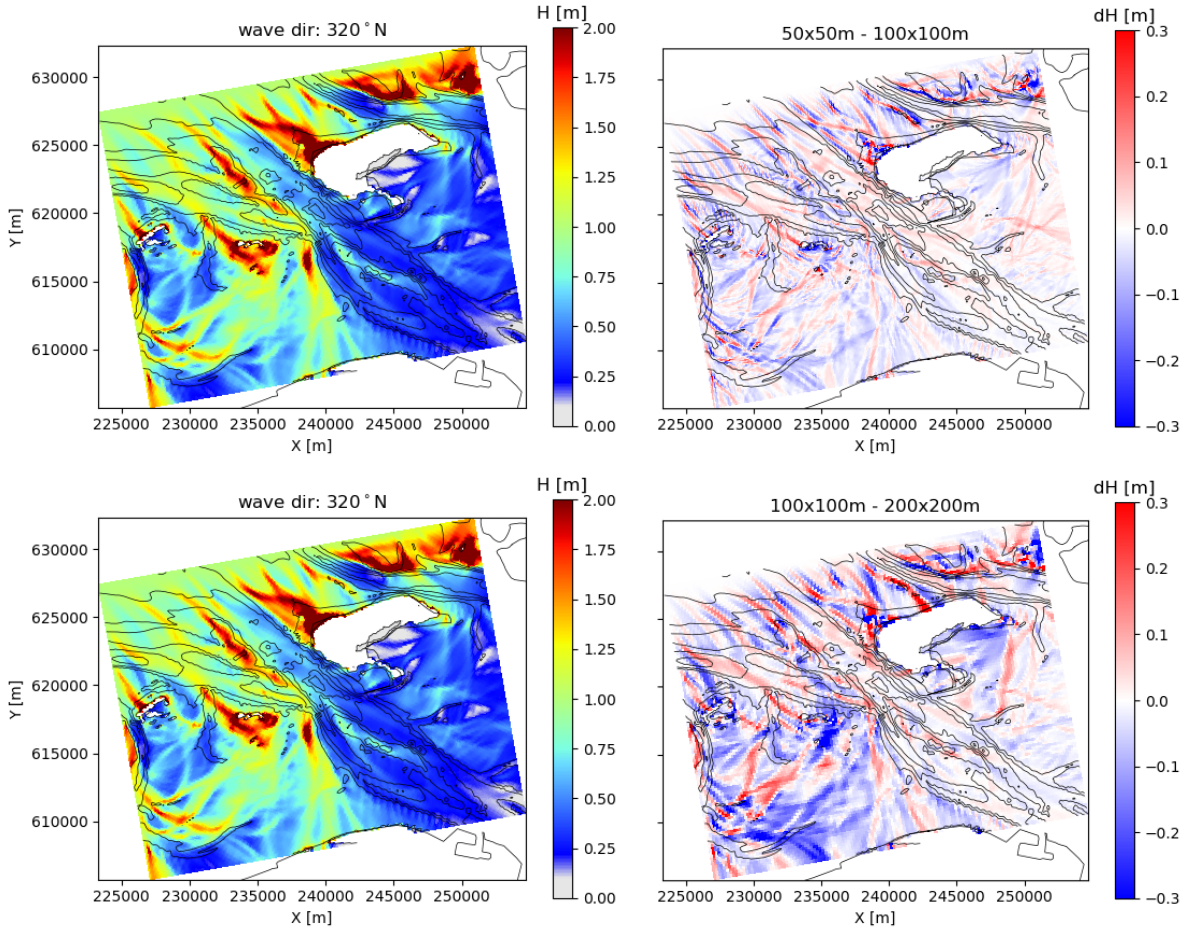

Figure 5.10: Left: wave height plot for a mesh width of 100m; Right: Wave height difference for the mesh width of 50m and 200m for respectively the upper and lower plot. conditions: wave direction of 320°N, T_p=10s and η=2m.

Subsequently, for a wave direction of 320°N, the wave height for a fine grid is higher in the channel at the ebb delta, see figure 5.10. This suggests that for a coarse grid the refraction is stronger, since a larger fraction of wave energy stays in the channel for the fine grid. This can be supported by the fact that south-west of the channel in the ebb-delta the wave height for a coarse grid is higher.

As was done previously, the error of the grid variants can be quantified with the RMSE in significant wave height, see appendix C for the definition. The grid variants will be compared to a reference grid of 25m, which is the smallest mesh width that is tested in this case. Since the domain consist of shallower and deeper parts, the error will vary dependent on the considered part. It is chosen to look at the tidal flat in front of the coast near Uithuizerwad, since this part is most relevant for hydraulic design. Figure 5.11 gives the considered domain in blue, which consists of in total 498 observation points.

The rms-errors are given in table 5.1. The errors are determined for different combinations of wave period, direction and water level. Only the errors of incoming wave directions 270 and 320°N are given here, since the largest errors are found to be between 270-350°N. From the table it follows that the RMSE varies between 0-11cm, where highest values are found for a water level of 2m in combination with T_p>10s and a wave direction of 320°N. Furthermore, coarser meshes lead to a larger RMSE. Figure 5.12 shows the dependency of the RMSE on mesh width for different combinations of water level, wave direction and period. The estimated order of accuracy varies between p=1.0-1.2 for η=0m and p=1.2-1.6 for η=2m. Considering a wave direction of 270°N, a period of 5s leads to largest order of accuracy, while the opposite is true for waves coming from 320°N. However, the differences for a wave direction of 320°N are less significant.

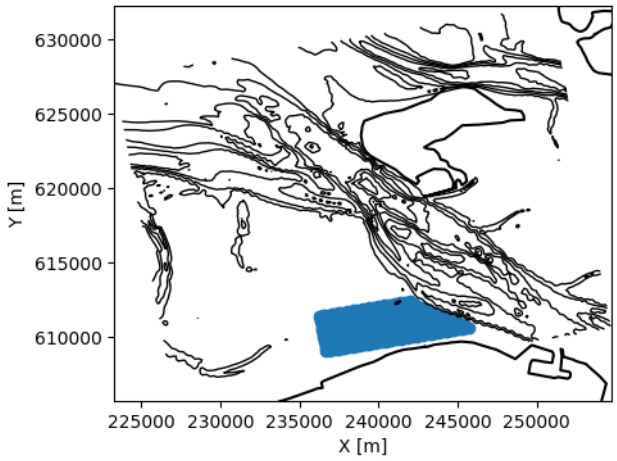

Figure 5.11: Selected part for which the RMSE will be determined, given in blue.

Table 5.1: RMSE in *m* for different combinations of wave period, wave direction, water level and mesh width. A mesh width of 25m is the the reference width, thus all errors are relative to the mesh width of 25m. The relative error RRMSE is determined by dividing the RMSE by the mean wave height in the considered area.

		η=0m, RMSE [m]		η=0m, RRMSE [%]		η=2m, RMSE [m]		η=2m, RRMSE [%]	
		270°N	320°N	270°N	320°N	270°N	320°N	270°N	320°N
T_p=5s	50m	0.007	0.022	*13.1*	*13.8*	0.015	0.016	*2.8*	*2.8*
	100m	0.015	0.042	*27.0*	*26.0*	0.040	0.044	*7.5*	*8.0*
	200m	0.026	0.075	*47.9*	*47.0*	0.122	0.094	*23.0*	*17.0*
T_p=10s	50m	0.016	0.019	*11.9*	*11.4*	0.021	0.019	*2.6*	*2.7*
	100m	0.032	0.042	*24.0*	*25.5*	0.050	0.051	*6.2*	*7.4*
	200m	0.055	0.064	*41.1*	*39.5*	0.077	0.104	*9.5*	*15.2*
T_p=15s	50m	0.015	0.017	*10.2*	*10.5*	0.022	0.021	*2.6*	*2.9*
	100m	0.032	0.039	*22.5*	*23.9*	0.047	0.057	*5.6*	*8.0*
	200m	0.057	0.064	*40.4*	*39.2*	0.078	0.108	*9.3*	*15.1*

The RMSE suggests that the error for a higher water level is larger, however also the mean wave height is larger. Therefore, the RRMSE, relative RMSE, is also given. This shows that the error relative to the mean wave height is significantly lower for a water level of 2m, with a maximum error of 15% instead of 40%. Concluding, the error due to coarse resolution reduces with increasing water level. This confirms the statement that was made based on the visual comparison to REFRAC results. Notable is that the RRMSE is almost independent of the incoming wave direction for relatively fine grids, i.e. 50m. For a 2m water level, also the RMSE is similar for all wave periods and direction with an error of 2cm (3%). Linking back to the schematic channel case, an equal conclusion with respect to mesh widths followed there, see figure C.2. Here the dependency of the RMSE to the wave direction was shown per mesh width, of which followed that the RMSE of large mesh sizes varied stronger over wave direction. Also for this case the error of smaller mesh sizes is almost independent of the wave direction. The study of Crosby et al. (2019) did a similar analysis for the coast from Santa Barbara to San Diego, USA. They compared SWAN with different spatial resolutions to a backward ray-tracing model, were they found that the misfit was almost independent of wave frequency for a 90m mesh width. On the other hand, coarser grids showed a significantly larger misfit for lower frequencies. Additionally, Crosby et al. (2019) concluded that a 90m mesh width was closest to the ray-tracing model, however this was also the smallest considered mesh width. The maximum RMSE was found to be 4cm for 90m resolution, i.e. around 4%, which is in the same order as the errors found in figure 5.12 for this study.

Concluding all, a resolution of 50m gives a sufficient prediction of refraction in this area. The difference between the 25m and 50m resolutions is maximum order 2cm in wave height for all considered cases. Comparing the crest turning, $\Delta\theta$, according to SWAN and Snel's law in the ebb-delta (here wave refraction is most

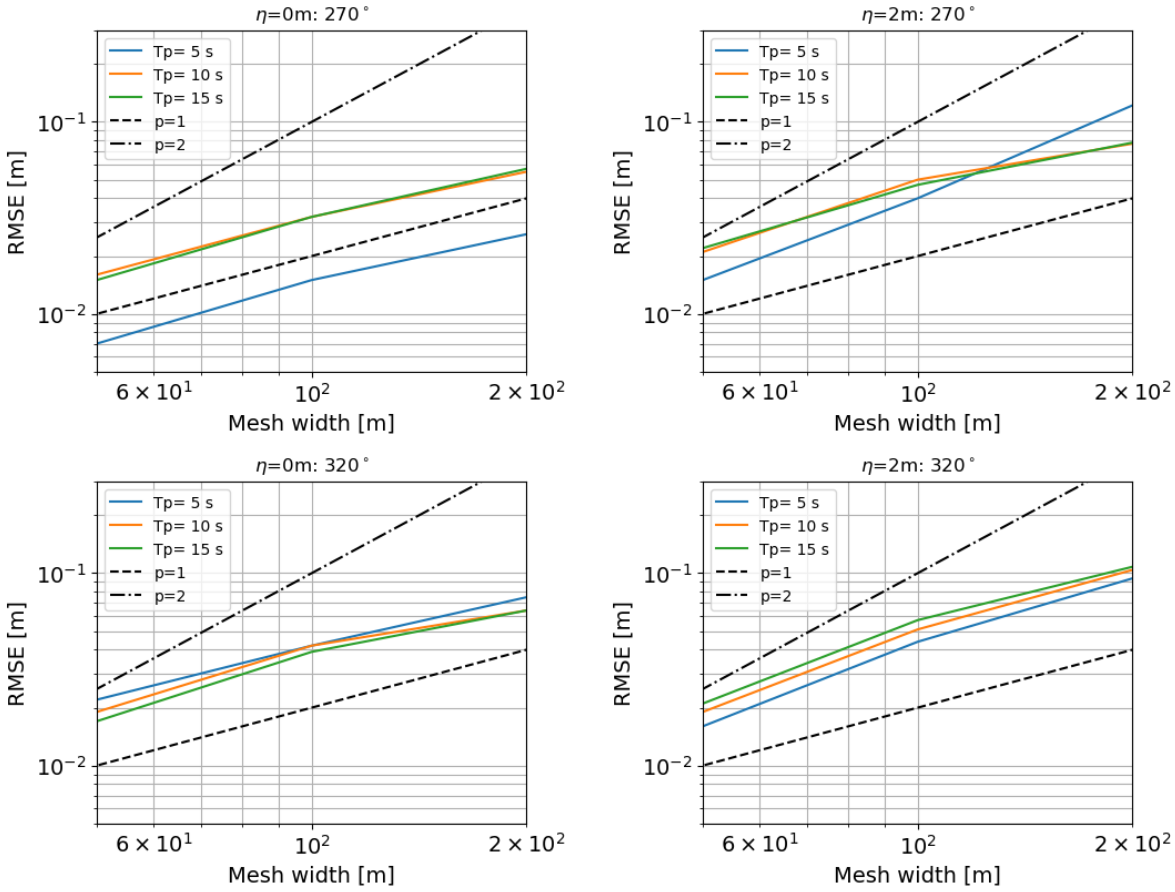

Figure 5.12: RMSE as function of mesh width for the different water levels, wave directions and periods. The lines p correspond with the order of accuracy, as mentioned in equation 4.5.

pronounced), gives a difference in crest turning of order 3°. On the other hand, a resolution of 25m and 100m gives a difference in turning of respectively 1° and 9°. These numbers are based on the maximum differences that will be found, hence a maximum difference of 3° is considered allowable. Appendix E gives further details about the crest turning, where section E.5 is specified to the Wadden Sea case.

Influence of directional resolution

In literature and in the previous schematic case it was found that also the directional resolution potentially influences the accuracy of modelling refraction (Alkyon, 2009a). This will be tested for the Ems estuary, where again a monochromatic wave will be used as first assessment. Two directional resolution variants are taken of 2° and 0.5° which correspond with respectively 180 and 720 bins. The results will be compared to the reference resolution of 1°, in other words 360 directional bins. The SORDUP scheme will be used in all cases.

Figure 5.13 shows the wave height difference plots compared to a resolution of 1° for a water level of 2m. Here, a wave direction of 320°N together with a period of T_p=10s is shown. It is found that the influence of the directional resolution is rather small. This could be due to the fact that the reference resolution is already quite small. However, this reference was chosen since a coarser resolution was not able to capture the narrow incoming wave spectrum, as was concluded in the schematic channel case. The colour scale is plotted equal to the other cases, to get a good vision of the relative importance of the sensitivities. However, in this case it also leads to a lack of details. From the figure it can be seen that the difference between the 180 bins and 360 bins case is larger than for the 720-360 bins case. For this last one the largest differences are in the order of 5cm, whereas the mean deviation in the domain is far less than 1cm. Therefore it is thought that the resolution of 1° was sufficient in this case. The observed effect is similar for other period and direction variants, hence for all cases the impact of directional resolution is small.

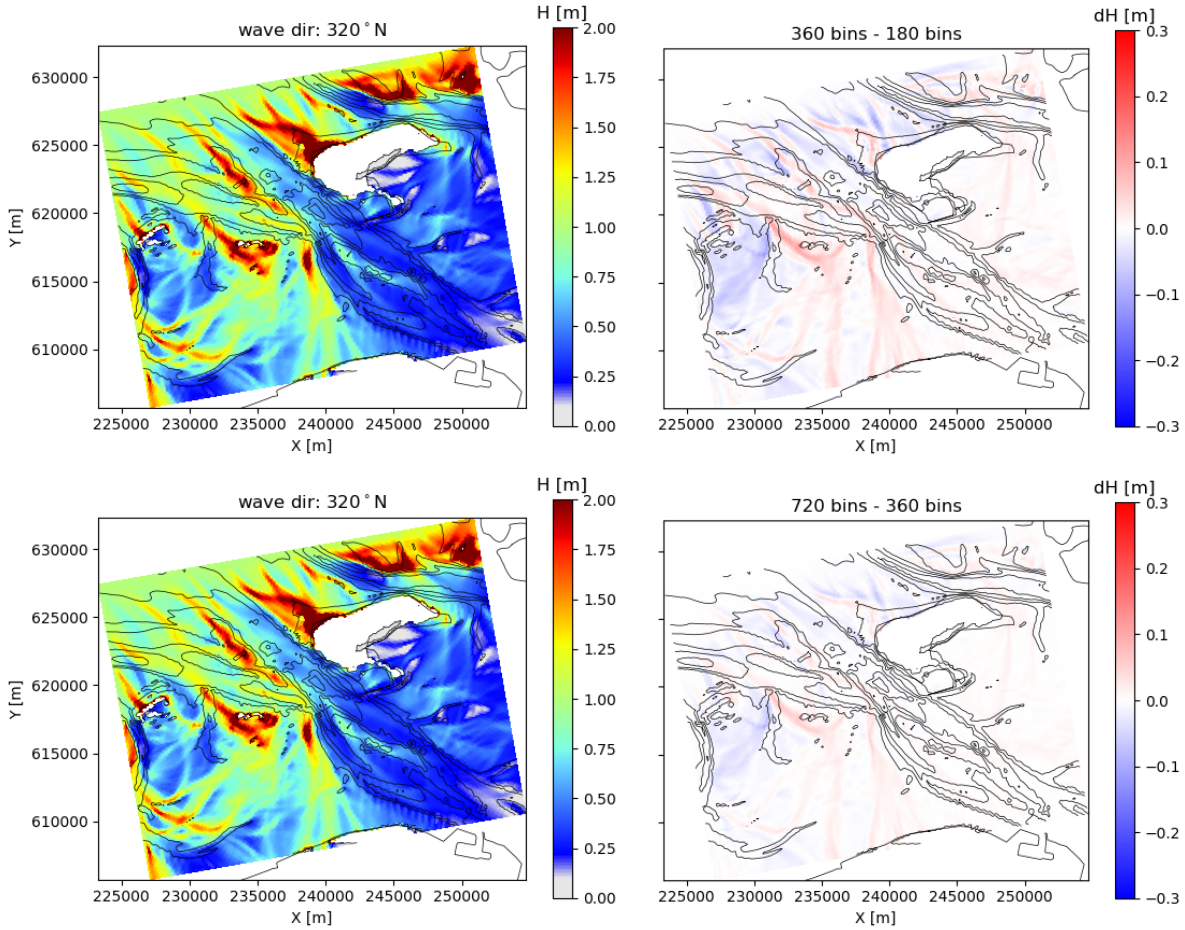

Figure 5.13: Left: wave height plot for a directional resolution of 1°; Right: Wave height difference for the directional resolution variants of 2° and 0.5° respectively. conditions: wave direction of 320°N, T_p=10s and η=2m.

Influence of numerical scheme

This part discusses the influence of the applied propagation scheme in SWAN, i.e. SORDUP and BSBT. In the previous chapter it was concluded that the overestimation of the critical angle was larger for the BSBT scheme, leading to enhanced refraction. This conclusion will be checked for a more complex bathymetry.

Figures 5.14 gives the wave height distribution for applying the SORDUP scheme and the wave height difference between SORDUP and BSBT. The wave directions are respectively 270°N and 320°N with a T_p=10s and a water level of 2m. It can be seen that the wave height for SORDUP is larger inside the Ems channel in both cases. These results support the conclusion that the BSBT scheme induces a stronger refractive behaviour, as was also found for the schematic channel case.

Subsequently, a combination of the spatial resolution variants and the numerical scheme variants will be assessed. Plotting the wave height difference of a 50m-100m mesh width for both BSBT and SORDUP gives the figures as presented in respectively figure 5.15 and 5.16. Considering the BSBT scheme, the wave energy that propagates through the Ems channel is higher for a finer grid, see figure 5.15. Therefore, a finer grid results in less wave refraction when the BSBT scheme is applied. In case SORDUP is used, the result is obviously equal to figure 5.10. Therefore the same conclusion can be made.

Two conclusions can be drawn from the above:

1. The BSBT scheme induces enhanced wave refraction compared to the SORDUP scheme.
2. The difference between the solutions of the numerical schemes reduce for finer grids.

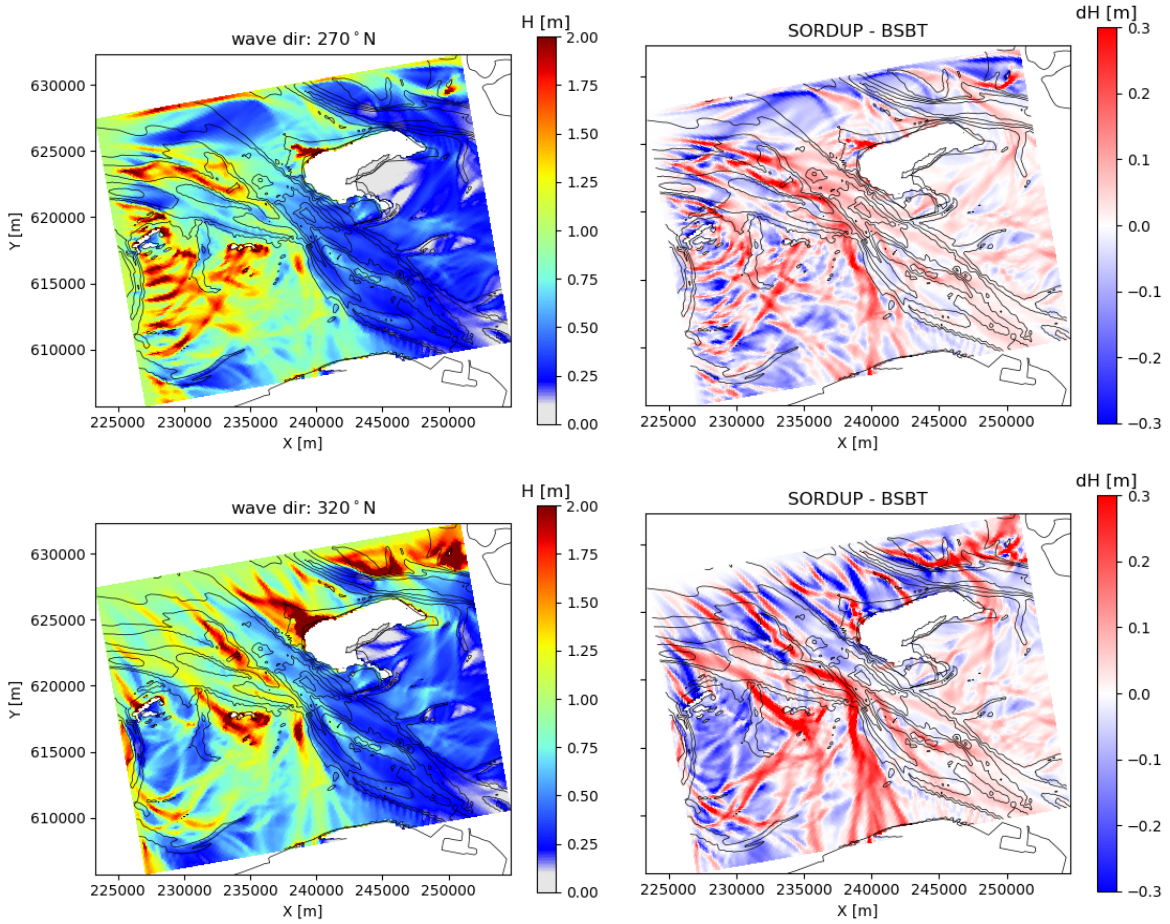

Figure 5.14: Wave height with left: SORDUP and right: SORDUP-BSBT; Upper plots: 270°N, lower plots: 320°N wave direction, conditions: T_p=*10s* and water level=2m.

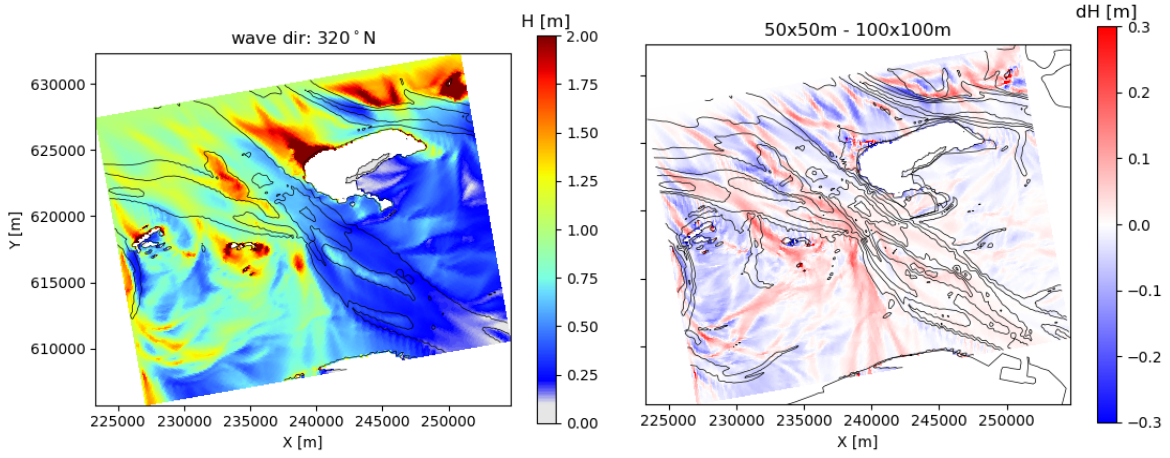

Figure 5.15: Wave height for BSBT scheme with left: dx=100m and right: dx=50m-100m, conditions: T_p=*10s* and water level=2m.

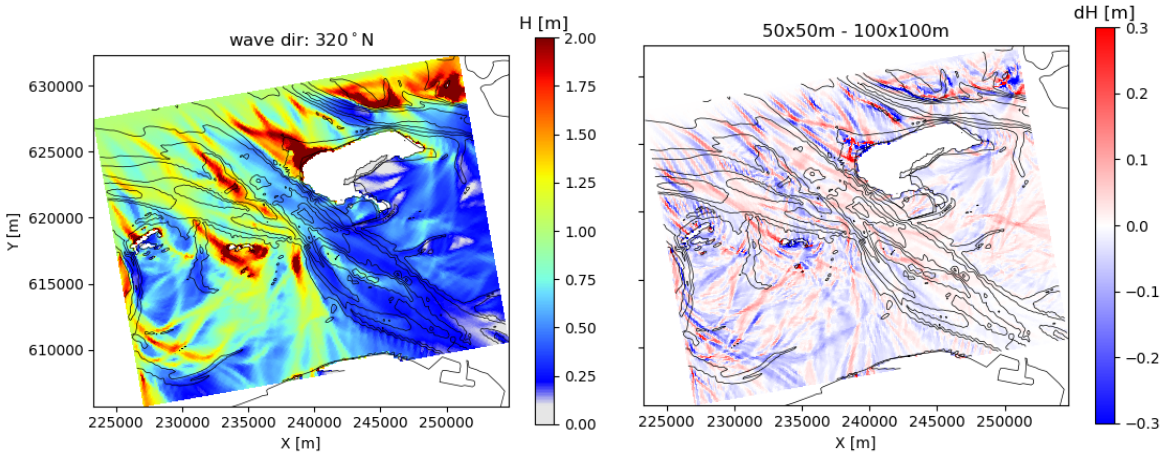

Figure 5.16: Wave height for SORDUP scheme with left: dx=100m and right: dx=50m-100m, conditions: T_p*=10s* and water level=2m.

Conclusion of SWAN approach

Summarising the above, the following conclusions can be made:

- Considering the wave height inside the Wadden Sea basin, SWAN deviates the most from REFRAC for waves coming from 310-360°N. For these directions, SWAN shows less wave penetration than REFRAC. For locations where REFRAC predicts refraction, SWAN also shows refraction to occur. The prediction of the wave height in SWAN corresponds better to REFRAC for a higher water level.
- It can be concluded that a coarser spatial resolution induces a stronger refractive behaviour. Considering the RMSE in wave height of a coastal flat, the error does increase with mesh width, where 25m is the reference width. The RMSE is proportional to the mesh width to power p=1.0-1.2 for a water level of 0m and p=1.2-1.6 for 2m water level. For T_p>10s, largest errors are found for a wave direction of 320°N and a water level of 2m, where the error becomes order 15%. For the grid size of 50m, the RMSE of the wave height in the domain is almost independent of wave period and direction and equals 2cm (3%) for a water level of 2m. For storm conditions it can thus be concluded that a resolution of order 50m is sufficient. This is in the same order as the study of Crosby et al. (2019), who suggested that a resolution of 90m is sufficient when comparing the SWAN results to a backward ray-tracing model.
- In general, a lower wave height is found at the coast for the fine grid if the waves come in from 270-300°N and the period is low. For these cases, the waves are not able to reach the coast if refraction would be absent. A stronger refraction for the coarse grids turns the waves inside the basin towards the coast. Furthermore, for wave directions parallel to the Ems channel, thus around 320°N, waves turn stronger out of the channel for coarser grids, after which they propagate over the tidal flats to the coast. Since wave breaking and other dissipation terms are not yet taken into account, the waves can freely propagate over these tidal flats such that all energy reaches the coast.
- The influence of the directional resolution is relatively small for this case. This is due to the imposed narrow spectrum, which requires a small resolution on itself. Therefore, coarser resolutions cannot be tested in this part. The influence of the directional resolution will also be analysed for a more realistic wave energy spectrum, which will be imposed in the coming part.
- The BSBT scheme gives enhanced wave refraction when comparing the results to a SORDUP scheme. Since it was already concluded that the results for applying SORDUP overestimated the refraction, this is certainly the case when the BSBT scheme is used. The difference between the schemes reduces with increasing spatial resolution.

Overall, It can be concluded that SWAN shows similar patterns to REFRAC. Subsequently, the RMSE in wave height compared to a resolution of 25m in SWAN showed a maximum error of 11cm, i.e. 15%, for a 200m mesh width and a water level of 2m. The RMSE of a 50m grid for a water level of 2m was found to be order 2cm, i.e. 3%, which is considered small. Concluding, a mesh size of order 50m is sufficient for modelling refraction at the Ems channel if the source terms are neglected. Furthermore, the SORDUP scheme shows a stronger wave penetration into the Wadden Sea basin compared to the BSBT scheme.

5.4. Realistic wave conditions

In the previous part of this chapter, the focus was on a monochromatic incoming wave direction. To obtain insight in the refractive behaviour for a realistic case, a more complex incoming wave spectrum will be chosen. From the year 2010, the most severe storms took place in the years 2013, 2015 and 2017. Buoy measurements are available for all of these years. Furthermore, additional measurement devices were placed on the Uithuizerwad which have measured the conditions during the 2015 and 2017 storms. Since extra data is available, one of these storms will be considered in this case study.

5.4.1. Storm selection

From the monochromatic wave case it was concluded that wave penetration was predominantly present for waves coming from 300-350°N. Therefore, the wind and hence wave direction largely influences the theoretical wave penetration. To get a quick overview of the prevalent wind direction, wind roses are generated as given in figure 5.17. This wind data is measured at measuring station Lauwersoog. In principle, data of Huibertgat would be preferred for the study area, since land-sea effects will be smaller at this location. However, at the time of both storms there is no measured data available for this station. Thus, while it is thought that the wind conditions at Lauwersoog are slightly less severe, it is closest to the actual wind that occurred during the storms in the area. It can be seen that the wind direction in 2015 was mostly from the SW for the peak of the storm. The wind varied between south and west during the considered time range. In 2017, the peak wind speed occurred for a wind from N-NW, with the spreading of the wind direction ranging mainly from west to north. The maximum absolute wind speed is in the same order for both storms. With respect to wave penetration and occurring wave refraction along the Ems channel it is thus chosen to look at the storm of January 2017. Atmospheric models have been used in previous studies to approximate the wind speed and direction at Huibertgat, which gives a better estimate than the situation at Lauwersoog. According to this data, the wind direction during the peak of the 2017 storm was 329°N with a magnitude of 20.3 m/s (Geleynse, 2017).

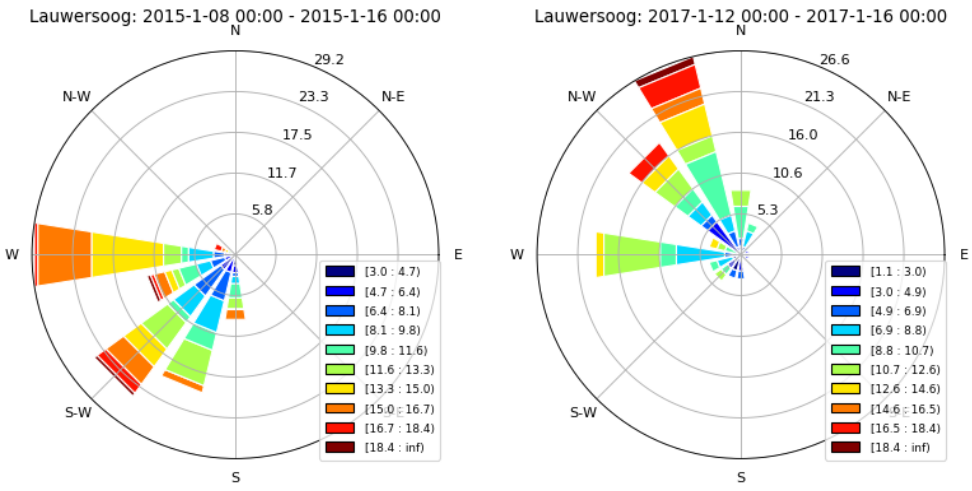

(a) January 2015 (b) January 2017

Figure 5.17: Wind roses at Lauwersoog for (a) 2015 and (b) 2017. The colours indicate the wind speed, whereas the height of the bar gives the frequency of occurrence. The data is retrieved from KNMI (2019).

5.4.2. Wave boundary conditions

Boundary conditions (BC) will be retrieved from the offshore buoy measurements taken at 'Westereems West' (WW), see figure 5.18. This is located close to the northern boundary of the curvilinear grid as can be seen in the figure, this also holds for the rectangular grid as applied in the previous sections. It is thought that these measurements are representative for the conditions in the area. Looking at the bathymetry, it is thought that buoy WW is located just offshore of the breaking zone. If the boundaries of the domain are placed outside the breaking zone, then the model is able to spin-up and the breaking process can be modelled without boundary effects. The location of Westereems Oost (WO) is fairly close and presumably in the breaking zone, therefore these measurements are less suitable for the BC.

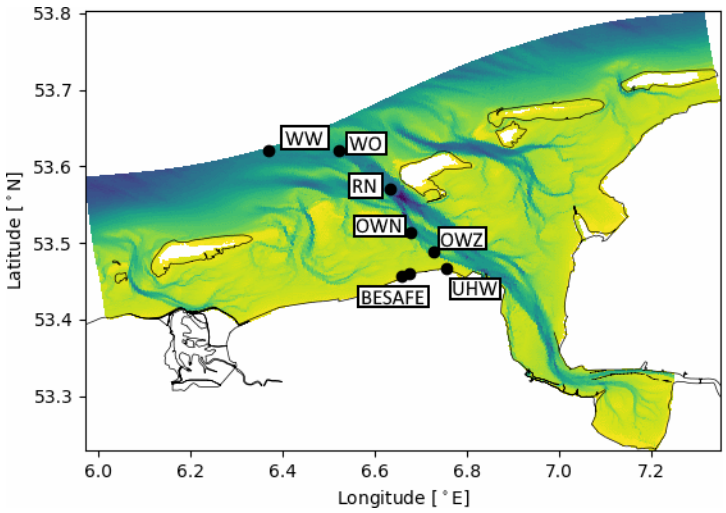

Figure 5.18: Locations of the used measurement stations. WW=Westereems West, WO=Westereems Oost, RN=Randzelgat Noord, OWN=Oude Westereems Noord, OWZ=Oude Westereems Zuid, UHW=Uithuizerwad.

Figure 5.19(a) gives the measured variance density spectra at WW during the peak of the storm at 13 January 2017, 23:50h. This data will be imposed to the Northern domain boundary in SWAN, hence the BC is chosen constant. The directional data is measured per frequency component, see figure 5.19(b). Here both the directional spreading and the absolute wave direction are given. It can be noted that the directional spreading is around 50°, which is relatively broad. The frequency data ranges from 0.03 to 0.5 Hz, with 47 frequency bins.

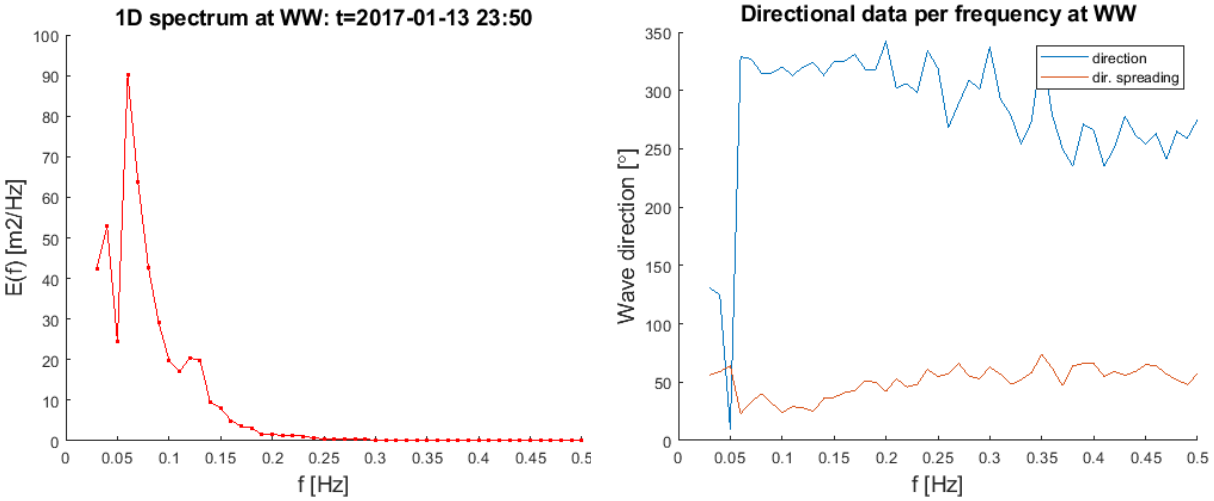

(a) Variance density spectrum

(b) Directional data over frequency

Figure 5.19: Left: Variance density spectrum; right: Wave direction and directional spreading over frequency. Both figures are from 13 January 2017, 23:50h at Westereems West (WW).

5.4.3. Hydrodynamic boundary conditions

For a proper prediction of the wave behaviour, it is important to know the hydrodynamic current as well as the water level that are present in the domain. Generally, the water level plus current velocity and direction are retrieved from flow models such as Delft3D. However, using an additional model will introduce other uncertainties. Therefore, it is chosen to work with SWAN only and exclude the current velocities. The water level will be based on Delft3D model results of Arcadis for the study of Geleynse (2017) at 14 January 00:00h,

see figure 5.20. This water level is thought to be representative for the situation at 13 January 23:50h. It is chosen to include the water level field because the spatial gradient is significant in this area.

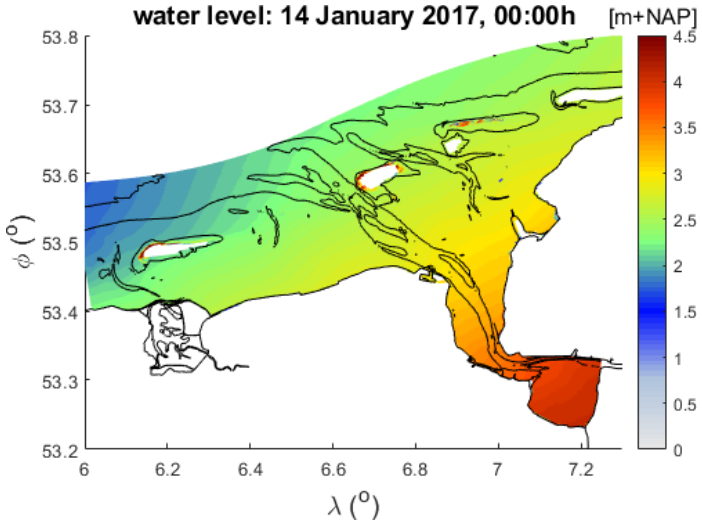

Figure 5.20: Water level at 14 January 2017, 00:00h in the Eastern Wadden Sea basin as used in the SWAN simulation.

5.4.4. Grid properties

Use will be made of a part of the 'Kustrook Wadden' grid, which was shown in figure 5.2. This is a curvilinear grid with (MxN)=(266,620) meshes, where the size ranges from 100-250m. When considering the influence of the spatial resolution, a nested grid will be applied, see 5.2(b). The meshes of the nested curvilinear grid are 3x3 refined, leading to a grid size of 50-70m. The default grid size ranges from 150-250m. Another nest grid with 6x3 refining of the reference grid leads to sizes of 35-55m. Both nests have equal boundaries and therefore cover an equal domain. The boundary conditions for the nest layers are retrieved from the kustrook Wadden grid, hence the reference grid. For all other cases, the Kustrook Wadden grid will be used for the computations. The bathymetry will be equal for all variants. In case the computational grid is refined, the bathymetry will thus be interpolated. This seems physically less correct, however it ensures that only numerical discretisations will be taken into account.

5.5. Contribution of wave breaking

Since the results of the SWAN simulations will be compared to measurements, the physical wave processes can no longer be neglected. Before turning all physics on simultaneously, a simulation with only whitecapping and depth-induced wave breaking will be made. This stepwise analysis is chosen to get a better insight in the effect of the different processes on the wave height distribution as well as the refraction process. For a clean comparison, it is first assumed that the wind velocity is 0 m/s. In previous studies it was found that whitecapping plays a significant role in deeper to intermediate water, while the depth-induced wave breaking plays a dominant role in shallow water (van Vledder et al., 2016). This was concluded for the southern North Sea, but it is thought that it is also true for the Wadden Sea domain that is considered here. Since the influence of these processes is significant and even dominant in shallow water, it is chosen to perform a computation with only these physics first. These computations will still be performed on the rectangular grid as was given in figure 5.3(b).

Generally, the method of Battjes and Janssen (1978) (BJ) is used for depth-limited wave breaking. Another more recent method is devised by Salmon and Holthuijsen (2015) known as $\beta - kd$ (BKD). In sense of the refraction process, it is hypothesised that the wave breaking does not influence the turning rate of waves. Wave breaking largely impacts the wave height but it should not influence the energy distribution over wave frequency in SWAN. Thus the wave period should be independent of wave breaking. This hypothesis can be tested by comparing the mean wave period $T_{m-1,0}$ of a situation with and without breaking. It is found that the period becomes shorter inside the basin in case wave breaking is included in the computation. To get a

better grip on this process, two simulations have been done with a *Gaussian* distribution spectrum. One simulation has a peak frequency of 0.2Hz whereas the other has a peak of 0.1Hz. Observing the 1D spectra, it can be concluded that the energy is equally dissipated over frequencies for both cases. However, the resolution in frequency space should be taken fine enough to avoid discretisation effects. This thus corroborates the hypothesis that wave breaking is independent of frequency. Figure 5.21 gives the $T_{m-1,0}$ without breaking and with BJ breaking for both simulations. Concerning the peak frequency of 0.2Hz, it follows that the difference in spatial distribution of mean wave period is negligible. However, for the low-frequency peak of 0.1Hz it is found that the case with wave breaking results in slightly lower wave periods inside the basin. It can be noted that without source terms, the spatial variation of the case with T_p=10s is larger than for T_p=5s. This is likely caused by the fact that processes like refraction act stronger for larger periods. Since a larger spatial variation is already present without breaking, turning breaking on will enhance these patterns. Hence, breaking does not impact the mean period on itself. However, in a complex bathymetry it indirectly affects other processes causing the local mean period to vary slightly.

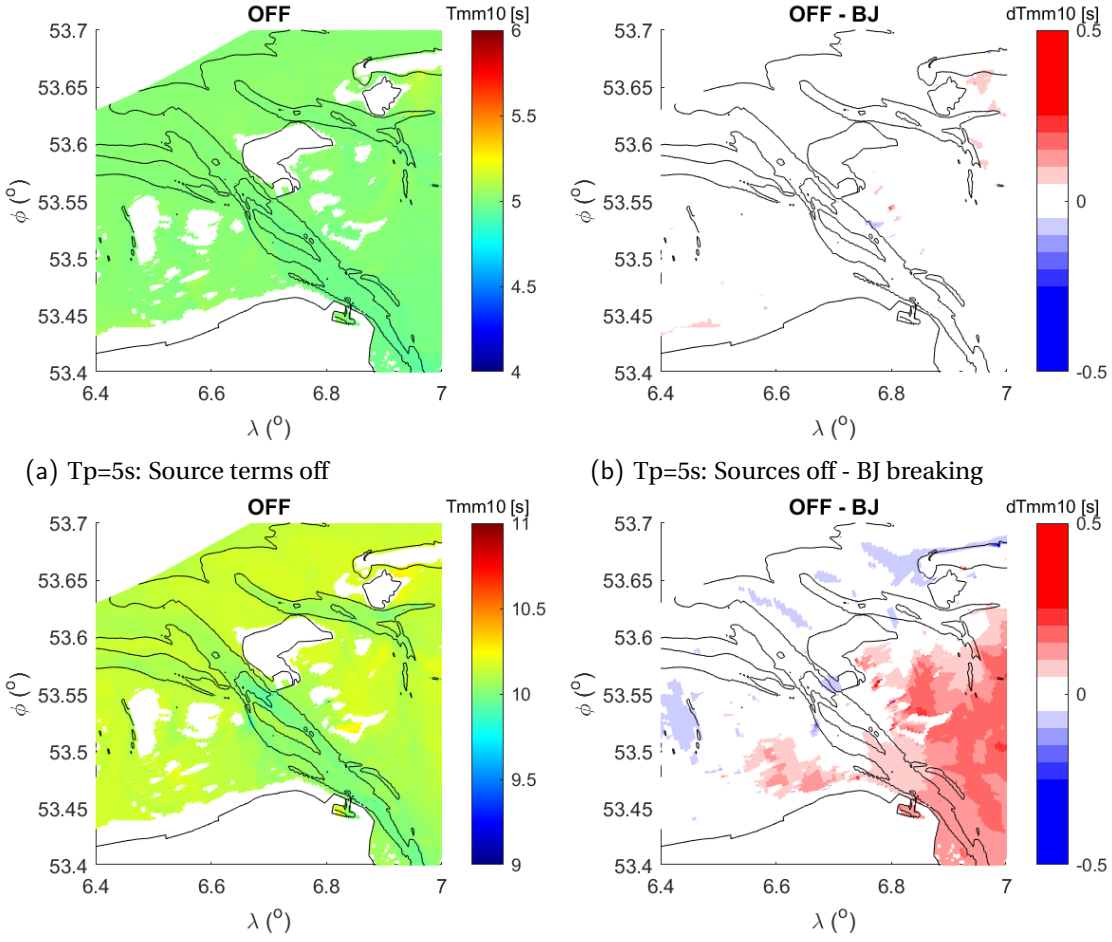

(a) Tp=5s: Source terms off

(b) Tp=5s: Sources off - BJ breaking

(c) Tp=10s: Source terms off

(d) Tp=10s: Sources off - BJ breaking

Figure 5.21: Mean wave period for the case without wave breaking and with wave breaking, where the last is a difference plot. Upper: peak frequency of 0.2Hz; lower: peak frequency of 0.1Hz.

Subsequently, the differences between applying the BJ and BKD formulation will be assessed. This comparison does not directly contribute to understanding of the refraction process, still it gives more insight in the relative importance of refraction compared to parametrisation of other processes. Figure 5.22 gives the comparison in $T_{m-1,0}$ between the two variants for the imposed peak frequency of 0.1Hz. The differences for a peak frequency 0.2Hz are comparable in this case. It follows that the differences between the formulations is negligible. This is also caused by the fact that wind growth is excluded from the computation. The spatial distribution of wave breaking is different for both formulations. In case wave growth by wind is taken into account, smaller waves grow faster. Therefore, this will influence the spatial distribution of the wave period.

According to Salmon and Holthuijsen (2015), the BKD tends to give more wave breaking for non-local waves at the start of the breaking zone. Additionally, the local wave generation is larger on the tidal flats, giving larger waves near the coast. Concluding, wave breaking does not influence the mean period and thus the refraction pattern significantly. However, in case wind is included in the computation this will cause more short wave energy and hence a shift in wave period.

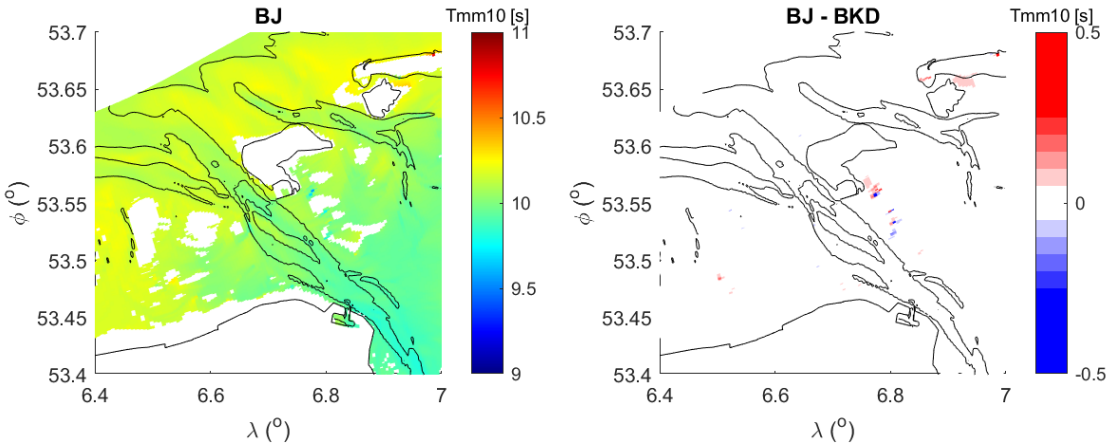

(a) Tp=10s: BJ breaking

(b) Tp=10s: BJ - BKD breaking

Figure 5.22: Mean wave period for a case with Battjes-Janssen (BJ) and the method of Salmon (BKD) for an imposed peak frequency of 0.1Hz.

5.6. Comparison with 2017 storm conditions

Finally, this section will treat the measurements that are made in the Eastern Wadden Sea and compare these with the results of SWAN. All relevant physical wave processes are included, where the settings are based on the default settings, see table 5.2. Two datasets will be used of respectively Rijkswaterstaat and the measurements in the context of the BE SAFE project. The SWAN simulation will be performed stationary with the conditions that occurred on 13 January 2017, 23:50h. This is around the peak of the storm.

Table 5.2: Overview of SWAN settings to be used in this research (SWAN-team, 2019a).

Wave process	**Formulation**	**Settings**
Wind input	Fit	Default
Whitecapping	Komen	Default
Quadruplets	DIA	Default
Bottom friction	JONSWAP	Default, with $c_f = 0.038\ m^2/s^3$
Surf breaking	Battjes-Janssen	Default α=1 and γ=0.73
Triads	LTA	itriad=11

Figure 5.23 gives the wave height distribution in the domain. The wave height inside the Ems channel is larger than at the surrounding tidal flats. In previous computations the opposite was found, there most wave energy left the channel leading to lower wave heights inside. It can thus be said that the other wave processes account for this difference and will thus increase the wave penetration in the channel.

5.6.1. Source term distributions

To verify, SWAN has the option to check the energy contribution of each wave process in the computation, see figure 5.24. Note that the upper plots have a larger colour scale range. It can be seen that the influence of refraction, i.e. Propth, is significant compared to whitecapping, bottom friction and triad interactions, respectively Swcap, Sfric and Snl3. Obviously, excluding refraction from the simulation leads to zero propagation in θ-space. Especially on the tidal flats in the ebb-delta and along the channel edges, refraction is

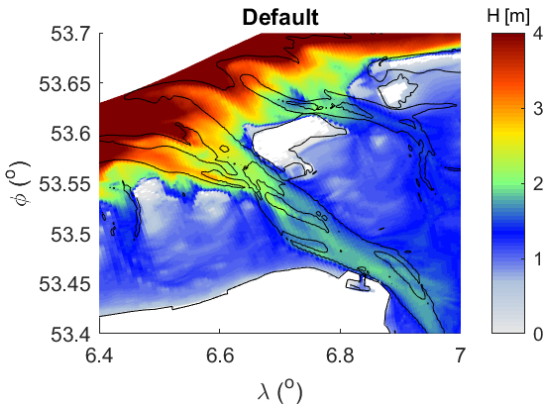

Figure 5.23: Wave height distribution according to SWAN when all relevant physical processes are included. Conditions are equal to 13 January 2017, 23:50h.

present and dominant. Thus, a proper modelling of this term is of importance for this area. Surf breaking, Ssurf, is also significant on the tidal flats in the ebb-delta.

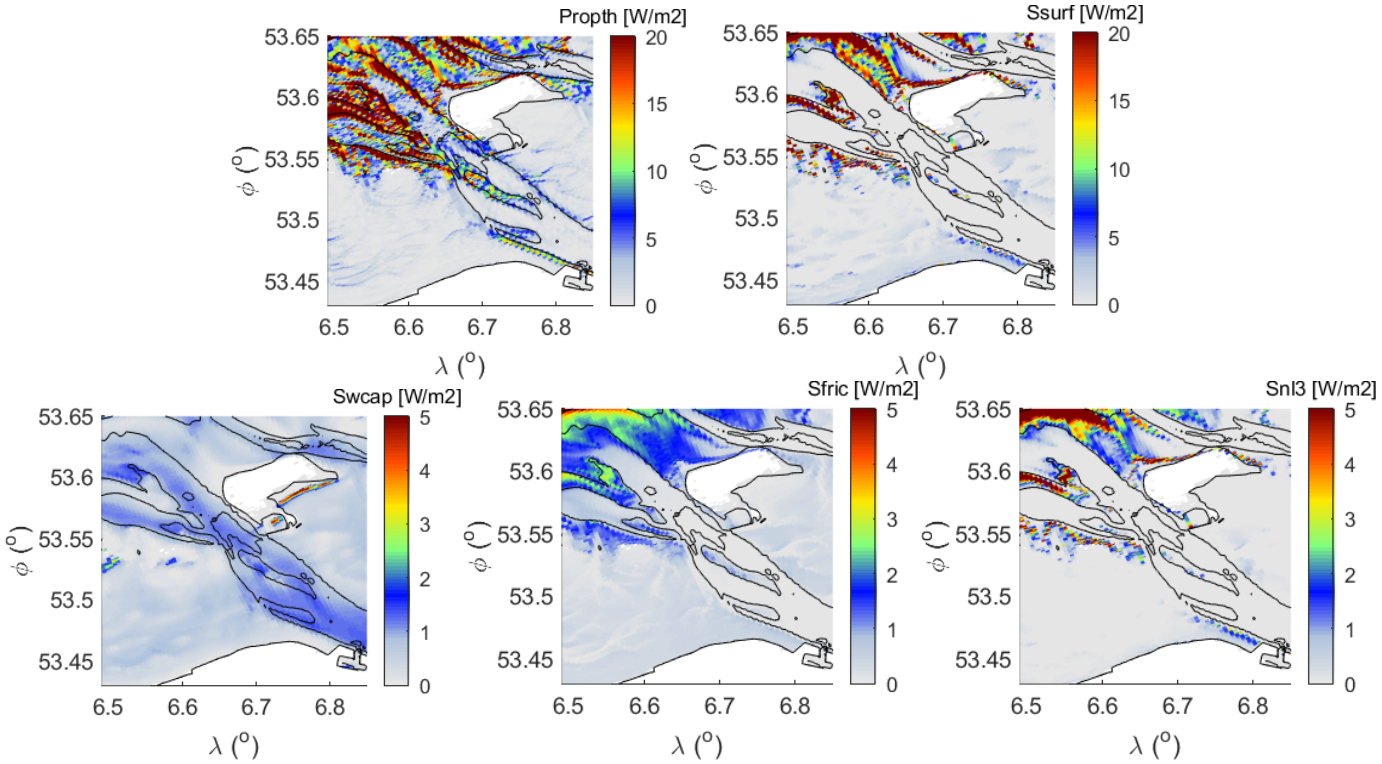

Figure 5.24: Source term distributions around the Ems channel for the SWAN calculation with standard settings.

5.6.2. Analysis of Rijkswaterstaat measurements

Most Rijkswaterstaat measurements are made by waveriders that are able to measure directional as well as wave energy data. As mentioned in figure 5.25, there are six locations present in this area along the south-western edge of the channel, see table 5.3 for the exact coordinates and spectral parameters. Notable is that for the nearshore location Uithuizerwad (UHW) *radar* is used for the measurements, which is not able to measure directional data. Location Uithuizerwad is found near the coast and is thus of most interest for the coastal protection. Therefore, it is interesting to observe the error that is made at this point. It should however be mentioned that the water depth at this location is rather small. Thus, the possibility exists that also

measurement errors are significant here. For the time being, this is neglected and the measurements are considered as the real conditions. In vision of refraction and directional results, locations along the channel edge or inside the channel are of greater interest.

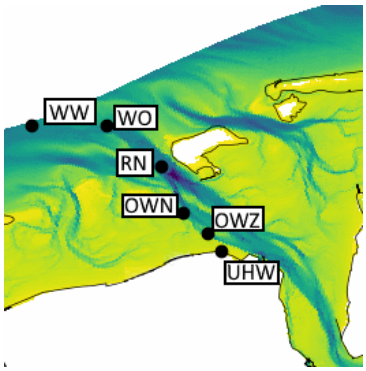

Figure 5.25: Locations of the measurement locations of Rijkswaterstaat; WW=Westereems West, WO=Westereems Oost, RN=Randzelgat Noord, OWN=Oude Westereems Noord, OWZ=Oude Westereems Zuid, UHW=Uithuizerwad.

Table 5.3: Spherical coordinates and spectral parameters of the measuring devices of Rijkswaterstaat.

Observation point	Longitude [°]	Latitude [°]	H_{m0} [m]	$T_{m-1,0}$ [s]	mean dir. [°]	dir. spreading [°]
WW	6.368616	53.620976	8.42	15.16	329.8	50.8
WO	6.522083	53.620351	4.53	11.52	315.7	48.4
RN	6.632476	53.570392	2.13	7.95	309.0	37.6
OWN	6.677245	53.513223	1.15	3.90	325.7	41.8
OWZ	6.726506	53.487975	1.33	4.09	318.5	41.3
UHW	6.755581	53.466622	1.08	4.42	-	-

The measured data gives the variance density per frequency and the mean directional data per frequency. Therefore, most focus will be on 1D spectra in the comparison. Directional data can be compared per frequency component. The frequency ranges from 0.03Hz-0.5Hz, with 47 equally spaced bins.

Comparison with SWAN

The 1D spectra at the six Rijkswaterstaat locations are given in figure 5.26. Notable is the dip in variance density at f=0.1Hz for RN in SWAN, this decrease is also present for location WO resulting in a bimodal spectrum. Contrary, the measurements at RN show a peak in energy at this frequency, hence the spectrum is unimodal at RN. Furthermore, at locations OWN and OWZ it follows that SWAN generally overestimates the amount of wave energy. On the other hand, at UHW it seems that SWAN gives an underprediction. Table 5.4 gives the spectral parameters at the Rijkswaterstaat locations according to SWAN.

Table 5.4: Spectral parameters at the measuring locations of Rijkswaterstaat according to SWAN.

Observation point	H_{m0} [m]	$T_{m-1,0}$ [s]	mean dir. [°]	dir. spreading [°]
WW	7.06	12.93	328.7	31.9
WO	4.18	11.07	311.3	35.7
RN	2.31	6.09	320.3	24.6
OWN	1.32	3.67	338.7	31.0
OWZ	1.64	4.29	337.6	24.7
UHW	0.70	3.97	350.7	23.3

Since refraction influences the wave direction, also the mean direction per frequency is compared with measurements. In this case the locations of interest are WO, OWN and OWZ, because refraction is thought to play

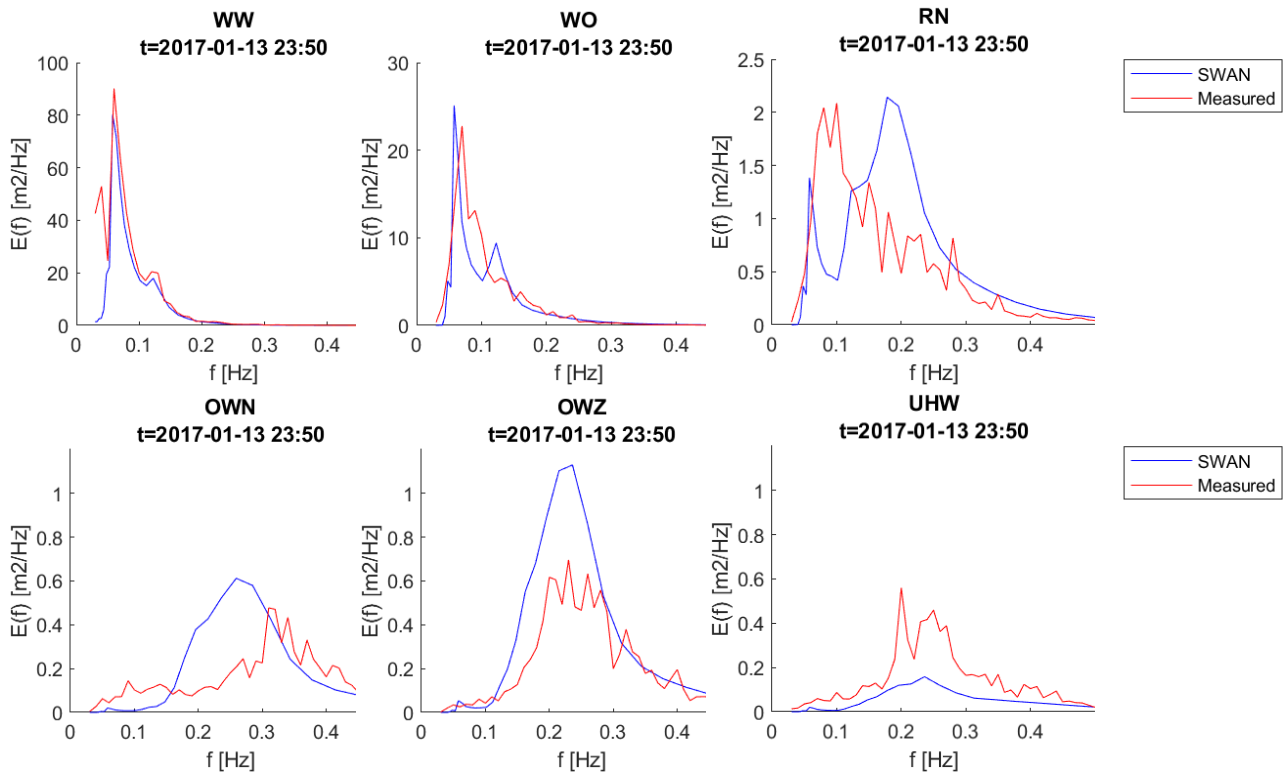

Figure 5.26: 1D variance density spectra at the six buoy locations of Rijkswaterstaat for time 13 January 2017, 23:50h.

an important role here. Figure 5.27 shows the mean wave directions as well as the directional spreading for these locations against frequency. It can be seen that SWAN overestimates the wave direction at WO and especially at OWZ. Hence more wave energy is directed off the channel at OWZ in SWAN. This together with the fact that the total wave energy here is higher in SWAN, leads to the conclusion that more wave energy leaves the channel in SWAN at OWZ.

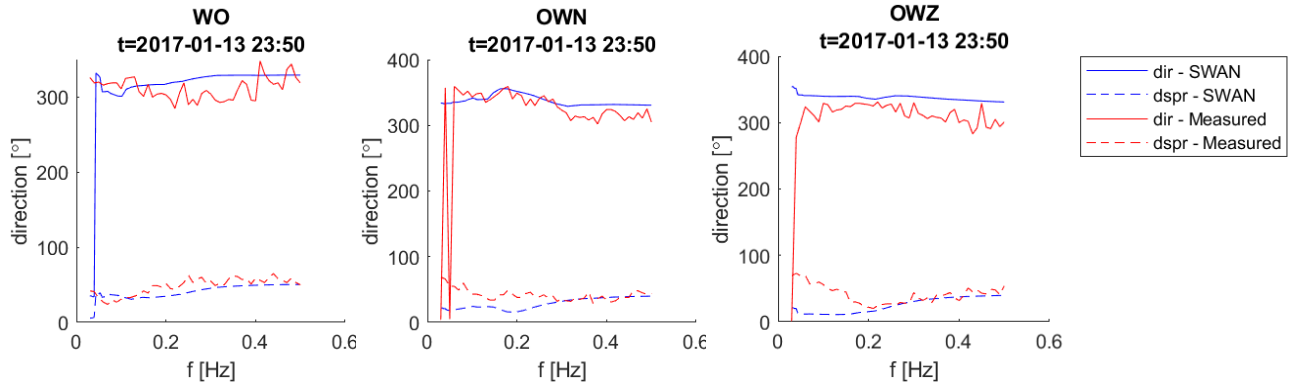

Figure 5.27: Wave direction and directional spreading for WO, OWN and OWZ for time 13 January 2017, 23:50h.

Before this point, the total amount of energy is comparable between the measurements and the model. At UHW it is the other way around, suggesting that more energy leaves the channel around UHW in reality. Based on these measurements only, a decisive conclusion about the origin of the error cannot be given. Yet, this conclusion is based on the default settings with the relatively coarse 'kuststrook' grid. The coming paragraphs aim to improve the prediction of SWAN by varying the resolution and schemes respectively.

Spatial resolution
The influence of the spatial resolution on bottom refraction is assessed by using the nested curvilinear grids as discussed in section 5.4.4. Largest differences are found inside the Wadden Sea basin, see figure 5.28 for the 1D spectra and table 5.5 for the parameters. The nested grids give a lower wave energy for a frequency range between 0.1-0.25Hz at OWN, OWZ and UHW. Interestingly, the difference between the nested grids is small. Also, the peak is shifted to higher frequencies for OWN and OWZ, which corresponds better to the measurements. At OWN and UHW the wave energy for frequencies<0.15Hz is underestimated by both the reference and the nested grids. Therefore, refining the spatial resolution does not seem to improve the prediction of low-frequency waves here. This suggests that the underprediction is not caused by refraction only.

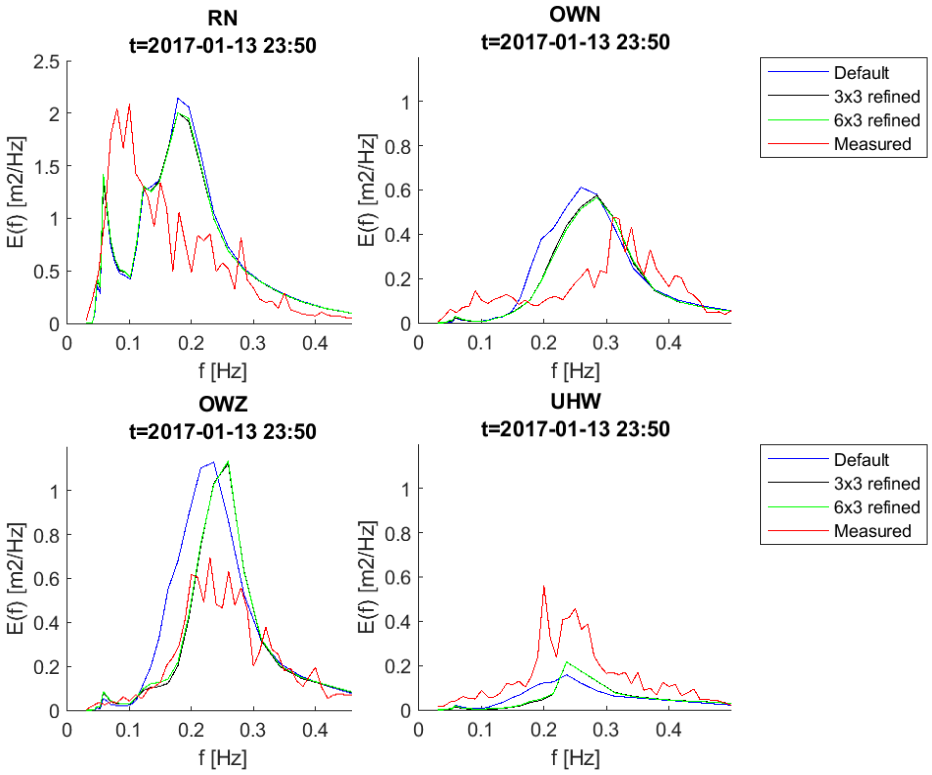

Figure 5.28: 1D variance density spectra at the six buoy locations of Rijkswaterstaat for time 13 January 2017, 23:50h.

Table 5.5: Spectral parameters of the Rijkswaterstaat stations for the different grid variants.

	Measured		default grid		3x3 refined		6x3 refined	
Observation point	H_{m0} [m]	$T_{m-1,0}$ [s]	H_{m0} [m]	$T_{m-1,0}$ [s]	H_{m0} [m]	$T_{m-1,0}$ [s]	H_{m0} [m]	$T_{m-1,0}$ [s]
RN	2.13	7.95	2.31	6.07	2.28	6.15	2.29	6.18
OWN	1.15	3.90	1.32	3.58	1.24	3.44	1.24	3.44
OWZ	1.33	4.09	1.64	4.25	1.50	3.92	1.52	3.95
UHW	1.08	4.42	0.70	3.85	0.70	3.22	0.71	3.31

Directional resolution
For the monochromatic wave case it was found that a refinement in directional space did not lead to significant changes in the solution. In that case a resolution of 1° was used, while in practice often a resolution of 10° is applied. Comparing the 1D variance spectra of these directional resolution variants shows again small differences. The largest difference is found at RN, where a coarser resolution of 10° decreases H_{m0} with 5cm. At all other locations, the differences are less than 1cm. Also for the mean periods $T_{m-1,0}$ and T_{m01} the differences are always less than 0.2s, where the coarser resolution gives higher periods.

It is found that the propagation energy in θ-space may become significantly larger near the channel edges for a finer directional resolution. Furthermore, this difference in propagation energy increases when the computational grid is also refined. Hence, a refinement in spatial resolution should include a refinement in directional resolution for a larger effect. Still, the effect of solely the directional resolution is limited when considering the variance spectra at all locations.

Propagation scheme

It is found earlier that largest differences between the SORDUP and BSBT scheme are found for coarser grids. Therefore, the reference Kuststrook Wadden grid will be used for the comparison. At the Rijkswaterstaat buoy locations there are no significant differences between the spectra. Largest differences are found at the ebb-delta and the Ems channel. The BSBT scheme leads to a higher peak around 0.05Hz for RN. At OWN, OWZ and UWH, the BSBT scheme results in slightly more energy in the frequency range 0.05-0.25Hz. This can be caused by the fact that more energy enters the basin at RN, or because the low-frequency waves stick to the channel edge stronger for BSBT. This last reason seems more likely, since there is negligible difference in energy for f>0.25Hz. Also, taking into account the difference in H_{m0} between the variants shows more energy propagation through the Ems channel for the SORDUP scheme, see figure 5.29. Yet, it can also be seen that the difference at the coast is negligible. this is consistent with the spectra found at UHW, which were almost identical.

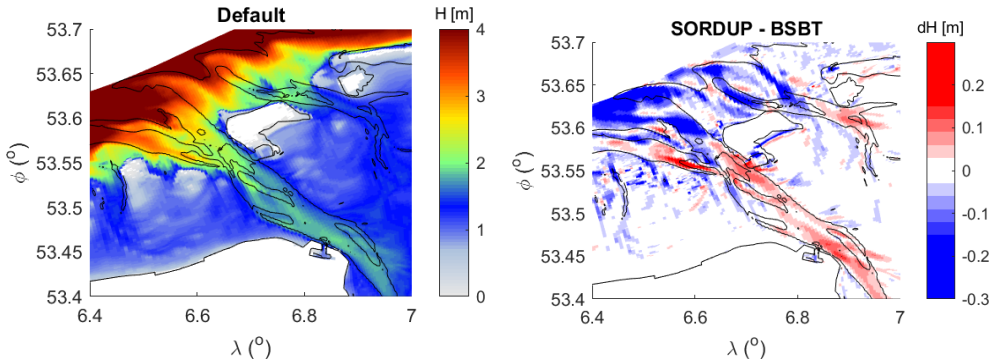

(a) SORDUP (b) SORDUP - BSBT

Figure 5.29: Left: Wave height plot when applying the SORDUP propagation scheme; right: difference in wave height distribution between the SORDUP and BSBT schemes.

2D variance density spectra

With respect to refraction, the 2D variance density spectra are of greater interest than the 1D spectra, even though a comparison to measurements is not possible. The 2D spectra for the six measuring locations are given in appendix H figure H.3. Offshore, there is wave energy present for frequencies <0.1Hz, with a directional spreading from 270-30°N. However, at RN this peak is shifted to 0.2Hz (wind waves), with a mean direction equal to the wind direction and channel axis. Two peaks are present in directional space at OWN, one around 300°N and the other around 350°N. This second peak follows approximately the channel direction. The first peak is caused by offshore waves that approach the channel from the western tidal flats. In theory these waves should be able to enter the channel. However, inside the channel this second peak is absent and all waves follow the channel axis. Figure 5.30 gives the 2D density spectrum at this location for respectively the reference grid and the 6x3 refined nest layer. It can be concluded that the amount of low-frequency wave energy as well as the directional spreading inside the channel is larger for the nest layer.

Figure H.6 shows the spectra for the cross-section around the channel edge at OWN as given in figure H.2. Here the aforementioned presence of the different directions on the tidal flats can be clearly seen. An additional cross-section is made around OWZ, see appendix H figure H.6. Also here it can be concluded that more low-frequency energy is present at the tidal flats for the nest layer and the directional spreading is larger.

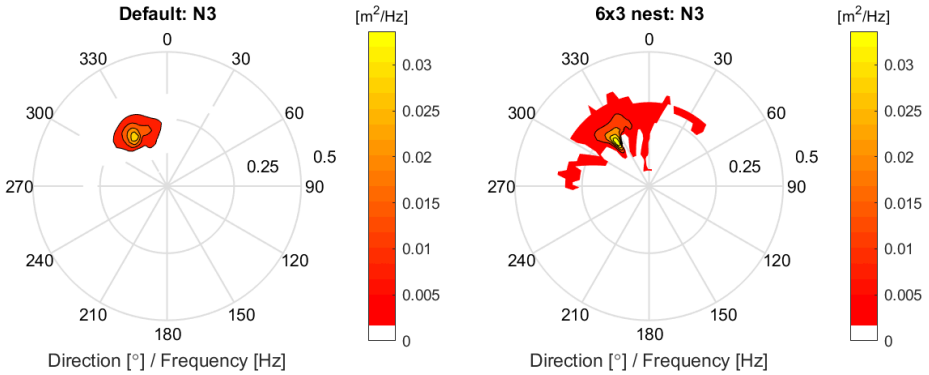

Figure 5.30: 2D variance density spectra inside the channel at the height of OWN for the reference grid and a 6x3 refined nest layer, using default SWAN settings for 13 January 2017, 23:50h.

5.6.3. Analysis of BE SAFE measurements

Another dataset is retrieved from the BE SAFE project, see figure 5.31 and table 5.6 for the locations. These measurements were taken to assess the influence of salt marsh vegetation on the wave conditions. To make sure that these vegetation effects do not disturb the comparison in this case, only p1 and p6 of figure 5.31 will be used. A disadvantage of this data is that no directional data is available, since the data is measured using pressure sensors. Despite this, it still gives information about the wave energy that is able to reach the coast.

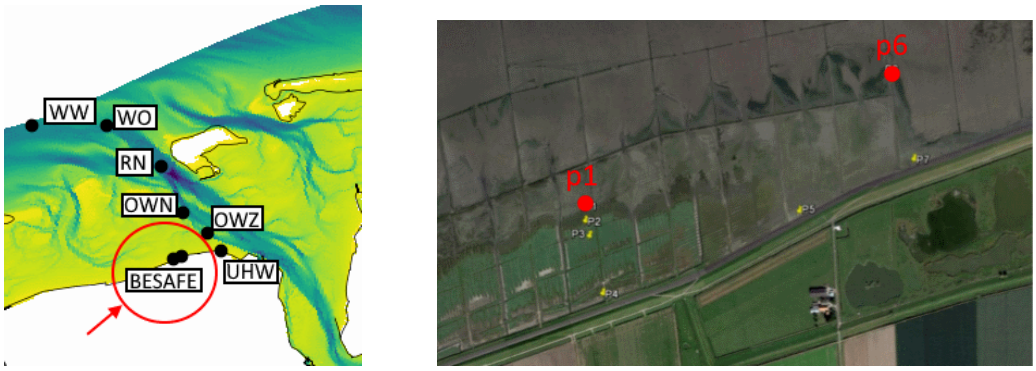

Figure 5.31: Locations of the measurement locations of the BE SAFE project (Geleynse, 2017).

Table 5.6: Spherical coordinates for p1 and p6 of the BE SAFE project and corresponding spectral parameters (Geleynse, 2017).

Observation point	Longitude [°]	Latitude [°]	H_{m0} [m]	$T_{m-1,0}$ [s]
p1	6.65887	53.45689	0.63	4.6
p6	6.67400	53.46059	0.79	4.2

The spectral energy is available for frequencies between 0.01-2Hz with 398 equally spaced bins. Since the SWAN model only ranges from 0.03-0.5Hz, hence equal to the Rijkswaterstaat measurements, the BE SAFE data is filtered such that an equal frequency range as SWAN is retrieved. This choice can be supported by the fact that errors may be introduced for low frequencies. For example, the post-processing with Fourier transformation into spectral data introduces errors that may cause too much energy in the low-frequency domain. Moreover, SWAN is unable to compute very low-frequency waves/infragravity waves. Therefore it is chosen to exclude these frequencies from the comparison.

Comparison with SWAN

Figure 5.32 gives the 1D variance density spectra at p1 and p6 according to the SWAN computation and measurements. It can be seen that SWAN predicts the variance density quite well, both show an almost uniform

spectrum. However, SWAN underestimates the low-frequency wave energy, while the peak energy is overestimated. Furthermore, the shape and order of values of the predictions here are similar but slightly higher to the one SWAN found for UHW. In the coming paragraphs, again the resolutions will be varied to check if this leads to improvements of the solution. It was already found that the numerical schemes had negligible effect at the coast.

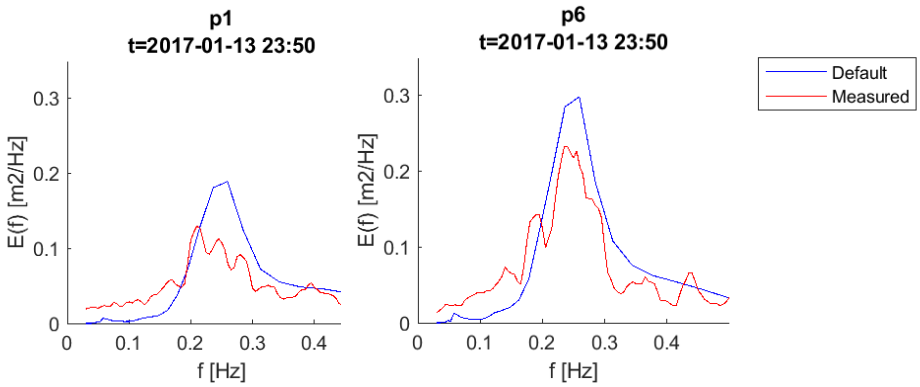

Figure 5.32: 1D variance density spectra at p1 and p6 of the BE SAFE project for time 13 January 2017, 23:50h.

Spatial resolution

For both p1 and p6, the peak wave energy is lower for a finer grid, which corresponds better to measurements, see figure 5.33. For frequencies>0.3Hz the fine grid gives slightly more wave energy. Although difference are present in the spectra, table 5.7 shows that the difference in the spectral parameters are negligible. In the monochromatic wave cases it was found that wave energy that left the channel propagated to the coast just west of Uithuizerwad. This is also the location of the BE SAFE instruments. Therefore, in case refraction is overestimated, it is expected that more low-frequency wave energy is found at this location. Yet, measurements give an even higher energy for frequencies <0.2Hz. Hence it is thought that also other processes play a role here.

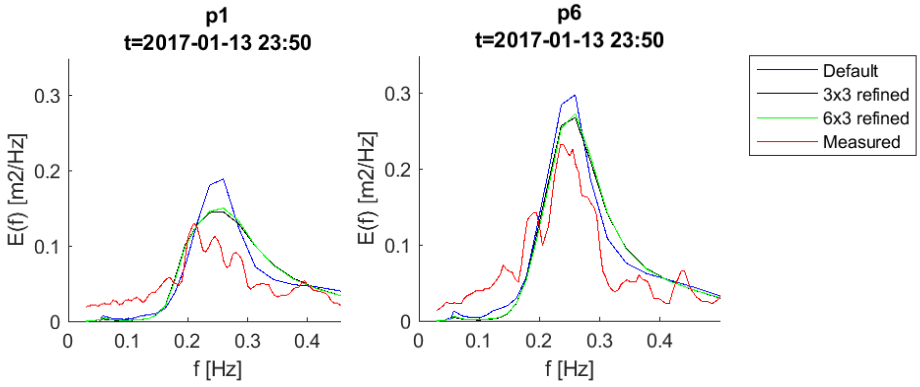

Figure 5.33: 1D variance density spectra at p1 and p6 of the BE SAFE project for different grid variants at time 13 January 2017, 23:50h.

Table 5.7: Spectral parameters for p1 and p6 of the BE SAFE project of the different grid variants.

	Measured		default grid		3x3 refined		6x3 refined	
Observation point	H_{m0} [m]	$T_{m-1,0}$ [s]	H_{m0} [m]	$T_{m-1,0}$ [s]	H_{m0} [m]	$T_{m-1,0}$ [s]	H_{m0} [m]	$T_{m-1,0}$ [s]
p1	0.63	4.6	0.72	3.4	0.71	3.4	0.71	3.4
p6	0.79	4.2	0.85	3.6	0.84	3.5	0.84	3.5

5.6.4. Comparison to Dutch safety assessment

As a short note, also a comparison is made between the standard SWAN settings and the settings as used by the Dutch safety assessment WBI2017. In the WBI approach, the van der Westhuysen formulation for breaking is used with SWAN version 40.72ABCDE. Specifically in the Ems area, a limiter is applied on refraction for f<0.2Hz by means of a factor (van Dongeren et al., 2011). This factor limits refraction for low-frequency waves and thus leads to a larger amount of low-frequency energy that reaches the coast. However, the limiter is not physically based. Therefore, it is chosen to exclude the limiter in the upcoming comparison.

The WBI settings should give better results for the Wadden Sea area, since the van der Westhuysen formulation is thought to be more suitable for flat bathymetries. From literature it is known that standard SWAN with Battjes-Janssen tends to overestimate wave dissipation compared to the WBI settings and measurements in this area (van der Westhuysen et al., 2012). This is consistent with the results found in this study, see appendix H for the 1D and 2D wave spectra. Where the standard SWAN showed an overestimation of the wave energy at OWN and OWZ, the WBI settings give an even larger overestimation, see figure 5.34. It could thus also be stated that van der Westhuysen underestimates wave dissipation compared to Battjes-Janssen at these locations. Furthermore, the overall differences in the 2D spectra are most significant at UHW. Here most wave energy comes from 0°N according to standard SWAN. However, the WBI settings show a bimodal spectrum with waves coming from 325°N and 20°N. Also the spreading over frequencies is larger.

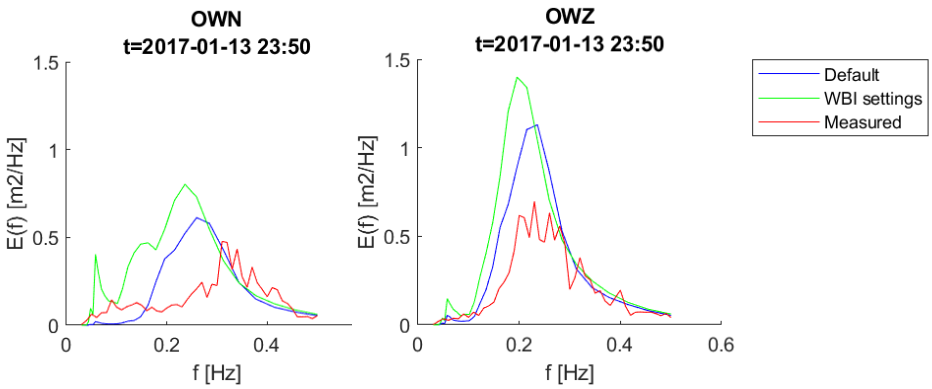

Figure 5.34: 1D variance density spectra at OWN and OWZ of Rijkswaterstaat with WBI2017 settings and default SWAN for 13 January 2017, 23:50h

The WBI spectra for the BE SAFE locations are given in figure 5.35. The prediction of the low-frequency energy shows a better agreement to measurements for the WBI settings. However, the higher frequency tail with f>0.3 Hz is overestimated in this case. Therefore, also the H_{m0} is stronger overestimated in case the WBI settings are applied.

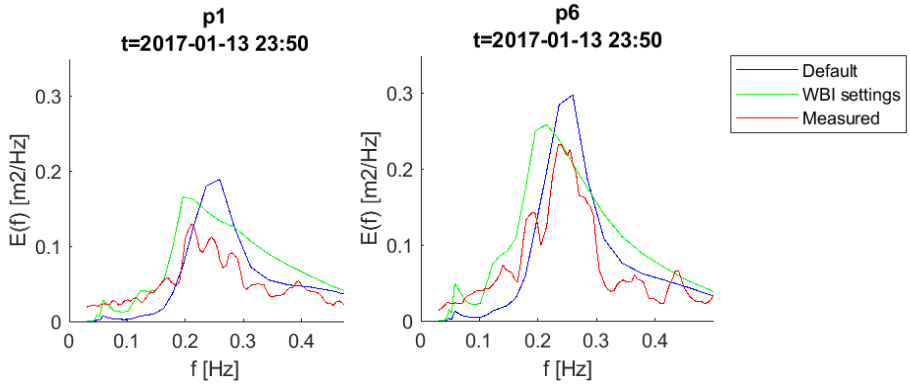

Figure 5.35: 1D variance density spectra at BE SAFE locations p1 and p6 with WBI2017 settings and default SWAN for 13 January 2017, 23:50h

5.6.5. Effects of wave growth, bottom friction and non-linear interactions

This section shortly discusses the role of the physical wave processes that are taken into account in SWAN and potentially adjust refraction. The physical wave processes alter the wave energy propagation, either by energy dissipation or energy shifting over frequencies. Wave breaking, both whitecapping and depth-limited, causes a decrease in wave energy for all frequencies. The wave breaking at the ebb tidal delta is significant, leading to only a small amount of energy that penetrates into the basin. In case wind is excluded from the simulation, one can indeed see negligible wave energy inside the basin. Hence, most energy inside the Wadden Sea basin is locally generated by wind, with a frequency around 0.25Hz = 4s. This wind-generated wave energy reduces the period and thus the turning rate of the waves.

Bottom friction impacts the mean period. Inside the basin, both in the channel and on the tidal flats, friction reduces T_{m01} as well as the wave length. Also on the tidal flats in the ebb-delta, T_{m01} reduces significantly due to bottom friction. This is conform with the findings of Steetzel et al. (2018), who stated that bottom friction affects low-frequency energy stronger. Also for $T_{m-1,0}$ a reduction is present in the basin, both on the tidal flats and in the channel. Since wave celerity c = L/T, it is found that c also reduces inside the channel when applying bottom friction. A lower celerity will result in a smaller turning rate and hence less wave refraction. Considering the mean wave direction gradient, it is found that the gradients at the channel edges are smaller when including bottom friction. Besides altering the wave period, bottom friction also leads to energy dissipation resulting in a lowering of wave height inside the basin.

Lastly, adding the non-linear triad term causes a redistribution of energy over frequencies. The LTA formulation (Eldeberky, 1996) as used by SWAN is only able to transfer energy to higher frequencies, while energy is able to shift back to lower frequencies in reality as well. T_{m01} and $T_{m-1,0}$ strongly reduce on the tidal flats at the ebb-delta. Therefore, the mean wave period is small inside the basin with values 2-5s, both at the tidal flats and in the channel. When also the non-linear quadruplets are added, the T_{m01} reduces slightly more. The shift of energy to higher frequencies causes the direction gradient to reduce significantly, suggesting the turning rate and hence the refraction term to be lower at the channel edges and on the tidal flats. The effect of the non-linear interactions is less significant when the wave height is concerned. The triads and quadruplets transfer a fraction of energy to the higher frequencies, resulting in slightly more wave energy that penetrates the channel, and hence reaches the coast. In absence of wind growth this effect is however small, hence the intrusion of swell into the basin is limited even when including all physical processes.

Concluding, all processes above reduce lower frequency wave energy, while a shift to these frequencies is absent. Therefore, all low-frequency energy, in this case approximately f<0.15Hz, should come in from offshore in SWAN and should not shift to higher frequencies. Excluding wind generation shows that this penetration is very limited. Hence, a combination of too strong refraction for low-frequency energy, stronger dissipation of long waves and shifting of energy to higher frequencies could cause the underestimation as found in the comparison to measurements. This makes the underestimation not solely a refraction problem.

5.7. Conclusion for the Ems estuary

Summarised, the most important conclusions of this chapter are:

- Wave penetration of SWAN agreed well with REFRAC in case no source terms were used and a monochromatic wave was applied. Both showed that small wave periods penetrate deeper into the channel and hence the Wadden Sea basin.
- In case the source terms are neglected, SWAN shows less wave turning towards the channel edge for finer spatial resolutions. Hence, the wave penetration into the Ems channel increased. Since the directional resolution was already very fine, refinement did not lead to improvements of the solution.
- It was found that the numerical scheme SORDUP leads to a larger wave penetration than the BSBT scheme. This conclusion holds both for cases without source terms and with source terms. As one would expect, the solutions of both schemes converge for smaller grid resolutions.
- The breaking process does not influence the patterns of the mean period significantly, since the energy is dissipated equally at all frequencies. Therefore the distribution of energy over frequencies does not change. However, other processes like refraction may cause a small spatial variation due to a lower or higher amount of energy. Hence, breaking indirectly influences the energy propagation in directional space.

- Comparing the SWAN results to measurements, it follows that SWAN underpredicted the wave energy at the coast for Uithuizerwad (UHW). However, SWAN seems to overpredict the wave energy at the western channel side inside the basin. This suggests that more energy leaves the channel in SWAN at these locations, while the energy stays inside the channel according to measurements. Here, more energy penetrates into the basin and leaves the channel near Uithuizerwad. Another explanation for the underprediction at UHW is the fact that the water depth was too small in the simulation, leading to too much dissipation. Yet, this is not thought to be the complete story as the difference in wave energy is significant.
- In general, the shape of the SWAN spectrum is similar to the measured spectra. Only at RN and OWN the shape differs significantly. For these locations, the variance at a frequency range of 0.05-0.15Hz is underestimated, while the variance at 0.15-0.3Hz is overestimated by SWAN.
- Increasing the spatial resolution of the computational grid showed a small improvement of the solution at the measurement locations, where largest differences where found along the channel edge. However, the prediction of the low-frequency energy did not seem to improve at the locations near the coast. In general, the spatial resolution did not affect the shape of the SWAN spectrum. Furthermore, the effect of the directional resolution and the numerical scheme were found to be negligible at most measuring locations.

Concluding all, refining the spatial resolution and using the SORDUP scheme does improve the prediction of refraction, which was clearly visible when the source terms were excluded. Along the western channel edge, this results in a significant wave height that is 12-14cm (6-9%) closer to the measured value. However, the spectra at the coast of Uithuizerwad do not show improvement for the SORDUP scheme, a finer spatial resolution or a finer directional resolution. Between the Ems channel and the Uithuizerwad coast, there is a coastal flat with a length of approximately 1km. This tidal flat causes the shallow water depth, local wave processes and bottom schematisation to be of greater importance than the refraction process at the channel. Hence, a finer resolution does improve the prediction of refraction. Yet solely refraction is not the main cause of the underestimation of (low-frequency) wave energy at the coast in this case.

6
Discussion

The results and conclusions of the previous chapters will be discussed in this chapter. There will be a distinction between the schematic case and the performed case study in the Eastern Wadden Sea.

6.1. Modelling wave refraction for a schematic channel

To obtain insight in the accuracy of modelling refraction, the considered cases were made as simplistic as possible. Energy source and sink terms were neglected and a monochromatic wave condition was imposed to the boundary. Furthermore, the channel was considered straight with a flat bottom and the flats had a constant depth. A first note to this is that al of these assumptions will never be present in reality, making this chapter purely academical.

6.1.1. Prediction of REFRAC

First, the results of REFRAC will be discussed. It was found that the prediction of REFRAC equalled the theoretical prediction well. They both showed a tendency of waves to refract off the channel edge at the same critical angle. Therefore, the approximation of REFRAC shows to model refraction accurately. However, some side notes should be placed concerning the model REFRAC:

- One thing that emerges from the results is the high sensitivity for the bathymetry and the corresponding resolution. For cases were wave turning was present but waves were still able to cross the channel, the wave rays did not remain parallel to each other as one would theoretically expect. Here the schematisation of the bathymetry plays an important role. This schematisation causes a small variation between the depth differences, leading to different turning rates for the wave rays. Hence, REFRAC shows a strong sensitivity to the applied bathymetric resolution.
- Since wave rays are solved independently, they are able to cross or even turn backwards. In reality, the occurrence of these behaviours is unlikely and hence the results of the model should not always be taken too literally. In this sense, the model REFRAC gives an indication of where to expect refraction instead of a correct prediction of the wave ray paths.
- REFRAC gives the wave rays for only one wave component. If the wave climate is complex, REFRAC will not represent the system properly and hence the applicability of the model is limited. Next to this, bottom friction, non-linear interactions and other wave processes are not taken into account. Therefore, the model REFRAC is not suitable to use on itself for realistic coastal environments. Still, for a simplified case as was considered here, REFRAC shows a proper prediction of the refraction process.

6.1.2. Prediction of SWAN

Subsequently, the SWAN model was used to predict the refractive behaviour for different scenarios. For wave angles where waves should refract off the channel edge, there was more wave energy that entered the channel for coarser resolutions. This is due to the formulation of c_θ in SWAN, which causes an underestimation of refraction when waves travel into deeper water. The difference between SWAN and theory increases for coarser resolutions, leading to a larger underestimation of c_θ and hence refraction. However, for wave angles where waves should enter the channel, SWAN generally overestimated the refraction with respect to REFRAC and critical angle theory based on Snel's law. Introducing a coarser resolution in both spatial or directional space, resulted in a larger fraction of waves that refract off the channel edge.

A reason for this can be found in the directional spreading. It is thought that the differences in refractive behaviour are primarily caused by the lack of diffusion for fine grids or on the other hand the abundant diffusion for coarser grids. Since the solution for a coarse grid is more diffusive over directions, i.e. larger directional

spreading, there is a larger fraction of waves with a direction smaller than the critical direction. Therefore, less energy will enter and cross the channel. Note that the diffusive behaviour is initiated by approximating refraction of the waves. If refraction would not play a role, the broadening of the spectrum over directions would be absent. The diffusivity is however dependent on the resolution of the computational grid.

As expected, the spectrum is bimodal just upwave of the channel edge if $\theta_{in} < \theta_{crit}$, see figure 6.1. However, large differences are visible between the different resolution variants. It can be seen that the prediction of the coarse mesh is more diffuse, leading to more energy present between the peaks and hence for larger wave directions.

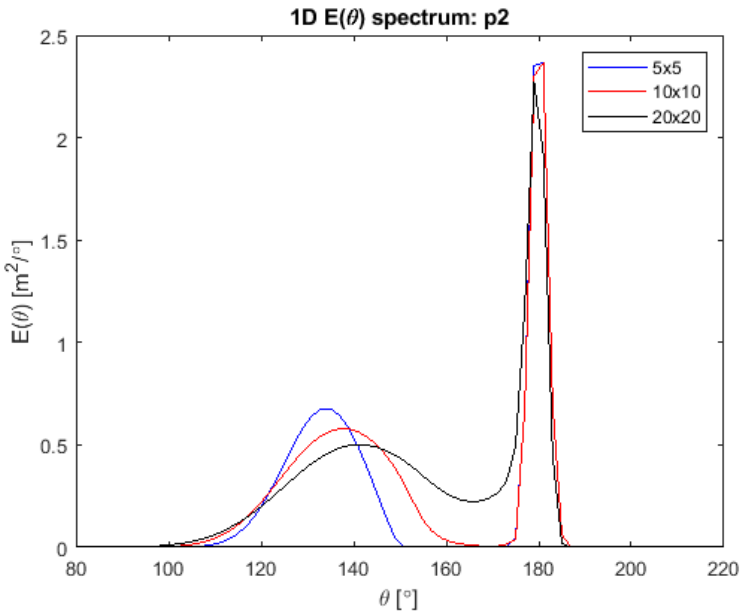

Figure 6.1: 1D variance density spectrum E(θ) for the three grid variants just upwave of the channel edge. Conditions: T_p=10s and θ=180°N.

Interestingly, the mean wave direction is approximately equal for all grid variants at all locations. When plotting the wave ray pattern, one will see that there are minor differences present between SWAN and REFRAC. When the case with T_p=10s and θ=180°N is considered, the mean wave direction will show wave rays that do not cross the channel for both the small and large resolutions. Therefore, wave rays based on the mean wave direction do not always properly represent the energy propagation.

Concerning the numerical schemes, it was found that the SORDUP scheme leads to better results than the BSBT scheme. It is thought that this is caused by the fact that the SORDUP is second order accurate instead of first order like BSBT. It is known that the SORDUP scheme approximates the solution faster due to the second order accuracy, hence a coarser step size is sufficient. Additionally, the introduction of numerical diffusion due to the BSBT scheme causes the prediction of the wave height distribution to be similar to the solution using a 20m mesh width. This comparable behaviour is due to the diffusivity that both cases induce.

Lastly, it is known that small schematisation errors are present in the bathymetry between the grid variants. The coarser bathymetries tend to have a slightly milder slope at the edge, which leads to weaker wave refraction. Therefore, this does not explain the overestimation of refraction.

One side note can be made on the fact that also for the finest grid size, an error is present in the critical angle. This is due to the fact that SWAN will always require a small directional spreading in the incoming wave spectrum. If the mean direction equals the critical angle, there will also be a part of energy smaller than the critical angle that will thus refract off the channel edge. This is partly captured in the tolerance of refraction that was allowed.

6.2. Application for the Wadden Sea case study

The SWAN results have been compared to measurements in the performed case study. Here two datasets were used, one retrieved from buoys and radar sensor of Rijkswaterstaat and the other from pressure sensor poles of the BE SAFE campaign.

6.2.1. Review of the measurements

First of all, it can be seen that the measurements contain many wiggles in the spectra compared to SWAN. This also holds for the direction distribution over frequencies. These wiggles are thought to be caused by a combination of observation noise and the number of sampling points that are underlying the dataset. In case the sampling number goes to infinity, the wiggles will be levelled out. Interestingly, at offshore measurements of for example WW and WO these wiggles are negligible. Since the wave spectrum is less affected by shallow water processes, the variation and hence the amount of wiggles is less. However, at WW a spike in energy can be seen around 0.04Hz. Even though this spectrum is used as input in the SWAN simulation, SWAN did not reproduce this spike at WW. This causes a lower mean period according to SWAN at this location.

6.2.2. Exclusion of currents

The SWAN simulations are performed stationary and exclude currents. It is known that the tidal current may become significant, order 1 m/s, in the area. In that case, wave-current interactions will be present and neglecting this will give a crude approximation. However, the time at which the computation takes place is around slack water, meaning the velocities are generally small. Moreover, the currents at 14 January 2017 00:00h where directed out of the basin meaning ebb tide initiated. A simulation has been performed with this current data retrieved from Geleynse (2017). Yet, this did not lead to any improvements of the solution, it only introduced extra uncertainties. Additionally, Alkyon (2009b) found that including currents did not lead to an improvement on the model performance at UHW for the 2007 storm. Therefore, excluding the currents is thought to be acceptable.

6.2.3. Comparison at Uithuizerwad

One fact that stands out is the underestimation of wave energy in SWAN at UHW compared to measurements. It is known that the water depth at this location equals 1.58m according to the SWAN output file. This leads to a H_{m0}/d of 0.44 and 0.68 according to SWAN and the radar measurement respectively. The ratio for the measurement is relatively high, since the maximum ratio is often around 0.5. This suggests that also the SWAN wave height is close to depth-limited. Observing the bathymetry of the SWAN output more closely, it is found that the bottom level is 1.24m+NAP at UHW. However, the bottom level is in the order of 0.67m+NAP at this location according to AHN2 (AHN, 2009). In this case the ratio of H_{m0}/d becomes 0.5 for the measurements, which corresponds to depth-limited conditions. In case the water depth is larger, also the wave height of SWAN becomes higher. The error in the bathymetry is thought to be the main cause of the underestimation of wave energy that is present at all frequencies. Taking a point further offshore with a similar bottom level to Uithuizerwad, i.e. NAP+0.61m, gives H_{m0}=0.86m and $T_{m-1,0}$=4.04s. This does improve the solution, yet the wave energy is still underestimated. Concluding, even with a correct bottom level SWAN underestimates the wave energy at UHW compared to measurements.

6.2.4. Effect of (spatial) resolution

This study was focussed on the effect of numerical properties such as resolution and schemes and less on the physical processes. Varying the resolution in spatial domain seemed to improve the solution slightly. However, the differences between the spectra are relatively small. In some cases the SWAN spectrum does not match the shape of the measurements. This seems to improve by increasing the resolution, but not convincingly. Also, SWAN still underestimates wave energy for f<0.15Hz, this does not change by a finer resolution. Following these conclusions, it is unlikely that a refinement in the computational domain will solve all discrepancies. Following theory it should hold that in case $\Delta x, y, \theta \rightarrow 0$, the exact solution to the equation is found. Yet, if errors exist in the equation to solve, a finer resolution will not solve the problem.

6.2.5. Effect of formulations for physical processes

Concerning the source terms, it is found that wave breaking and non-linear triad interactions are most pronounced in the Wadden Sea basin, whereas bottom friction was present in the ebb-delta. Here the bottom

friction is chosen according to JONSWAP with c_f=0.038, which is based on the study of Zijlema et al. (2012). It is thought that changing this coefficient will not improve the model physically.

The triad interactions are implemented by the 'old' LTA method, with itriad=11 in SWAN. The limitations of the LTA method are thought to impact the wave period and hence refractive behaviour in complex bathymetries like the Wadden Sea basin according to Groeneweg et al. (2015). In some cases, it might even be preferred to neglect triad interactions. Therefore, this has been tested for this study as well. It is found that at most measuring locations the wave energy for f<0.15Hz is overestimated by SWAN in case triads are excluded from the simulation. Interestingly, the energy for f<0.15Hz is equal for both the case with and without triads at UHW. Hence they both underestimate this compared to measurements. Additionally, the total energy at UHW is stronger underestimated by SWAN when triads are turned off. Since the low-frequency energy is higher without triad interactions, the refractive behaviour is stronger leading to less wave penetration. Therefore, less energy is able to reach the coast at UHW.

7
Conclusions & recommendations

7.1. Conclusions

This study concerned the modelling of wave bottom refraction, focusing on channels in tidal environments. Use was made of the spectral wave model SWAN, which was compared to a wave ray-tracing model called REFRAC. Additionally, a comparison was made between a SWAN simulation and measurements for the Eastern Wadden Sea. The central topic of this study is defined in the following main question:

How can the representation of wave refraction over tidal channels be improved in spectral wave models?

This question can be answered by dividing it into multiple sub-questions. The following sub-questions were proposed, where the answers are given per question. Thereafter, the answer to the main question is given.

1. **How does the refraction process in SWAN compare with the analytical solution of REFRAC?**
   SWAN and REFRAC show similar wave ray patterns in a schematic as well as a more complex bathymetric environment. In case the bathymetry and computational grid are taken differently, bathymetric characteristics are altered. Obviously, this results in a different equation to solve and hence a different solution.
2. **How well is the refraction process over channels in tidal basins represented by both wave models?**
   Considering a simplistic channel, REFRAC agrees well with the theoretical solution. It is found that SWAN shows a small overestimation of the critical angle for refraction compared to theory and REFRAC, leading to enhanced refraction. This is partly caused by the directional spreading that is present in SWAN, but also by the computational resolution and propagation scheme that is applied. SWAN overestimates the critical angle for refraction by 7-16° for a simplistic channel with side-wall slope 1:5, where the larger errors were found for coarser computational grids. In the complex Wadden Sea area it is found that both SWAN and REFRAC show a similar refraction pattern in case source terms are neglected. However, the wave processes bottom friction, non-linear interactions and wave growth are not taken into account by REFRAC, whereas it is known that they affect wave refraction. Hence this model is not capable of simulating refraction properly in a complex wave environment. SWAN is able to include these processes and thus gives a preferable result over REFRAC in these cases.
3. **What spatial resolution is required to accurately predict bottom refraction of waves?**
   For a simplistic channel it is found that SWAN performs well for a depth gradient of 2m over two grid points. A resolution of 10m, corresponding with a depth gradient of 2m, leads to a maximum underestimation of 7cm (7%) in significant wave height at the upwave side of the channel compared to a 1m mesh width for a side-wall slope of 1:5. However, the error in the prediction largely depends on the critical angle for refraction and the incoming wave direction. If these are in the same order, maximum errors are found. For the Wadden Sea case, a decrease of 0-11cm (2.5-15%) in wave height is found for coarser resolutions at the coastal flats for a 2m water level and for excluding physical source terms. In case these source terms are taken into account, the wave energy is overestimated by SWAN along the upwave channel edge and underestimated at Uithuizerwad. However, it can be noted that the low-frequency waves here are underestimated by SWAN. Refining the resolution does improve the prediction along the channel edge, where the overestimation in significant wave height is 12-14cm (6-9%) less for a finer grid. Hence a smaller resolution along the channel edges positively impacts the prediction, where a grid size of order 50m is sufficient. Furthermore, refraction does not play a significant role on the coastal flats. Other processes alter the wave energy, making the solution mostly dependent on local characteristics. Where the impact of resolution on refraction was significant for a case with no source terms, including these terms diminishes this effect.

The bottom depth at Uithuizerwad was poorly implemented, leading to a limit in wave energy that was too low. Therefore, a finer resolution in both bathymetry and computational space should be used for near coast locations. However, this is needed for a proper schematisation of the bathymetry and hence unrelated to refraction by channels.

4. **How does the directional resolution influence the bottom refraction process?**
   For a simple navigation channel where waves propagate into deeper water, it was found that a coarser directional resolution resulted in an underestimation of the refraction process. The effect was similar to the spatial resolution. However, refining the directional resolution in a more complex bathymetry only slightly improved the solution. Even the difference between a 1° resolution and a 10° bin size, which is often chosen in practice, did not lead to significant differences in the solution for a realistic wave climate and bathymetry. Therefore, it is concluded that the directional resolution does influence the solution, however, the effects are minor compared to other sensitivities. Especially at the coast the effects where found to be negligible.
5. **What is the sensitivity of the model accuracy with respect to the wave propagation scheme in SWAN concerning the refractive behaviour?**
   Two propagation schemes were tested, namely the SORDUP and BSBT scheme which are respectively second and first order accurate. From theory it is known that the BSBT scheme tends to be more diffusive, this is supported by the results found in this thesis. Furthermore, the BSBT scheme showed to overestimate the refraction process compared to the SORDUP scheme. Additionally, the negative influence of a coarser computational mesh width became larger in case the BSBT scheme was applied. This is most likely caused by the first order accuracy. The Wadden Sea case study showed that the SORDUP scheme led to more wave energy penetrating through the Ems channel than the BSBT scheme. However, the differences in wave energy on the flats and at the coast were negligible.
6. **How do other nearshore wave processes influence the refraction process in SWAN inside the Wadden Sea basin?**
   Wave breaking did not influence the mean period, since the energy dissipation is equally distributed over frequencies. However, it allows for generation of local wind waves that lower the mean wave period. Similarly, non-linear triad interactions shift energy to lower wave periods decreasing the mean wave period. Lastly, the bottom friction dissipates energy from lower wave frequencies stronger, again reducing the mean wave period. Therefore all these processes lower the mean wave period, generally this leads to a weaker refraction. These processes thus essentially keep the wave energy inside the Ems channel, leading to significantly more wave penetration into the Wadden Sea basin compared to the case without source terms. However, no energy transfer to lower frequencies is present in the model. In the measurements it can be seen that low-frequency energy is present near the coast, which cannot be modelled properly with the current settings.

With help of the above sub-questions, the answer to the main question can be summarised by the following statement:
Bottom refraction is overestimated in SWAN if a coarse spatial resolution of the computational grid is used and waves travel from deep to shallower water. The wave height at the upwave channel side may become order 10% larger for coarser grids compared to finer grids. In case waves propagate from shallow to deeper water, the opposite can be true where SWAN underestimates refraction. For the considered case study, it was found that the low-frequency energy, f<0.15Hz, was underestimated by SWAN compared to measurements along the coast. It was thought that this was caused by a lack of wave penetration into the channel from offshore due to too strong wave refraction. Increasing the spatial resolution did lead to an improvement of this wave penetration. However, SWAN still underestimates the wave energy for f<0.15Hz at the coast compared to measurements. Focusing on all frequencies, increasing the spatial resolution does improve the significant wave height prediction along the channel edge by 12-14cm (6-9%). Hence, the prediction of refraction at the channel edges improves by a finer resolution. Besides spatial resolution, also the resolution in directional space and the propagation scheme modified the solution in case only propagation terms were taken into account. However, the directional resolution had minor influence on the solution for the Wadden Sea case. For the propagation scheme it was found that the BSBT scheme led to an overestimated refraction, therefore this option will not improve the prediction of wave refraction and is thus not recommended.

7.2. Recommendations

The following recommendations are made with respect to practical use of this study:

- The currently used 'Wadden kuststrook' grid is too coarse for proper modelling of refraction at the transition of channels to flats. However, the difference at the coast is small in case a three times finer grid is used. It is found that refraction is modelled sufficiently in case the grid size along the channel becomes in the order of 50 meters;
- The required grid size depends on bottom depth and slope as well as the wave conditions. In an ideal situation, a grid is thus made based on the boundary conditions (BC) that are imposed. However, these will vary in an instationary computation, making this customisation almost impossible. For instationary calculations the normative BC can be used as guideline;
- The required spatial resolution is smallest in case the role of refraction is significant. Therefore, it is suggested to visualize the gradient of the group velocity or the turning rate c_θ. At locations were these are significantly large, refraction will be present and a finer grid is needed.

For research purposes the following recommendations are given:

- Following the previous recommendation, it is recommended to investigate the possibilities of an unstructured simulation, where the resolution is based on the group velocity and turning rate;
- It is recommended to further investigate the role of physical processes on the solution. It is already found that the triad terms do influence the spectral shape significantly, however none of the existing formulations in SWAN seem to fit all measurements properly. Especially the implementation of the depth-induced wave breaking and non-linear triad interactions should be further investigated.
- The influence of a coupled wave-flow model should be tested. In this study a stationary, spatially varying water level without currents is imposed. An instationary coupled wave-flow model could potentially lead to different water levels and wave characteristics.
- This study concerns the storm of January 2017 in the Eastern Wadden Sea. It is recommended to observe the refraction behaviour for other storms with different characteristics or for different locations. Especially locations where a tidal channel is close to the coast, such as at 'Vierhuizergat', are of interest. Here the effects of refraction could be more pronounced. Additionally, the added value of an instationary computation can be investigated, since this study only concerned stationary simulations;
- Finally, it is recommended to verify the quality of measurements. If errors exist in this data, the model results are falsely labelled as wrong. By increasing the number of measurement stations or by using multiple techniques, one can get better insight in the correctness of the measured data.

Bibliography

Adytia, D. and van Groessen, E. (September 2012). Phase resolved and averaged wave simulations in Jakarta harbour. *APHydro2012*, pages 218–223.

AHN (2009). Actueel Hoogtebestand Nederland - Viewer. https://www.ahn.nl/ahn-viewer?origin=/common-nlm/viewer.html. Accessed on January 4th, 2020.

Alkyon (2009a). Analysis of wave penetration into the Eastern Wadden Sea. Technical report, Authors: G.Ph. van Vledder and O.R. Koop.

Alkyon (2009b). SWAN hindcast in the Eastern Wadden Sea and Eems-Dollard estuary. Storm of 9 November 2007. Technical report, Authors: G.Ph. van Vledder, J. Adema and O.R. Koop.

Arcadis (2015). Een rekenexperiment voor de Waddenzee, 4 stormen van 2006, 2007, 2013 en 2014. Technical report, Alkyon, Marknesse.

Battjes, J. and Janssen, J. (1978). Energy loss and set-up due to breaking of random waves. *Coastal Engineering*.

Booij, N. and Holthuijsen, L. (1987). Propagation of ocean waves in discrete spectral wave models. *Journal of Computational Physics*, 68:307–326.

Booij, N., Ris, R., and Holthuijsen, L. (1999). A third generation wave model for coastal regions: 1. model description and validation. *Journal of Geophysical Research: Oceans*, 104:Issue C4.

Cavaleri, L., Abdalla, S., Benetazzo, A., Bertotti, L., Bidlot, J.-R., Breivik, Ø., Carniel, S., Jensen, R., Portilla-Yandun, J., Rogers, W., Roland, A., Sanchez-Arcilla, A., Smith, J., Staneva, J., Toledo, Y., van Vledder, G., and van der Westhuysen, A. (2018). Wave modelling in coastal and inner seas. *Progress in Oceanography*, 167:164–233.

Crosby, S., Kumar, N., O'Reilly, W., and Guza, R. (2019). Regional swell transformation by Backward Ray Tracing and SWAN. *JOURNAL OF ATMOSPHERIC AND OCEANIC TECHNOLOGY*, 36:217–229.

Deltares (2015). D-flow FM user manual. Technical report, Deltares.

Dingemans, M. W. (1997). *Water Wave Propagation Over Uneven Bottoms: Part 1 - Linear Wave Propagation*. World Scientific Publishing Co. Pte. Ltd., Farrer Road, Singapore.

Dusseljee, D., Klopman, G., van Vledder, G. P., and Riezebos, H. (2014). Impact of harbor navigation channels on waves: a numerical modelling guideline. *Coastal Engineering*.

Eldeberky, Y. (1996). Nonlinear transformation of wave spectra in the nearshore zone. Technical report, Delft University of Technology.

Geleynse, N. (2017). Memo: Werkrapportage POV voorlanden fase C; onderdeel c1-1/4 - storm 2017. *Projectnummer: C03011.000544*.

Google (2019). Google earth pro.

Groeneweg, J., van Gent, M., van Nieuwkoop, J., and Toledo, Y. (2015). Wave propagation into complex coastal systems and the role of nonlinear interactions. *J. Waterway, Port, Coastal, Ocean Eng*, 141(5):04015003.

Groeneweg, J., van Nieuwkoop, J., and Toledo, Y. (2014). On the modelling of swell wave penetration into tidal inlet systems. *Coastal Engineering Proceedings*.

Hasselmann, K., Barnett, T., Bouws, E., Carlson, H., Cartwright, D., Enke, K., Ewing, J., Gienapp, H., Hasselmann, D., Kruseman, P., A.Meerburg, Müller, P., Olbers, D., Richter, K., Sell, W., and Walden, H. (1973). Measurements of wind-wave growth and swell decay during the joint north sea wave project (JONSWAP). Technical report, Deutches Hydrographisches Institut.

Helpdesk-Water (2020). Beoordelingsinstrumentarium (WBI2017). Accessed on February 3rd, 2020.

Herbers, T., Elgar, S., and Guza, R. (1999). Directional spreading of waves in the nearshore. *Journal of geophysical research*, 104:7683–7693.

Holthuijsen, L. (2007). *Waves in oceanic and coastal waters*. Cambridge university press, Delft.

Ilia, A. and ODonnell, J. (2018). An assessment of two models of wave propagation in an estuary protected by breakwaters. Technical report, University of Connecticut, Journal of Marine Science and Engineering.

KNMI (2019). Potential wind speed of the netherlands - download. http://projects.knmi.nl/klimatologie/onderzoeksgegevens/potentiele_wind/index.cgi?language=eng. ROYAL NETHERLANDS METEOROLOGICAL INSTITUTE. Accessed on August 29th, 2019.

Lorenzo, A. M., van der Meer, J., and Hawkes, P. (2000). Effects of bi-modal waves on overtopping: application of UK and Dutch prediction methods. http://www.vandermeerconsulting.nl/downloads/functional_b/2000_vandermeer_regeling.pdf. Accessed on October 4th, 2019.

Oosterlo, P., van der Meer, J., Hofland, B., and van Vledder, G. (2018). Wave modelling in a complex estuary: Study in preparation of field measurement campaign Eems-Dollard estuary. *Coastal Engineering*, -:–.

Refrac-team (2019). Refrac user manual. Technical report, Delft University of Technology.

Riezebos, H. (2014). Additional thesis: Validation of SWASH for wave-channel interactions. Technical report, Delft University of Technology.

Rijkswaterstaat (2019). Buoy locations. Retrieved from Henk Steetzel of Arcadis.

Salmon, J. and Holthuijsen, L. (2015). Modeling depth-induced wave breaking over complex coastal bathymetries. *Coastal Engineering*, 105:21–35.

Steetzel, H. (2019). Risicoanalyse HR onderzoeksrapportage: Fase B. Technical report, POV Waddenzeedijken HWBP.

Steetzel, H., Groeneweg, J., and Vuik, V. (2018). Effectiviteit Voorlanden HR: Onderzoeksrapportage fase C. Technical report, POV-W.

SWAN-team (2019a). SWAN Scientific and Technical documentation. Technical report, Delft University of Technology.

SWAN-team (2019b). SWAN user manual. Technical report, Delft University of Technology.

van der Westhuysen, A., van Dongeren, A., Groeneweg, J., van Vledder, G., Peters, H., Gautier, C., and van Nieuwkoop, J. (2012). Improvements in spectral wave modeling in tidal inlet seas. *Journal of Geophysical research*, 117:C00J28.

van Dongeren, A., van der Westhuysen, A., Groeneweg, J., van Vledder, G., Lansen, J., Smale, A., Gautier, C., Peters, H., and Wenneker, I. (2011). Spectral wave modelling in tidal inlet seas: Results from the SBW Wadden Sea project. *Coastal Engineering Proceedings*, 1:32.

van Vledder, G., Hulst, S., and McConochie, J. (2016). Source term balance in a severe storm in the Southern North Sea. *Ocean Dynamics*, 66:1681–1697.

Waterschap-Noorderzijlvest (2020). Project meerjarige veldmetingen. Accessed on January 24th, 2020.

Zijlema, M. (2020). On grid dependence of refraction in SWAN. Retrieved from author in January 2020.

Zijlema, M., van Vledder, G., and Holthuijsen, L. (2012). Bottom friction and wind drag for wave models. *Coastal Engineering*, 65:19–26.

A

Scripts used for all computations

```
$************************HEADING************************
$
PROJ 'refractie' '1'
$

inp grid 0. 0. 0. 184 400 5 5
read bottom -1 'channel.bot' 1
set level 0.
period 10
set whinc 1.

area 0. 0. 0. 920 2000 1 1
num 0.01
bb 'hs.tab' 'x.tab'  'y.tab'  avg 2 2
mark file='rays.tab'
rays par angle 50. dist 20
bb comput
stop
```

Figure A.1: Script as used by REFRAC for the monochromatic cases in the schematic channel case. Conditions: T_p=10s, direction=220°N.

```
$************************HEADING************************
$
PROJ 'refractie wz' '[nr]'
$

inp bot xpinp=227123. ypinp=605736. alpinp=10. 280 220 100 100
read bottom 1 'wz3_rect.bot' 3
set level 0 fasmax=2000
period 10.0
set whinc 1

area 227123. 605736. 10. 280 220 100 100
num 0.01
bb 'hs.tab' 'x.tab'  'y.tab'  avg 2 2
mark file='rays.tab'
rays par angle -50 dist 10
bb comput
stop
```

Figure A.2: Script as used by REFRAC for the monochromatic cases in the Eastern Wadden Sea. Conditions: T_p=10s, direction=320°N.

```
$*************HEADING*************************************************
PROJECT 'IR' '1'
'Modelling the harbour of Riezebos - Tp, theta =10.0, 180'

$***************MODEL INPUT*****************************************
$---------------Standard settings-----------------------------------
SET LEVEL=0 NOR = 90.0 MAXMES=200 MAXERR = 2 grav=9.81 rho=1025 inrhog=1 NAUT
MODE STATIONARY TWOD
$-------------------------------------------------------------------
$ Specify coordinate system
COORD CART

$-----------Computational domain--------------------------------
CGRID REG xpc=0. ypc=0. alpc=0.  xlenc=920. ylenc=2000. mxc=184 myc=400 CIRcle &
  mdc=360 flow=0.095 fhigh=0.105  msc=2

$-----------Grid BC---------------------------------------------
INPgrid BOT REG xpinp=0. ypinp=0. alpinp=0. mxinp=184 myinp=400 dxinp=5 dyinp=5 EXC excval=-999.

$-----------Read input files BC---------------------------------
READinp BOTtom fac=-1 'grid\channel.bot' 1 0 FREE

$-----------BOUNDARY spectra------------------------------------
BOUnd SHAPespec BIN PEAK DSPR POWer
BOUndspec SIDE S CON PAR hs=1. per=10.0 dir=180 dd=1000
BOUndspec SIDE W CON PAR hs=1. per=10.0 dir=180 dd=1000
$-----------INITIAL conditions----------------------------------
INITial DEFault

$----------PHYSICS-------------------------------------------
OFF SOURCES

$----------NUMERICS-----------------------------------------
$
NUMeric STOPC dabs=0.005 drel=0.01 curvat=0.005 npnts=100 &
       STAT mxitst=40 alfa=0.01 $


$----------OUTPUT-------------------------------------------
$ Define locations
POINTS 'obs' FILE 'gauges.obs'

$ Write output parameters to output points
TABLE 'obs' HEADer 'output\TAB\[outfile].tab' XP YP DEPTH HSIGN TMM10 RTP DIR WLEN &
    LWAVP PROPT DISSU DISW DISB FOR
OUTPut OPTIons BLOck ndec=6 len=10 SPEC ndec=5
BLOCK 'COMPGRID' NOHEADer 'output\MAT\[outfile].mat' XP YP DEPTH HSIGN TMM10 RTP DIR WLEN DSPR &
   WATLEV DHSIGN DRTM01 PROPT DISSU DISW DISB FOR
$
SPEC 'obs' SPEC2D  ABS 'output\spec\[outfile].sp2'


$
COMPUTE
STOP
```

Figure A.3: Script as used by SWAN for the monochromatic cases in the schematic channel case. Conditions: T_p=10s, direction=180°N.

```
$**************HEADING*******************************************
PROJECT 'IR' '[nr]'
'Modelling the Eastern Wadden Sea - Tp, theta =10.0, -40'

$***************MODEL INPUT*****************************************
$--------------Standard settings-----------------------------
SET LEVEL=0 NOR = 90.0 MAXMES=200 MAXERR = 2 grav=9.81 rho=1025 inrhog=1 NAUT
MODE STATIONARY TWOD
$-----------------------------------------------------------------
$ Specify coordinate system
COORD CART

$-----------Computational domain--------------------------------
CGRID REG xpc=227123. ypc=605736. alpc=10.  xlenc=28000 ylenc=22000 mxc=280 myc=220 CIRcle &
  mdc=360 flow=0.095 fhigh=0.105  msc=2

$-----------Grid BC---------------------------------------------
INPgrid BOT REG xpinp=227123. ypinp=605736. alpinp=10. mxinp=280 myinp=220 dxinp=100 dyinp=100 EXC excval=-999.

$-----------Read input files BC---------------------------------
READinp BOTtom fac=1 'grid\wz3_rect.bot' 3 0 FREE

$-----------BOUNDARY spectra------------------------------------
BOUnd SHAPespec BIN PEAK DSPR POWer
BOUNDspec SIDE N CON PAR hs=1 per=10.0 dir=-40 dd=1000
BOUNDspec SIDE W CON PAR hs=1 per=10.0 dir=-40 dd=1000
$ SIDE E CON PAR hs=1 per=10.0 dir=-40 dd=1000
$-----------INITIAL conditions----------------------------------
INITial DEFault

$----------PHYSICS-------------------------------------------
OFF SOURCES

$----------NUMERICS-----------------------------------------
$
NUMeric STOPC dabs=0.005 drel=0.01 curvat=0.005 npnts=100 &
        STAT mxitst=50 alfa=0.01 $

$----------OUTPUT-------------------------------------------
$ Define locations
POINTS 'obs' FILE 'buoys_cart.obs'

$ Write output parameters to output points
TABLE 'obs' HEADer 'output\wlev0\TAB\[outfile].tab' XP YP DEPTH HSIGN TMM10 RTP DIR WLEN &
    LWAVP PROPT DISSU DISW DISB FOR
OUTPut OPTIons BLOck ndec=6 len=10 SPEC ndec=5
BLOCK 'COMPGRID' NOHEADer 'output\wlev0\MAT\[outfile].mat' XP YP DEPTH HSIGN TMM10 RTP DIR WLEN DSPR &
   WATLEV DHSIGN DRTM01 PROPT DISSU DISW DISB FOR
$
SPEC 'obs' SPEC2D  ABS 'output\wlev0\spec\[outfile].sp2'

$
COMPUTE
STOP
```

Figure A.4: Script as used by SWAN for the monochromatic cases in the Eastern Wadden Sea. Conditions: T_p=10s, direction=320°N.

```
$**************HEADING*************************************************
PROJECT 'IR' '1'
'Modelling the Eastern Wadden Sea'

$***************MODEL INPUT*********************************************
$--------------Standard settings-----------------------------------
SET NOR = 90.0 MAXMES=200 MAXERR = 2 grav=9.81 rho=1025 inrhog=1 NAUT
MODE STATIONARY TWOD
$-------------------------------------------------------------
$ Specify coordinate system
COORD SPHE CCM

$-----------Computational domain--------------------------------
CGRID CURVilinear mxc=266 myc=620 EXC excval=0.0 alpc=0 CIRcle &
  mdc=180 flow=0.030 fhigh=0.500  msc=30
READgrid COORdinates fac=1 'grid\wz3.grd' idla=3 nhedf=3  FORMAT '(10x,5f12.6)'
$-----------Grid BC---------------------------------------------
INPgrid BOT CURVilinear mxinp=266 myinp=620 EXC excval=-999.
INPgrid WLEV CURVilinear mxinp=266 myinp=620 EXC excval=-999.
$-----------Read input files BC---------------------------------
READinp BOTtom fac=1 'grid\wz3.bot' 3 0 FREE
READinp WLEV fac=1 'bc\wz3_2017Jan14_0000_UHWmask.wlev' 3 0 FREE
$-------------------------------------------------------------
$ Input a constant wind
WIND 20.3 329 DRAG FIT

$-----------BOUNDARY spectra------------------------------------
$
BOUNDspec SEGMENT IJ i=0 j=0 i=266 j=0 CON FILE 'bc\spec_2017_1_13_2350.bnd'
$-----------INITIAL conditions----------------------------------
INITial DEFault

$----------PHYSICS-------------------------------------------
GEN3 KOMEN
WCAP KOMEN DELTA=1
QUAD 2
BRE CON 1.0 0.73
FRIC JONswap CONstant 0.038
TRIad itriad=11
LIMiter ursell=10.0 qb=1.

$----------NUMERICS-----------------------------------------
$
NUMeric STOPC dabs=0.005 drel=0.01 curvat=0.005 npnts=99.5 &
        STAT mxitst=60 alfa=0.01 $

$----------OUTPUT-------------------------------------------
$ Define locations
POINTS 'NGRID001' FILE 'fine1'
POINTS 'NGRID002' FILE 'fine2'
POINTS 'obs' FILE 'buoys.obs'
POINTS 'obs1' FILE 'besafe.obs'


$ Write output parameters to output points
TABLE 'obs' HEADer 'output\TAB\grid1_SET00.tab' XP YP DEPTH HSIGN TMM10 TM01 RTP DIR DSPR &
    WATLEV BOTLEV WLEN LWAVP PROPT DISSU DISW DISB REDTRIAD FOR
TABLE 'obs1' HEADer 'output\TAB\besafe_grid1_SET00.tab' XP YP DEPTH HSIGN TMM10 TM01 RTP DIR DSPR &
    WATLEV BOTLEV WLEN LWAVP PROPT DISSU DISW DISB REDTRIAD FOR
OUTPut OPTIons BLOck ndec=6 len=10 SPEC ndec=5
BLOCK 'COMPGRID' NOHEADer 'output\MAT\grid1_SET00.mat' XP YP DEPTH HSIGN TMM10 TM01 RTP DIR WLEN DSPR &
 WATLEV DHSIGN DRTM01 PROPT DISSU DISW DISB REDTRIAD FOR
$
SPEC 'NGRID001' SPEC2D  ABS 'bc\fine1_grid1_SET00.sp2'
$SPEC 'NGRID002' SPEC2D  ABS 'bc\fine2_grid1_SET00.sp2'

SPEC 'obs' SPEC2D  ABS 'output\spec2\grid1_SET00.sp2'
SPEC 'obs' SPEC1D  ABS 'output\spec1\grid1_SET00.sp1'
SPEC 'obs1' SPEC1D  ABS 'output\spec1\besafe_grid1_SET00.sp1'

$
COMPUTE
STOP
```

Figure A.5: Script as used by SWAN for the realistic cases in the Eastern Wadden Sea. Conditions: Spectral data of 13 January 2017, 23:50h. In this case mdc=180, however, this is a variable.

```
$*************HEADING*************************************************
PROJECT 'IR' '1'
'Modelling the Eastern Wadden Sea'

$**************MODEL INPUT*********************************************
$--------------Standard settings-----------------------------------
SET NOR = 90.0 MAXMES=200 MAXERR = 2 grav=9.81 rho=1025 inrhog=1 NAUT
MODE STATIONARY TWOD
$-------------------------------------------------------------------
$ Specify coordinate system
COORD SPHE CCM

$-----------Computational domain--------------------------------
CGRID CURVilinear mxc=105 myc=831 EXC excval=0.0 alpc=0 CIRcle &
  mdc=360 flow=0.030 fhigh=0.500  msc=30
READgrid COORdinates fac=1 'grid\fine1.grd' idla=3 nhedf=3  FORMAT '(10x,5f12.6)'
$-----------Grid BC---------------------------------------------
INPgrid BOT CURVilinear mxinp=105 myinp=831 EXC excval=-999.
INPgrid WLEV CURVilinear mxinp=105 myinp=831 EXC excval=-999.
$-----------Read input files BC---------------------------------
READinp BOTtom fac=1 'grid\fine1.bot' 3 0 FREE
READinp WLEV fac=1 'bc\fine1_2017Jan14_0000_UHWmask.wlev' 3 0 FREE
$-------------------------------------------------------------------
$ Input a constant wind
WIND 20.3 329 DRAG FIT

$-----------BOUNDARY spectra------------------------------------
$
BOUN NEST 'bc\fine1_grid1_SET00.sp2' CLOSED
$-----------INITIAL conditions----------------------------------
INITial DEFault

$----------PHYSICS-------------------------------------------
GEN3 KOMEN
WCAP KOMEN DELTA=1
QUAD 2
BRE CON 1.0 0.73
FRIC JONswap CONstant 0.038
TRIad itriad=11
LIMiter ursell=10.0 qb=1.

$
$----------NUMERICS-----------------------------------------
$
NUMeric STOPC dabs=0.005 drel=0.01 curvat=0.005 npnts=99 &
        STAT mxitst=50 alfa=0.01 $

$----------OUTPUT-------------------------------------------
$ Define locations
POINTS 'obs' FILE 'fine1'
$POINTS 'obs1' FILE 'besafe.obs'


$ Write output parameters to output points
TABLE 'obs' HEADer 'output\TAB\grid2_SET00.tab' XP YP DEPTH HSIGN TMM10 TM01 RTP DIR WLEN &
    LWAVP PROPT DISSU DISW DISB REDTRIAD FOR
TABLE 'obs1' HEADer 'output\TAB\besafe_grid2_SET00.tab' XP YP DEPTH HSIGN TMM10 TM01 RTP DIR WLEN &
    LWAVP PROPT DISSU DISW DISB REDTRIAD FOR
OUTPut OPTIons BLOck ndec=6 len=10 SPEC ndec=5
BLOCK 'COMPGRID' NOHEADer 'output\MAT\grid2_SET00.mat' XP YP DEPTH HSIGN TMM10 TM01 RTP DIR WLEN DSPR &
   WATLEV DHSIGN DRTM01 PROPT DISSU DISW DISB REDTRIAD FOR
$
SPEC 'obs' SPEC2D  ABS 'output\spec2\grid2_SET00.sp2'
SPEC 'obs' SPEC1D  ABS 'output\spec1\grid2_SET00.sp1'
SPEC 'obs1' SPEC1D  ABS 'output\spec1\besafe_grid2_SET00.sp1'

$
COMPUTE
STOP
```

Figure A.6: Script as used by SWAN for the nest of the realistic case in the Eastern Wadden Sea. Conditions: Spectral data of 13 January 2017, 23:50h..

B

Harbour channel additional figures

B.1. REFRAC figures

This section contains the additional figures for a period of T=5s and 15s. The first two figures show the wave rays for incoming wave directions of respectively 180, 200 and 220°N.

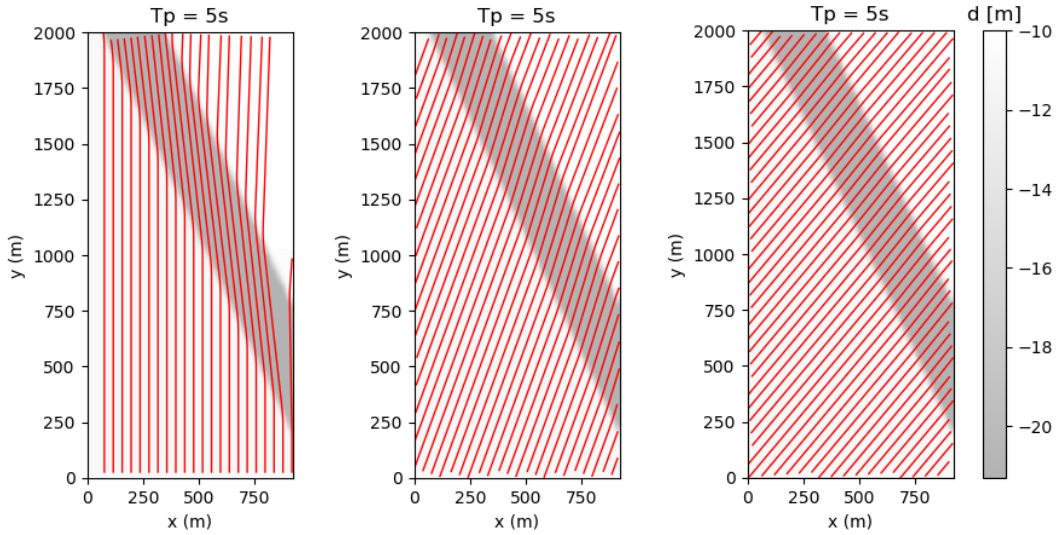

(a) Incoming wave 180°N (b) Incoming wave 200°N (c) Incoming wave 220°N

Figure B.1: Wave rays according to REFRAC for different incoming wave directions for T=5s, H_{in}=1m.

It can be noted that for T=5s, the wave rays are able to cross the channel for all considered directions. The wave ray pattern of T=15s shows a similar behaviour as was seen for T=10s, since the critical angles of these frequencies are very close to each other.

Figures B.3 and B.4 give the wave ray pattern for T=5s and 15s respectively for incoming wave directions around the corresponding critical angle. It can be seen that refraction turns the waves away from the channel for incoming directions smaller than the critical angle. For wave directions above the critical angle, wave rays are able to enter the channel.

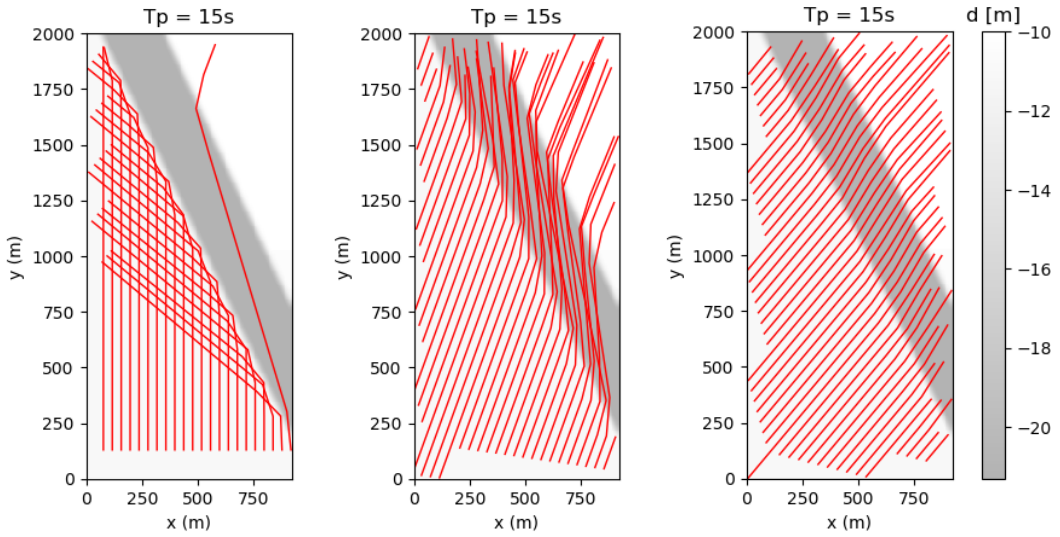

(a) Incoming wave 180°N (b) Incoming wave 200°N (c) Incoming wave 220°N

Figure B.2: Wave rays according to REFRAC for different incoming wave directions for T=15s, H_{in}=1m.

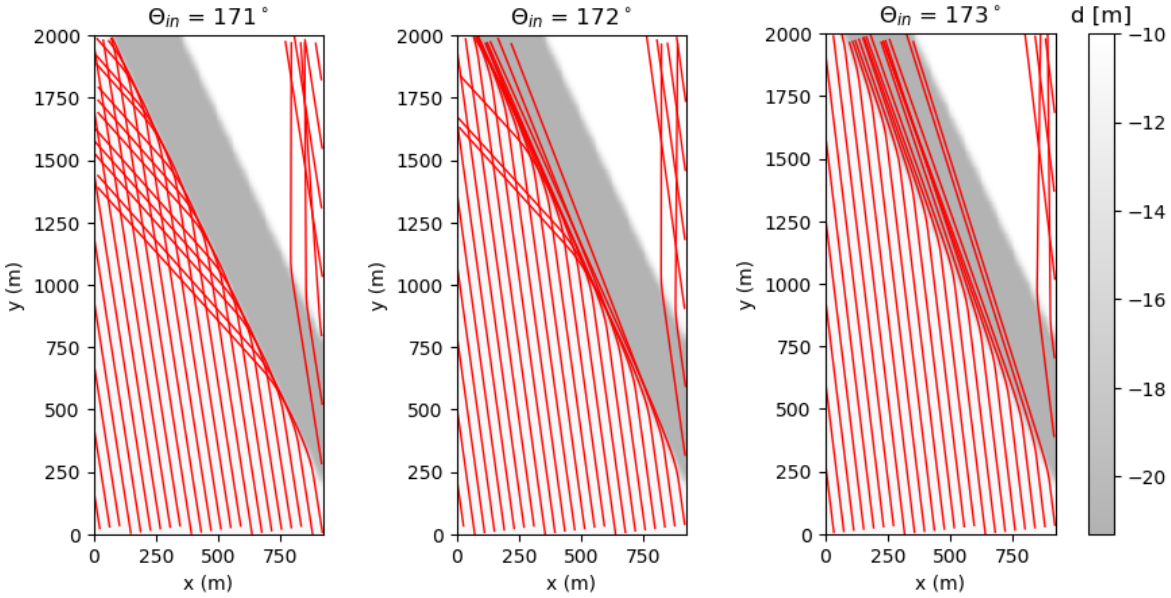

(a) Incoming wave 171°N (b) Incoming wave 172°N (c) Incoming wave 173°N

Figure B.3: Wave rays according to REFRAC for wave directions around the critical angle of 172°N for T=5s, H_{in}=1m.

B.2. Refraction off

In case refraction is turned off in SWAN, the significant wave heights become as given in figure B.5. The boundary effect at the right side of B.5(b) is caused by waves refracting off the boundary. This effect can not be prevented properly and thus results close to the east boundary should not be taken into account. Furthermore, the wave heights for a directional resolution of 6° are larger than for all other cases. Hence the wave field is not properly modelled for this coarser resolution. Both of the other directional resolution variants showed the same result as well as the grid variants, which are all equal to figure B.5(a). For the frequency variants some differences where found.

The lowering in wave height inside the channel and increase at the downwave side of the channel are both

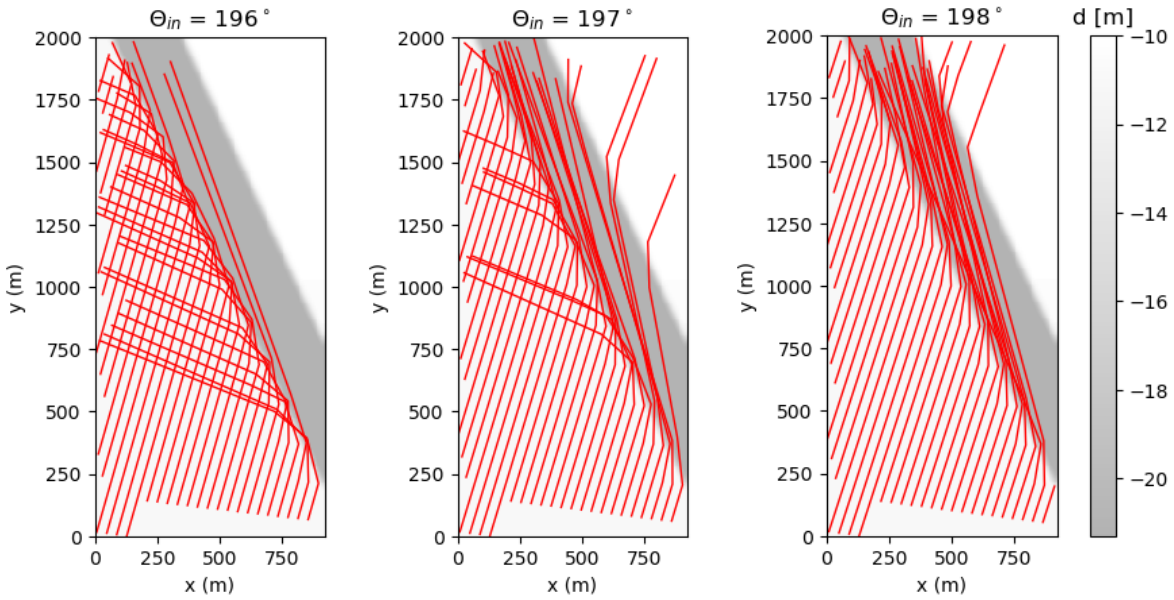

(a) Incoming wave 196°N (b) Incoming wave 197°N (c) Incoming wave 198°N

Figure B.4: Wave rays according to REFRAC for wave directions around the critical angle of 197°N for T=15s, H_{in}=1m.

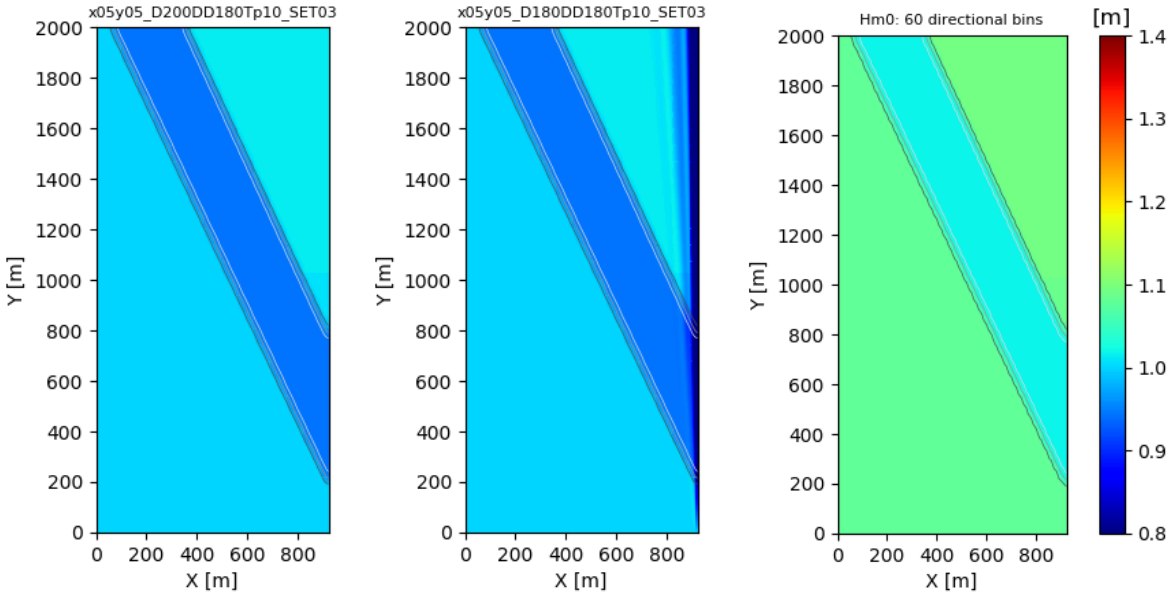

(a) Incoming wave 200°N (b) Incoming wave 180°N (c) Incoming wave 200°N, 60 directional bins

Figure B.5: Significant wave height according to SWAN when refraction is excluded. T_p=10s.

caused by shoaling effects. The influence of shoaling on the wave height is determined by:

$$H_2 = \sqrt{\frac{c_{g,1}}{c_{g,2}}} H_1 \tag{B.1}$$

Where the wave group celerity is equal to nc and c is determined by the dispersion relationship:

$$c_g = nc = \frac{1}{2}\left(1 + \frac{2kd}{\sinh 2kd}\right)\sqrt{\frac{g}{k}\tanh kd} \tag{B.2}$$

Thus the group velocities for a peak period of 10s in front of and inside the channel respectively become:

$$\begin{aligned} d_1 = 11m \quad &\rightarrow \quad c_{g,1} = 8.30 m/s \\ d_2 = 21.3m \quad &\rightarrow \quad c_{g,2} = 9.33 m/s \end{aligned} \tag{B.3}$$

With an incoming wave height of 1m, the wave height inside the channel then becomes:

$$H_2 = \sqrt{\frac{8.296}{9.327}} \cdot 1 = 0.94\, m \tag{B.4}$$

This is exactly the wave height SWAN gives inside the channel, hence the wave height is only affected by shoaling. To verify, the above calculation is also performed for T_p=5s and T_p=15s. This gave a wave height inside the channel of respectively 1.05m and 0.89m.

B.3. Direction dependency

This section gives the absolute figures corresponding to different grid resolutions, incoming wave directions and frequencies. Also relative wave height plots for wave directions and periods that are not in the main report are presented here. First, figures B.6 and B.7 show the relative wave height for a wave period of respectively 5s and 15s for wave directions around the critical angle. These figures are similar to the one as presented in the main report.

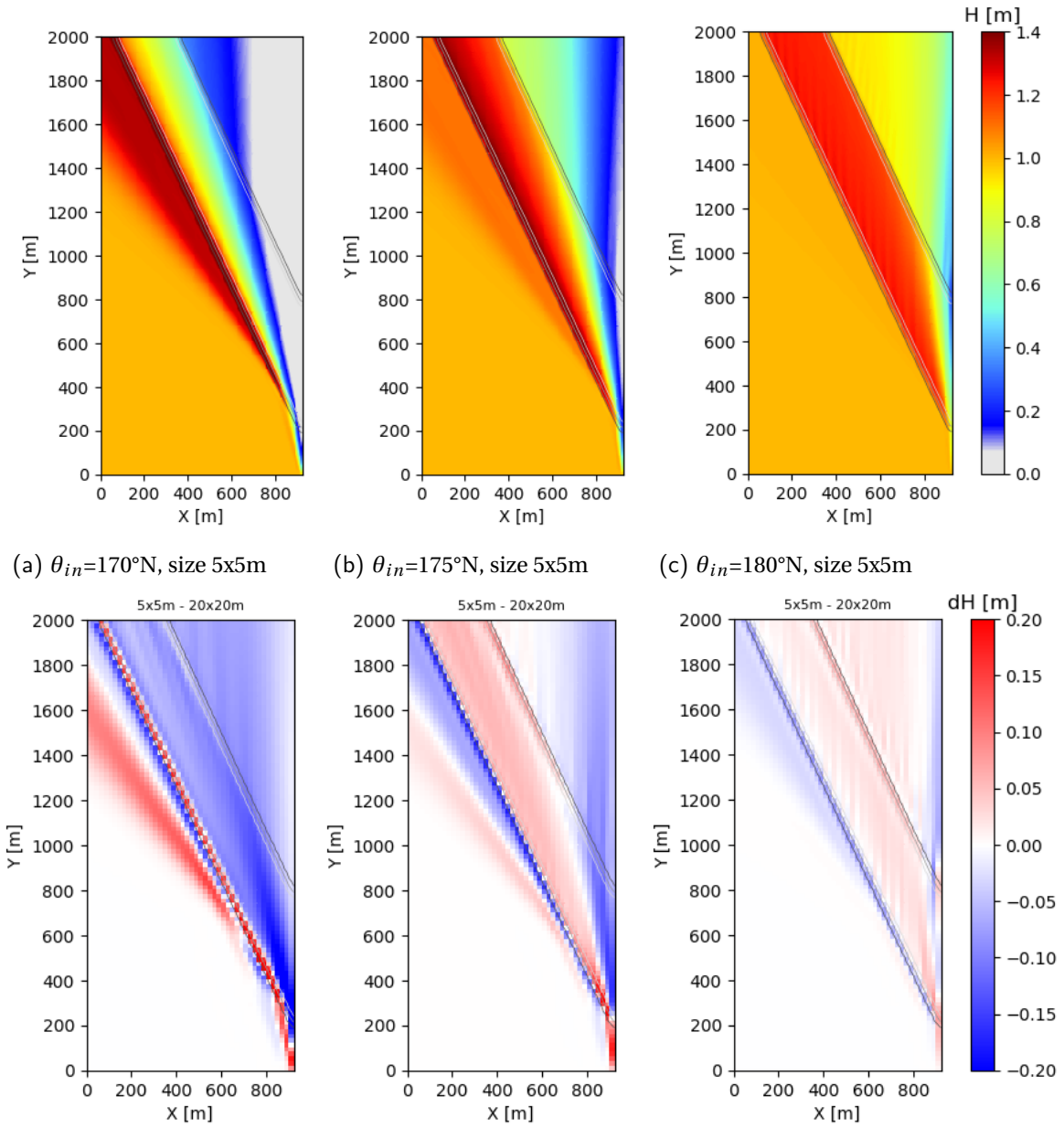

(a) θ_{in}=170°N, size 5x5m (b) θ_{in}=175°N, size 5x5m (c) θ_{in}=180°N, size 5x5m

(d) θ_{in}=170°N, size 5x5-20x20m (e) θ_{in}=175°N, size 5x5-20x20m (f) θ_{in}=180°N, size 5x5-20x20m

Figure B.6: Upper: absolute significant wave height of a 5x5m grid; Lower: relative height of a 20x20m grid to 5x5m grid, for different incoming wave directions. For all plots T_p=5s.

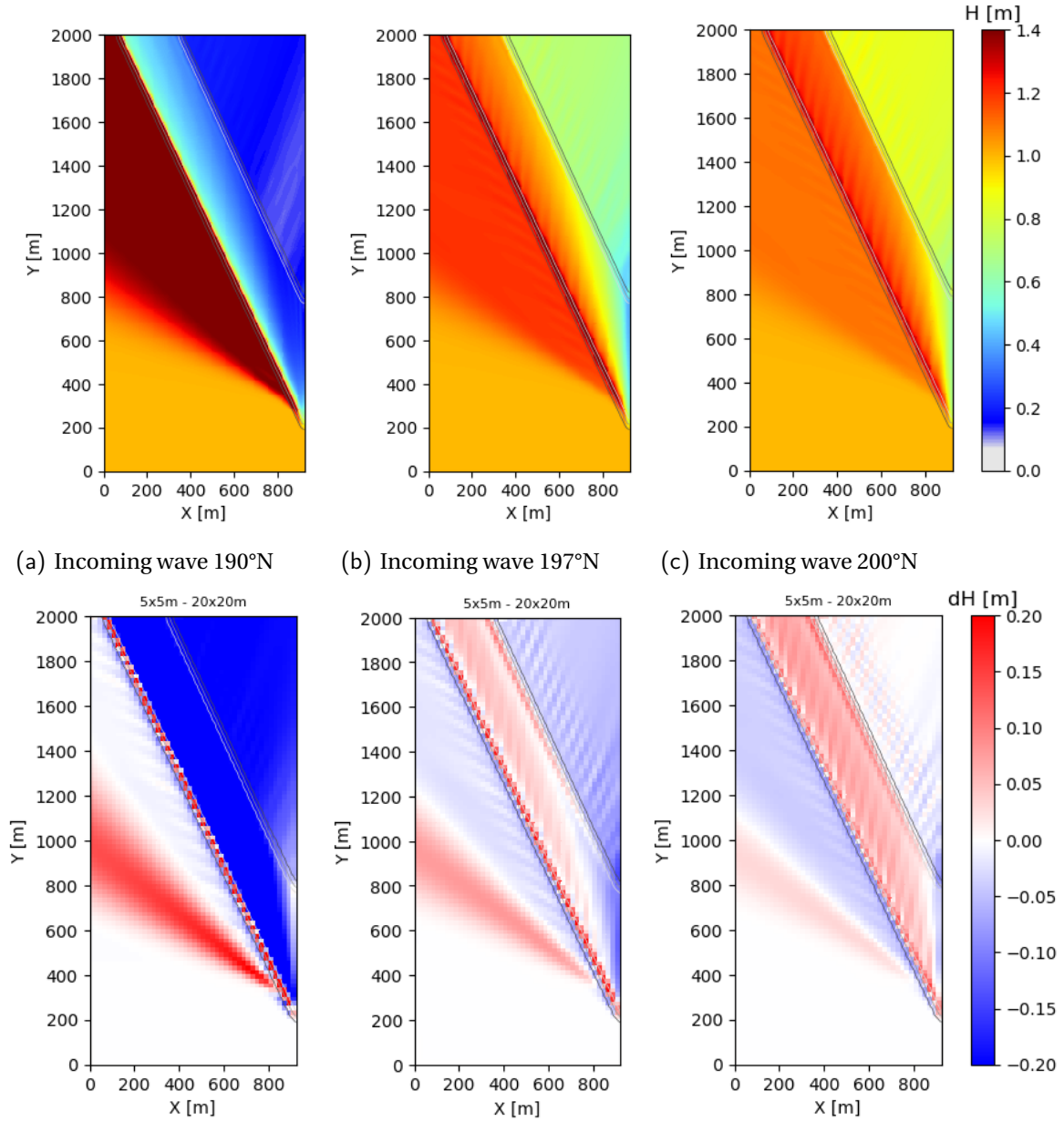

(a) Incoming wave 190°N (b) Incoming wave 197°N (c) Incoming wave 200°N

(d) Incoming wave 190°N (e) Incoming wave 197°N (f) Incoming wave 200°N

Figure B.7: Upper: absolute significant wave height of a 5x5m grid; Lower: relative height of a 20x20m grid to 5x5m grid, for different incoming wave directions. For all plots T_p=15s.

Subsequently, absolute wave height plots are for multiple directions are given in figures B.8 to B.13. Here each figure corresponds to a wave period and a spatial resolution of respectively 5m or 20m mesh width.

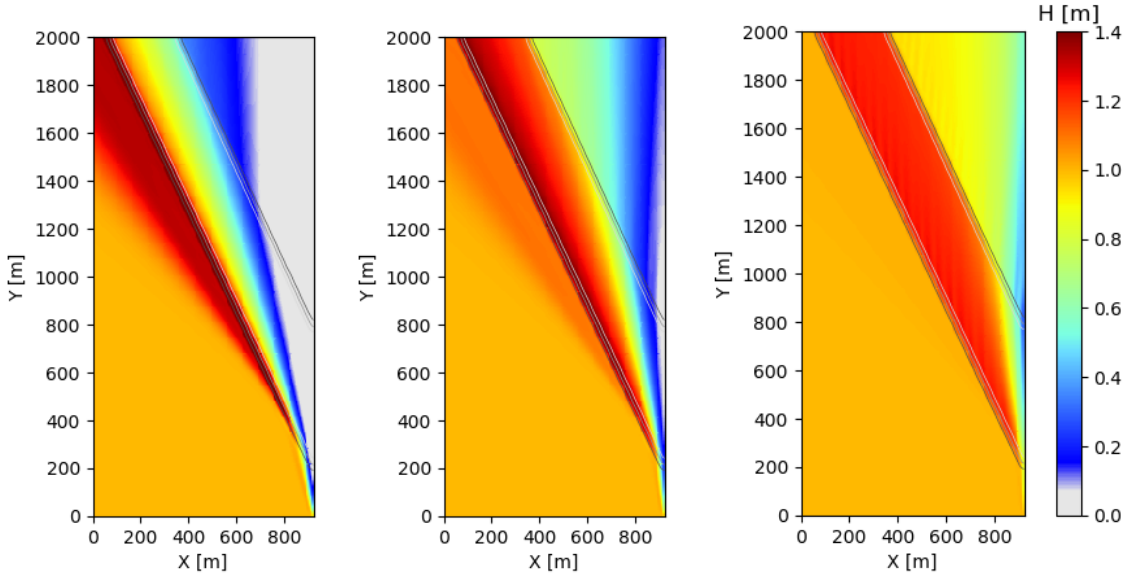

(a) Incoming wave 170°N (b) Incoming wave 175°N (c) Incoming wave 180°N

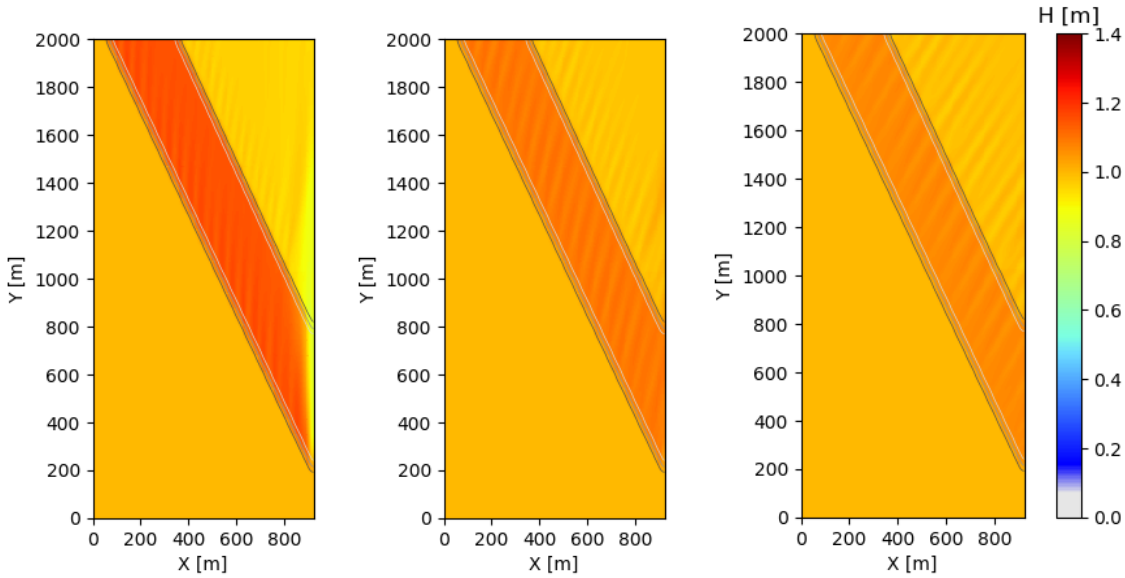

(d) Incoming wave 185°N (e) Incoming wave 195°N (f) Incoming wave 210°N

Figure B.8: Absolute significant wave height of a 5x5m grid for different incoming wave directions. For all plots T_p=5s.

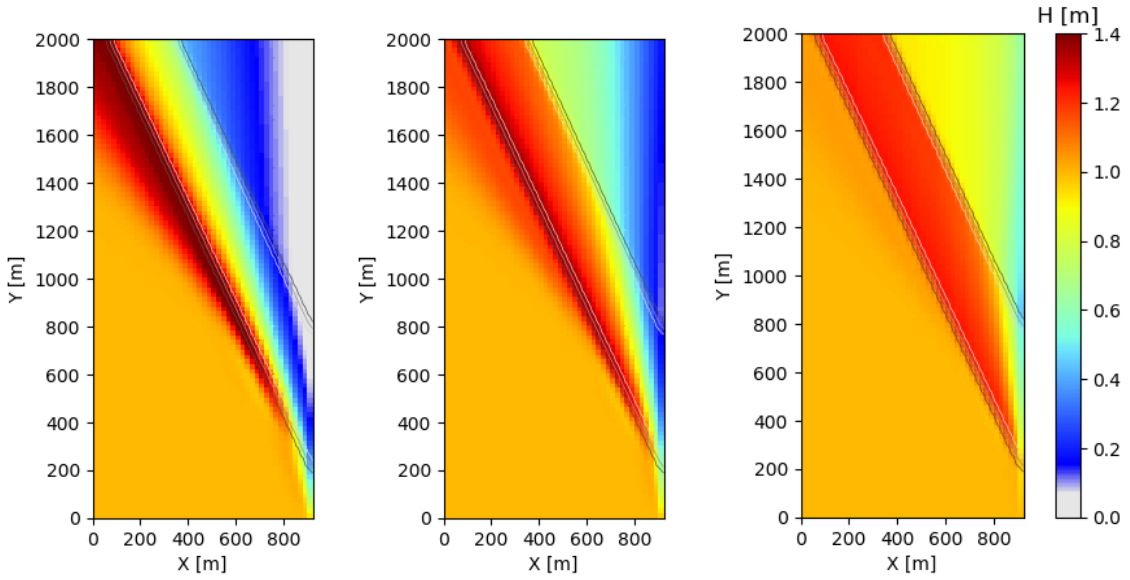

(a) Incoming wave 170°N (b) Incoming wave 175°N (c) Incoming wave 180°N

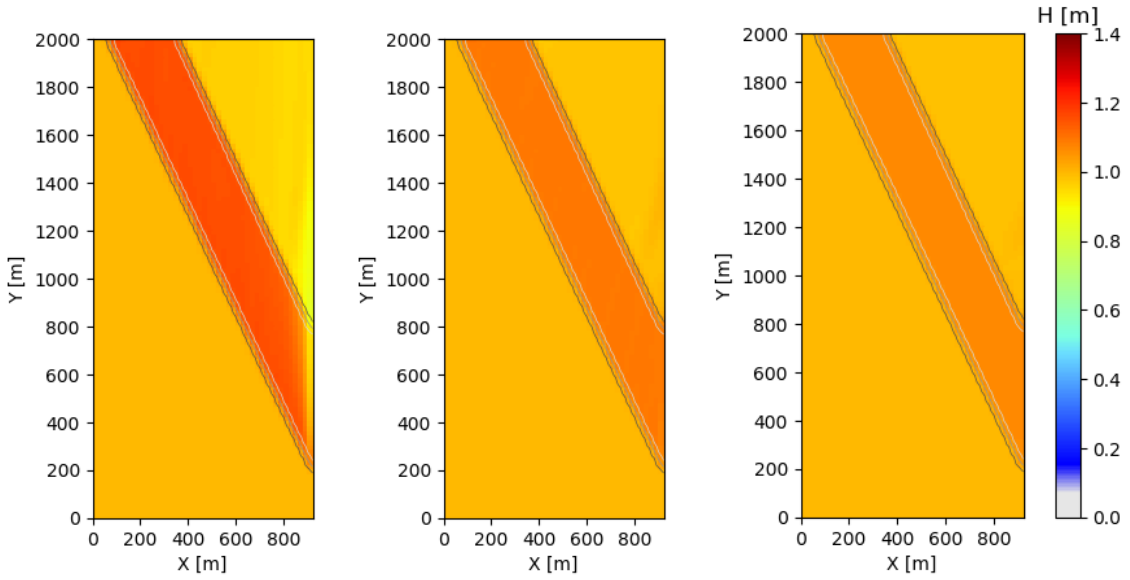

(d) Incoming wave 185°N (e) Incoming wave 195°N (f) Incoming wave 210°N

Figure B.9: Absolute significant wave height of a 20x20m grid for different incoming wave directions. For all plots T_p=5s.

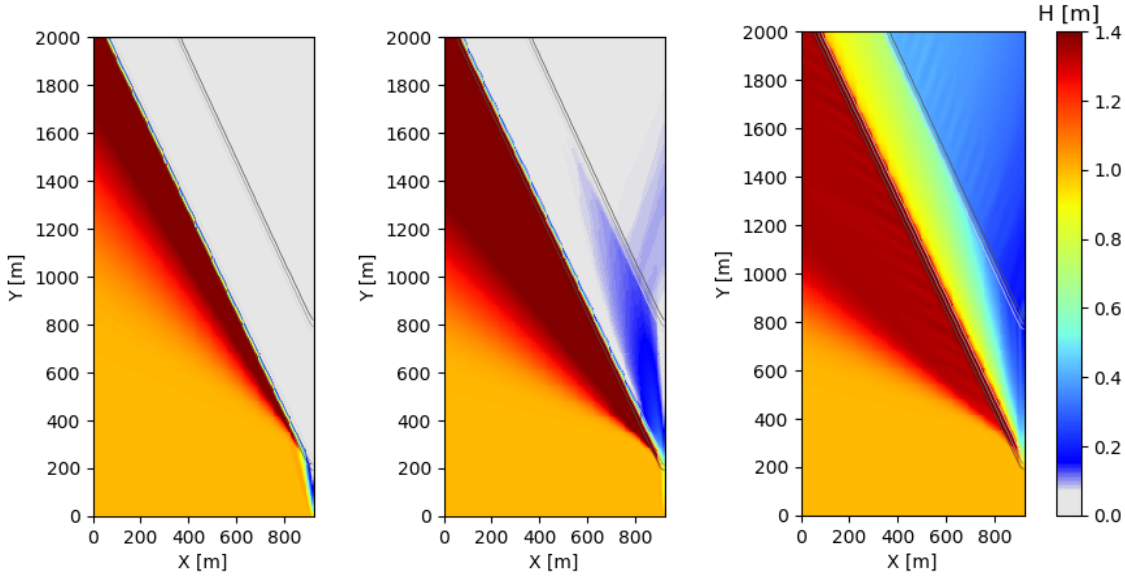

(a) Incoming wave 170°N (b) Incoming wave 180°N (c) Incoming wave 190°N

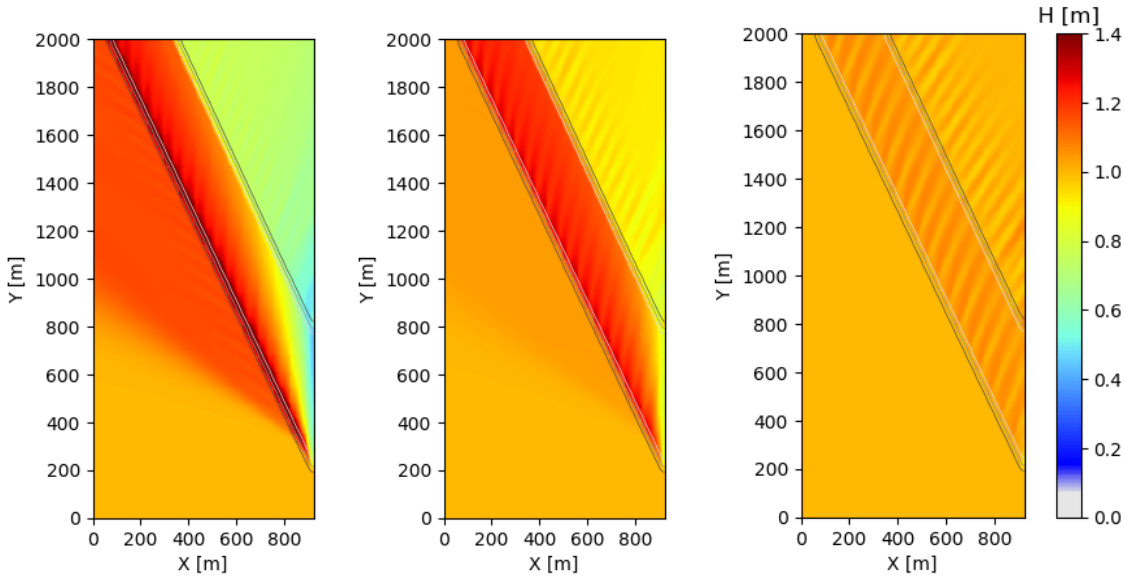

(d) Incoming wave 195°N (e) Incoming wave 200°N (f) Incoming wave 210°N

Figure B.10: Absolute significant wave height of a 5x5m grid for different incoming wave directions. For all plots T_p=10s.

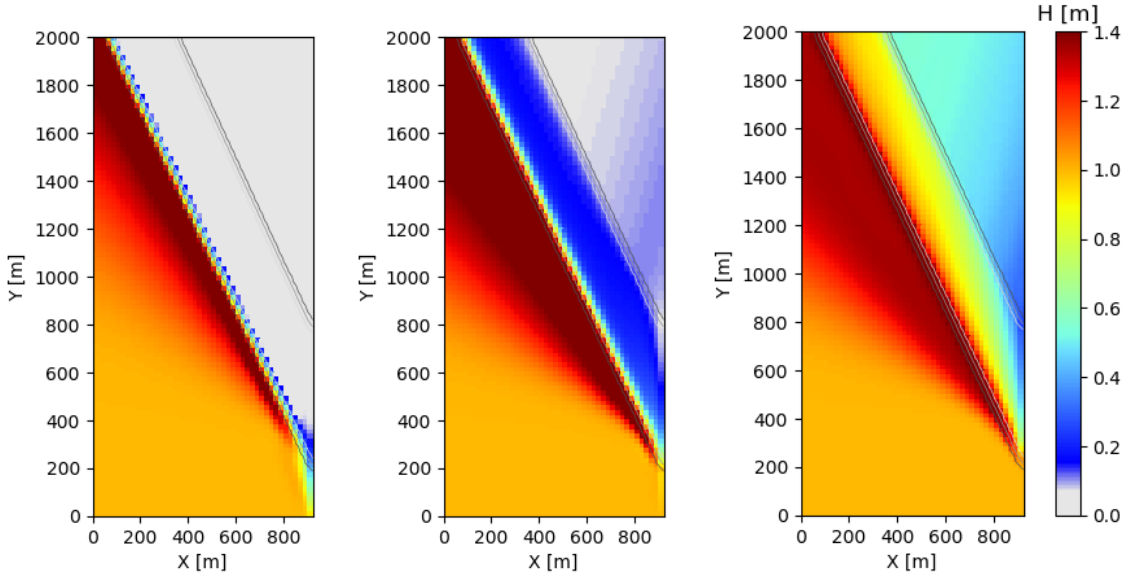

(a) Incoming wave 170°N (b) Incoming wave 180°N (c) Incoming wave 190°N

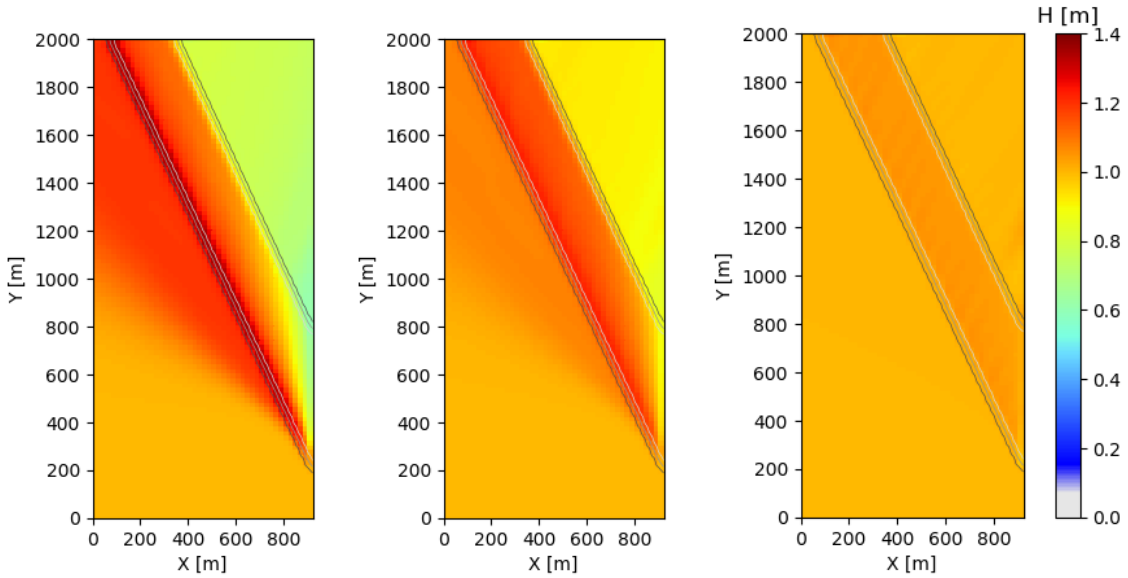

(d) Incoming wave 195°N (e) Incoming wave 200°N (f) Incoming wave 210°N

Figure B.11: Absolute significant wave height of a 20x20m grid for different incoming wave directions. For all plots T_p=10s.

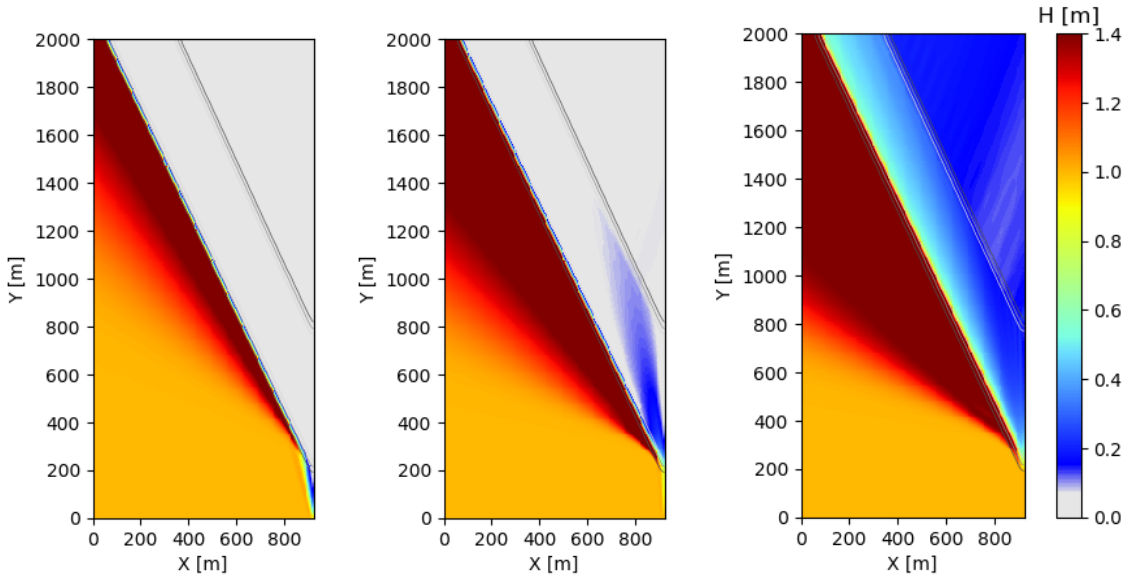

(a) Incoming wave 170°N (b) Incoming wave 180°N (c) Incoming wave 190°N

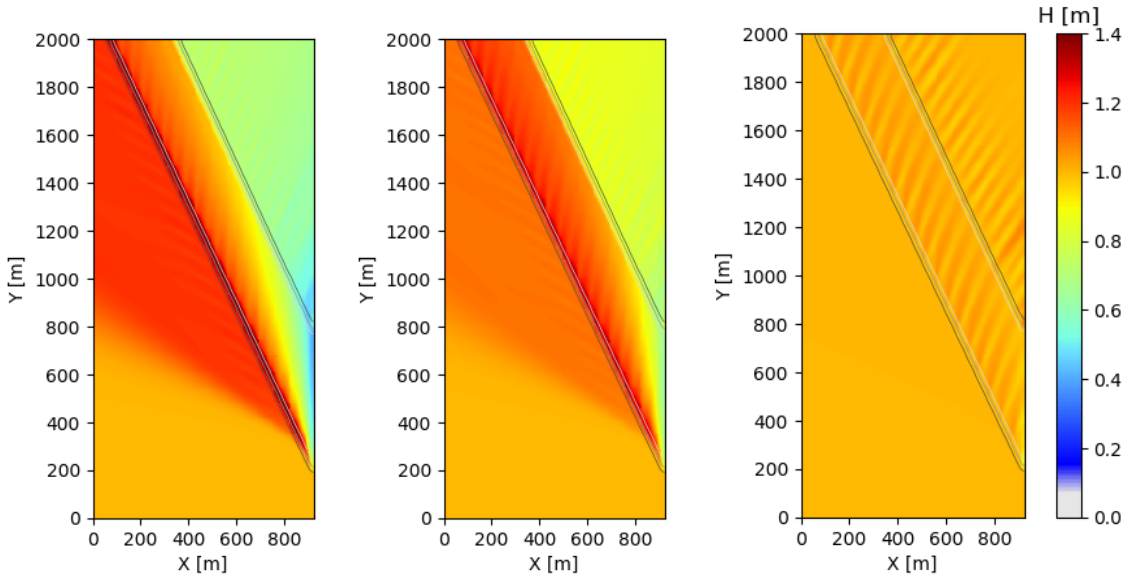

(d) Incoming wave 197°N (e) Incoming wave 200°N (f) Incoming wave 210°N

Figure B.12: Absolute significant wave height of a 5x5m grid for different incoming wave directions. For all plots T_p=15s.

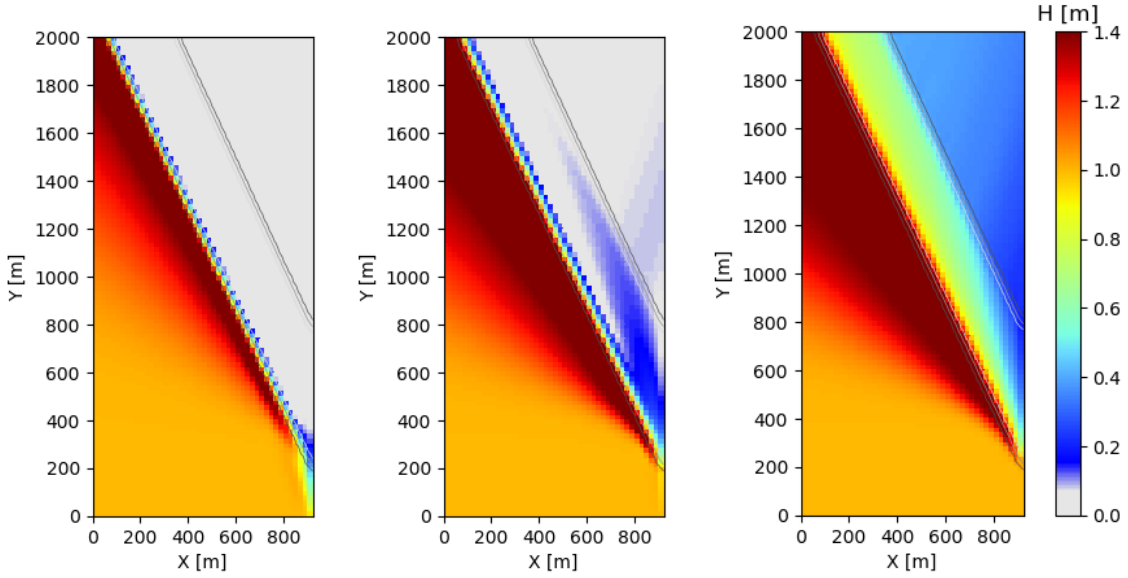

(a) Incoming wave 170°N (b) Incoming wave 180°N (c) Incoming wave 190°N

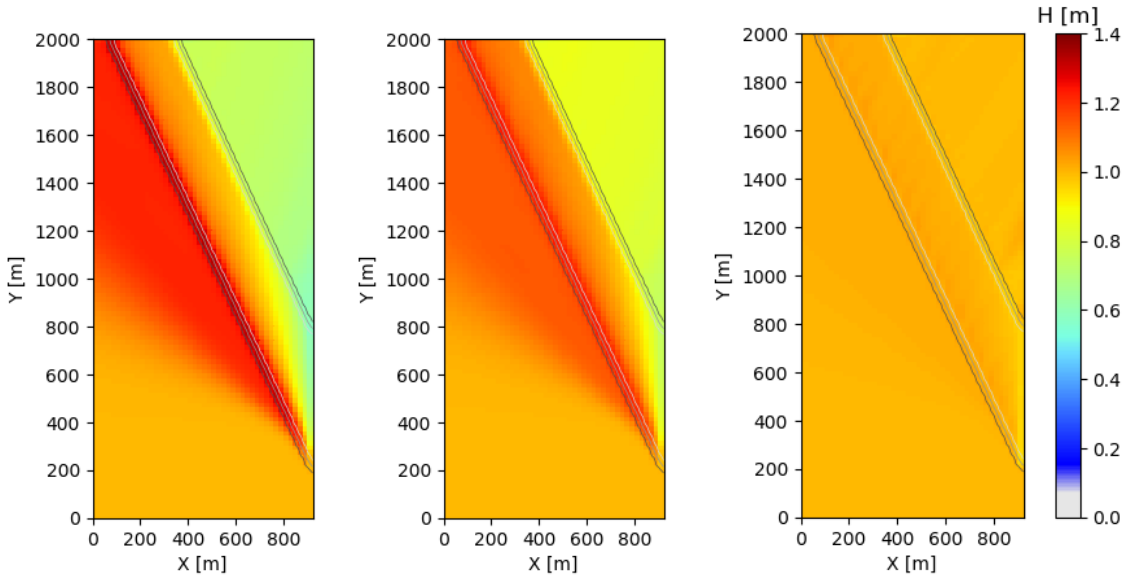

(d) Incoming wave 197°N (e) Incoming wave 200°N (f) Incoming wave 210°N

Figure B.13: Absolute significant wave height of a 20x20m grid for different incoming wave directions. For all plots T_p=15s.

B.4. Directional resolution

The wave heights for a wave direction of 200°N and a directional resolution of 1° and 0.1° are given in figure B.14. It can be seen that the amount of wave refraction is less for the finest resolution, hence the modelling of refraction is improved. However, the absolute difference is quite small, suggesting that the resolution of 1° already was close to sufficient. Considering the diffuseness of both graphs, it can be seen that they both have an equal 'streaky' behaviour. Hence the coarseness of the directional resolution did not cause this behaviour. On the contrary, the non-diffusive behaviour strengthens with finer resolutions.

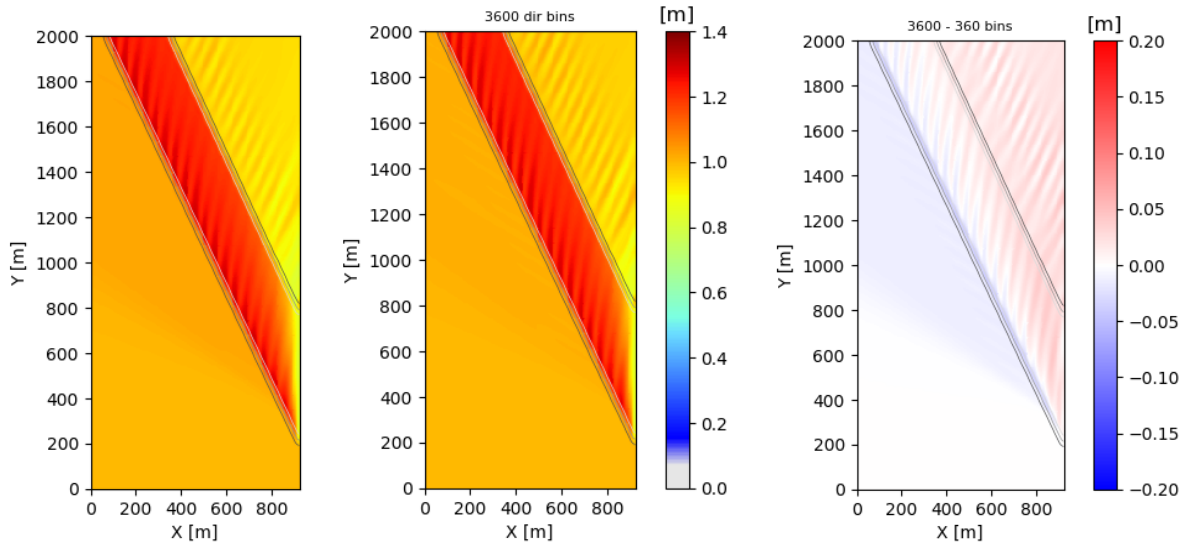

(a) DR4, incoming wave: 200°N (b) Dr3, incoming wave: 200°N (c) DR4 - DR3, incoming wave: 200°N

Figure B.14: Significant wave height of a 5x5m grid for different incoming wave directions and directional resolutions, for all plots T_p=10s. DR3=1°(360 bins), DR4=0.1°(3600 bins).

C

Mesh width analysis

This appendix gives a more detailed overview of the influence of the chosen grid resolution for the harbour channel as given in chapter 4. Here it is assumed that a grid size of 1x1m, 920 by 2000 meshes in respectively x- and y-direction, gives the best approximation. Therefore, this will be chosen as reference grid. Additional information about the applied settings and boundary conditions is given in table C.1.

Table C.1: Boundary conditions and additional settings as used in the SWAN simulation for the mesh study.

Setting	**Value**
Bathymetric resolution	920 by 2000 meshes (1x1m grid size)
Numerical scheme	SORDUP
Wave height	1 m
Periods	5, 10 or 15s
Wave directions	170-200°, with steps of 5°

Only a rectangular grid with equal size in x and y direction will be tested. Since the refraction pattern is dependent on the wave frequency and direction, these will be varied to observe the response of the mesh variants. The used variations for wave period and direction are given in table C.1.

To determine the accuracy of the different mesh widths, use will be made of the root mean squared error, RMSE or rms-error, of the significant wave height distribution. This error is defined in equation C.1. Here N is the number of grid points for which the wave height is computed. $H_{s,ref}$ is the reference wave height from the 1x1m mesh size and H_s is the significant wave height of the variant mesh size.

$$RMSE = \sqrt{\frac{\sum^i \left(H^i_{s,ref} - H^i_s\right)^2}{N}} \tag{C.1}$$

Also the relative bias, RB, is determined to observe the systematic error that is made by the different mesh widths. The RB is defined according to equation C.2.

$$RB = \frac{\sum^i \left(H^i_s - H^i_{s,ref}\right)}{\sum^i H^i_{s,ref}} \tag{C.2}$$

These two statistical parameters are calculated for mesh widths between 1 and 40m. It is important to notice that the RB can become negative, while the RMSE cannot be smaller than zero due to the square and square root. Since the sum components of RB can be either positive and negative, it will occur that they cancel each other. This has to be taken into account and care should be taken in making conclusions based on the RB.

The following mesh sizes are applied:

- 1m
- 2m
- 5m
- 10m
- 20m
- 40m

First the rms-error of the wave height is considered. Figure C.1 gives the RMSE against the mesh width for various wave directions per wave period. The RMSE increases with increasing mesh width in a logarithmic shape, therefore the plots are made on log-log scale. In general, a sufficient grid size is found if the change in error is limited. It can be noted that the difference between the 1m and 2m grid sizes is relatively small for all cases. Still, taking for example a 5m mesh width leads to an RMSE of 2-7cm for T_p=10s compared to the reference mesh width. The error could thus become more than 5%, if this is not allowed the grid size of 5m is insufficient and 2m should be used. In this case the computational time and hence efficiency is left out of consideration.

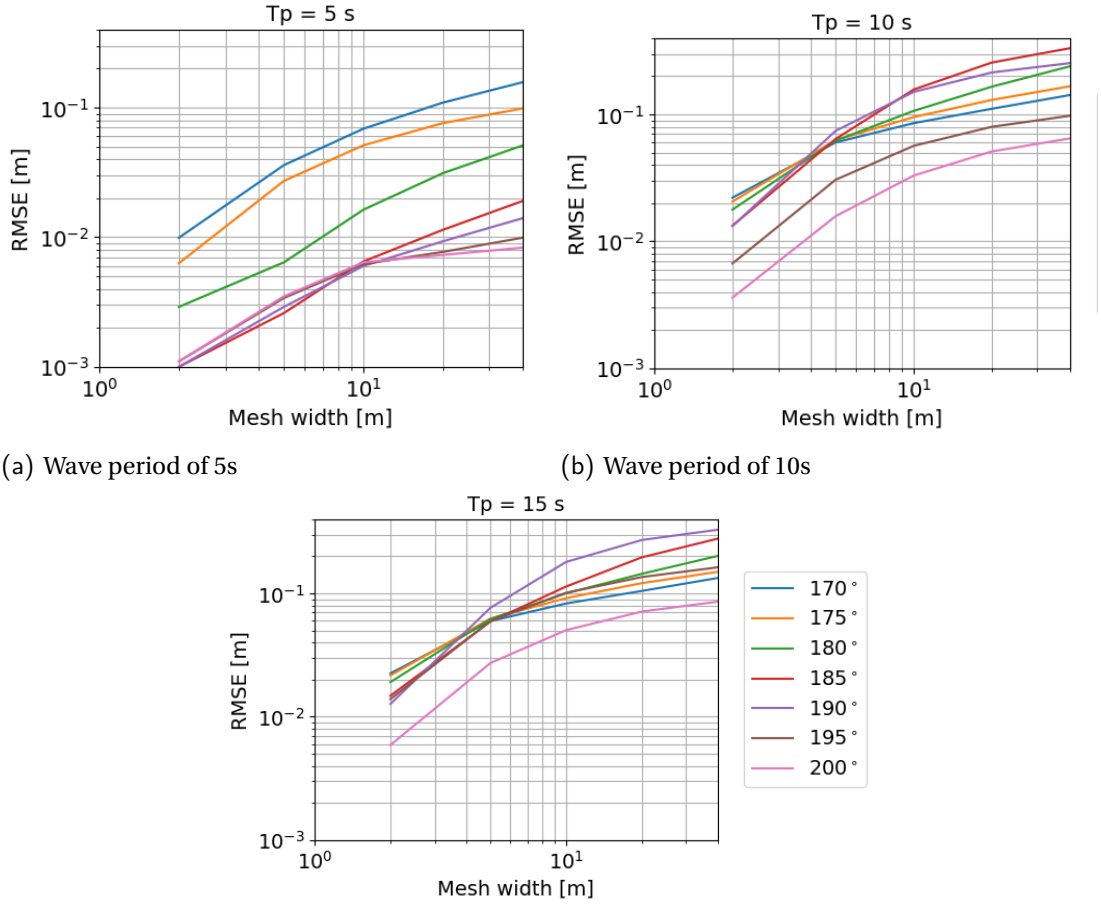

(a) Wave period of 5s

(b) Wave period of 10s

(c) Wave period of 15s

Figure C.1: RMSE as function of mesh width for different wave directions and periods on a log scale.

Furthermore, figure C.1 shows that in general the largest errors are found for large wave periods and angles around 5-10° lower than the corresponding critical angle for refraction. This pattern cannot be observed in figure C.1(a) since here the lowest incoming wave angle is approximately equal to the critical angle. Both the T_p=10s and 15s cases show a maximum RMSE of around 0.33m for a mesh width of 40m. When observing the rms-error of the critical wave directions, one finds an approximately equal error for all period variants. The maximum error at the critical direction is around 0.12 for all cases at a mesh width of 40m.

Figure C.2 gives the same RMSE as before, only now as function of the wave direction. This representation clearly shows the development of the rms-error over wave directions. Also, the maximum error is not yet reached within the considered directions for the T_p=5s case. What can be clearly seen here is that for high wave directions the errors reach to a minimum value, which is slightly higher for larger mesh widths. This minimum error will in all cases be present and is due to discretisation errors of the bathymetry and lack of diffusion, causing the garden-sprinkler effect to be present in fine grid variants. Since coarse grids show a more diffuse solution, the wave height distribution differs slightly causing a minimum RMSE value to be

present.

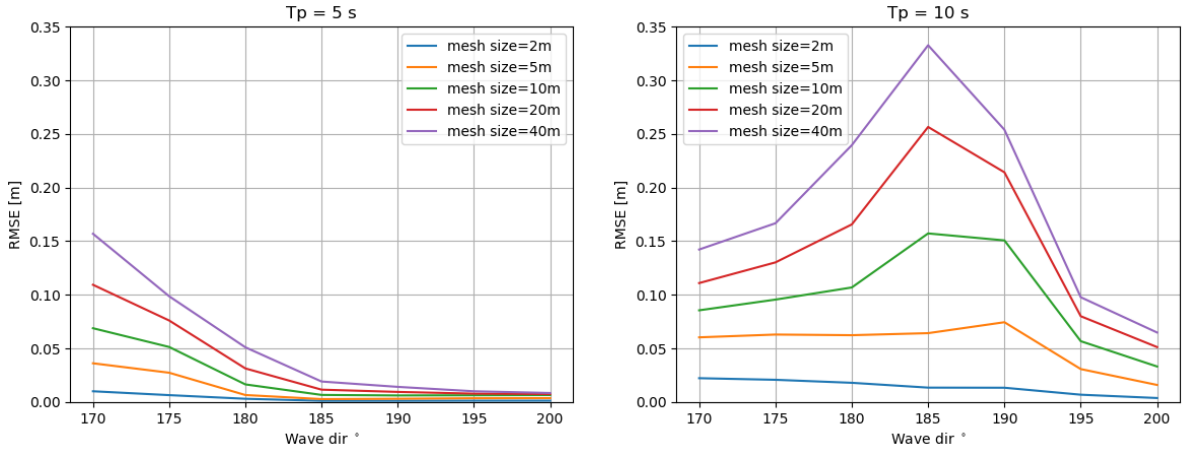

(a) Wave period of 5s

(b) Wave period of 10s

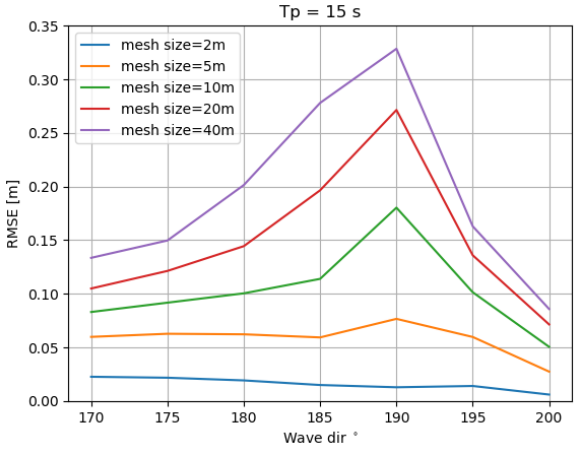

(c) Wave period of 15s

Figure C.2: RMSE as function of wave direction for different mesh widths wave periods.

It can be observed from figure C.2 that the RMSE is always lower than 0.03m for a mesh size of 2m for all period variants. Also, the peak error just before the critical wave direction which is present for all other mesh sizes, is absent for a 2m mesh width.

Figures C.3 and C.4 give the RMSE as function of mesh width, where each plot shows a different wave direction. This again shows that irrespective of the specific peak period, the error is largest if the wave direction is approximately 10° below the critical wave direction. Therefore, from 175-185°, the error is largest for T_p=10s. For higher wave directions, the largest errors are found for T_p=15s. It can also be noticed that for the range from 170-190° the error for these two period variants is equal for all mesh widths below 5m. Hence, the error is independent of the specific wave period for wave directions in the range 170-190°N, T_p>10s and relatively fine grids. When observing figure C.3(a) specifically, one can see that the RMSE has the same order of values for all wave periods. This was also visible in figure C.2. Here, the error of the lowest period variant is still increasing with decreasing wave direction, while the RMSE reduces with decreasing direction for the other period variants. Apparently, they cross at an incoming wave direction of around 170°.

From this point the focus will be on the relative bias. Figure C.5 gives the relative bias as function of the mesh width for different wave directions per period. It can be clearly seen that RB approaches zero for mesh widths≤2m for all periods and directions. Also, for incoming wave directions larger than the critical directions the RB approaches zero for all cases and becomes negative. A negative RB holds that the sum of all H_s^i –

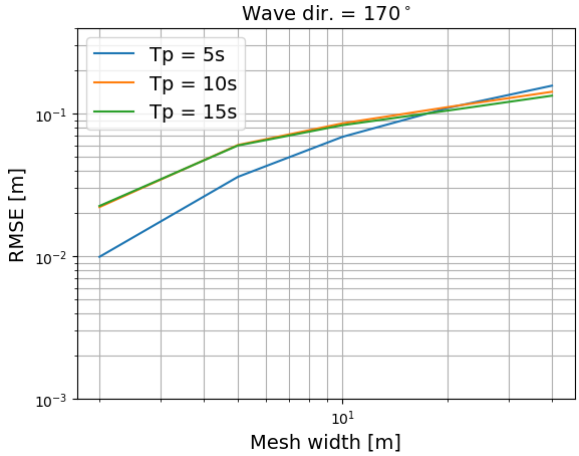

(a) Wave direction = 170°

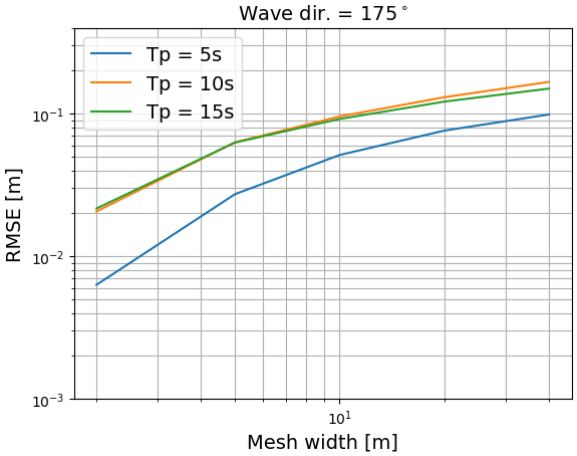

(b) Wave direction = 175°

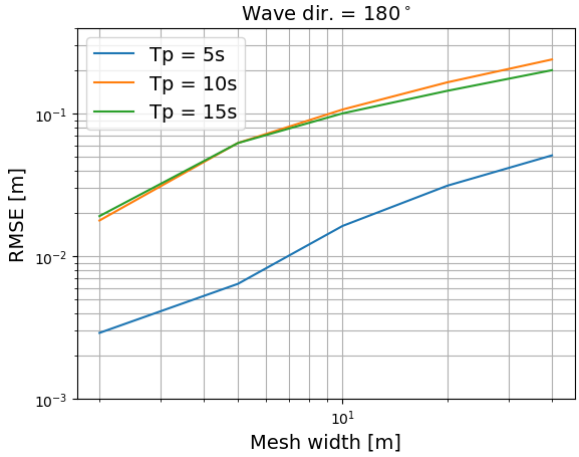

(c) Wave direction = 180°

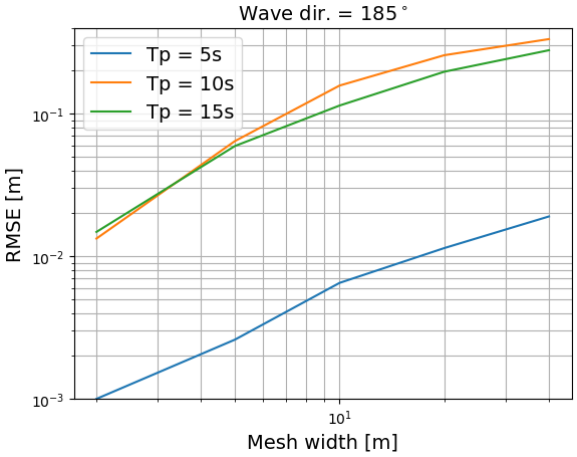

(d) Wave direction = 185°

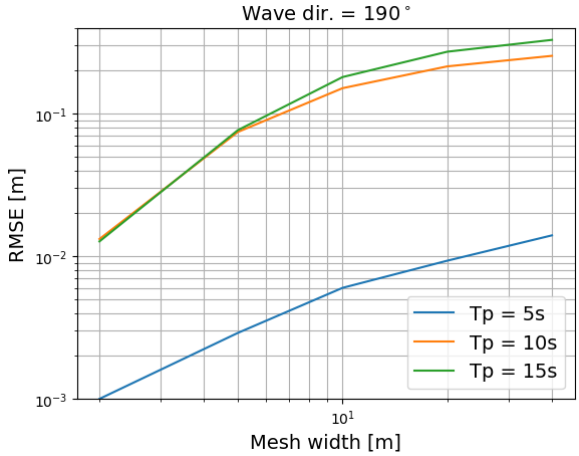

(e) Wave direction = 190°

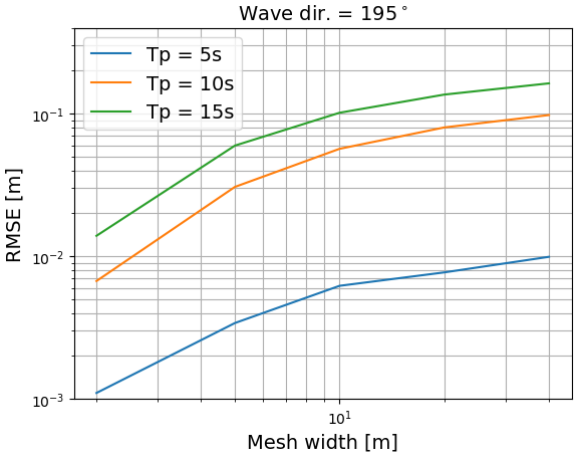

(f) Wave direction = 195°

Figure C.3: RMSE as function of mesh width for different wave periods and directions 170-195°N.

$H^i_{s,ref} < 0$. Hence, the average wave height is higher for the reference grid. This can be explained by the fact that more wave energy is refracted off the channel edge for coarser grids, leading to lower wave heights in and across the channel. The refracted energy will leave the domain at the left boundary.

For the RMSE there will always remain an error present, since all differences are taken in absolute sense

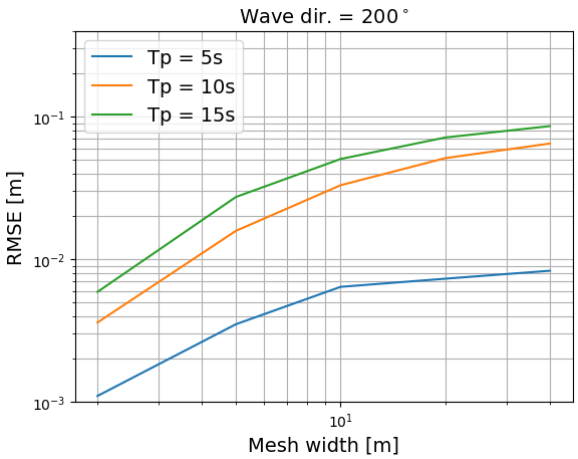

Figure C.4: RMSE as function of mesh width for different wave periods and direction 200°N.

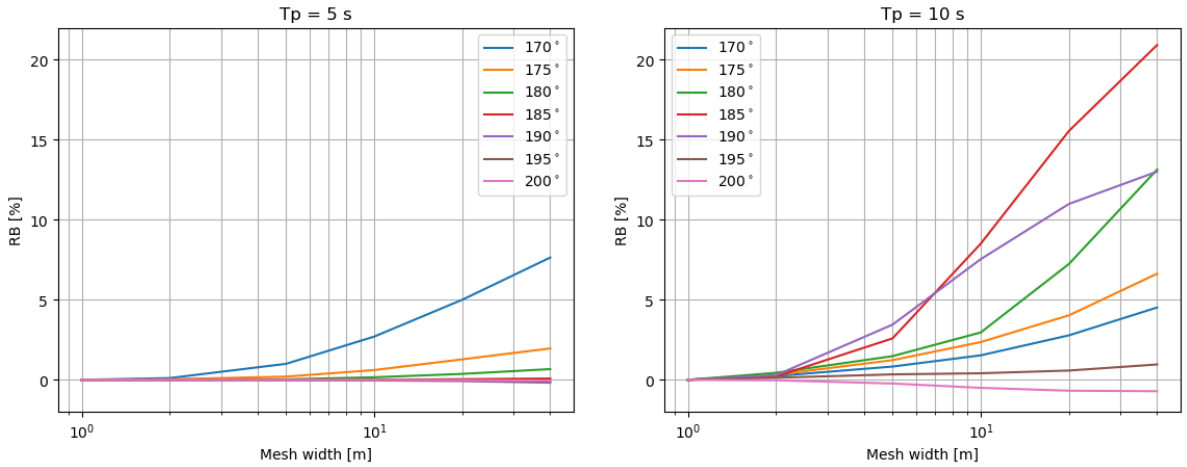

(a) Wave period of 5s

(b) Wave period of 10s

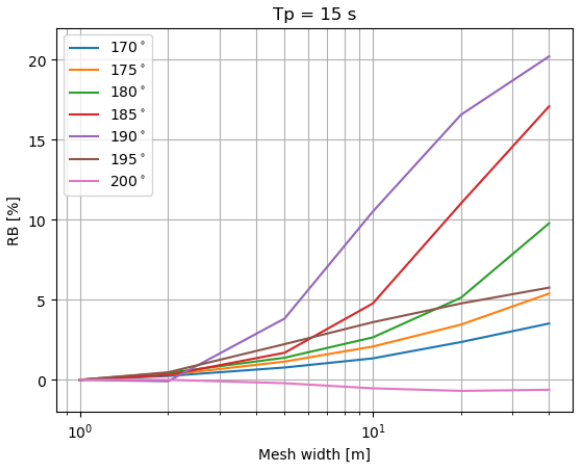

(c) Wave period of 15s

Figure C.5: RB as function of mesh width for different wave directions and periods.

and hence they will only sum up without cancellation. Therefore, the lack of diffusion for small mesh sizes resulted in the garden-sprinkler effect and hence an error. This error is cancelled out in the RB, since the

difference in wave height between two grids is allowed to become negative. A switching negative and positive value that is in equal order will thus cancel each other.

Interesting is that for most cases the RB is positive, meaning that the wave height for coarser grids is on average larger than the reference wave height. Taking in mind the previously presented wave height plots, this showed a similar result. However, this is the case if the entire domain is considered. For a proper assessment of refraction, it may be better to split the area up into two areas, one upwave of the channel and the second covering the area inside and across the area. In this case a positive RB in front of the channel does not cancel out a negative value across the channel and vice versa.

The domain is split as in figure C.6, where the red area denotes the part of the domain that is taken into account. Tables C.2 to C.5 give the rms-error and relative bias for both side 1 and side 2. It is found that for side 2 the differences in wave height can become very large due to presumably a combination of refraction and boundary effects that are propagating into the domain. The RB exceeds 100% for side 2 in some cases, meaning that the wave height of the coarser grid is on average more than two times larger than for the fine grid. Observing the absolute wave height values, it can be seen that these are order 10^{-3} or lower for the fine grid. Since most waves do not enter the channel there is little wave energy and hence the absolute error is minimal. Yet, this potentially leads to extreme relative errors.

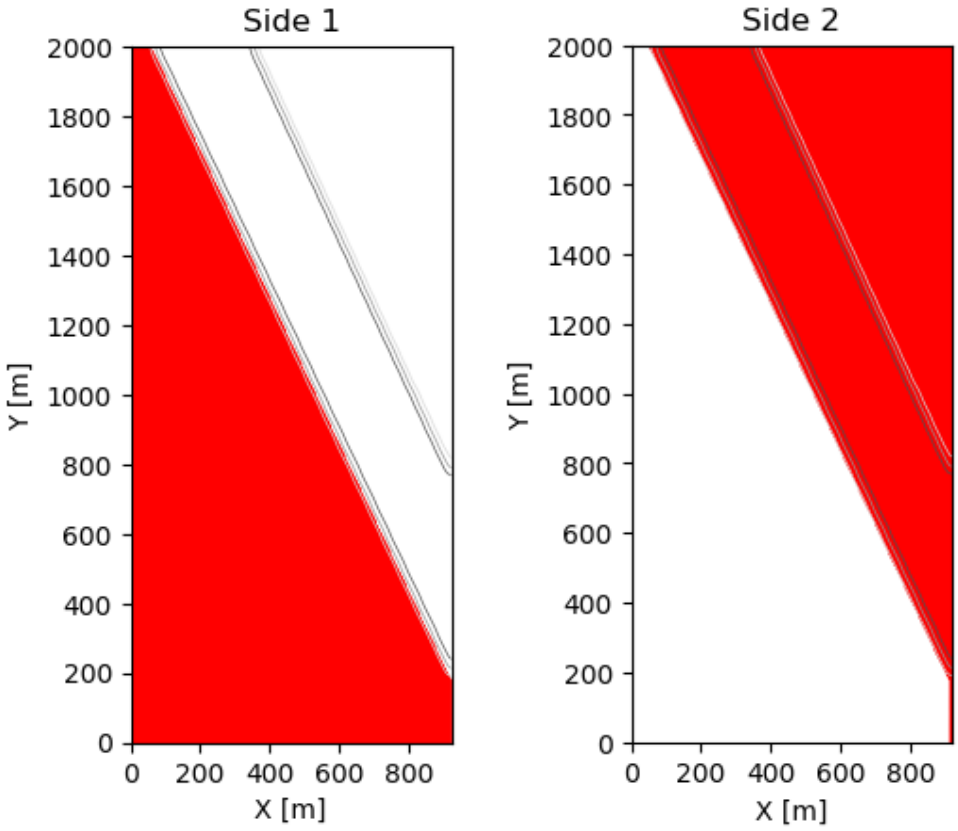

(a) Upwave side of the channel (b) Downwave side of the channel

Figure C.6: Split of the domain in an upwave and downwave channel part. The red area shows the part that is used.

Figure C.7 shows the RMSE against mesh width following from the values of table C.2 for side 1. In case the wave direction is below the critical angle, the slope of the lines becomes milder for lower directions. On the other hand, the start error is lower for higher wave conditions.

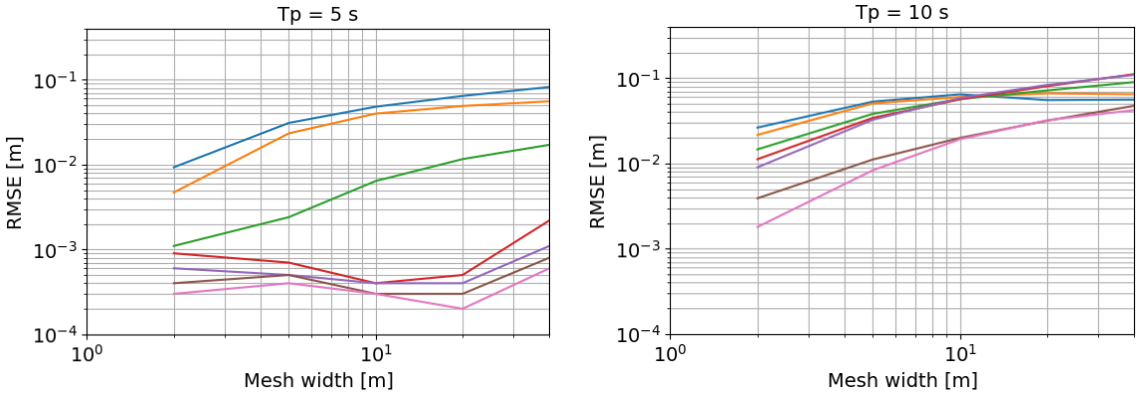

(a) Wave period of 5s

(b) Wave period of 10s

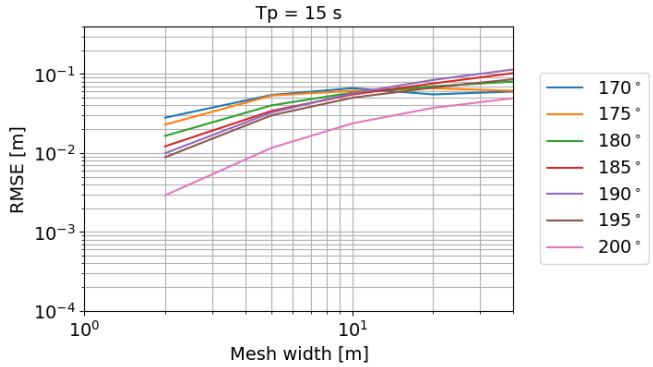

(c) Wave period of 15s

Figure C.7: RMSE as function of mesh width for different wave directions and periods for side 1.

Table C.2: RMSE in meters of side 1 for all considered combinations of wave period, direction and mesh widths.

	5s					**10s**					**15s**				
	2m	5m	10m	20m	40m	2m	5m	10m	20m	40m	2m	5m	10m	20m	40m
170	0.01	0.03	0.05	0.06	0.08	0.03	0.05	0.06	0.06	0.06	0.03	0.05	0.07	0.05	0.06
175	0.00	0.02	0.04	0.05	0.06	0.02	0.05	0.06	0.07	0.06	0.02	0.05	0.06	0.07	0.06
180	0.00	0.00	0.01	0.01	0.02	0.01	0.04	0.06	0.07	0.09	0.02	0.04	0.06	0.07	0.08
185	0.00	0.00	0.00	0.00	0.00	0.01	0.03	0.06	0.08	0.11	0.01	0.03	0.05	0.08	0.10
190	0.00	0.00	0.00	0.00	0.00	0.01	0.03	0.06	0.08	0.11	0.01	0.03	0.06	0.08	0.11
195	0.00	0.00	0.00	0.00	0.00	0.00	0.01	0.02	0.03	0.05	0.01	0.03	0.05	0.07	0.09
200	0.00	0.00	0.00	0.00	0.00	0.00	0.01	0.02	0.03	0.04	0.00	0.01	0.02	0.04	0.05

Table C.3: RMSE in meters of side 2 for all considered combinations of wave period, direction and mesh widths.

	5s					**10s**					**15s**				
	2m	5m	10m	20m	40m	2m	5m	10m	20m	40m	2m	5m	10m	20m	40m
170	0.01	0.04	0.09	0.15	0.21	0.02	0.07	0.11	0.15	0.20	0.01	0.07	0.10	0.14	0.19
175	0.01	0.03	0.06	0.10	0.13	0.02	0.08	0.13	0.18	0.24	0.02	0.07	0.12	0.17	0.21
180	0.00	0.01	0.02	0.04	0.07	0.02	0.08	0.15	0.23	0.34	0.02	0.08	0.14	0.20	0.29
185	0.00	0.00	0.01	0.02	0.03	0.02	0.09	0.23	0.37	0.48	0.02	0.08	0.16	0.28	0.40
190	0.00	0.00	0.01	0.01	0.02	0.02	0.11	0.22	0.31	0.36	0.02	0.11	0.26	0.39	0.47
195	0.00	0.01	0.01	0.01	0.01	0.01	0.04	0.08	0.11	0.14	0.02	0.08	0.14	0.19	0.22
200	0.00	0.01	0.01	0.01	0.01	0.00	0.02	0.04	0.07	0.08	0.01	0.04	0.07	0.10	0.12

Table C.4: RB of side 1 for all considered combinations of wave period, direction and mesh widths. For % multiply all values by 100%.

	5s					**10s**					**15s**				
	2m	5m	10m	20m	40m	2m	5m	10m	20m	40m	2m	5m	10m	20m	40m
170	0.00	0.00	0.00	-0.01	-0.02	0.00	0.00	0.00	0.00	0.00	0.00	0.00	0.00	0.00	0.00
175	0.00	0.01	0.02	0.02	0.01	0.00	0.00	0.00	0.00	0.00	0.00	0.00	0.00	0.00	0.00
180	0.00	0.00	0.00	0.00	0.01	0.00	0.00	0.01	0.00	0.00	0.00	0.00	0.01	0.01	0.00
185	0.00	0.00	0.00	0.00	0.00	0.00	0.00	0.00	-0.01	-0.02	0.00	0.00	0.01	0.00	0.00
190	0.00	0.00	0.00	0.00	0.00	0.00	-0.01	-0.02	-0.03	-0.04	0.00	0.00	-0.01	-0.02	-0.04
195	0.00	0.00	0.00	0.00	0.00	0.00	0.00	0.00	0.00	0.00	0.00	-0.01	-0.02	-0.03	-0.04
200	0.00	0.00	0.00	0.00	0.00	0.00	0.01	0.01	0.02	0.02	0.00	0.01	0.01	0.02	0.02

Table C.5: RB of side 2 for all considered combinations of wave period, direction and mesh widths. For % multiply all values by 100%.

	5s					**10s**					**15s**				
	2m	5m	10m	20m	40m	2m	5m	10m	20m	40m	2m	5m	10m	20m	40m
170	0.00	0.04	0.13	0.26	0.41	1.42	2.66	1.25	0.74	1.08	2.35	3.89	1.42	0.66	0.87
175	0.00	-0.01	-0.01	0.01	0.03	0.18	0.57	0.67	0.77	1.19	0.25	0.75	0.70	0.70	1.02
180	0.00	0.00	0.00	0.00	0.01	0.04	0.18	0.33	0.75	1.29	0.05	0.19	0.32	0.56	1.02
185	0.00	0.00	0.00	0.00	0.00	0.01	0.26	0.82	1.34	1.72	0.03	0.18	0.47	1.03	1.54
190	0.00	0.00	0.00	0.00	0.00	0.02	0.19	0.40	0.55	0.64	-0.01	0.34	0.91	1.29	1.52
195	0.00	0.00	0.00	0.00	0.00	0.00	0.01	0.01	0.01	0.02	0.02	0.10	0.17	0.21	0.25
200	0.00	0.00	0.00	0.00	0.00	0.00	-0.01	-0.03	-0.04	-0.04	0.00	-0.01	-0.03	-0.04	-0.04

D

Critical angle analysis

This appendix gives further information about the comparison of the critical angle in SWAN with theory. The critical angle for refraction can be found in SWAN by searching the wave direction for which refraction no longer occurs. Or in other words, in case the wave height in front of the channel is approximately equal to the incoming wave height. This is assessed by choosing eight points in front of the channel, see table D.1 for the coordinates of the locations. Figure D.1 gives the geographic location of the points.

Output point	x-coordinate	y-coordinate
point 1	150	1600
point 2	200	1500
point 3	250	1400
point 4	300	1300
point 5	350	1200
point 6	400	1100
point 7	450	1000
point 8	500	900

Table D.1: Coordinates of the output points as used to determine the presence of refraction.

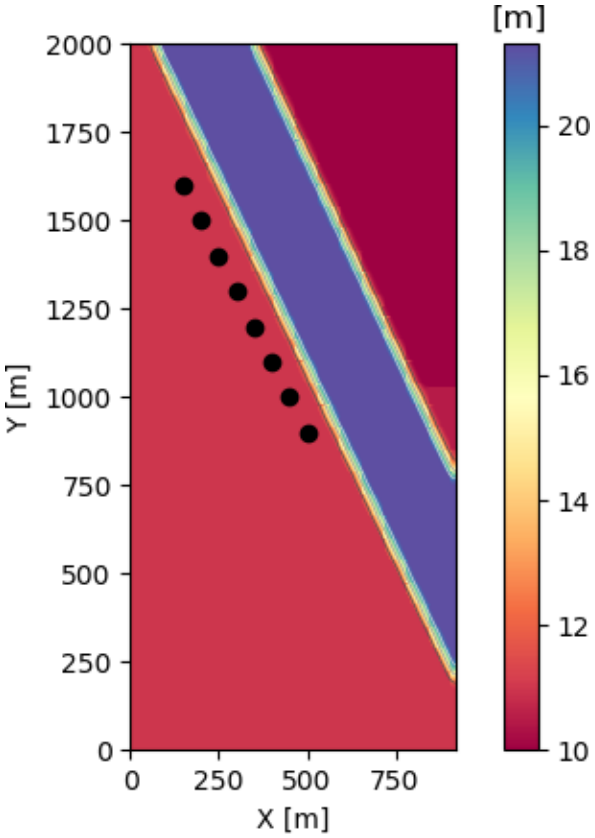

Figure D.1: Geographical locations of the considered output points of table D.1.

D.1. Lower limit for the critical angle

The relative difference in wave height should be smaller than 0.5%, where this 0.5% is chosen arbitrarily. Therefore, an additional test is performed for the case where 5% difference is allowed. Considering a 1m wave, the allowed wave setup due to refraction is thus around 5cm in this case. This is already significant and is thus chosen as upper limit for the wave height difference that is allowed. Hence, this leads to the lower limit for the critical angle as given by SWAN.

Table D.2 gives critical angles according to theory and SWAN in case more wave height difference is allowed in SWAN. It can be observed that the critical angle is still overestimated by SWAN. Figure D.2 gives a graphical

representation of the found critical wave angles according to SWAN and theory. Also the critical angle of SWAN for an allowed wave height difference of 0.5% is plotted here. Presumably, the critical angle according to SWAN will be somewhere inside the blue area. Hence, for all frequencies SWAN will overestimate the critical angle for refraction.

Table D.2: Lower limit for critical wave directions according to SWAN for different wave periods. The critical angle is expressed as the nautical wave direction in the table. Conditions: mesh width=5m, numerical scheme=SORDUP.

Tp [s]	**4**	**5**	**6**	**7**	**8**	**9**	**10**	**11**	**12**	**13**	**14**	**15**
theoretical angle	161.7	172.1	180.8	186.6	190.1	192.3	193.8	194.8	195.5	196	196.4	196.8
SWAN angle	164.0	176.3	185.0	191.1	194.8	196.8	198.3	199.3	200.1	200.6	201.0	201.4
error [degr]	*2.3*	*4.2*	*4.2*	*4.5*	*4.7*	*4.5*	*4.5*	*4.5*	*4.6*	*4.6*	*4.6*	*4.6*
error [%]	1.4%	2.4%	2.3%	2.4%	2.5%	2.3%	2.3%	2.3%	2.4%	2.3%	2.3%	2.3%

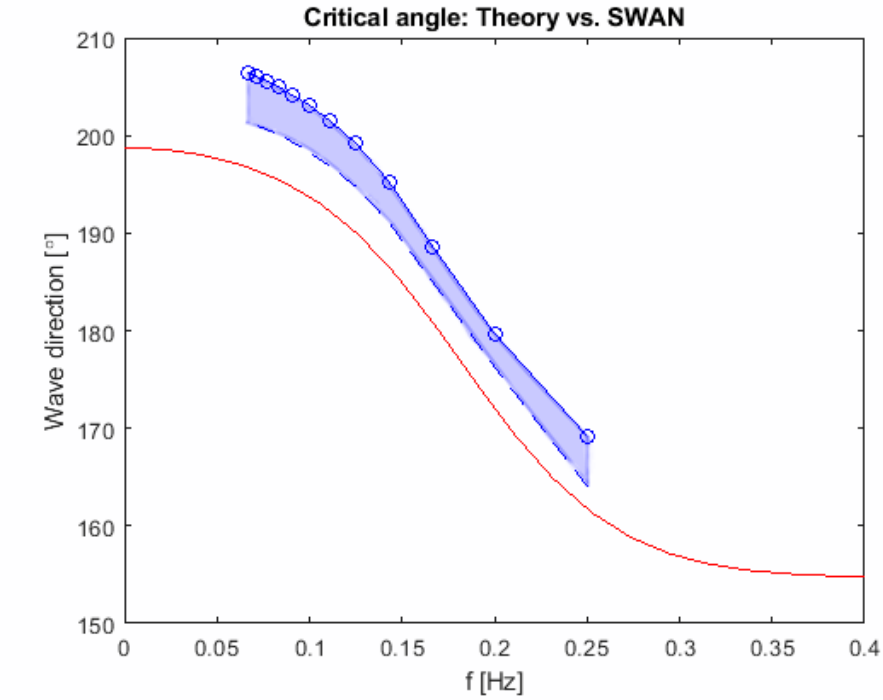

Figure D.2: Critical wave direction as function of wave frequency according to theory (red line) and SWAN (dotted blue line). The dashed blue line gives the lower limit as calculated in table D.2

D.2. Wave height distribution at critical angle

This section gives the distributions of the wave height for the wave direction where no refraction is present anymore in SWAN. These figures correspond to the variants as given in table 4.6, hence where the relative difference in wave height should be smaller than 0.5%. The plots are given in figures D.3, D.4 and D.5 for the grid resolution variants, for all these cases the SORDUP scheme is used. A very thin colour of red can be observed in front of the channel. This represents a small amount of wave energy that refracts off the channel since a little refraction is allowed. Figure D.6 gives the wave height distributions for the BSBT scheme per wave period. Here a mesh width of 5m is used.

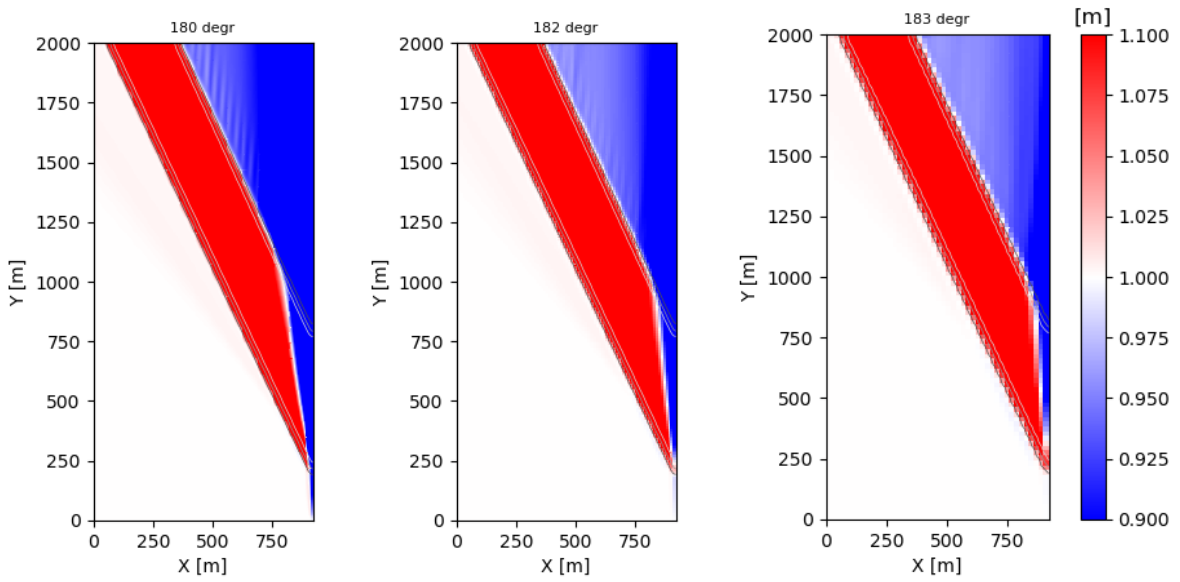

(a) 5m mesh width (b) 10m mesh width (c) 20m mesh width

Figure D.3: Wave height distribution of SWAN at the critical wave direction for different mesh widths. T_p=5s and H_{in}=1m.

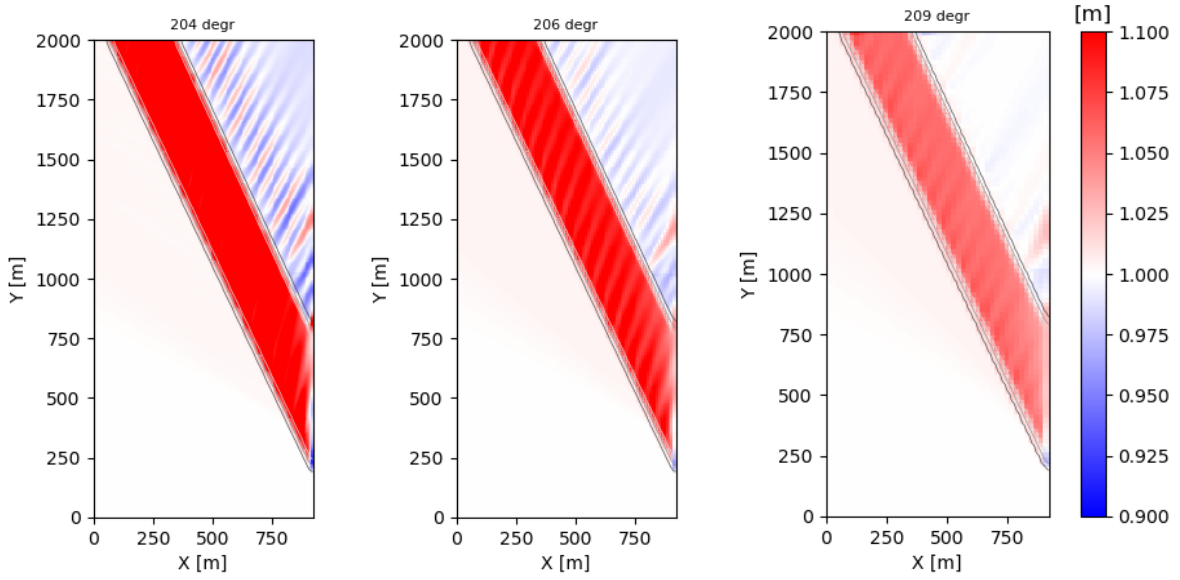

(a) 5m mesh width (b) 10m mesh width (c) 20m mesh width

Figure D.4: Wave height distribution of SWAN at the critical wave direction for different mesh widths. T_p=10s and H_{in}=1m.

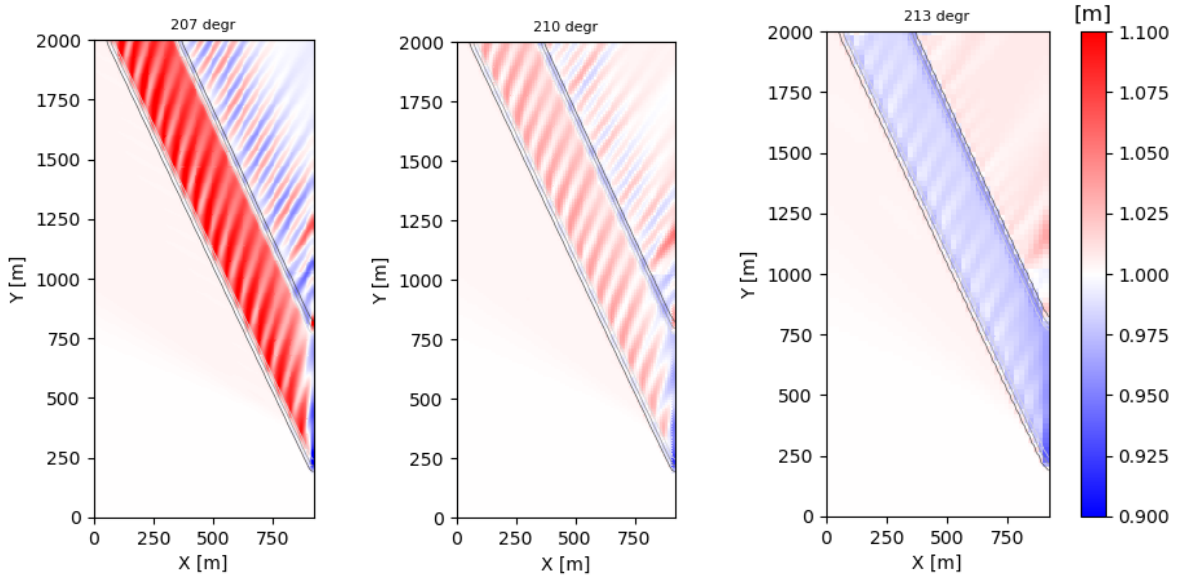

(a) 5m mesh width (b) 10m mesh width (c) 20m mesh width

Figure D.5: Wave height distribution of SWAN at the critical wave direction for different mesh widths. T_p=15s and H_{in}=1m.

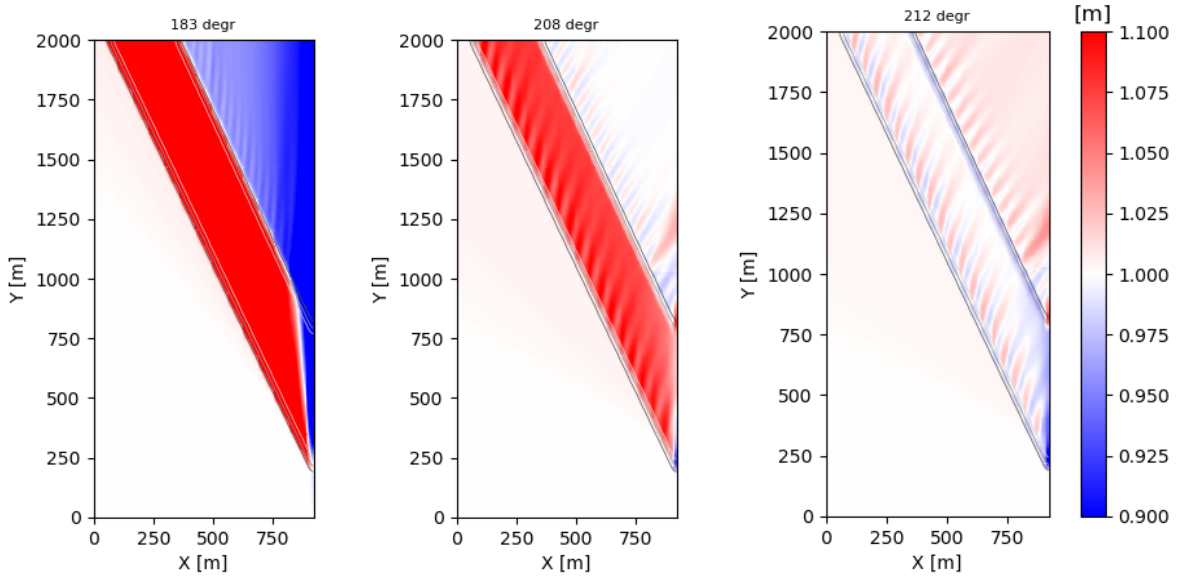

(a) T_p=5s (b) T_p=10s (c) T_p=15s

Figure D.6: Wave height distribution of SWAN at the critical wave direction for different wave periods applying the BSBT scheme. H_{in}=1m.

E

Interpretation 'grid dependence of refraction'

This appendix is based on the memo of M. Zijlema: "On grid dependence of refraction in SWAN" (Zijlema, 2020). This memo stated that refraction in SWAN is independent of the bed slope. Even with a bed slope that fulfils the mild slope criterion, excessive wave turning can occur if the change in depth over grid points is relatively large. Therefore, the change in turning rate is dependent on the change in water depth, Δd.

E.1. Turning rate in SWAN

As mentioned in the main text, the turning rate can be determined using equation E.1 in Cartesian coordinates, which is based on the wave number.

$$\begin{aligned} c_\theta &= -\frac{c_g}{c}\frac{\partial c}{\partial m} = \frac{c_g}{c}\left(\sin\theta\frac{\partial c}{\partial x} - \cos\theta\frac{\partial c}{\partial y}\right) \\ &\approx \frac{c_g}{c}\left(\sin\theta_1\frac{c_2-c_3}{\Delta x} - \cos\theta_1\frac{c_2-c_1}{\Delta y}\right) \end{aligned} \tag{E.1}$$

Here θ is the angle between the wave ray and the normal to the depth-contours, see figure E.1, also grid points 1,2 and 3 are given here. Taking a more Lagrangian approach, i.e. following the wave ray, the turning rate can be described as given in equation E.2. Here c_1 is a point somewhere on the wave ray.

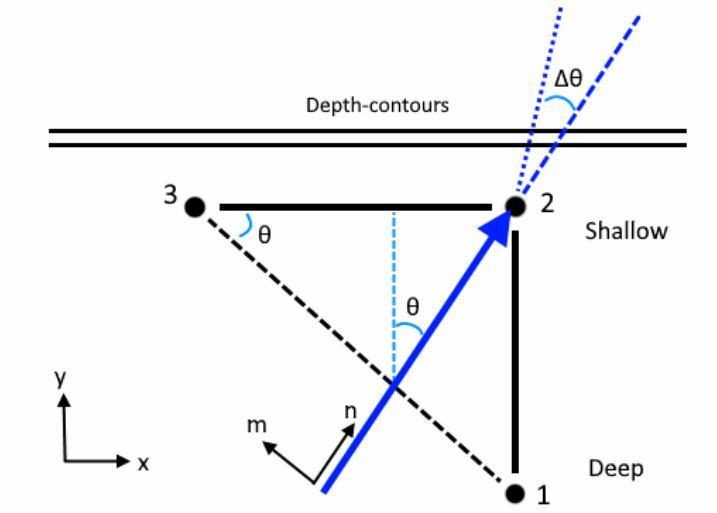

Figure E.1: Convention of wave direction θ and x,y-directions, the turning rate will be calculated in point 2. This figure is based on a similar figure of M. Zijlema

$$c_\theta = -\frac{c_g}{c}\frac{\partial c}{\partial m} \approx \frac{c_g}{c}\frac{c_2-c_1}{\Delta n}\tan\theta_1 \tag{E.2}$$

In principle, both equation E.1 and E.2 give an equal answer. Following the Lagrangian method, which is consistent with Snel's law, the c of the term c_g/c should equal c_1 which is somewhere on the wave ray. Since

it is known that $\Delta\theta = c_\theta \Delta n c_g$, equation E.3 can be derived. However, SWAN is not able to compute this c_1, because it is not on a grid point and lies somewhere in between points 1,2 and 3. To solve this problem, it is chosen to use grid point c_2 instead in SWAN, see the second of equation E.3. If point 2 is located in shallower water, c_2 will be lower and thus the resulting $\Delta\theta$ is higher. Concluding, the wave turning is larger in SWAN in that case meaning a stronger refraction.

$$\begin{aligned} \Delta\theta &= -\frac{1}{c_1}(c_2 - c_1)\tan\theta_1 \quad \text{, consistent with Snel's law} \\ \Delta\theta &= -\frac{1}{c_2}(c_2 - c_1)\tan\theta_1 \quad \text{, as used by SWAN} \end{aligned} \tag{E.3}$$

This crest turning of SWAN can be compared to Snel's law, which gives the value of θ_2 based on c_1, c_2 and θ_1. The difference between θ_2 and θ_1 equals the crest turning, see equation E.4.

$$\begin{aligned} \frac{\sin\theta_1}{\sin\theta_2} &= \frac{c_1}{c_2} \\ \theta_2 &= \arcsin\left(\frac{c_2}{c_1}\sin\theta_1\right) \\ \Delta\theta &= \theta_2 - \theta_1 \end{aligned} \tag{E.4}$$

E.2. Example crest turning

The memo gives an example of the comparison between the crest turning according to Snellius and SWAN. Additionally, distinction is made between calculating the turning rate in SWAN based on wave number and on water depth, respectively options WNUM and DEP. An example is given for a grid size of 100m, with Δd=5m (from deep to shallower) and a wave period of 12s. With an incoming wave angle of 30° from the normal to the depth contours, it is found that the crest turning equals -70° and -150° with respectively WNUM and DEP, where minus means 'towards the channel normal'. However, the turning according to Snel's law equals -20° (θ_2=10°). Hence this difference is significant, while the slope was considered relatively mild. Taking a grid size of 10m, i.e. Δd=0.5m, the crest turning from one grid point to the other becomes -1.7°, -1.8° and -1.6° for respectively WNUM, DEP and Snel's law. Concluding, the prediction of SWAN greatly depends on the grid size and following Δd. An equal slope leads to larger differences for coarser grids, whereas a fine resolution shows good agreement between SWAN and Snel's law.

E.3. Numerical effect of refining resolution

Another effect of a finer spatial resolution can be found by taking a simplified action balance:

$$\frac{\partial c_g N}{\partial x} + \frac{\partial c_\theta N}{\partial \theta} = 0 \tag{E.5}$$

This balance can be discretised by applying the first order backward scheme, as done in the memo of M. Zijlema. This gives the following result, with 1 ≤ m ≤ M:

$$c_{g,m} N_m = c_{g,m-1} N_{m-1} - \Delta x \frac{\partial c_\theta N}{\partial \theta}|_m \tag{E.6}$$

When the grid is refined by a factor two, the number of grid points doubles with 1 ≤ j ≤ 2M. Then, the action balance at point j can eventually be discretised as:

$$c_{g,j} N_j = c_{g,j-2} N_{j-2} - \frac{1}{2}\Delta x \left(\frac{\partial c_\theta N}{\partial \theta}|_{j-1} + \frac{\partial c_\theta N}{\partial \theta}|_j\right) \tag{E.7}$$

As can be clearly seen in figure E.2, equation E.6 and E.7 can only be equal in case $\partial c_\theta N/\partial\theta$ is equal at j-1 and j. For all other cases, the sum of these components cannot be equal to the value at j=m. Hence, refining the grid will lead to a different equation to solve. This and the fact that the turning rate itself changed due to a different resolution both cause differences in wave turning.

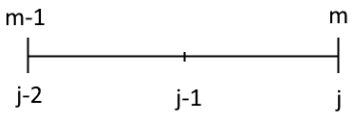

Figure E.2: Schematisation of grid points m, m-1 and j, j-1, j-2.

E.4. Crest turning for schematic channel case

The knowledge above will now be projected to the cases that are treated in this thesis. First, the schematic channel case is considered. This case is different from the example cases given in the memo, because waves travel from shallower to deeper water. Taking c_2 in deeper water implies that c_2 will be larger than c_1. Considering equation E.3, this means that the predicted crest turning in SWAN will be lower than in Snel's law, hence less refraction in SWAN for the same depth difference.

The gradient of the channel side-wall slope was 1:5, with a depth of 11m on the shallower part, i.e. d_1=11m. Considering Δx=20m, this leads to d_2=15m and thus Δd=4m. For a period of 10s and an incoming wave angle of θ_1=50° with respect to the channel normal (θ_{in}=195°N, channel normal=245°N), SWAN predicts a crest turning of 8° and 7°, for respectively options WNUM and DEP. According to Snel's law the turning equals 10°, because θ_2= 60°. Hence the difference is order 2°. In case Δx=10m, the crest turning becomes 4.5°, 4.2°and 5.2° for respectively WNUM, DEP and Snel's law. Lastly, for Δx=5m the crest turning becomes 2.4°, 2.3°and 2.6° for respectively WNUM, DEP and Snel's law. Here the differences are very small. Concluding, in case directional spreading would be absent in SWAN, a grid size of Δx=5m shows an almost equal result to Snel's law. Allowing a certain margin, a resolution of 10m is thought to be sufficient in this case.

E.5. Crest turning for Eastern Wadden Sea case

The situation for the Ems channel is similar to the example case, since waves start inside the channel and thus travel from deep to shallower water. It was found that most wave turning was present in the ebb-delta, hence a cross-section is made at this location, see figure E.3. The left point in the figure is the starting point. From this it follows that the side-wall slope is approximately 1:40 with the shallowest point at 3m+NAP. Assuming a water level of 2m, this results in a water depth of 5m at the shallowest part, i.e. d_2=5m. The incoming wave direction at this location is approximately 330°N, leading to an angle of around θ_1=65° with the channel normal. Note that the western channel edge is concerned in this case.

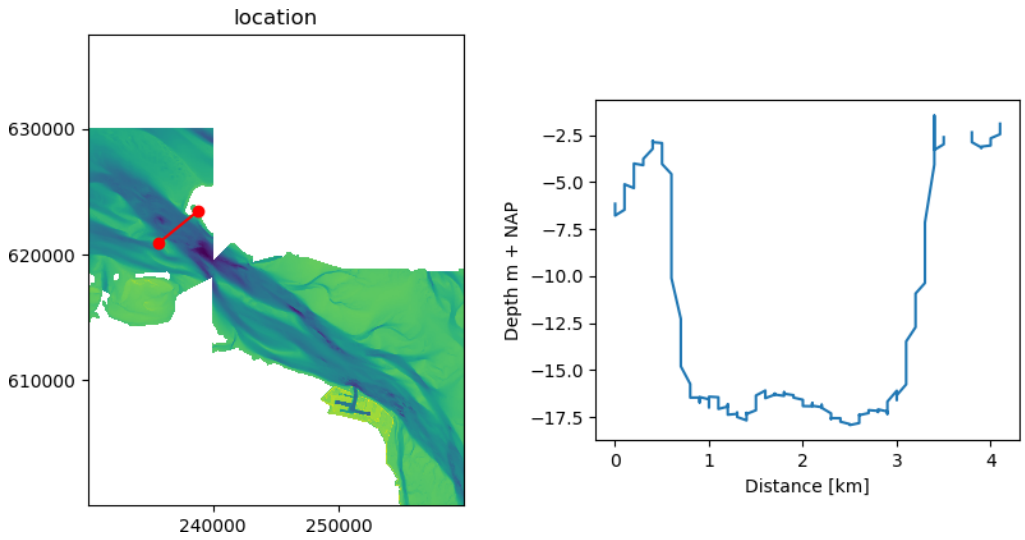

Figure E.3: Cross-section of the Ems channel at the ebb-delta.

With a grid size of Δx=100m, it follows that d_1=7.5m. For a period of 10s, SWAN predicts a crest turning of -25° and -29° for respectively options WNUM and DEP. On the other hand, Snel's law gives a turning of -16°. Here

the minus sign means clockwise and in this case towards the channel normal. It can thus be concluded that SWAN overestimates the crest turning. Considering a grid size of Δx=50m results in a crest turning of -13°, -14° and -10° for respectively WNUM, DEP and Snel's law. It can be seen that the differences are significantly smaller for a resolution of 50m compared to the resolution of 100m. Noteworthy is that in case c_1 is used in equation E.3, the resulting crest turning is -12° for a resolution of 50m. Apparently, the equation based on the turning rate gives a larger difference compared to Snel's law in case the resolution becomes more coarse. Hence, the 'error' of using a different celerity, i.e. c_2 instead of c_2, in SWAN is only order 1°.

Table E.1: Crest turning for different resolutions and formulations in the Wadden Sea case.

Resolution	Snel's law	SWAN with 1/c1	SWAN with 1/ c2	SWAN option DEP
200m	-23.4	-32.8	-44.8	-57.2
100m	-16.1	-20.8	-25.0	-28.6
50m	-10.1	-12.0	-13.3	-14.3
25m	-5.9	-6.5	-6.9	-7.1

F

Case study: Monochromatic wave REFRAC

F.1. Results for water level 0m

Figures F.4 to F.4 give the wave rays for different wave directions for a wave period of respectively 5s, 10s and 15s.

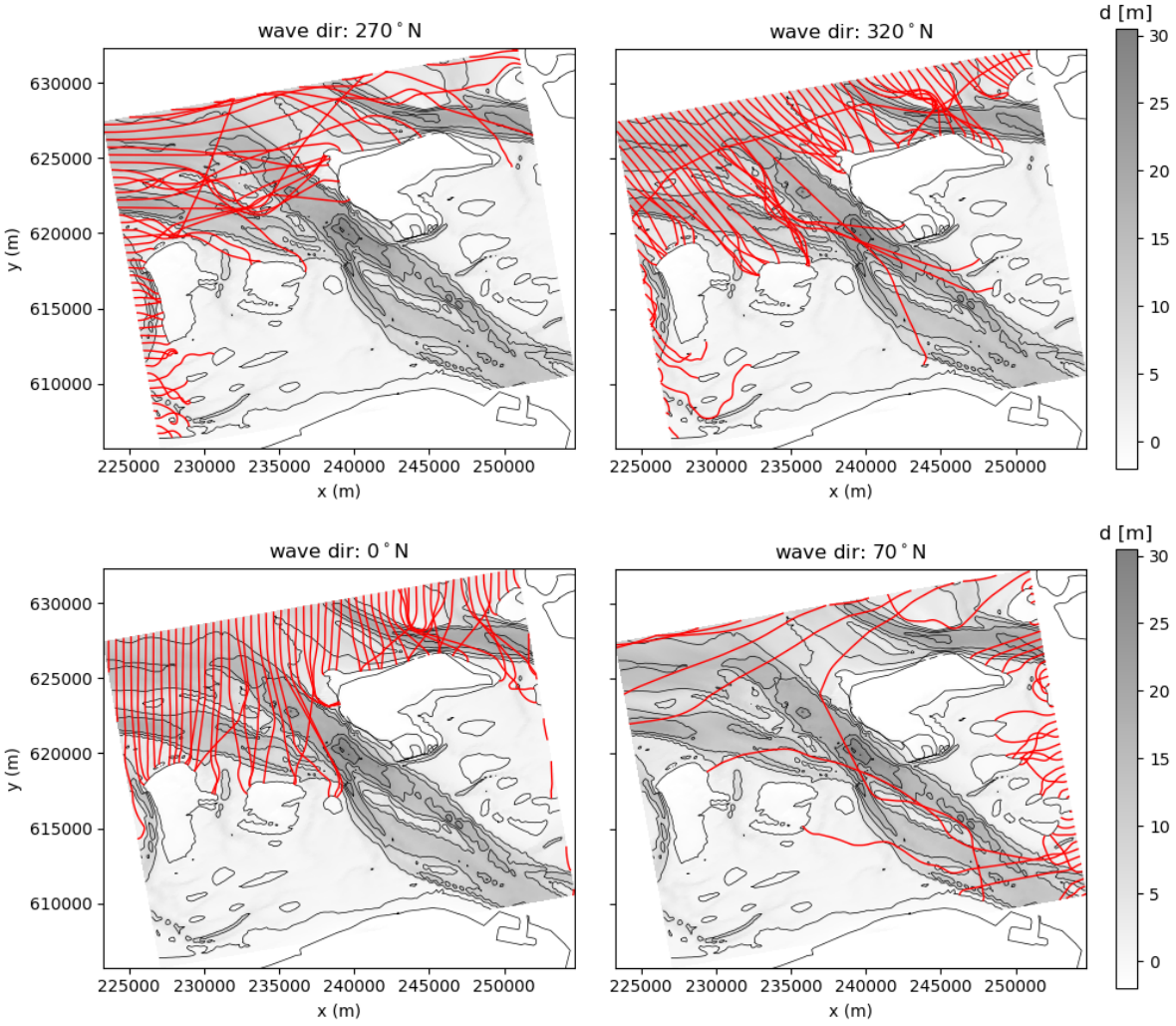

Figure F.1: Wave rays according to REFRAC for a *period of T=5s.*

Figures F.4 to F.6 give the wave height as calculated by REFRAC for a water level of 0m. These wave height plots correspond to the wave ray plots that were given in the main text. For most directions, there is a large dark red spot above Borkum. At this location there is a strong ray convergence due to refraction, leading to energy accumulation.

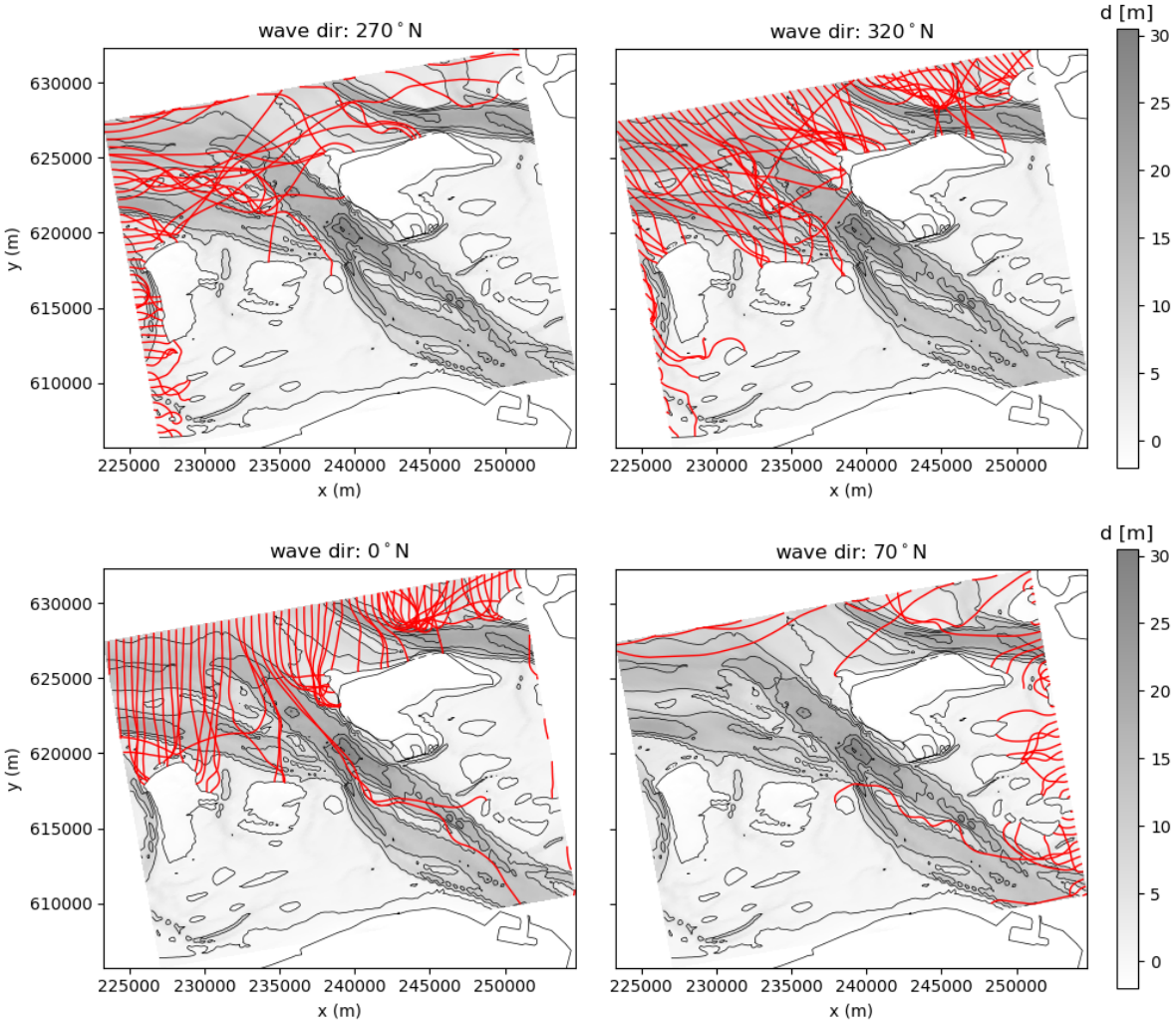

Figure F.2: Wave rays according to REFRAC for a *period of T=10s*.

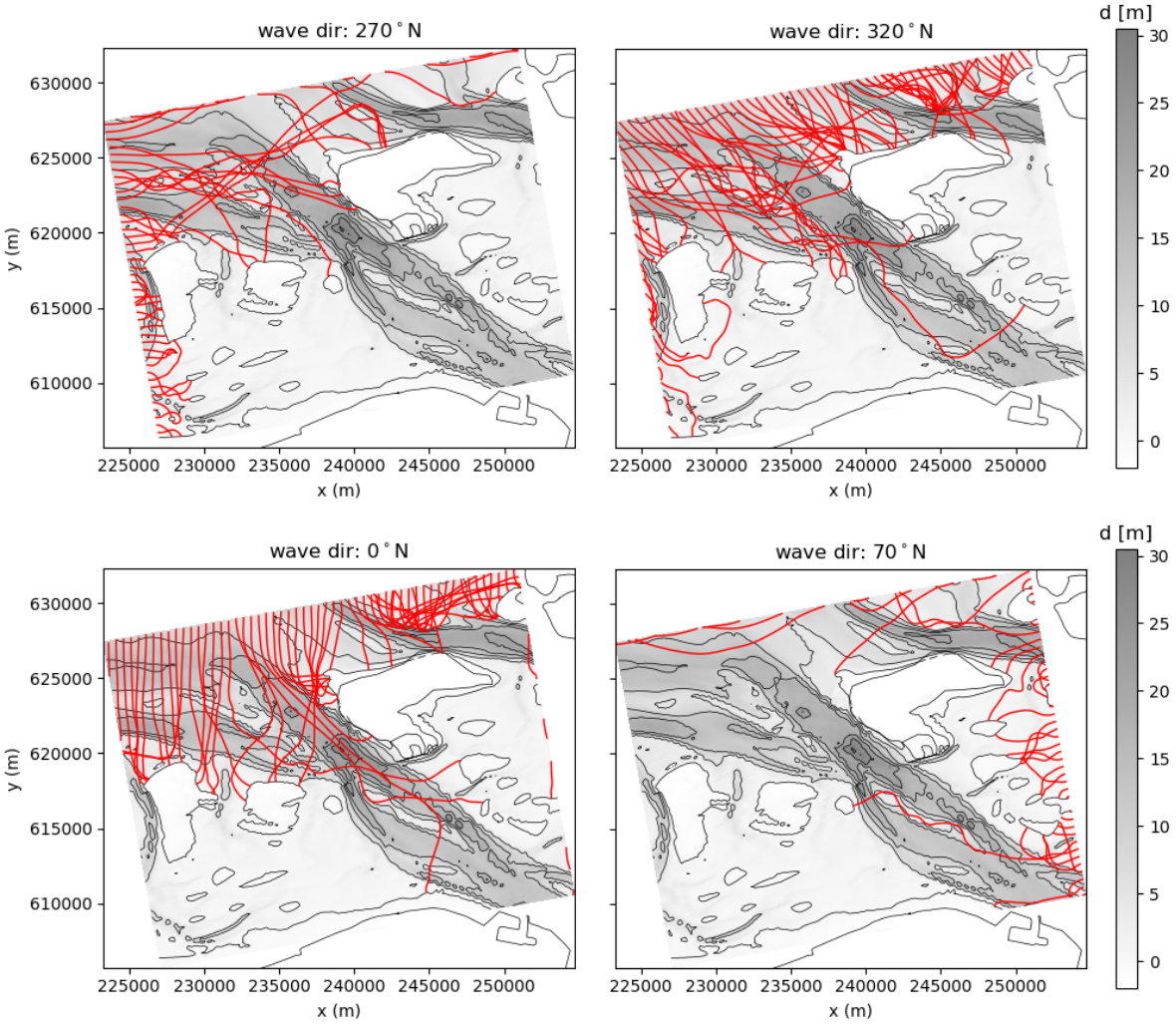

Figure F.3: Wave rays according to REFRAC for a *period of T=15s.*

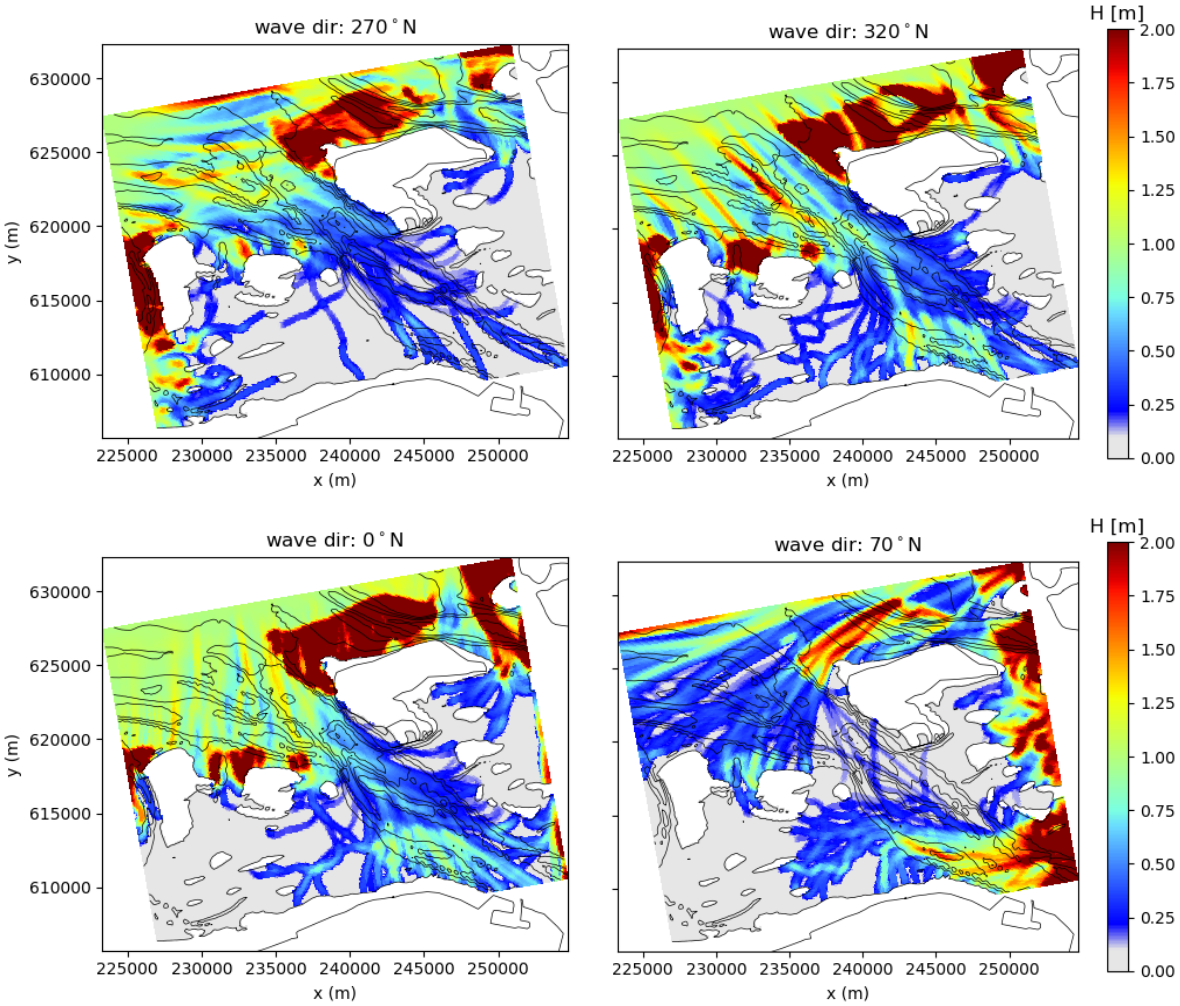

Figure F.4: Wave height according to REFRAC for a *period of T=5s.*

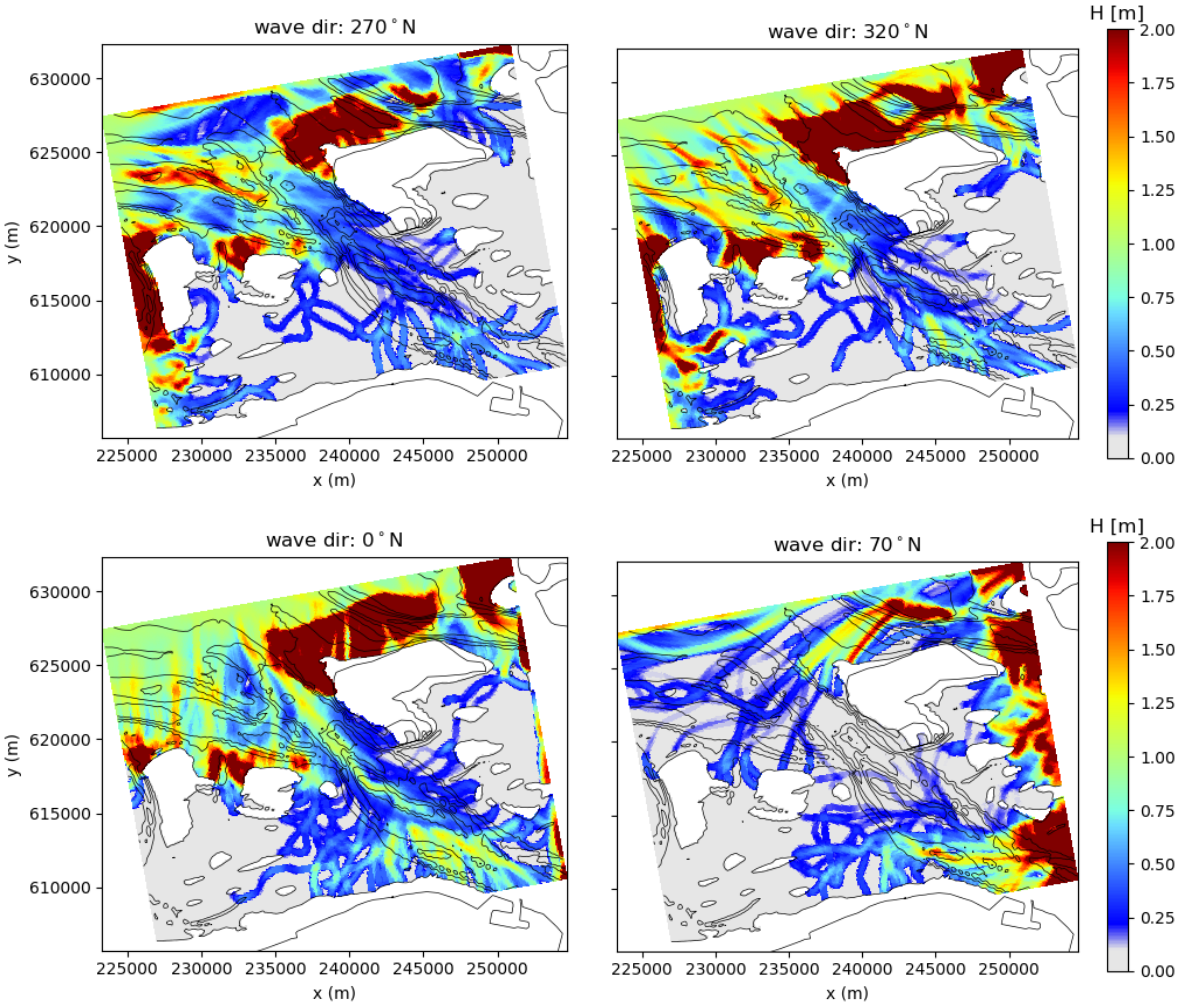

Figure F.5: Wave height according to REFRAC for a *period of T=10s.*

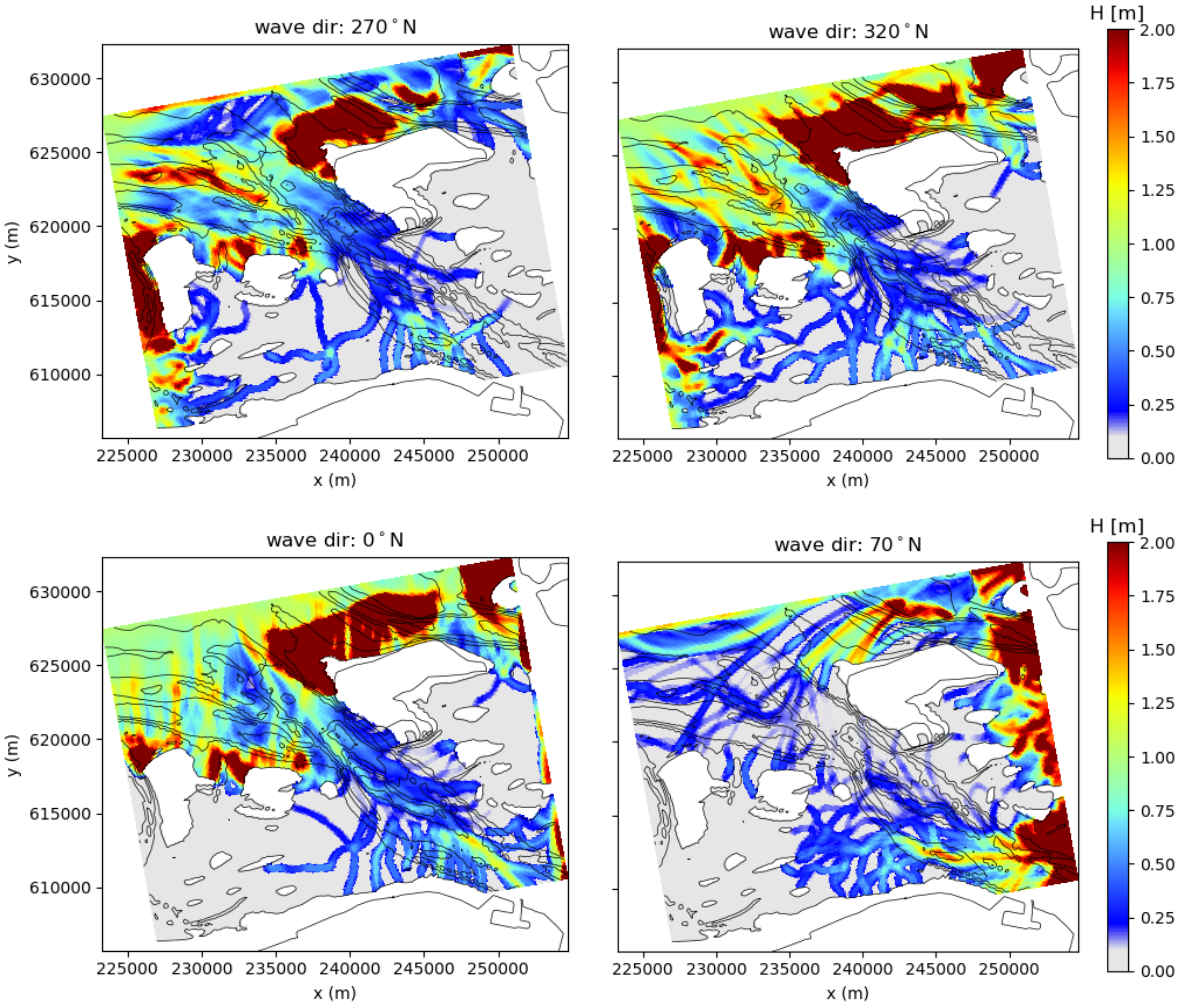

Figure F.6: Wave height according to REFRAC for a *period of T=15s.*

F.2. Results for water level 2m

Also the situation for a water level of 2m is considered. The results are given in figures F.7 to F.12. The first three figures give the wave rays, whereas the other three figures show the wave height calculated based on the wave rays.

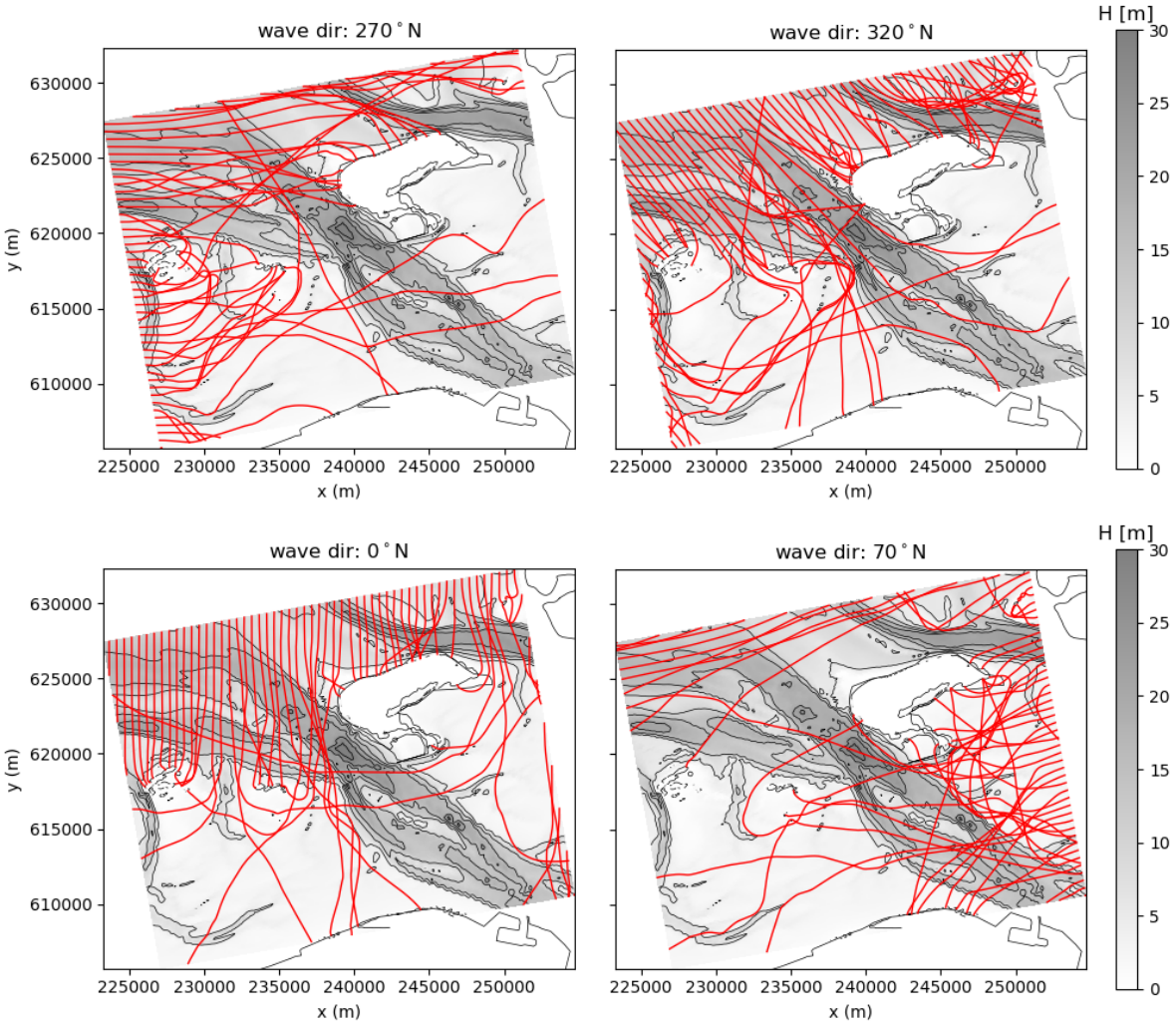

Figure F.7: Wave rays according to REFRAC for water level=2m and a *period of T=5s.*

It can be observed that the wave penetration is significantly larger than in the case a 0m water level is used. Furthermore, waves coming in from the east and west sides are now able to reach the Ems channel. Focusing on waves coming from 270°N, the plots show that in case T=5s almost all wave energy approaching the western channel side is able to enter and cross the channel, see figures F.7 and F.8. Looking at a period of 10s, there is still wave energy that is able to enter the channel, however some rays are turned too much to cross the channel in the considered domain. Lastly, for a period of 15s the pattern is similar to the 10s case, only with slightly less energy that is able to enter and cross the channel. The similarities between T=10s and 15s where also present in the schematic channel case and can be explained by the critical angle theory. For low frequencies, the critical angle approaches a constant value which is higher for larger relative depth differences. Since all wave directions smaller than the critical angle get refracted, a larger fraction of waves will thus refract for large differences in depth. For the depth differences present in the Wadden Sea, the critical angle for T=10s is approximately equal to the wave period of 15s.

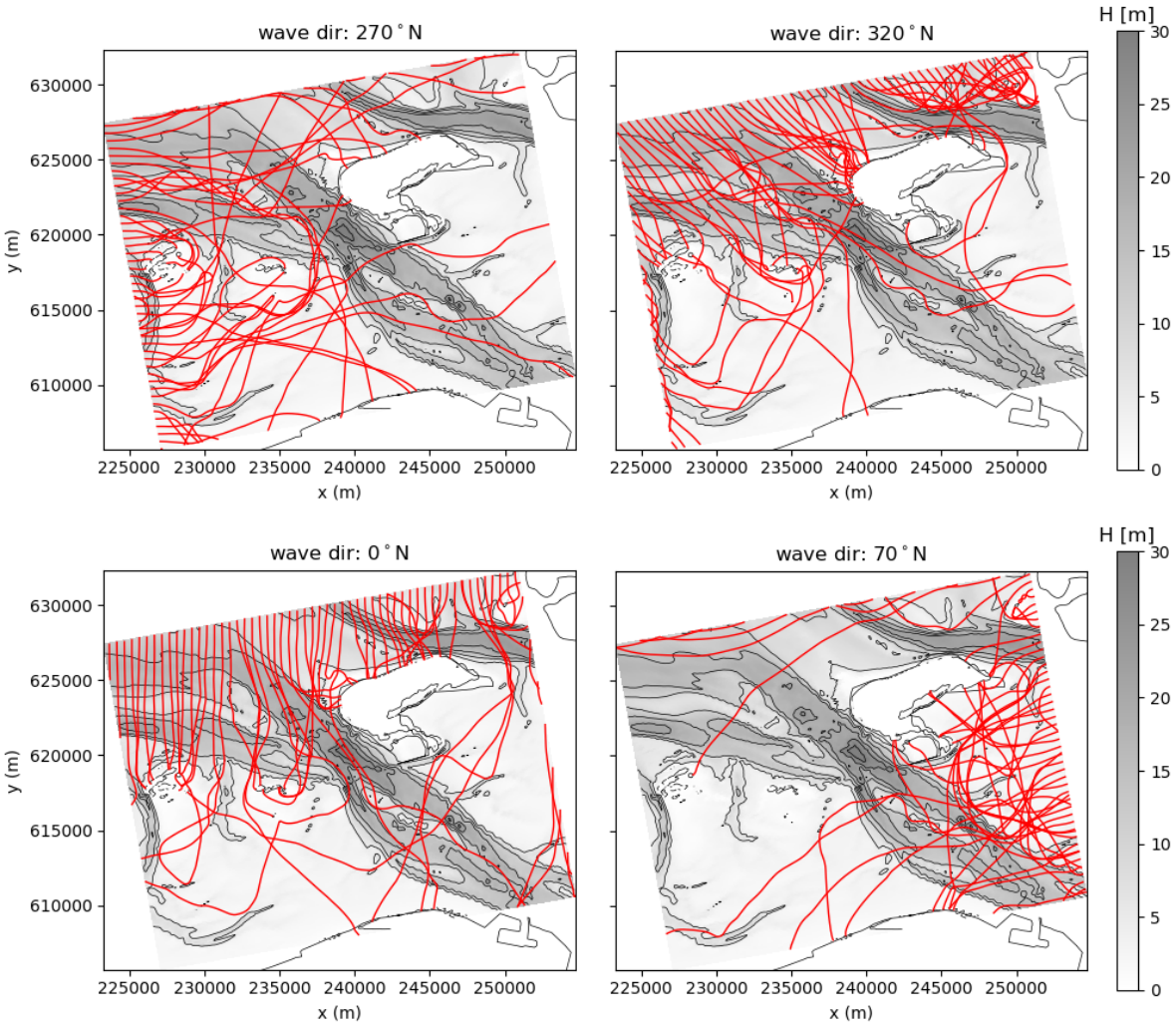

Figure F.8: Wave rays according to REFRAC for water level=2m and a *period of T=10s*.

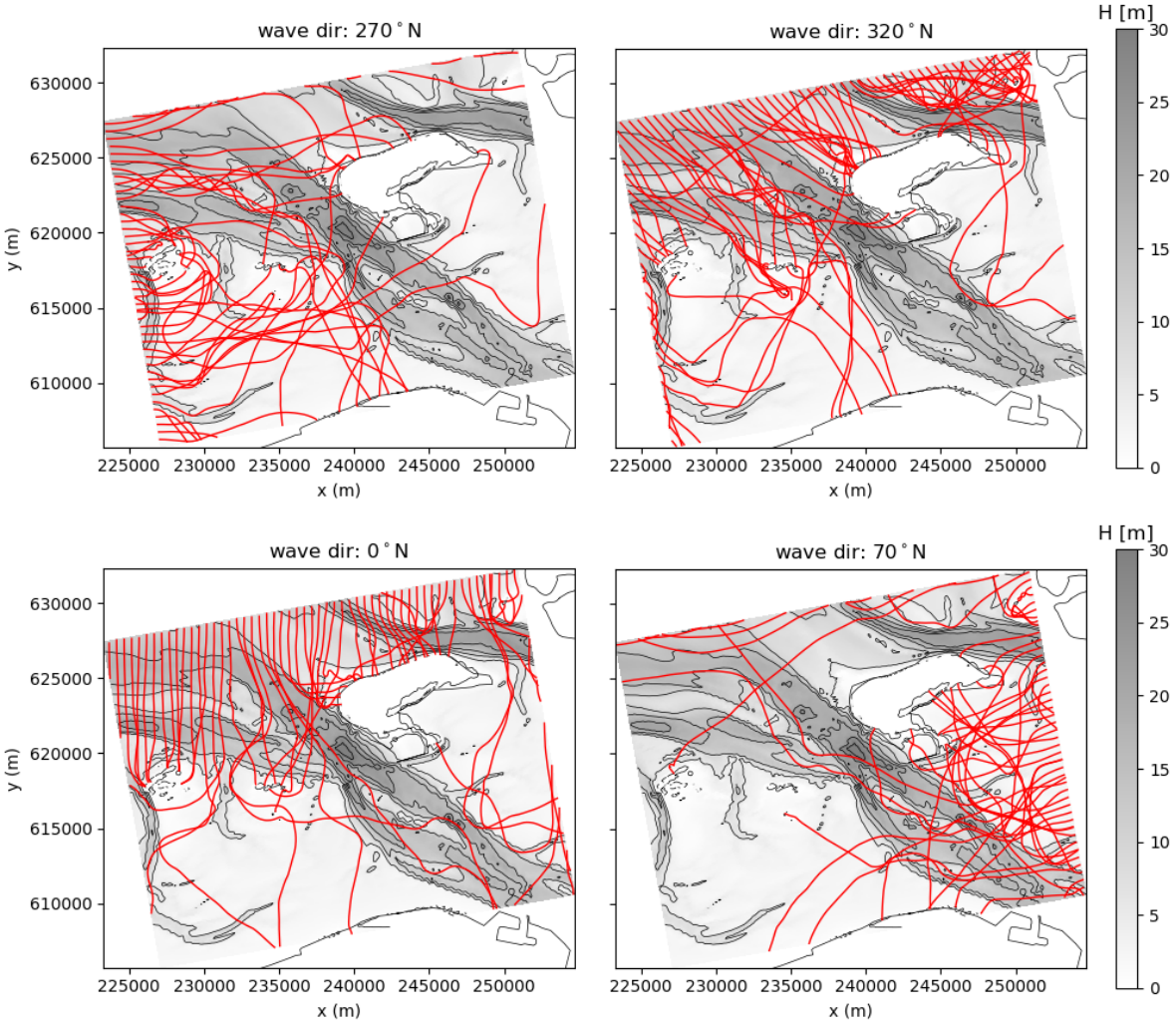

Figure F.9: Wave rays according to REFRAC for water level=2m and a *period of T=15s*.

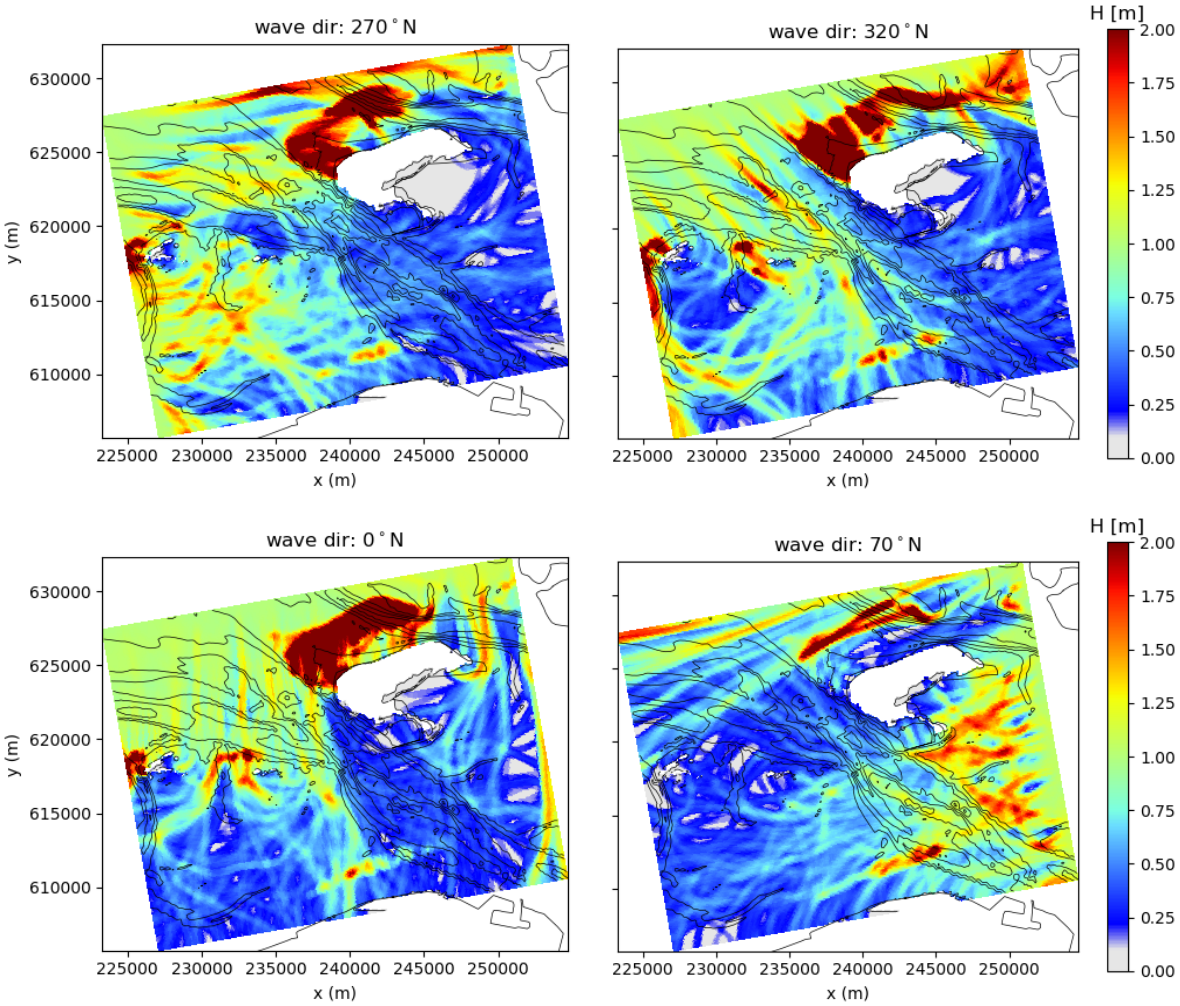

Figure F.10: Wave height according to REFRAC for for water level=2m and a *period of T=5s.*

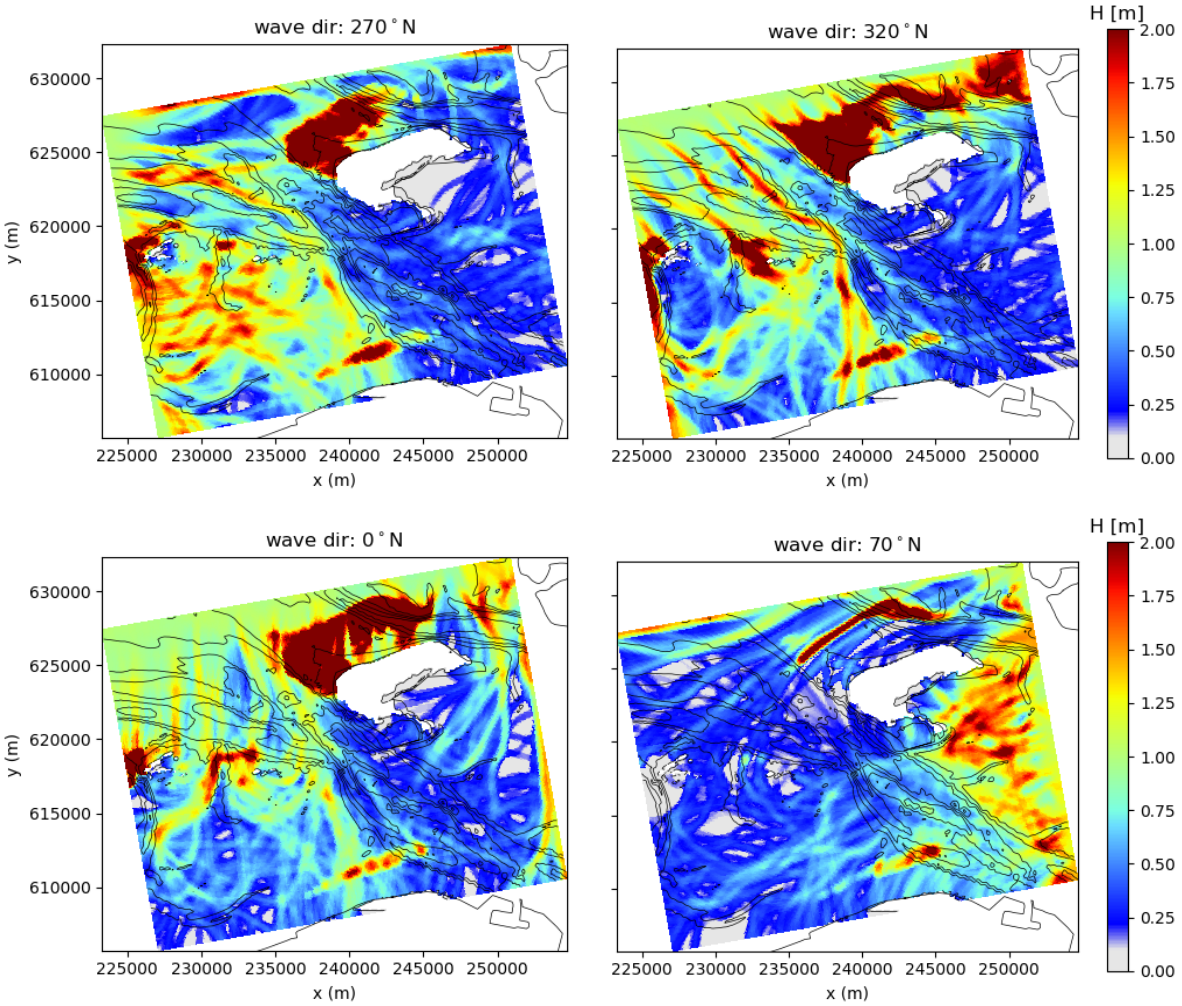

Figure F.11: Wave height according to REFRAC for for water level=2m and a *period of T=10s.*

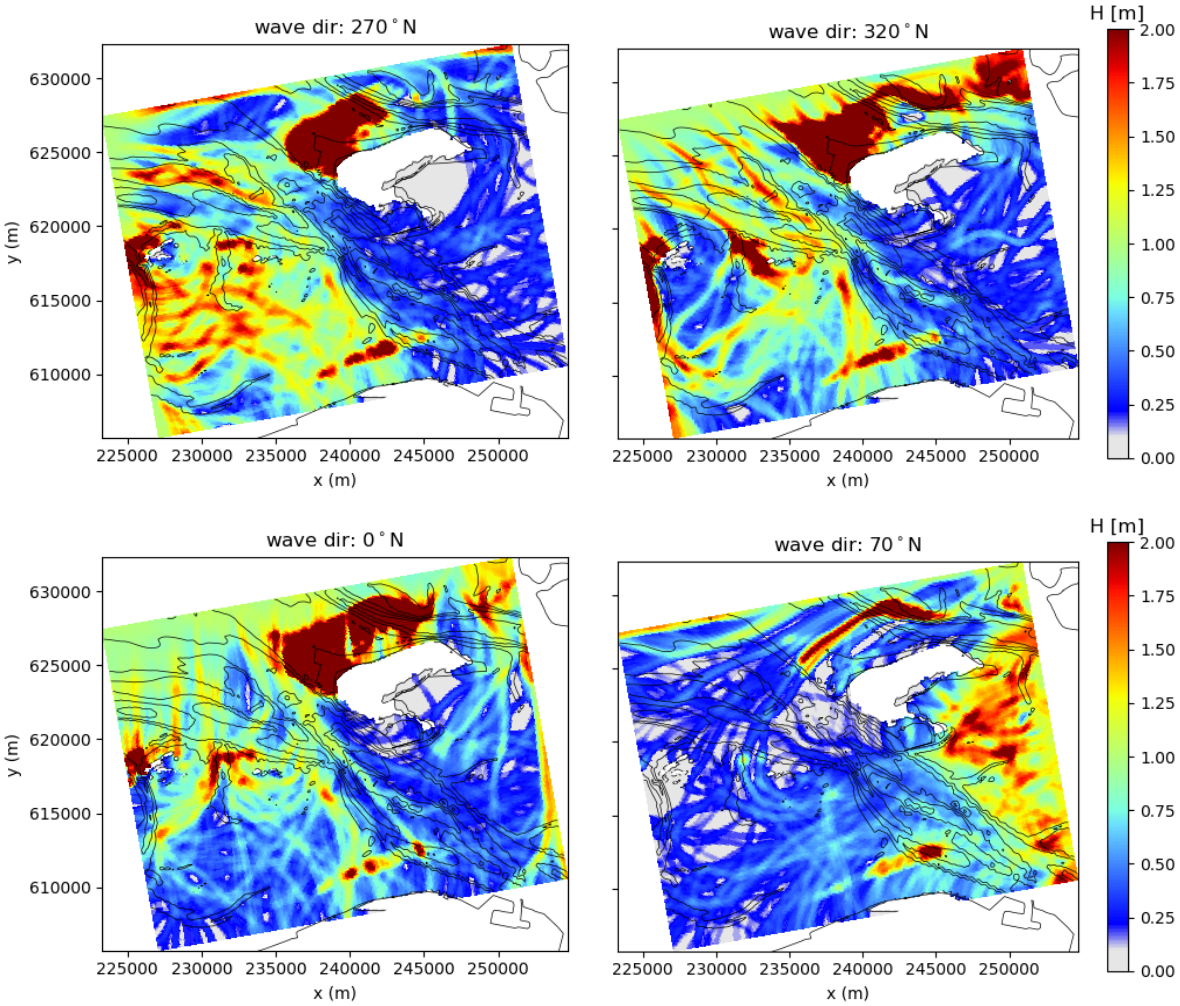

Figure F.12: Wave height according to REFRAC for for water level=2m and a *period of T=15s*.

G

Case study: Monochromatic wave SWAN

G.1. Results for water level 0m

Figures G.1 and G.3 give the wave height distributions for respectively T_p=5s and 15s. It follows that the results of the period of 15s is similar to the case with a wave period of 10s. Additionally, for wave directions approximately parallel to the channel axis, the penetration of waves is larger for lower wave periods. Furthermore, figures G.4 to G.6 show the wave rays according to SWAN for the same three period cases. It should be mentioned that the figures are rotated by 10 degrees compared to the other figures, therefore the north is oriented 10° clockwise from the y-axis.

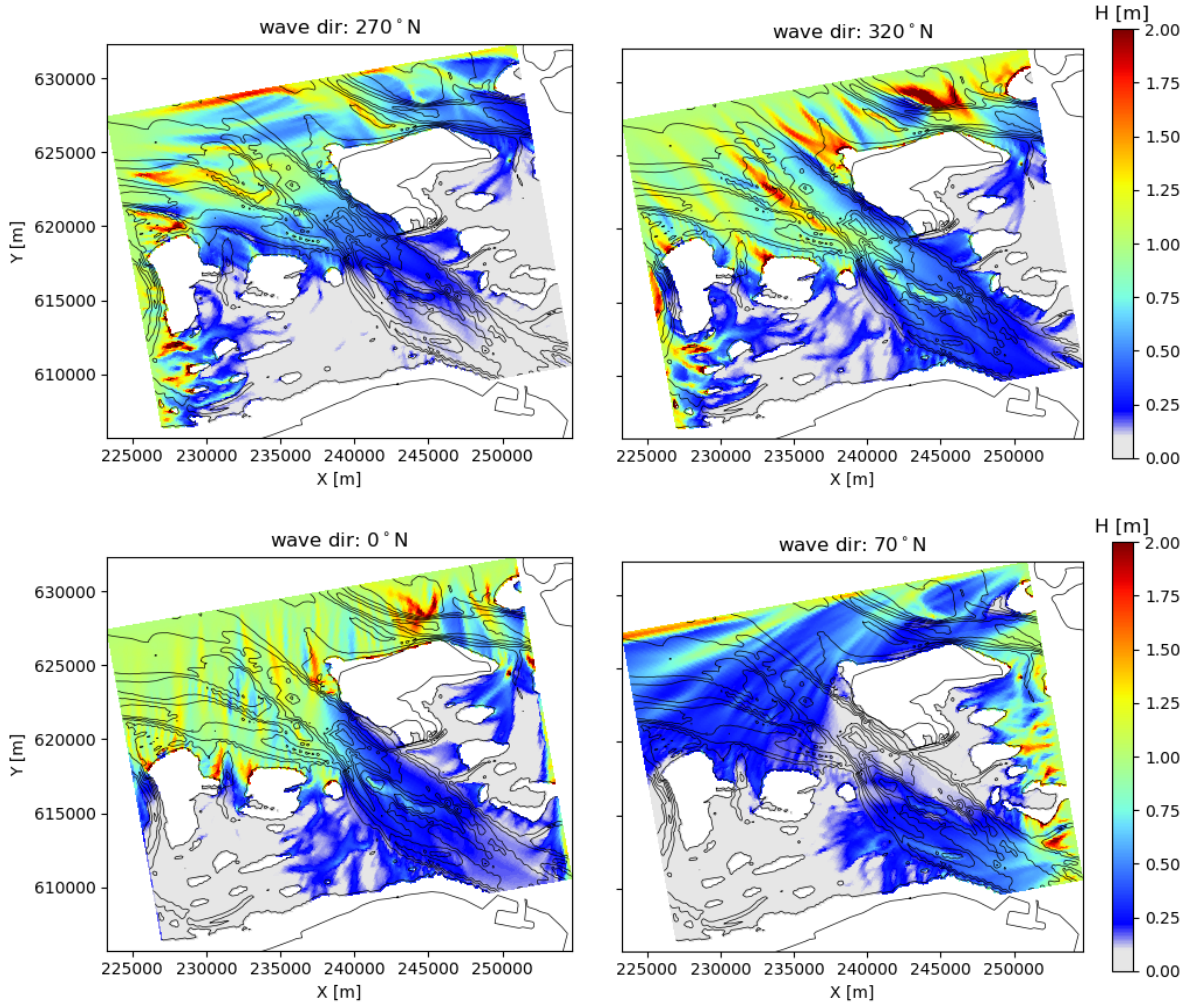

Figure G.1: Wave height according to SWAN for a *period of* T_p=5s.

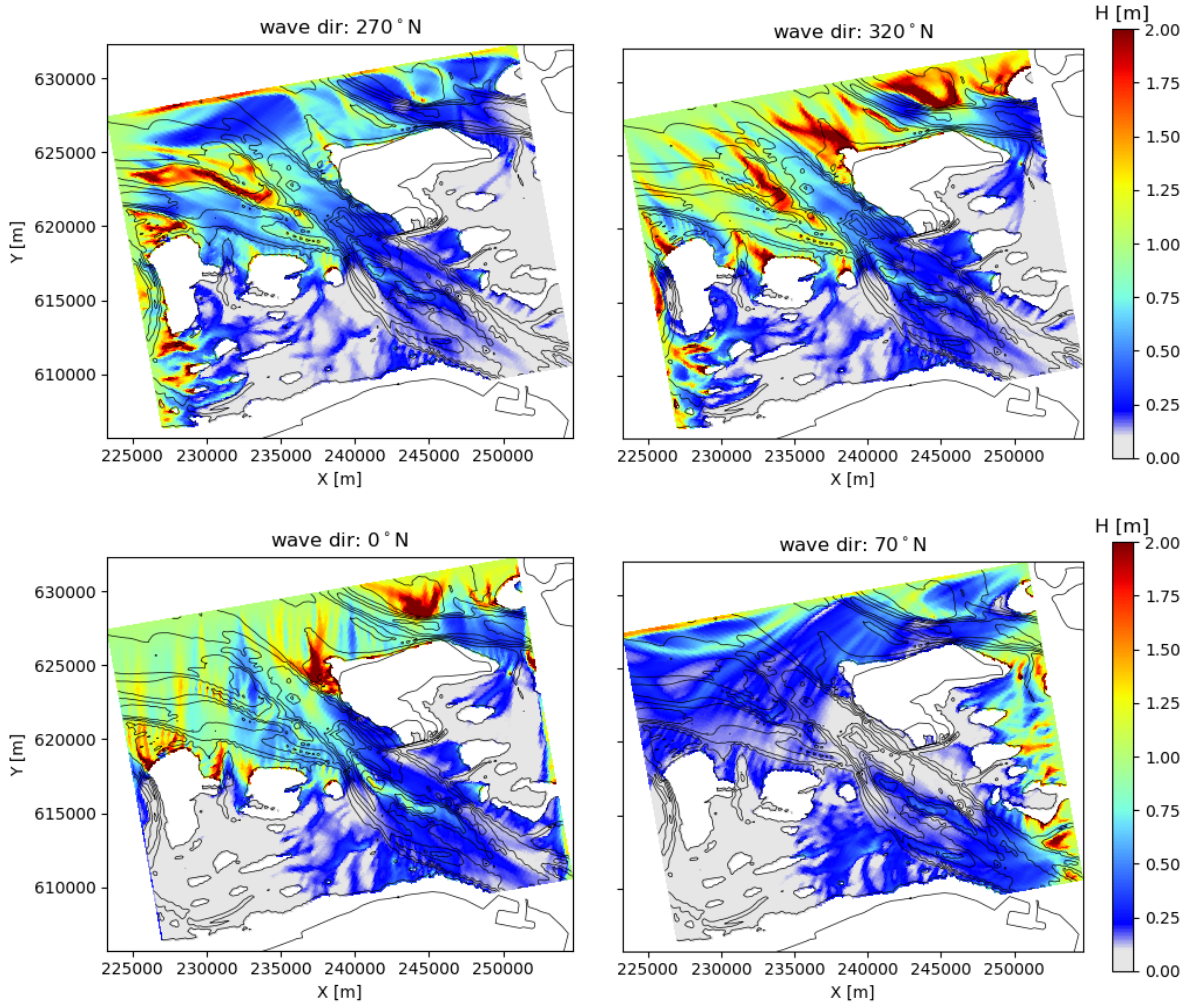

Figure G.2: Wave height according to SWAN for a *period of* T_p*=10s.*

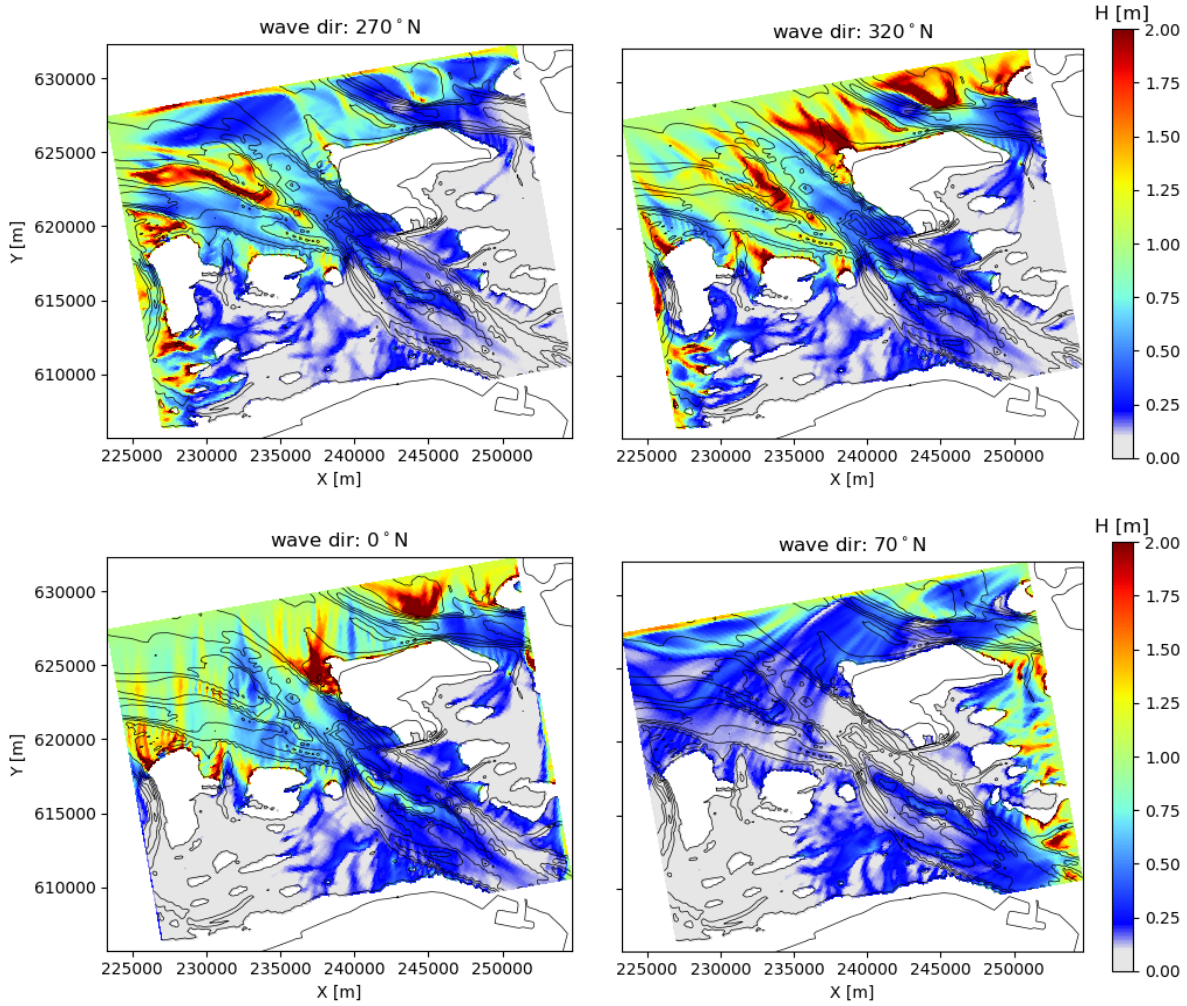

Figure G.3: Wave height according to SWAN for a *period of* T_p*=15s.*

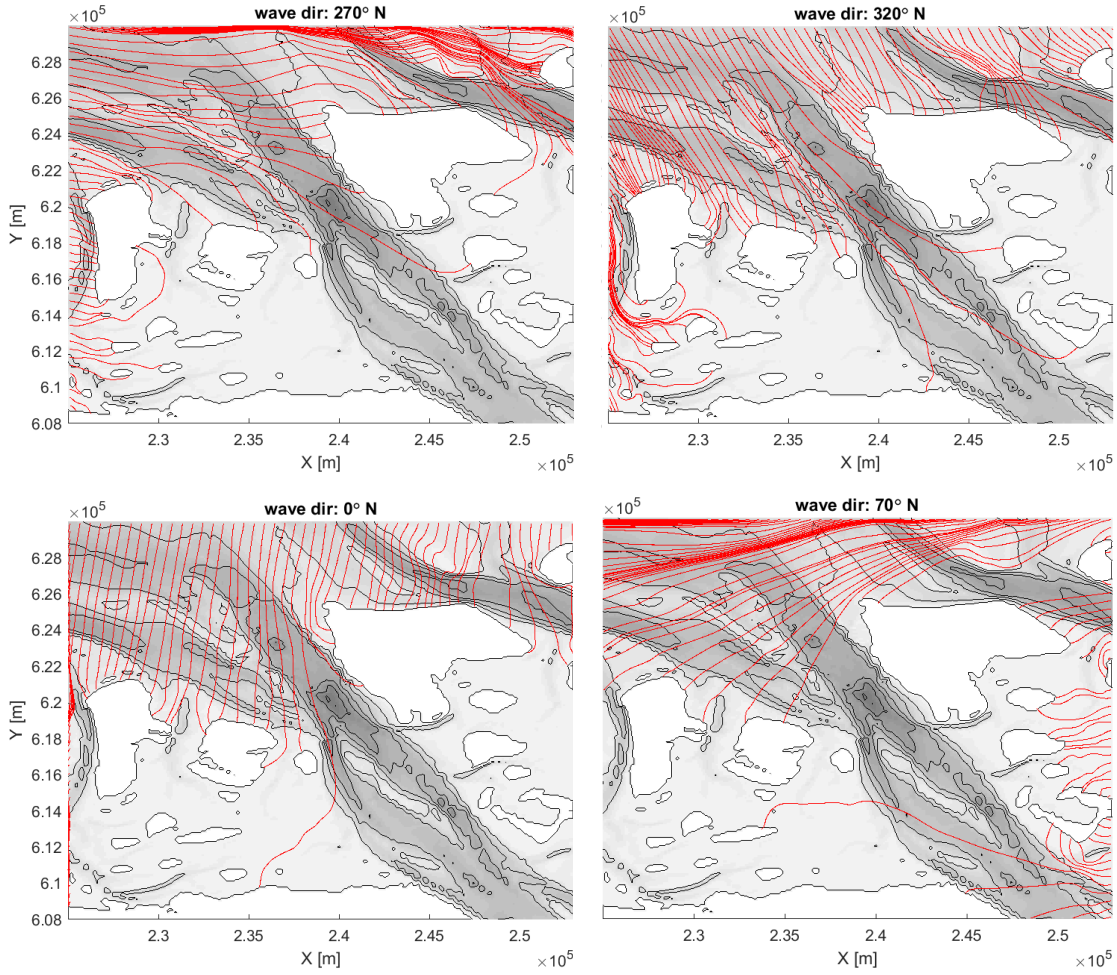

Figure G.4: Wave rays according to SWAN for a water level of 0m and a *period of T=5s.*

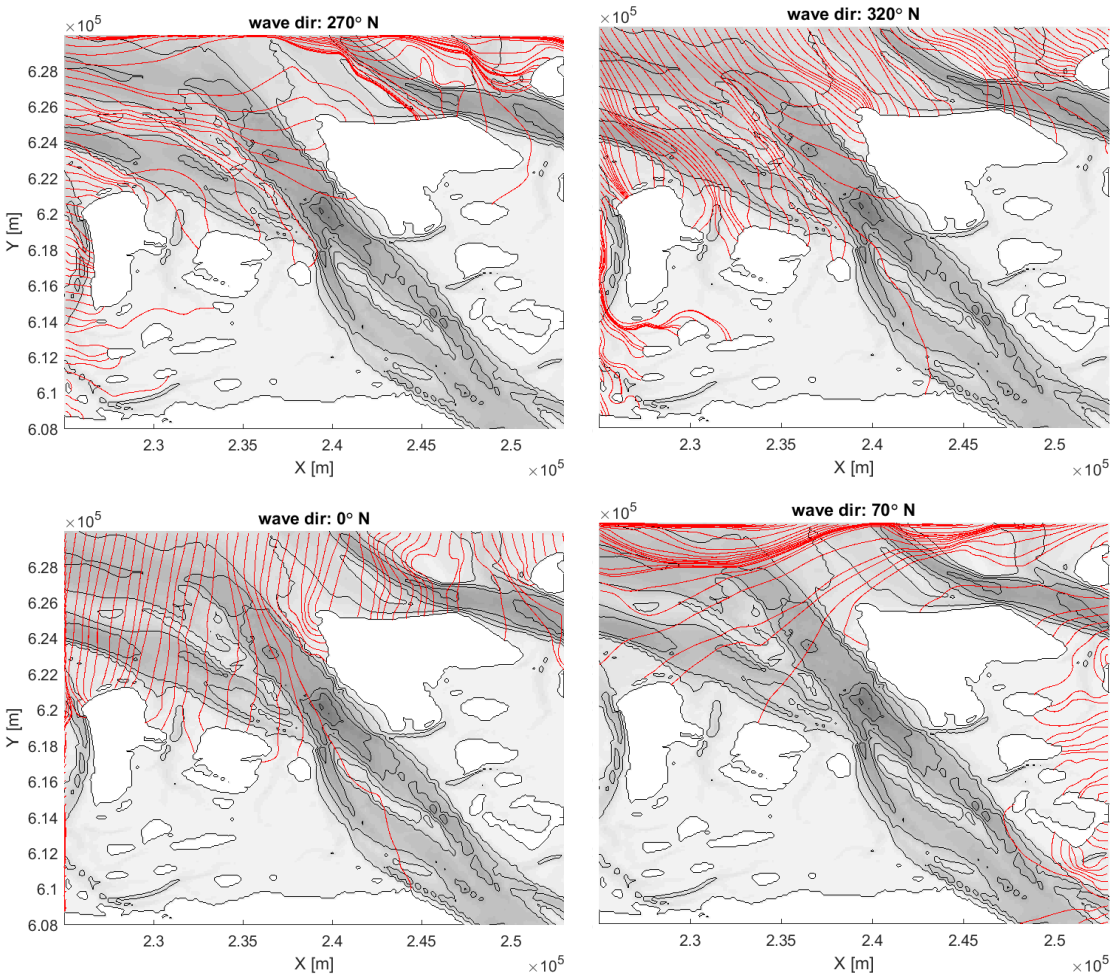

Figure G.5: Wave rays according to SWAN for a water level of 0m and a *period of T=10s.*

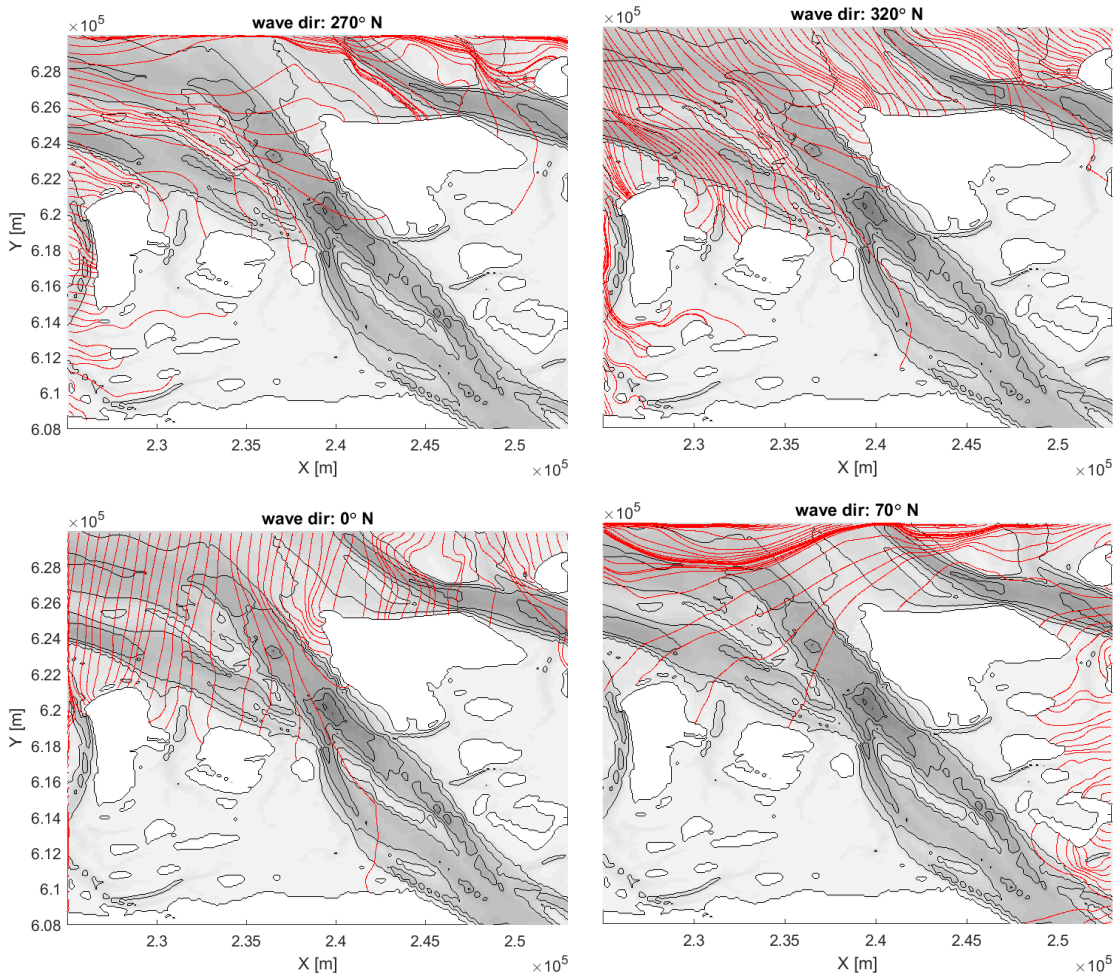

Figure G.6: Wave rays according to SWAN for a water level of 0m and a *period of T=15s.*

G.2. Results for water level 2m

Figures G.7 to G.12 show the same cases as before, only now for a water level of 2m. The first three figures show the wave height distributions, whereas the other three figures give the wave rays. Just as REFRAC, SWAN shows a larger wave penetration for this water level.

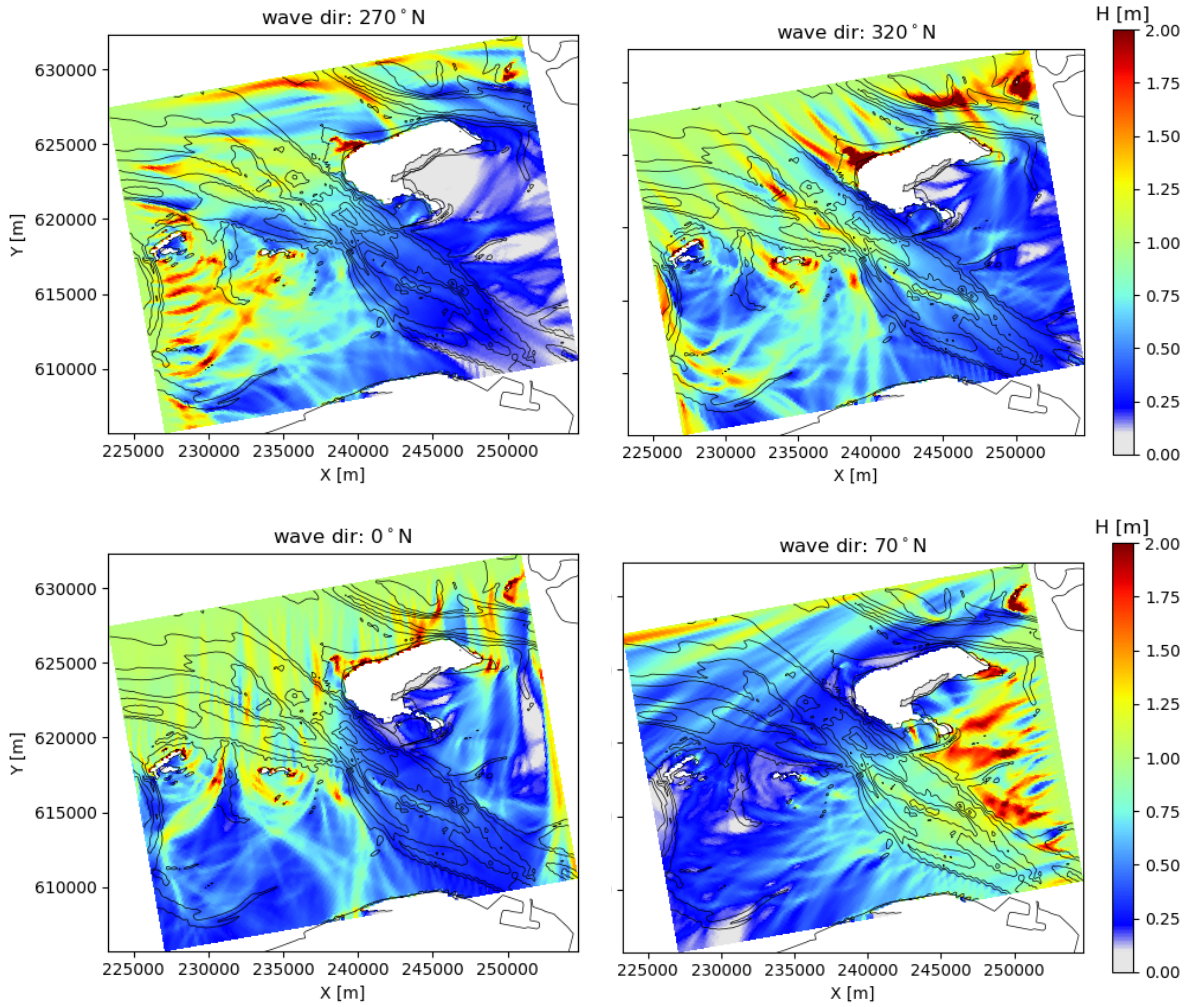

Figure G.7: Wave height according to SWAN for a water level of 2m and a *period of T=5s.*

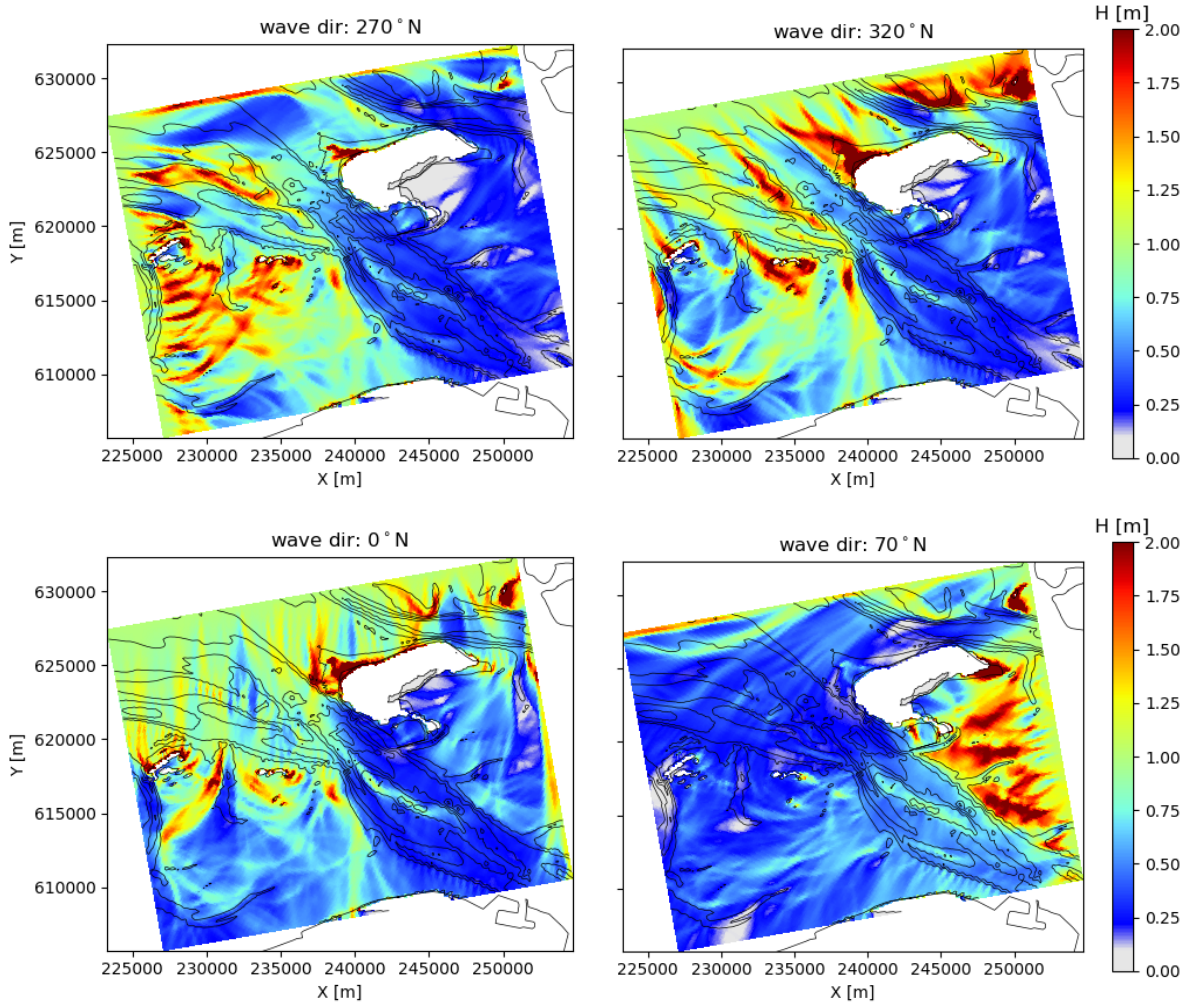

Figure G.8: Wave height according to SWAN for a water level of 2m and a *period of T=10s.*

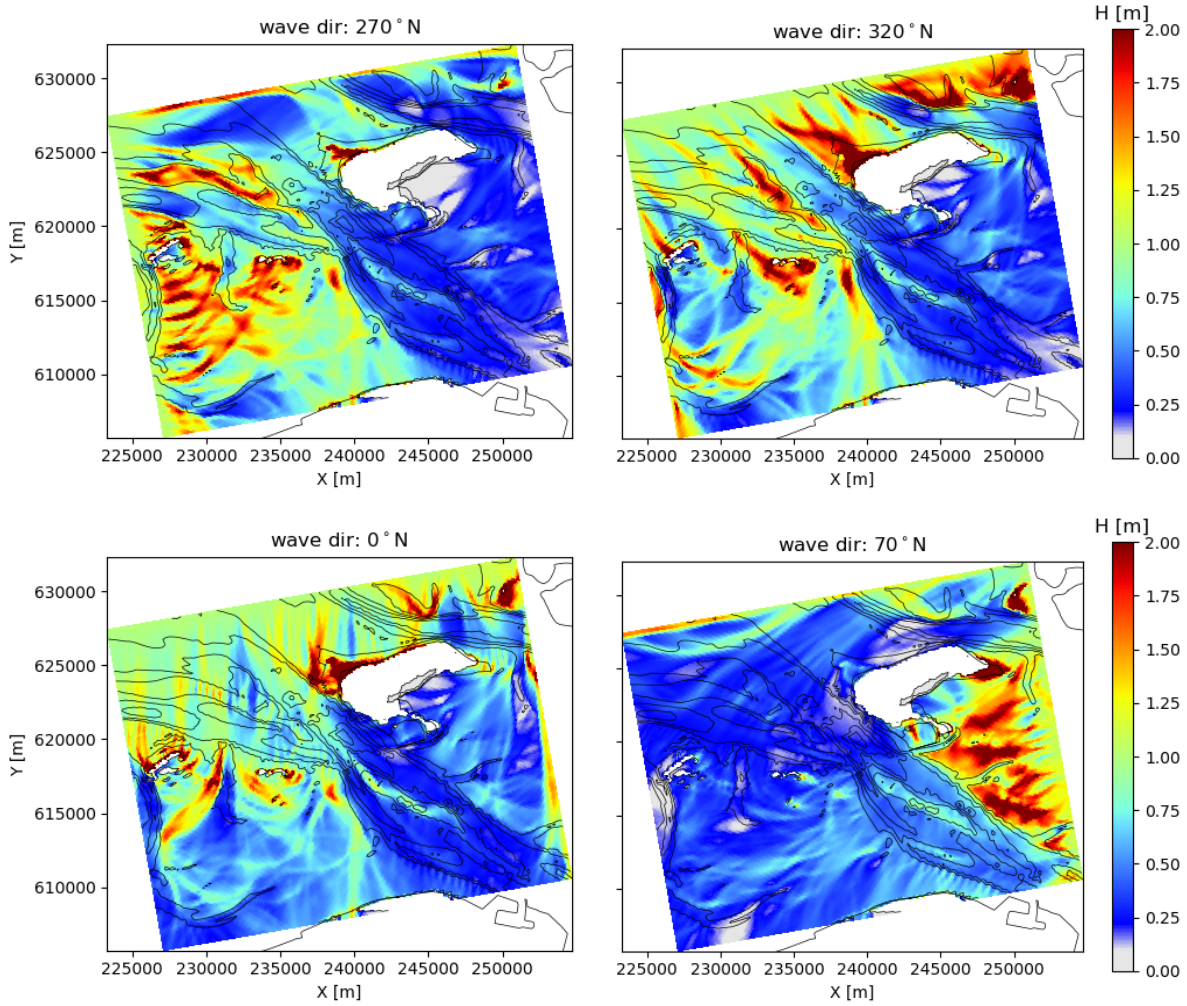

Figure G.9: Wave height according to SWAN for a water level of 2m and a *period of T=15s.*

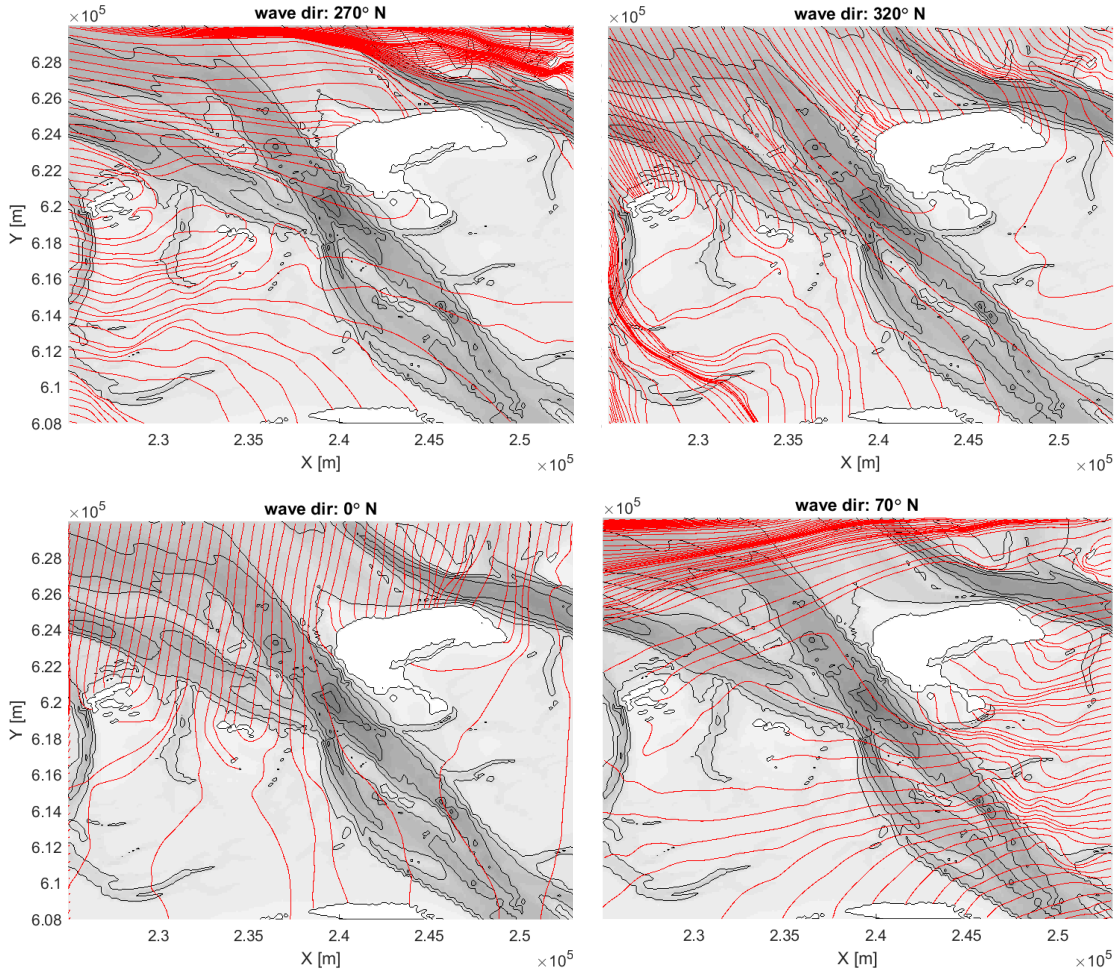

Figure G.10: Wave rays according to SWAN for a water level of 2m and a *period of T=5s.*

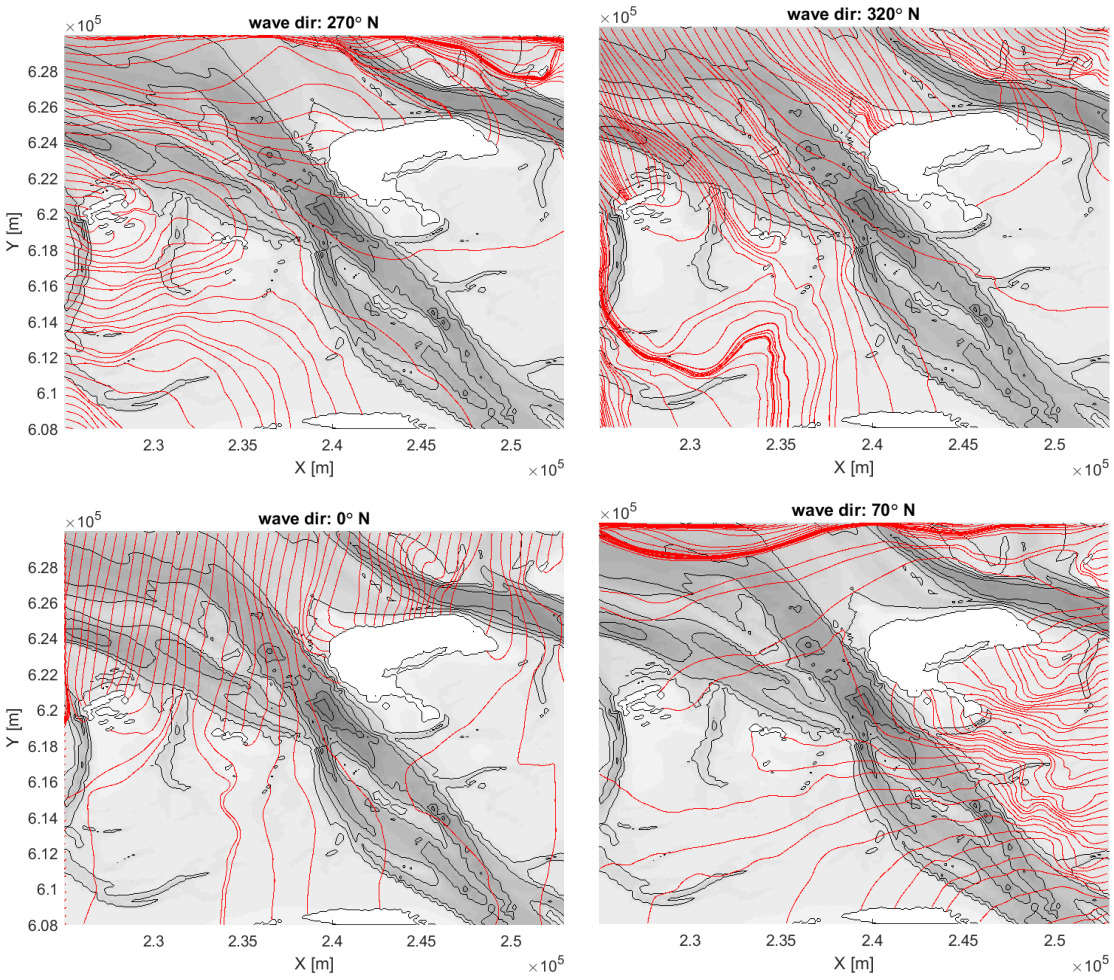

Figure G.11: Wave rays according to SWAN for a water level of 2m and a *period of T=10s.*

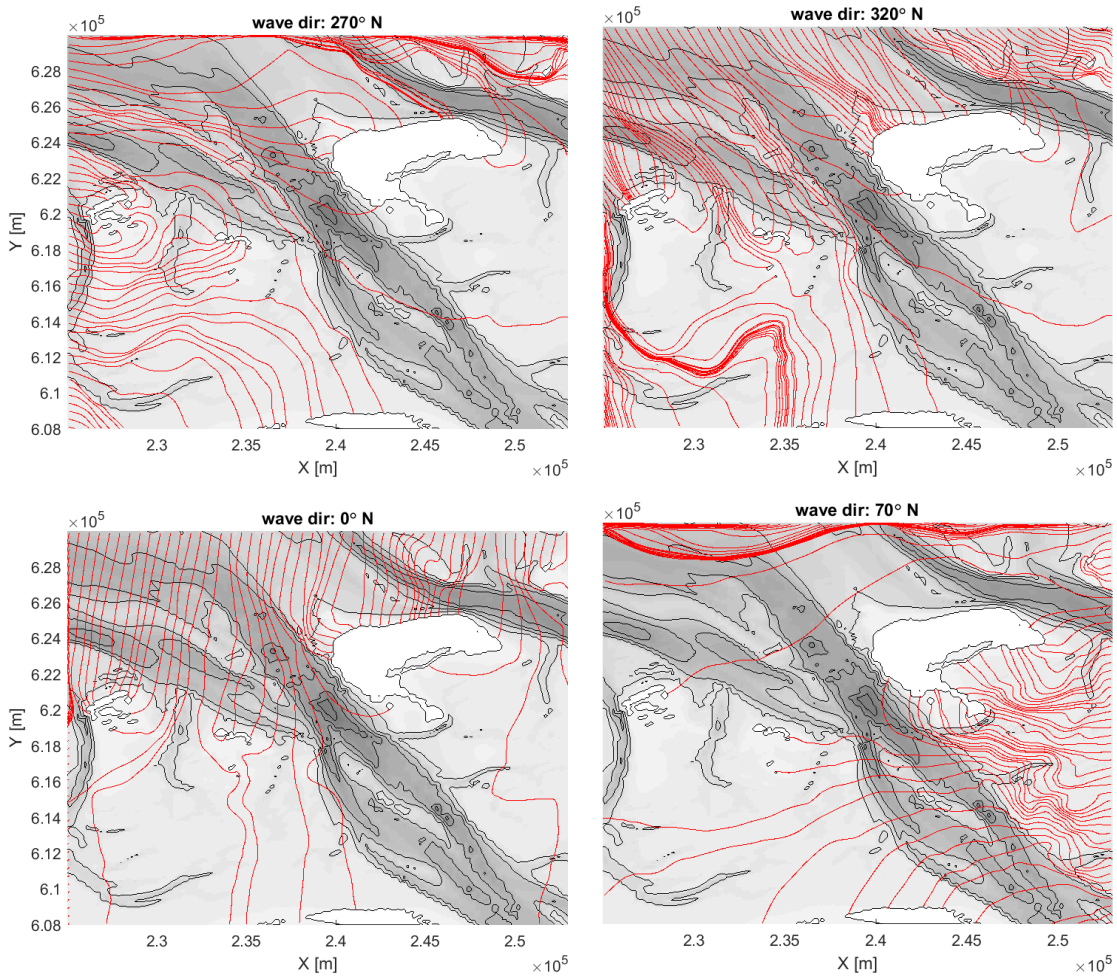

Figure G.12: Wave rays according to SWAN for a water level of 2m and a *period of T=15s.*

G.3. Results for spatial resolution variants

This part of the appendix contains the additional figures concerning the spatial resolution. First the results for a water level of 2m will be presented for the mesh width variants of 50m and 200m. These will both be given relative to the mesh width of 100m, just as was done in the main text. Subsequently, a case will be presented were a mesh width of 25m is applied. This resolution is only possible with running SWAN MPI and is nearly the finest possible resolution to prevent memory issues.

G.3.1. Results for a water level of 0m

Figures G.13 and G.14 give the wave height difference plots for the grid variants and the conditions as were also used in the main text. The patterns and order of the differences in wave height are similar to those observed in case the water level was set to 2m.

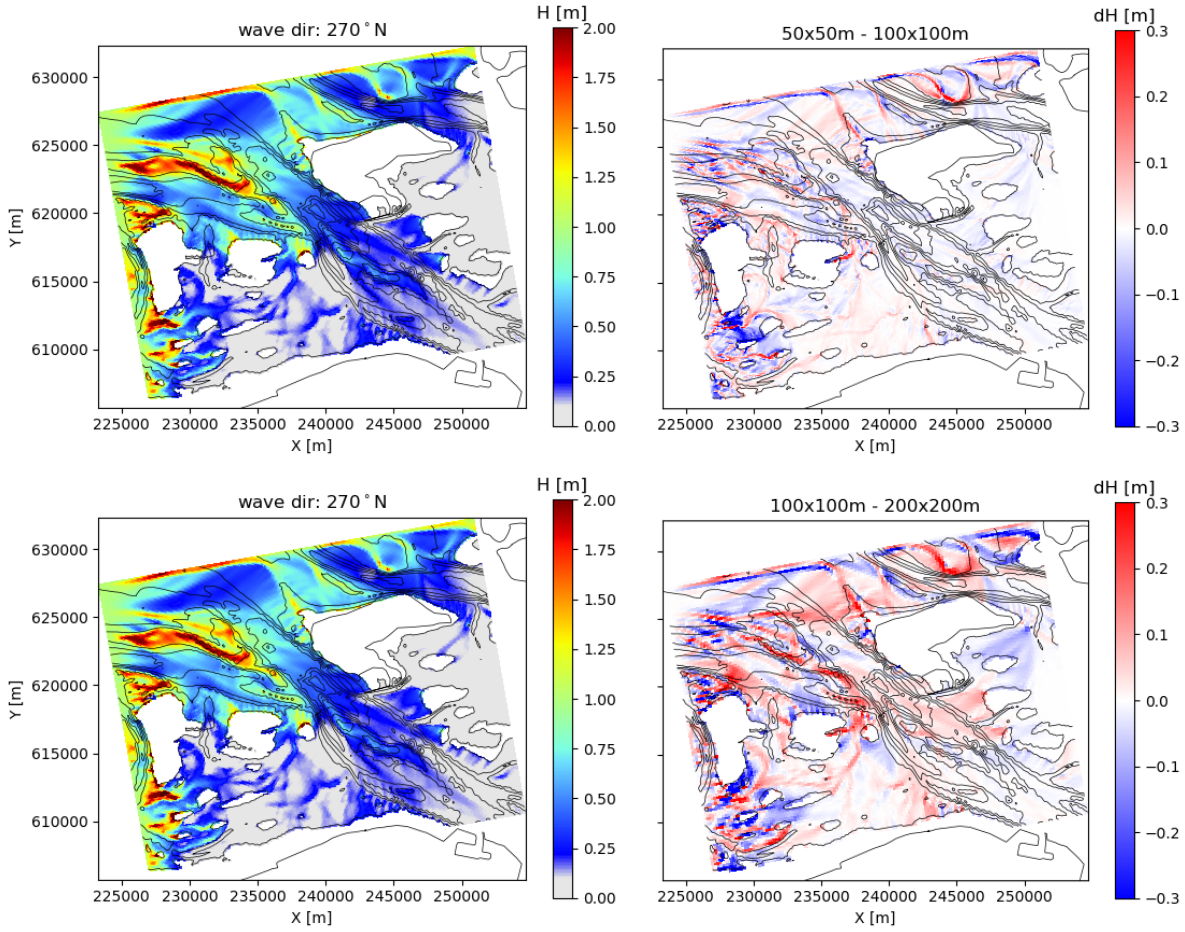

Figure G.13: Left: wave height plot for a mesh width of 100m; Right: Wave height difference for the mesh width of 50m and 200m respectively. conditions: wave direction of 270°N, T_p=10s and η=0m.

Also for figure G.14 the results are similar to those found for a higher water level. However, the results found for a 2m water level were more comprehensible. For a water level of 0m, the 50m mesh width resulted in slightly higher wave heights at the coast. An equal pattern is not found for the comparison with the 200m mesh width. Therefore, it is thought that the different patterns in the 0m water level cases are caused by the emerged flats. These are far less pronounced when the water level is set to 2m and hence they do not adjust the wave propagation that much.

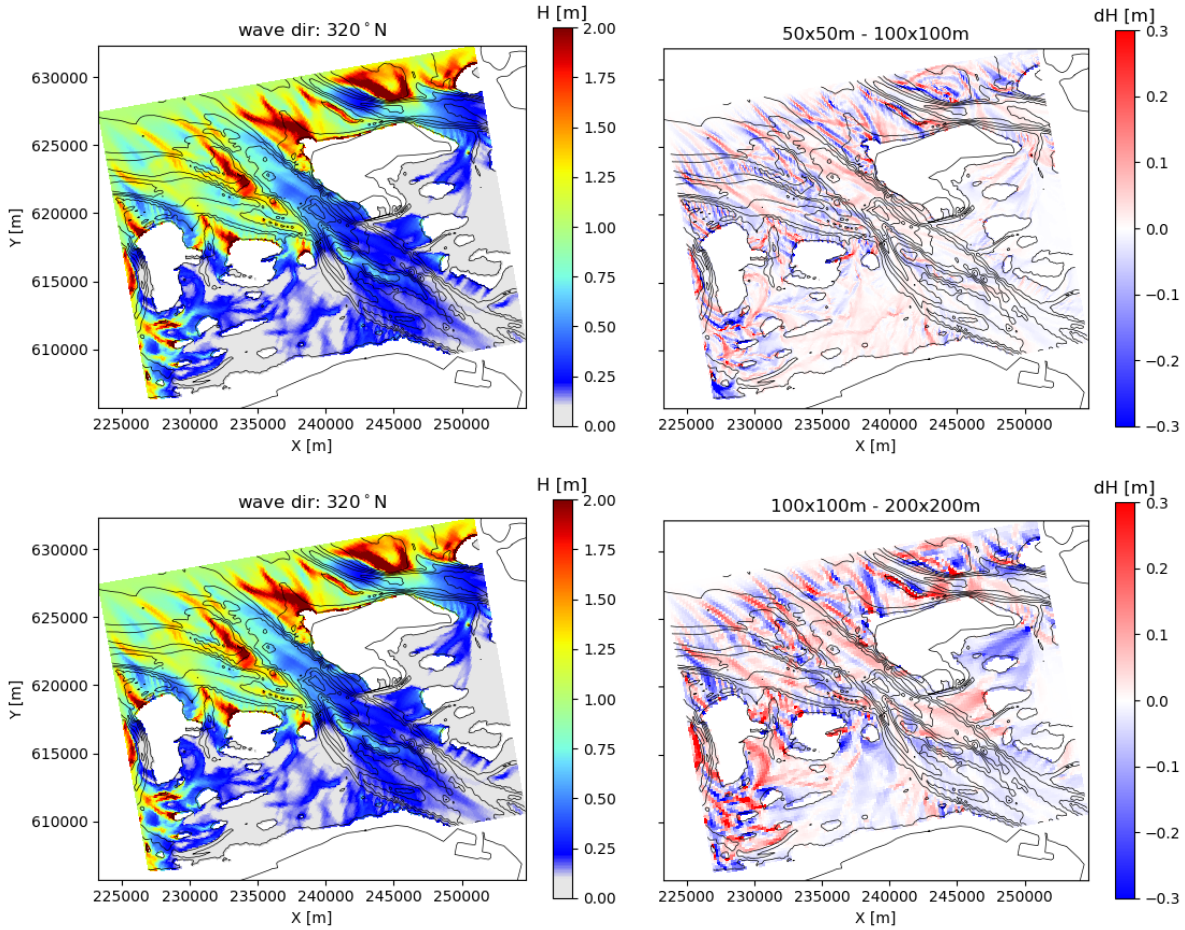

Figure G.14: Left: wave height plot for a mesh width of 100m; Right: Wave height difference for the mesh width of 50m and 200m respectively. conditions: wave direction of 320°N, T_p=10s and η=0m

G.3.2. Fine grid with mesh width = 25m

Figures G.15 to G.20 give the wave height differences for a mesh width of 25m compared to 50m for a water level of 0m. It can be seen that the differences are already relatively small.

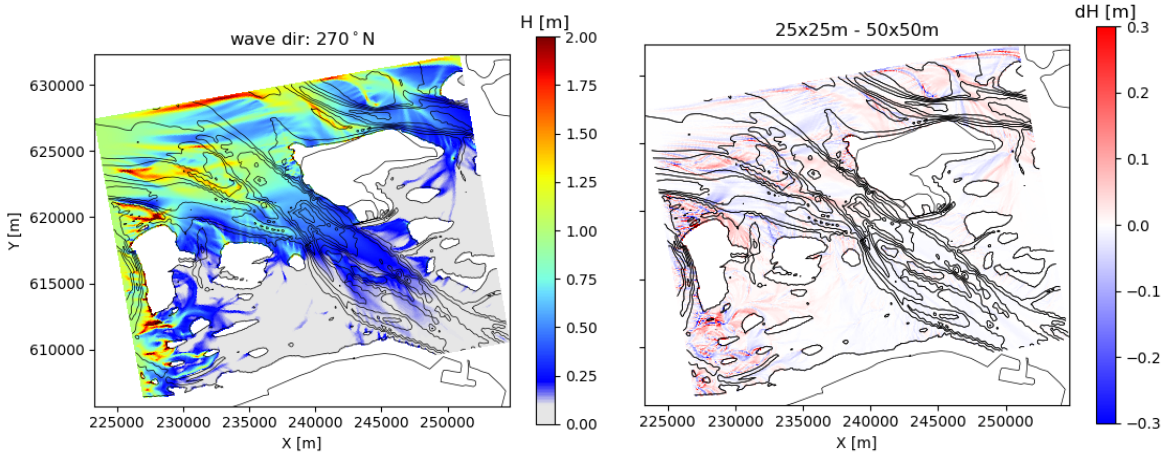

Figure G.15: Wave height with left: 50m mesh width and right: 25m-50m mesh width, conditions: T_p=5s, direction=270°N and water level=0m.

Especially inside the channel, the differences are not significant. Considering the situation near the coast, the absolute difference in wave height is between 0-0.05m in all cases. Observing the wave direction of 270°N, the largest differences in wave height are found at the western channel side. This is especially true for higher wave periods.

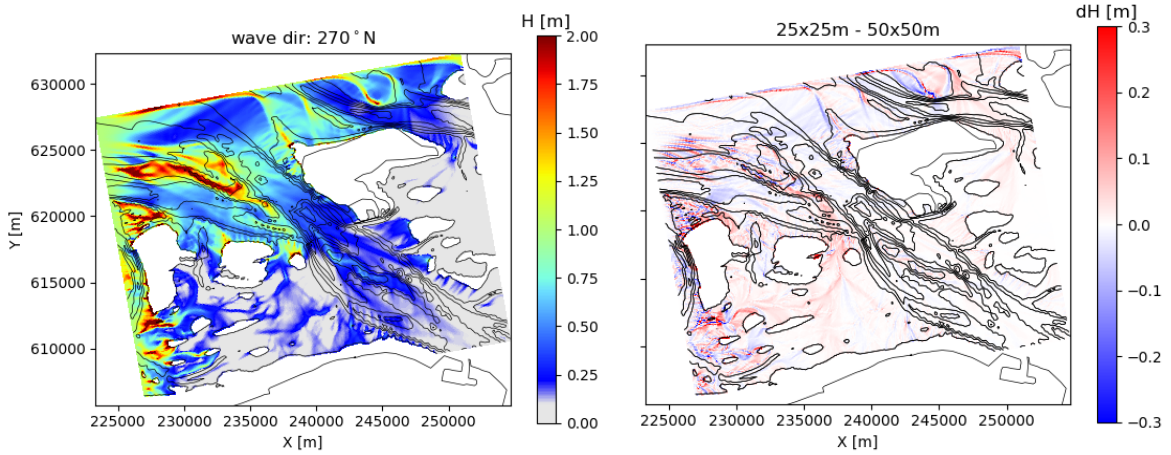

Figure G.16: Wave height with left: 50m mesh width and right: 25m-50m mesh width, conditions: T_p=10s, direction=270°N and water level=0m.

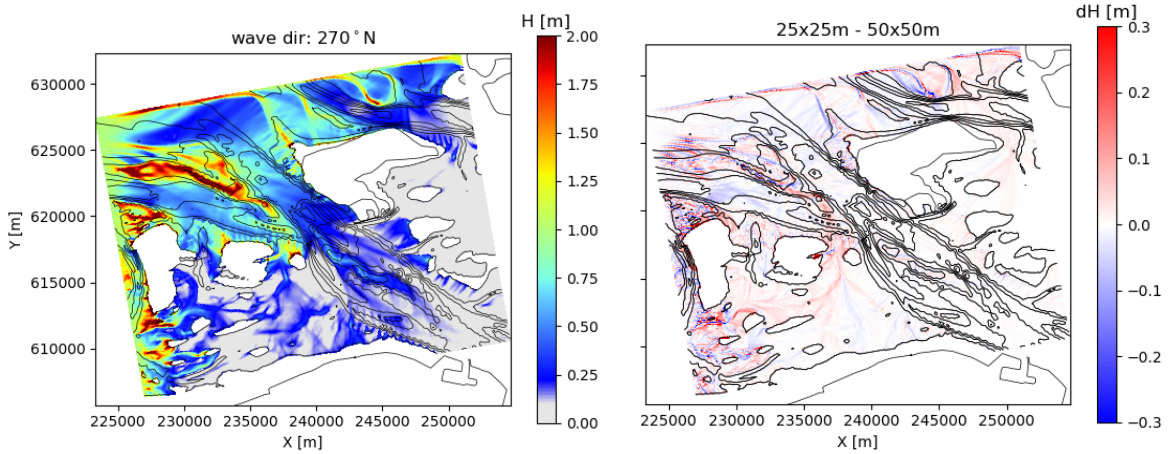

Figure G.17: Wave height with left: 50m mesh width and right: 25m-50m mesh width, conditions: T_p=15s, direction=270°N and water level=0m.

For the incoming direction of 320°N, it can be seen that the wave energy refracts out of the channel stronger for the 50m mesh width. Additionally, this behaviour is stronger for higher wave periods, leading to larger differences in this case.

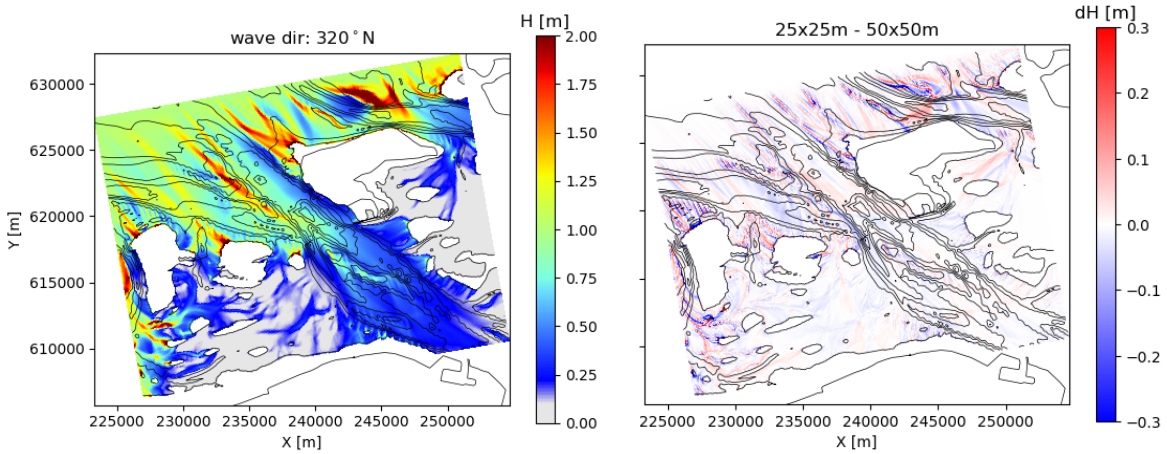

Figure G.18: Wave height with left: 50m mesh width and right: 25m-50m mesh width, conditions: T_p=5s, direction=320°N, and water level=0m.

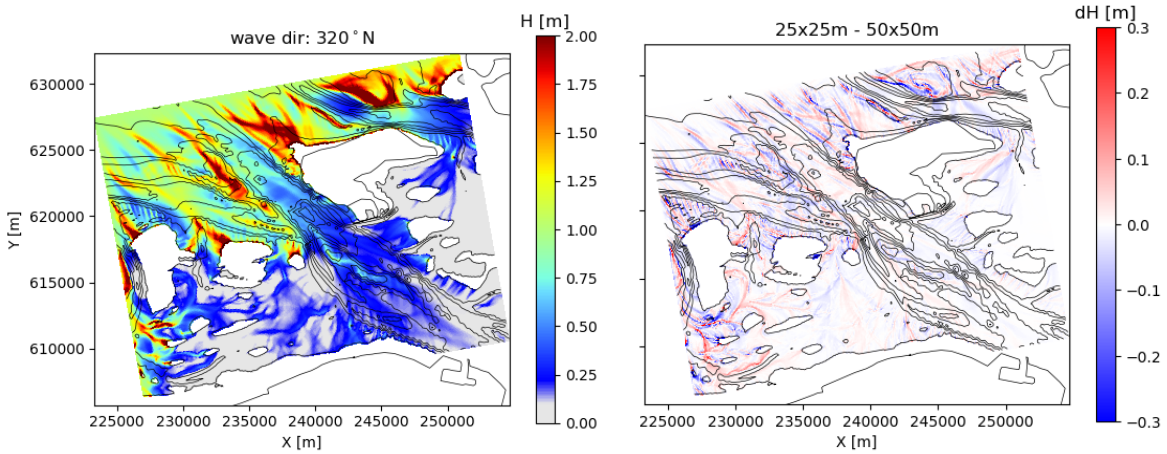

Figure G.19: Wave height with left: 50m mesh width and right: 25m-50m mesh width, conditions: T_p=10s, direction=320°N and water level=0m.

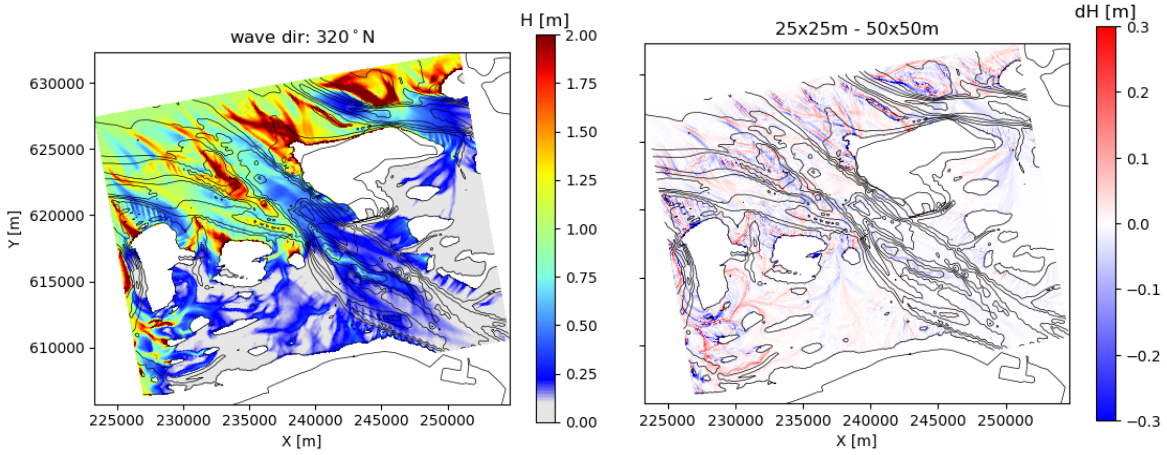

Figure G.20: Wave height with left: 50m mesh width and right: 25m-50m mesh width, conditions: T_p=15s, direction=320°N and water level=0m.

H

Additional wave spectra Wadden Sea

This appendix contains the additional spectra that are not given in the main report. These spectra belong to the conditions at 13 January 2017, 23:50h similar to the figures in the main report.

H.1. WBI settings

Applying the WBI2017 settings leads to the spectra at the buoy locations in the Ems area as given in figure H.1. As mentioned, Uithuizerwad (UHW) is not a wave buoy but a radar device.The default settings are equal to the standard SWAN settings as used in the main report. The WBI settings that are used with SWAN version 40.72ABCDE are given in table H.1.

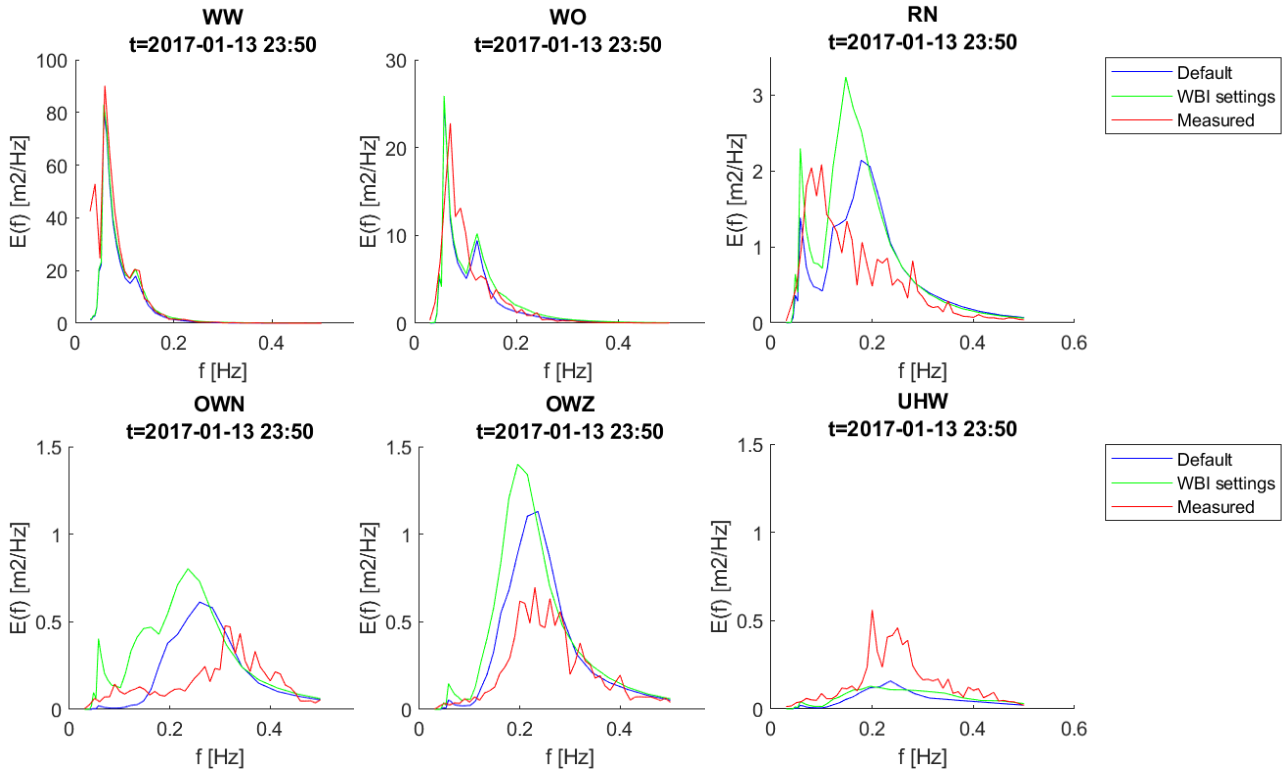

Figure H.1: 1D variance density spectra at the six locations of Rijkswaterstaat with WBI2017 settings and default SWAN for 13 January 2017, 23:50h.

Table H.1: Overview of the settings as used by WBI2017 (Oosterlo et al., 2018).

Wave process	Settings
Wave growth	GEN3 WESTH
Whitecapping	WCAP WESTH cds2=5e-05 br=0.00175 p0=4 powst=0 powk=0 nldisp=0 cds3=0.8 powfsh=1
Quadruplets	QUAD iquad=2 lambda=0.25 cnl4=3.0e+07
Bottom friction	FRIC JONSWAP cfjon=0.038
Surf breaking	BREA WESTH alpha=0.96 pown=2.5 bref=-1.39630 shfac=500
Triads	TRIAD trfac=0.10 cutfr=2.5
Quadruplet limiter	LIMiter ursell=10.0 qb=1.0

H.2. 2D variance density spectra

Figures H.3 and H.4 give the 2D spectra for the Rijkswaterstaat measurement locations for respectively the default and WBI2017 SWAN settings. The color scales are set equal for both versions at a certain location. Variance densities that are more than 30 times smaller than the maximum value are neglected from the figure by means of NaN values. Additionally, the first colour bin is made white for visual purposes.

Furthermore, the 2D spectra are given at the locations of figure H.2, these are shown in figure H.5 and H.6. The upper row gives the variance density spectra for the reference grid, where the lower plots show the spectra for a finer nest layer with 6x3 refinement. Location Z1 is not shown here, but this spectrum is similar to the one of Z2.

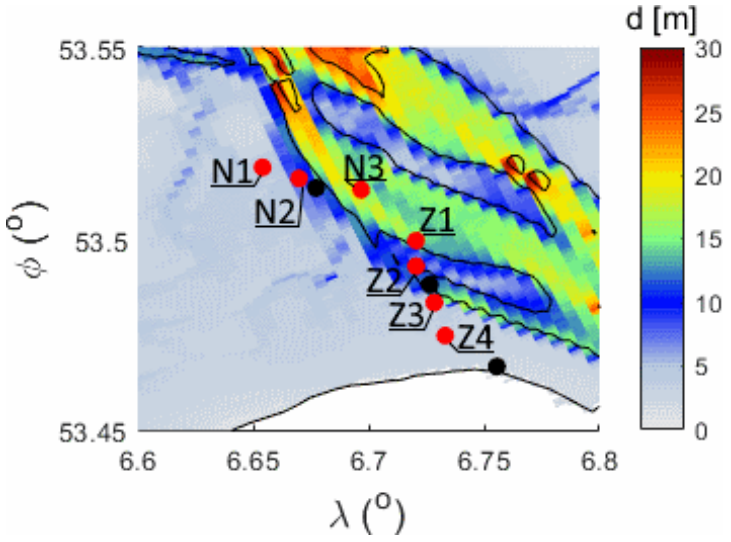

Figure H.2: Locations of the cross-sections around OWN and OWZ.

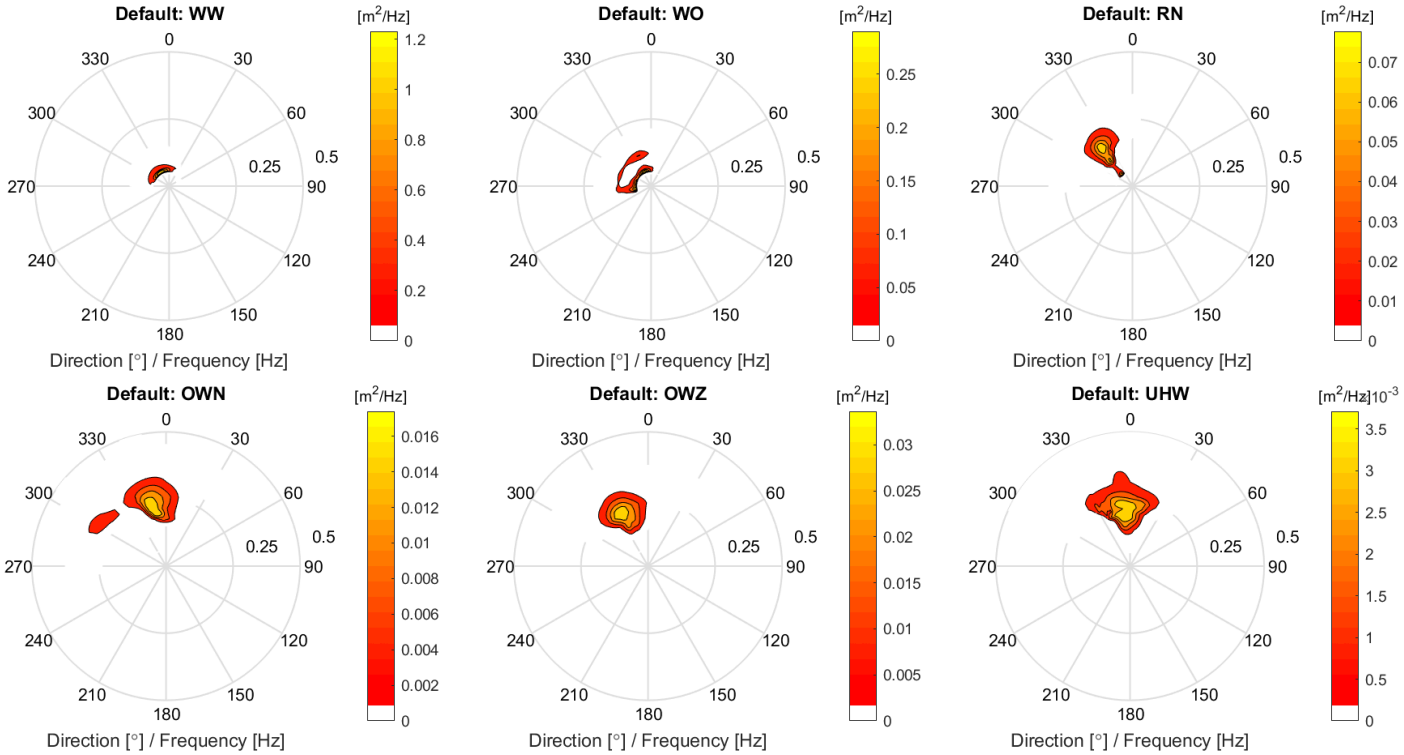

Figure H.3: 2D variance density spectra at the six locations of Rijkswaterstaat with default SWAN settings for 13 January 2017, 23:50h.

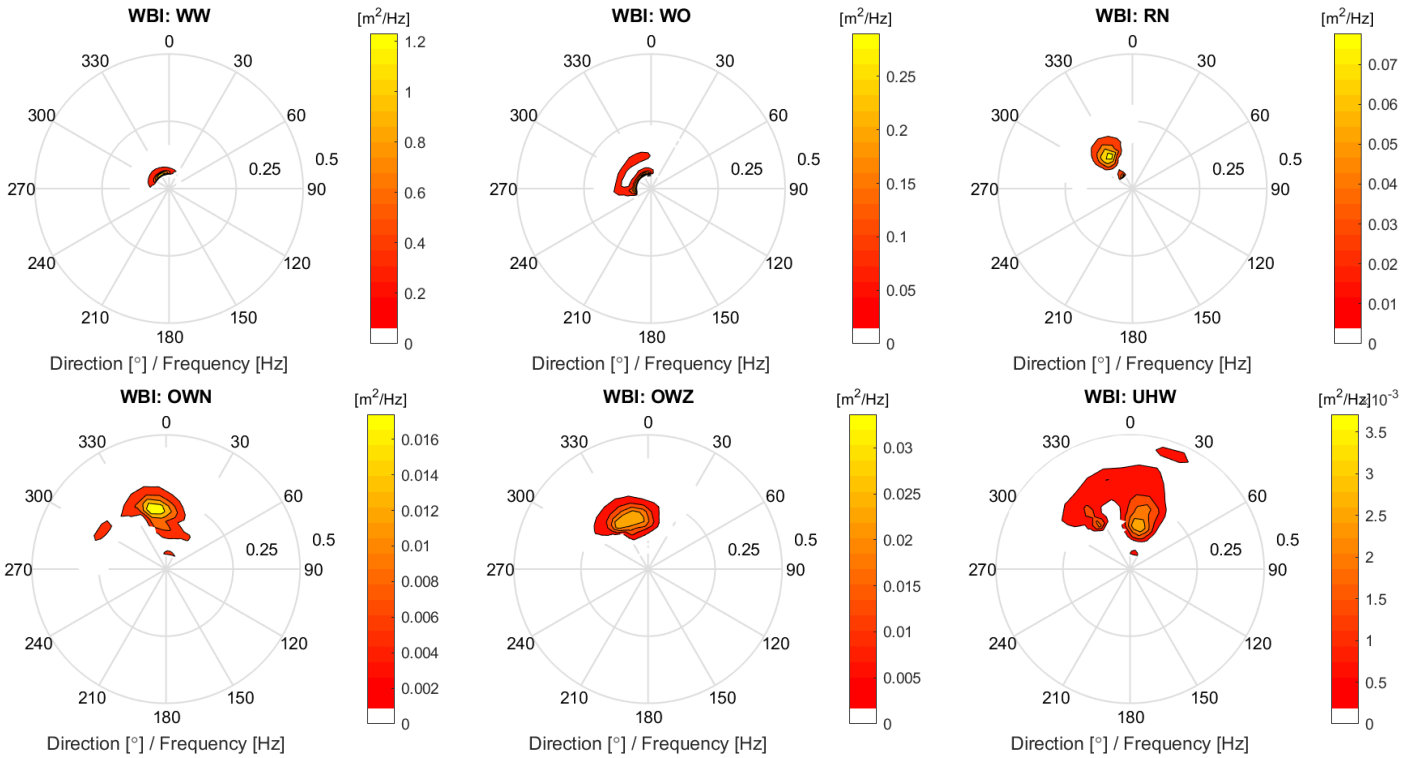

Figure H.4: 2D variance density spectra at the six locations of Rijkswaterstaat with WBI2017 settings for 13 January 2017, 23:50h.

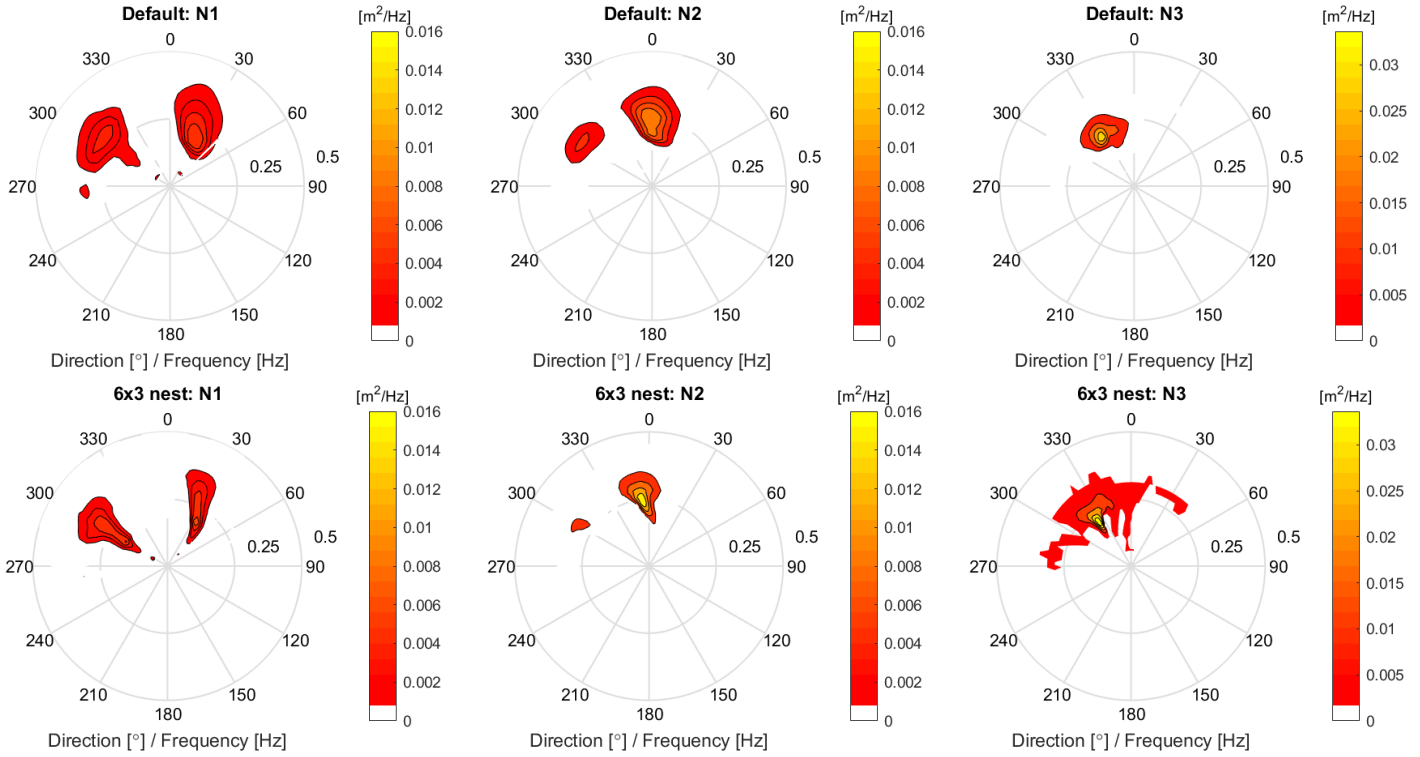

Figure H.5: 2D variance density spectra at the N locations of figure H.2 for the reference grid and a 6x3 refined nest layer, using default SWAN settings for 13 January 2017, 23:50h.

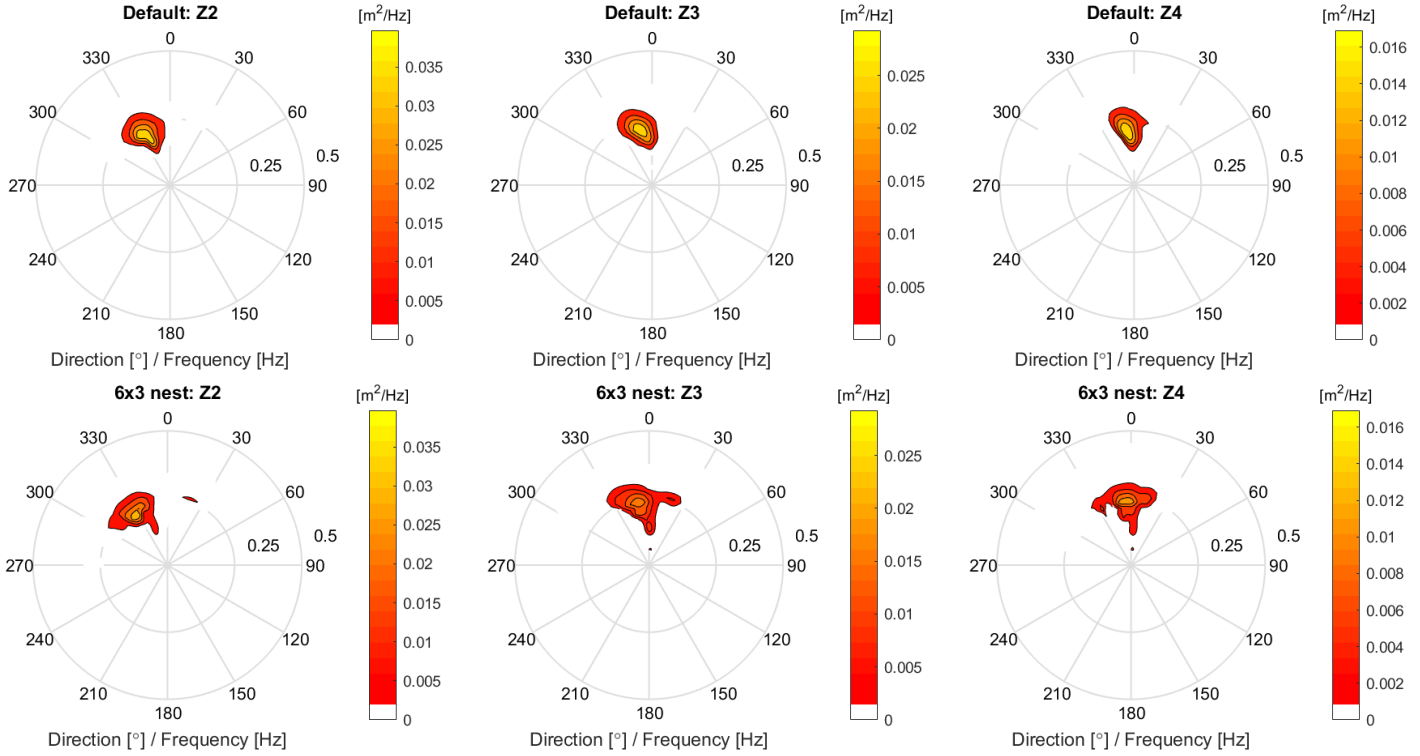

Figure H.6: 2D variance density spectra at the Z locations of figure H.2 for the reference grid and a 6x3 refined nest layer, using default SWAN settings for 13 January 2017, 23:50h.